Nanostructured NiO thin films for electrochemical and colorimetric biosensors

by

Anuja Tripathi

A thesis submitted in partial fulfillment of the requirements for the degree of

Doctor of Philosophy

in

Chemical Engineering

Department of Chemical and Materials Engineering
University of Alberta

Abstract

Biosensors are devices that detect biological or chemical responses by generating signals that are proportional to the concentration of the analyte. An ideal biosensor should be highly sensitive, selective, and reproducible, with a low detection limit and rapid response time. Nanostructured porous materials are advancing the development of new types of electrochemical and colorimetric biosensors that can detect chemical compounds associated with food spoilage and medical conditions. In this thesis, I developed both electrochemical and colorimetric biosensors, which are united by fabrication technique and material systems.

An electrochemical biosensor is a simple and low-cost sensing device. The working electrode material has a significant impact on the analytical performance of such biosensors, and methods that increase the surface area, such as nanoparticle incorporation, have been shown to improve sensor performance. Enzymes act as highly selective catalysts, which means they only speed up one type of reaction at a time and generate a product that can be used to detect desired compound selectively. Electrode incorporated with nanoparticles exhibit high surface area and porosity, which allows enhanced enzyme immobilization towards the development of a selective and sensitive sensor with high response time. Amongst several nanoparticle types, metal and metal oxides based nanoparticles have been widely investigated for serving this purpose.

Colorimetric biosensing platforms, which are counterparts of electrochemical sensors, often use enzymes as catalysts, which require well-controlled operating conditions (temperature, pH, and purity) for proper functioning. However, precise control of the operating and storage conditions can be difficult to achieve. Nanozymes are high surface area nanostructures that mimic enzyme-like catalytic properties. However, most of the reported nanozymes are dispersed in solution,

which makes them hard to recover after use. Moreover, nanozymes tend to have a low density of active sites which result in lesser catalytic activity than natural enzymes.

This thesis investigates the glancing angle deposition (GLAD) technique to explore inexpensive transition metal oxides such as NiO for developing enzymatic electrochemical and colorimetric biosensors. GLAD is a physical vapor deposition technique that exploits atomic shadowing and dynamic motion control to engineer nanostructures with high surface area and controlled porosity. The high specific surface area leads to the high concentration of catalytic active sites, which can improve the physicochemical properties of electrochemical and colorimetric biosensors.

In the first project, macroporous NiO electrodes were fabricated using the GLAD technique to develop an enzymatic electrochemical sensing of xanthine (XA), an indicator for fish freshness. GLAD NiO electrodes were used due to their high isoelectric point, biocompatibility, chemical stability, and well-defined porosity. This provided an accessible surface for enzyme (xanthine oxidase, XO) immobilization using physisorption technique which was used to selectively monitor XA. The developed XA electrochemical sensor showed the dynamic range of 0.1 μM to 650 μM, limit of detection of 37 nM, good reproducibility (relative standard deviation of ~ 4%, n=18), rapid response time (~7 s), and a high sensitivity (1.1 $\mu A \cdot \mu M^{-1} \cdot cm^{-2}$ in the low concentration range from 0.1-5 μM, and 0.3 $\mu A \cdot \mu M^{-1} \cdot cm^{-2}$ in the higher concentration range from 5-650 μM). Overall, the sensor was more sensitive in comparison to the flat NiO-based enzymatic sensor (0.03 $\mu A \cdot \mu M^{-1} \cdot cm^{-2}$). Moreover, the sensor showed less interference from common fish sample matrices (such as glucose, uric acid, hypoxanthine) and the common fish preservative (sodium benzoate). The sensor also did not loose its performance when stored in buffer at 4ºC for over a week.

Natural enzyme such as horseradish peroxidase (HRP) is used as a catalyst in the colorimetric detection of uric acid (UA), which is a biomarker for gout, arthritis, and high blood pressure.

Hence, in my second work, Ni GLAD film on Si substrate was used to mimic HRP for accelerating the oxidation reaction of colorless 3,3',5,5'-tetramethybenzidine (TMB) to blue colored (oxTMB) in the presence of hydrogen peroxide (H_2O_2). This reaction is dependent on UA, allowing the concentration of UA to be determined based on the solution color. The absorbance of oxidized TMB solutions was measured by UV-VIS spectroscopy to detect the concentration of UA added to the solution, while surface characterization and morphology studies of Ni GLAD films were done by XPS and SEM. In the first phase of this study, the concentration of TMB, amount of H_2O_2, contact time between GLAD films and reacting mixture, and pH of reactants were optimized to achieve high optical absorbance at 652 nm as measured by UV VIS (corresponding to a blue solution). As these thin films were surface-anchored structures, they could be easily recovered after use and be reused. Next, the catalytic activity of the nanostructured film was compared to a flat Ni reference sample. Results showed the excellent reusability of the GLAD film in 1.6 mM TMB and 0.29 M H_2O_2 solution, with LOD of 3 μM, exhibiting its practical relevancy to detect UA under physiological conditions. Furthermore, the developed colorimetric sensor was also tested against glucose and urea to examine its potential for use as a UA biomarker in clinical diagnosis. Calculated Michaelis Menten constant (K_m) of the Ni GLAD film ranged ~1 mM, which confirmed high peroxidase-like activity in comparison to mono metal nanoparticles-based nanozymes. However, the fabricated Ni GLAD-based nanozyme was not up to the mark of natural peroxidase enzyme (K_m = 0.43 mM). Low Michaelis-Menten constant (K_m) demonstrates the high effectivity of the catalyst. Therefore, in the third work, further enhancement of the surface energy of nanozymes were conducted via N plasma functionalization. Surface characterization and morphology studies by XRD, TEM, XPS and SEM, confirmed the presence of adsorbed N^{3-} ions as catalytically-active centers for accelerating electron transfer. Hence, an improved catalytic activity was achieved which resulted in low UA LOD (1 μM) and improved K_m (0.17 mM). The

functionalized Ni GLAD nanozyme with N plasma even exhibited high peroxidase-like activity for colorimetric sensing of UA. The potential application of functionalized GLAD nanozymes was also demonstrated through a gravity-driven continuous catalytic reaction device for colorimetric sensing of UA using paper based point of care device.

Preface

Parts of this thesis have been previously published in the literature, as explained below.

A version of chapter 3 has been submitted for consideration in a peer-reviewed journal by Anuja Tripathi, Anastasia L. Elias, Abebaw B. Jemere, Kenneth D. Harris, "Amperometric determination of xanthine using nanostructured NiO electrodes loaded with xanthine oxidase". As the primary author in this chapter, A. Tripathi performed the experiments and wrote the manuscript. Dr. Jemere and Dr. Harris conceived the project idea. It is fully acknowledged that Dr. Elias, Dr. Jemere, and Dr. Harris, supervised the project and contributed to the experiments planning, analysis, and writing the manuscript.

Chapter 4 of this thesis has been published as Anuja Tripathi, Kenneth D. Harris, Anastasia L. Elias, "Peroxidase-Like Behavior of Ni thin films deposited by Glancing Angle Deposition for Enzyme-Free Uric Acid Sensing", *ACS Omega*, 2020, 5, 9123-9130, 10.1021/acsomega.9b04071. A. Tripathi and Dr. Elias conceived the project. A. Tripathi designed and performed all the experiments and wrote the manuscript. Dr. Harris and Dr. Elias supervised the project and contributed to designing the research, analyzing the data, and writing the manuscript.

Chapter 5 of this thesis has been published as Anuja Tripathi, Kenneth D. Harris, Anastasia L. Elias, "High surface area nitrogen-functionalized Ni nanozymes for efficient peroxidase-like catalytic activity", *PLOS ONE,* 2021, 16(10): e0257777. https://doi.org/10.1371/journal.pone.0257777. A. Tripathi, Dr. Harris, and Dr. Elias conceived the project idea. A. Tripathi designed and performed all the experiments and wrote the manuscript. Dr. Harris and Dr. Elias supervised the project and contributed to designing the research, analyzing the data, and writing the manuscript.

This thesis is dedicated to my parents, brother, and family..!

Acknowledgments

This research work would not have been possible without the help and support of many people. I am sincerely thankful to everyone, who has supported and helped me throughout, not only in the scientific field but also on a personal level.

First and foremost, I want to thank my advisors, Prof. Anastasia Elias and Dr. Ken Harris, who have been exceptional advisors, great role models, and always guided me in the right direction with their incredible support and continuous encouragement. I am grateful that you believed in me, cared about my projects, and checked on me on a personal level. I am very fortunate to have you both as my supervisors and could not have imagined having better advisors and mentors for my Ph.D. I am going to miss working with both of you.

I would also like to thank Dr. Abebaw Jemere for believing in me. I am grateful to have worked with you. You make even the most tedious job a lovely learning process.

I sincerely thank all my committee members, especially Prof. Ravin Narain, who provided me access to their research facilities. Thank you, Dr. Janet Elliott, for your valuable suggestions to improve my teaching skills. I am also thankful to all the current and past members of Elias research group and my colleagues at NRC and UofA, for their help and encouragement. A special thanks to Dr. Rajesh Pillai for always helping with my experiments, Dr. Adrian Lopera Valle for helping me during my candidacy, and Dr. Dan Li for being an excellent friend who always helped and listened my ideas. The fabrication and characterization would not have been possible without Scott Munro, Shihong Xu, and Glenn Elaschuk. Thank you for being very patient!

I would like to thank Natural Sciences and Engineering Research Council of Canada for all their financial support, and University of Alberta & National Research Council Canada, for education, professional development, and outreach opportunities during my Ph.D. studies.

Before concluding, most importantly, I would like to thank my family members for their continuous support and encouragement, and my friends, for being there for me and making my Ph.D. journey enjoyable. I owe my immense gratitude to my parents and brother for their boundless love and support. Papa, thank you for always cheering me up and having confidence in me. You are my role model and the most influential character in my life. Last, I would like to thank you, Tamoghna Saha, for the infinite support, unbounded care, love, and for always having my back.

Table of Contents

List of Tables

List of Figures

Chapter 1: Introduction

1.1 Background

Monitoring of biomarkers – substances whose presence is indicative of some phenomenon such as infection or disease – is helpful for the early detection of medical conditions, which increases the chances of successful treatment. Similarly, early-stage detection of food-freshness biomarkers can prevent billions of tons of food waste due to spoilage (1,2). Most techniques for quantifying biomarkers are time-consuming, require skilled labor, and require large sample volumes (3,4). There is a need to develop reliable biosensors that can offer fast response, low limit of detection, that are easy to operate, and have high sensitivity to desired biomarkers.

Point of care testing (POCT) or near-patient testing is defined as an investigation taken at the time of consultation with immediately available results to make decisions about patient care (5). With the advancement in POCT devices development, they can also be used to monitor water and food quality (6,7). POCT requires the test to fall under ASSURED category: **A**ffordable, **S**ensitivity, **S**pecificity, **U**ser-friendly, **R**apid and robust, **E**quipment-free, and **D**eliverable (8). Some of the commonly used POCTs, such as glucometers to detect "glucose", and pregnancy kits to detect "human chorionic gonadotropin", are already commercially available. However, other important biomarkers, for instance, uric acid (which is found in blood and sweat are associated with a variety of diseases) or xanthine (a metabolite associated with fish and meat freshness), do not have such quantitative estimation techniques available or the techniques that exist are rather costly and time-consuming (9).

Biosensors are widely used in POCT. A biosensor is an analytical device that detects biological or chemical responses by producing signals proportional to the analyte concentration. The signals can

be in form of temperature, current, and color change, classified into thermal, electrochemical, and optical biosensors (10). Electrochemical biosensors translate electrochemical reactions into electrical signals such as current. Ideally, the current changes in proportion to the concentration of a desired chemical compound. Electrochemical biosensors are simple, rapid, and provide sensitive detection in a portable arrangement; however, target-specific transduction surface modification is vital to achieve the selectivity of a functional biosensor. Therefore, biorecognition elements such as enzyme, cells, tissue, or biomimetic materials have been used in biosensors. Integration of nanomaterials in electrochemical biosensors can improve sensitivity, limit of detection, response time, and can act as scaffold to immobilize enzymes (13). Enzymes are highly selective catalysts, which means that each enzyme speeds up only one type of reaction. One of the major step in an enzymatic reaction is the substrate binding at the active site of the enzyme, which yields a product to detect the target compound selectively (11). Enzymatic electrochemical biosensors have been demonstrated for the detection of glucose, lactate, uric acid, and other biomarkers (12). Natural enzymes perform great when stored in a well-controlled environment. Poor handling can cause change in the active site, which can modify the structure of the enzyme, resulting in poor stability and shelf life (14,15).

Optical biosensors are based on the change of optical properties that can produce intuitive color change visible to naked eye, making them user-friendly due to their simplified operation (16). Enzymes, or natural catalysts, play a crucial role in catalyzing colorimetric reactions which can be used to visually monitor chemical compounds such as glucose, ascorbic acid, and uric acid (17). However, some of the pitfalls are the low stability of the natural enzyme in extreme environmental conditions, as well as the high cost of synthesis, separation, and purification (14,18). As a result,

numerous ways for replacing natural enzymes have recently emerged, including the creation of nanoparticles that mimic natural enzymes' catalytic properties, also known as nanozymes (19).

Nanostructured materials have a high surface-to-volume ratio, chemical activity, mechanical strength, and electrocatalytic properties (20). Incorporating porous nanostructured materials in both optical and electrochemical biosensors has led to improved their performance (21). The catalytic properties of nanomaterials are greatly influenced by their synthesis techniques, shape, and surface morphology, as well as their surface area, which can be influenced by electrical charge, doping, loading, and external fields (22). In literature, numerous nanomaterials such as Pt nanoparticles, Au nanoparticles, polymers, multiwalled nanotubes, have been used to enhance the surface area of working electrodes for electrochemical biosensing of xanthine (23). Similarly, a wide variety of nanozymes were explored to mimic natural enzyme's catalytic activity to develop a uric acid colorimetric sensor (24). However, these solution-dispersed nanozymes are difficult to recover, which prevents the reuse of nanozymes. The most effective nanoparticle activity can be achieved if the nanoparticles remain in their stable form during the synthesis process while maintaining their surface activity. Loading nanoparticles on other surfaces would reduce the aggregation while still behaving as nanomaterials with high sensitivity, reusability, and non-tedious synthesis process. Furthermore, these loaded nanoparticles on a surface may also offer the freedom to be reused.

One way of engineering surface-anchored materials with a high surface area and high concentration of catalytic active site is the glancing angle deposition (GLAD) technique. GLAD is a physical vapor deposition technique that is based on atomic shadowing and dynamic motion control to engineer nanostructures with high surface area and controlled porosity (25). As a result, I propose developing GLAD based nanostructured thin film working electrode and a reusable

nanozyme for biosensing application. These films were first pioneered by Prof. Michael Brett's research group of the Department of Electrical and Computer Engineering at the University of Alberta (26).

Two particular biomarkers of interest are xanthene and uric acid in this thesis. Xanthine is a food freshness biomarker and its concentration (in µM range) increases with storage time. Measuring xanthine concentration is considered an important means to assess fish meat freshness (27). Xanthine is also a precursor of uric acid, which is generated from purine and found in blood and body fluids. An unusual range (normal range in blood: 155-357 µM (females), 208-428 µM (males)) of uric acid induces disorders such as gout, hypertension, high blood pressure, heart diseases, and kidney diseases (28).

1.2 Objective and Approach

In this thesis, the GLAD-based technique is used to create surface-anchored nanostructured NiO thin films for electrochemical and optical biosensors. In the first part of the work, a GLAD film-based enzymatic electrochemical biosensor was developed to monitor xanthine. The high surface area and porosity of the GLAD films should allow the enzyme immobilization of large quantities that can result in biosensors of low LOD, high selectivity and sensitivity, and fast response time. In the second part of the work, GLAD-based nanozymes were explored with peroxidase-like activity for colorimetric sensing of uric acid. These nanozymes can be removed from the solution after use, washed with solvent, and reused.

Overall, the objective of this dissertation is to develop GLAD nanostructured materials, and:

1. To develop a GLAD based nanostructured electrode for enzymatic electrochemical sensing of xanthine.

2. To mimic the catalytic activity of natural enzymes using GLAD nanozymes for colorimetric sensing of uric acid.

3. To enhance the surface energy of GLAD nanozymes for colorimetric sensors and develop a proof of concept demonstration for colorimetric sensing of uric acid.

1.3 Organization of Thesis

Chapter 2 presents a broad overview of the literature about biosensors, enzymatic electrochemical biosensing for xanthine using nanomaterials, enzyme immobilization techniques, nanozymes for peroxidase mimicking, and colorimetric sensing of uric acid. Further, role of high surface area and porosity in nanomaterials for biosensing is discussed. Glancing angle deposition is also highlighted as a method for creating porous nanostructured surfaces with a high surface area.

Chapter 3 demonstrates GLAD mesoporous NiO electrodes for enzymatic electrochemical sensing of xanthine. Xanthine is a food freshness biomarker, whose concentration increases with food spoilage. Different working conditions such as temperature, potential, and enzyme concentrations were optimized in order to develop a reliable, selective, and efficient electrochemical biosensor. The fabricated biosensor was used to detect xanthine in fish samples over a week.

Chapter 4 presents the fabrication of Ni film by GLAD technique to mimic peroxidase activity for colorimetric sensing of uric acid. Peroxidase mimicking activity for a flat film and GLAD film was compared using the Michaelis-Menten theory. Furthermore, interference from glucose and urea was studied to explore the potential for use in the clinical diagnosis of UA biomarker.

Chapter 5 explores methods to enhance the catalytic performance of GLAD Ni thin films using nitrogen-functionalization. Ammonia plasma was used to improve the peroxidase-mimicking of GLAD films for colorimetric detection of uric acid. The application of N-functionalized GLAD

films in a gravity-driven, continuous catalytic reaction device for potential application in flow-driven point-of-care devices was also demonstrated.

Chapter 6 provides a summary of the contributions, impacts, and conclusions made in this thesis. The future direction and suggestions of the GLAD films for nanozymes, catalysts, and biosensors are also briefly discussed.

References

1. Ishangulyyev R, Kim S, Lee S. Understanding Food Loss and Waste—Why Are We Losing and Wasting Food? Foods [Internet]. 2019 Jul 29;8(8):297. Available from: https://www.mdpi.com/2304-8158/8/8/297
2. Gibbons A. Disgusted by spoiled food? You may be protecting yourself from disease. Science (80-) [Internet]. 2021 Feb 15; Available from: https://www.sciencemag.org/news/2021/02/disgusted-spoiled-food-you-may-be-protecting-yourself-disease
3. Mustafa F, Andreescu S. Chemical and Biological Sensors for Food-Quality Monitoring and Smart Packaging. Foods [Internet]. 2018 Oct 16;7(10):168. Available from: https://www.mdpi.com/2304-8158/7/10/168
4. Falohun T, McShane MJ. An Optical Urate Biosensor Based on Urate Oxidase and Long-Lifetime Metalloporphyrins. Sensors [Internet]. 2020 Feb 11;20(4):959. Available from: https://www.mdpi.com/1424-8220/20/4/959
5. Vashist S. Point-of-Care Diagnostics: Recent Advances and Trends. Biosensors [Internet]. 2017 Dec 18;7(4):62. Available from: http://www.mdpi.com/2079-6374/7/4/62
6. Dodero A, Escher A, Bertucci S, Castellano M, Lova P. Intelligent Packaging for Real-Time Monitoring of Food-Quality: Current and Future Developments. Appl Sci [Internet]. 2021 Apr 15;11(8):3532. Available from: https://www.mdpi.com/2076-3417/11/8/3532
7. Jin B, Li Z, Zhao G, Ji J, Chen J, Yang Y, et al. Upconversion fluorescence-based paper disc for multiplex point-of-care testing in water quality monitoring. Anal Chim Acta [Internet]. 2022 Feb;1192:339388. Available from: https://linkinghub.elsevier.com/retrieve/pii/S0003267021012149
8. Rasmi Y, Li X, Khan J, Ozer T, Choi JR. Emerging point-of-care biosensors for rapid diagnosis of COVID-19: current progress, challenges, and future prospects. Anal Bioanal Chem [Internet]. 2021 Jul 18;413(16):4137–59. Available from: https://link.springer.com/10.1007/s00216-021-03377-6
9. Land KJ, Boeras DI, Chen X-S, Ramsay AR, Peeling RW. REASSURED diagnostics to inform disease control strategies, strengthen health systems and improve patient outcomes.

Nat Microbiol [Internet]. 2019 Jan 13;4(1):46–54. Available from: http://www.nature.com/articles/s41564-018-0295-3

10. Wang X, Li F, Guo Y. Recent Trends in Nanomaterial-Based Biosensors for Point-of-Care Testing. Front Chem [Internet]. 2020 Oct 16;8. Available from: https://www.frontiersin.org/article/10.3389/fchem.2020.586702/full

11. Bucur B, Purcarea C, Andreescu S, Vasilescu A. Addressing the Selectivity of Enzyme Biosensors: Solutions and Perspectives. Sensors [Internet]. 2021 Apr 26;21(9):3038. Available from: https://www.mdpi.com/1424-8220/21/9/3038

12. Navaee A, Salimi A. Enzyme-based electrochemical biosensors. In: Electrochemical Biosensors [Internet]. Elsevier; 2019. p. 167–211. Available from: https://linkinghub.elsevier.com/retrieve/pii/B9780128164914000073

13. Cho I-H, Kim DH, Park S. Electrochemical biosensors: perspective on functional nanomaterials for on-site analysis. Biomater Res [Internet]. 2020 Dec 4;24(1):6. Available from: https://biomaterialsres.biomedcentral.com/articles/10.1186/s40824-019-0181-y

14. Caves MS, Derham BK, Jezek J, Freedman RB. Thermal Inactivation of Uricase (Urate Oxidase): Mechanism and Effects of Additives. Biochemistry [Internet]. 2013 Jan 22;52(3):497–507. Available from: https://pubs.acs.org/doi/10.1021/bi301334w

15. Çete S, Yaşar A, Arslan F. An Amperometric Biosensor for Uric Acid Determination Prepared from Uricase Immobilized in Polypyrrole Film. Artif Cells, Blood Substitutes, Biotechnol [Internet]. 2006 Jan 11;34(3):367–80. Available from: http://www.tandfonline.com/doi/full/10.1080/10731190600684116

16. Zhu D, Liu B, Wei G. Two-Dimensional Material-Based Colorimetric Biosensors: A Review. Biosensors [Internet]. 2021 Jul 31;11(8):259. Available from: https://www.mdpi.com/2079-6374/11/8/259

17. Harpaz D, Eltzov E, Ng TSE, Marks RS, Tok AIY. Enhanced Colorimetric Signal for Accurate Signal Detection in Paper-Based Biosensors. Diagnostics [Internet]. 2020 Jan 7;10(1):28. Available from: https://www.mdpi.com/2075-4418/10/1/28

18. Njagi JI, Kagwanja SM. The Interface in Biosensing: Improving Selectivity and Sensitivity. In 2011. p. 225–47. Available from: https://pubs.acs.org/doi/abs/10.1021/bk-2011-1062.ch011

19. Zhang R, Yan X, Fan K. Nanozymes Inspired by Natural Enzymes. Accounts Mater Res [Internet]. 2021 Jul 23;2(7):534–47. Available from: https://pubs.acs.org/doi/10.1021/accountsmr.1c00074

20. Wu J, Li S, Wei H. Integrated nanozymes: facile preparation and biomedical applications. Chem Commun [Internet]. 2018;54(50):6520–30. Available from: http://xlink.rsc.org/?DOI=C8CC01202D

21. Park H, Kim G, Seo Y, Yoon Y, Min J, Park C, et al. Improving Biosensors by the Use of Different Nanomaterials: Case Study with Microcystins as Target Analytes. Biosensors

[Internet]. 2021 Dec 20;11(12):525. Available from: https://www.mdpi.com/2079-6374/11/12/525

22. Feng L, Zhang L, Zhang S, Chen X, Li P, Gao Y, et al. Plasma-Assisted Controllable Doping of Nitrogen into MoS 2 Nanosheets as Efficient Nanozymes with Enhanced Peroxidase-Like Catalysis Activity. ACS Appl Mater Interfaces [Internet]. 2020 Apr 15;12(15):17547–56. Available from: https://pubs.acs.org/doi/10.1021/acsami.0c01789

23. Dervisevic M, Dervisevic E, Şenel M. Recent progress in nanomaterial-based electrochemical and optical sensors for hypoxanthine and xanthine. A review. Microchim Acta [Internet]. 2019 Dec 6;186(12):749. Available from: http://link.springer.com/10.1007/s00604-019-3842-6

24. Wu, J.; Wang X.; Wang Q.; Lou Z.; Li S.; Zhu Y.; Qin L.; Wei H. Nanomaterials with enzyme-like characteristics (nanozymes): next-generation artificial enzymes (II). Chem Soc Rev. 2019;48(4):1004–76.

25. Sit JC, Vick D, Robbie K, Brett MJ. Thin Film Microstructure Control Using Glancing Angle Deposition by Sputtering. J Mater Res [Internet]. 1999 Apr;14(4):1197–9. Available from: http://link.springer.com/10.1557/JMR.1999.0162

26. Hawkeye MM, Brett MJ. Glancing angle deposition: Fabrication, properties, and applications of micro- and nanostructured thin films. J Vac Sci Technol A Vacuum, Surfaces, Film [Internet]. 2007;25(5):1317. Available from: http://scitation.aip.org/content/avs/journal/jvsta/25/5/10.1116/1.2764082

27. Sen S, Sarkar P. A novel third-generation xanthine biosensor with enzyme modified glassy carbon electrode using electrodeposited MWCNT and nanogold polymer composite film. RSC Adv [Internet]. 2015;5(116):95911–25. Available from: http://xlink.rsc.org/?DOI=C5RA18889J

28. Kushiyama A, Nakatsu Y, Matsunaga Y, Yamamotoya T, Mori K, Ueda K, et al. Role of Uric Acid Metabolism-Related Inflammation in the Pathogenesis of Metabolic Syndrome Components Such as Atherosclerosis and Nonalcoholic Steatohepatitis. Mediators Inflamm [Internet]. 2016;2016:1–15. Available from: https://www.hindawi.com/journals/mi/2016/8603164/

Chapter 2: Background and Review of the Literature

A biomarker is an objective measure of a physiological characteristic that can be used to characterize the freshness of food or an individual's health. The irregular concentration of associated biomarkers can indicate food spoilage or medical condition. Monitoring such substances in real-time can detect early stages of food degradation and sickness, allowing medical interventions focused on preventing or treating diseases (29,30). Two biomarkers of interest for food freshness monitoring and health monitoring are xanthine and uric acid, respectively.

The focus of this chapter is to give a broad review of biosensors for monitoring two closely-related metabolites: xanthine and uric acid, and about the glancing angle deposition technique (GLAD) used to fabricate nanostructured materials with high surface area.

Background on Xanthine

Xanthine is a biomarker for food freshness, and it is derived from purines, which contain adenine and guanine as nucleobases. Adenosine triphosphate (ATP), an energy carrier within cells, is formed when adenine base joins with ribose sugar and three phosphate groups (144). After the death of a fish, ATP degrades into hypoxanthine, which further deteriorates the muscle tissue and yields the final metabolite product by producing xanthine (XA) and uric acid (UA) (31,32). Xanthine (3,7-dihydropurine-2,6-dione) is formed from hypoxanthine by xanthine oxidase (XO), which is an enzyme containing two cofactors of FAD (flavin adenine dinucleotide), two atoms of molybdenum, and eight atoms of nonheme iron in its molecule (33). XA concentration increases with storage time and considered as an indicator for food freshness. The concentration of XA in fresh fish ranges ~2.2 nM to 5 μM, which increases with the storage time (34–37). Therefore, by

detecting xanthine, we can determine the freshness and shelf life of fish and meats. Moreover, xanthine oxidase (XO) also catalyzes XA to uric acid by the following reaction:

$$\text{Xanthine} + H_2O + O_2 \xrightarrow{XO} \text{Uric acid} + H_2O_2 \qquad (1)$$

Background on uric acid

Uric acid is the end product of purine metabolism (28). Purine is used by the cells to build DNA and RNA. According to most health and nutrition examinations, purine-rich food such as fish and meat raises the level of uric acid in the blood (38). When the body is unable to filter this uric acid adequately from blood, hyperuricemia (UA level > 155-357 μM in men and >208-428 μM in women) can occur, which can contribute to gout, diabetes, cerebral ischemia, nonalcoholic fatty liver disease, and cardiovascular diseases (39,40). Thus, timely monitoring of UA in serum plays an important role in early diagnosis and cure.

Conventional measurement methods for biomarkers

Monitoring and regulating chemical compounds such as xanthine and uric acid are becoming increasingly important in the food industry and clinical diagnosis. The conventional technique to measure these biomarkers includes standard analytical methods such as photometric, spectrometry, fluorometry, isoelectric focusing, capillary electrophoresis, chemiluminescence, and electromagnetic sensing techniques (41–47). All these analytical methods are well established and exhibit a wide range of advantages such as reliability and accuracy. However, these methods still have limitations, such as being labor-intensive, costly, difficult to perform outside a laboratory setting, and require trained technicians to operate these instruments. On the other hand, biosensors have been substantially developed for monitoring such chemical compounds with efficient

performance (48). The unique physical and chemical properties of nanomaterials have been exploited to enhance the analytical performance of biosensors. Hence, the use of nanomaterials for biosensing applications has advanced rapidly during the last decade. Boron nitride (BN), graphite carbon nitride (g-C_3N_4), transition metal dichalcogenides (TMDs, e.g. MoS_2 and WS_2), and transition metal oxides (such as MoO_3, WO_3, and MnO_2) have all been widely explored for biosensor development (49–53).

2.1 Biosensor

A biosensor is an analytical device that detects biological or chemical responses by producing signals proportional to the analyte concentration. Biosensors typically use a biorecognition element to sense biomarkers selectively. A biorecognition element, such as enzymes, antibodies, cell receptors, or biomimetic components interacts with, binds to, or otherwise identifies the biomarker (54). The critical role of these elements are to interact specifically with the target biomarkers, and produce a measurable signal in form of current, temperature, or color, classifying them as electrochemical, thermal, or colorimetric biosensors, respectively (55). The important part of a biosensor fabrication is the immobilization of biorecognition elements, which highly depend on factors such as their physical conditions (pH, temperature and contaminants) and stability.

2.1.1 Components

A typical biosensor consists of, (a) The **biorecognition element** - enzymes, nanozymes, cells, aptamers, antibodies, DNA, or RNA – which recognizes the target biomarker, and (b) The **transducer** of a biosensor converts biochemical reactions into a measurable signal (optical or electrical) that is proportional to the quantity of the biological target. The other important part of a biosensor is (c) **data processing,** which quantifies the transduced signals and processes them

with the display unit of the biosensor. The display can be numeric, graphic, color, depending on the user's requirements.

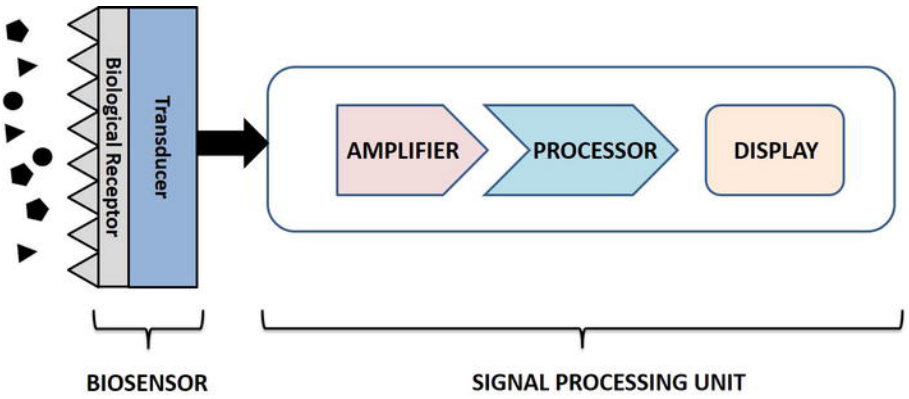

Figure 2.1: Biosensor components (56).

2.1.2 Analytical performance of the biosensors

Biosensors are characterized based on the following parameters:

(1) **Sensitivity (S)** is defined as the ratio of change in output signal (y) to change in concentration of analyte (x).

$$\text{Sensitivity (S)} = \frac{y}{x} \qquad (2)$$

An ideal biosensor should generate a signal in response to the concentration of the target analyte. Low sensitivity signifies the biosensor is less responsive to change in the analyte concentration. High sensitivity can reduce the sampling time and speed the detection of chemical compounds.

(2) **Linear range** is the concentrations where the signals are directly proportional to the concentration of the analyte in the sample (Fig 2.2) or, the range over which the sensitivity of the sensor is defined, mathematically represented as $y=S\ x$, where x is the concentration of the

analyte, *y* is the output signal, and *S* is the sensitivity of the biosensor. For xanthine sensors, a linear range of ~5 µM to 30 µM is desirable (34–37). For uric acid sensors, the desired linear range depends on the medium: in blood a range of 1 to 100 mM is needed, whereas in sweat a range of 18 to 35 µM is needed (57,58).

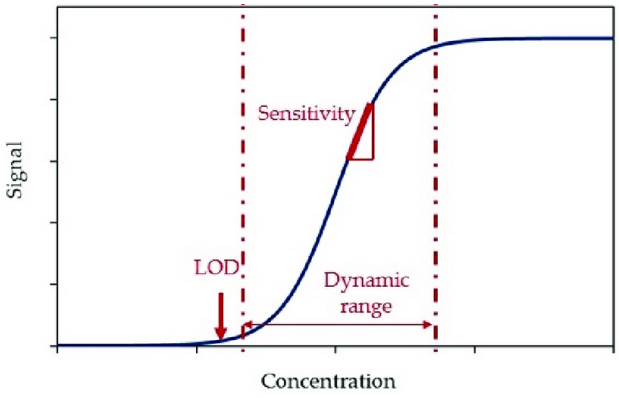

Figure 2.2: Sensitivity, limit of detection (LOD), and dynamic range of a calibration curve (59).

Dynamic range: In dynamic range, the response changes as the analyte concentration vary, but the relationship can be non-linear. Expanding the dynamic range of the biosensor to allow the broader sensing to monitor a target analyte is advantageous, but must not compromise on sensitivity and selectivity (60).

(3) **Response time** is the time required for the sensor to achieve 90% of its final response due to a change in analyte concentration. Sensors do not change the output state immediately when an input parameter change occurs. Rather, it will change to the new state over a period of time, called the response time. For the development of a reliable biosensor, a short response time is required. Typical values that have been achieved in xanthine biosensors are around 15 to 30 seconds (61,62).

(4) **Reproducibility** is the ability of the biosensor to generate identical responses for a duplicated experiment, and is defined by the precision (similar output when the sample is measured more than once) and accuracy (capability of a sensor to generate a mean value closer to the actual value when

sample is measured every time). The implication of the results on a biosensor's response is more reliable and robust when the signals are repeatable. Signals measured at a fixed concentration of desired compound, for instance, should have a small standard deviation. To achieve high repeatability, many factors can be optimized such as compatibility of electrodes with electrolyte, and optimized position of electrodes, and accurate spotting of the sample.

(5) **Limit of detection (LOD)** is the lowest concentration at which an analyte can be detected, but not necessarily quantifiable, under the specified experimental conditions (63). LOD is calculated based on the standard deviation of the lowest concentration (σ) of an analyte in the sample and the slope of the calibration curve (S). Calibration curves are used to predict unknown concentrations of analyte based on the instrument's response to known standards. The standard deviation of the response can be determined based on the y-intercept of the regression line.

$$\text{LOD} = 3\,\frac{\sigma}{S} \qquad (3)$$

A biosensor that detects xanthine concentration with a low LOD (1-5 μM) would be able to detect the earliest sign of food spoilage (27).

(6) **Selectivity** is one of the most important features of a biosensor, which means that in the presence of various admixtures and pollutants, the sensor should only respond to the target compound. Various compounds such as tissues, proteins, fats, and other chemicals may be present in food samples such as fish meat. An ideal xanthine-based biosensor should only respond to xanthine and nothing else. For measurements of xanthine in fish samples, commonly used enzyme is xanthine oxidase.

2.1.3 Standard addition method

The standard addition method is commonly used to quantify the concentration of an analyte in a complex matrix sample such as biological fluids. The matrix effect occurs when the interfering compounds contributes to the analytical signal, making it difficult to compare the analytical signal between sample and standard using the typical calibration method. Below is an example of the standard addition plot.

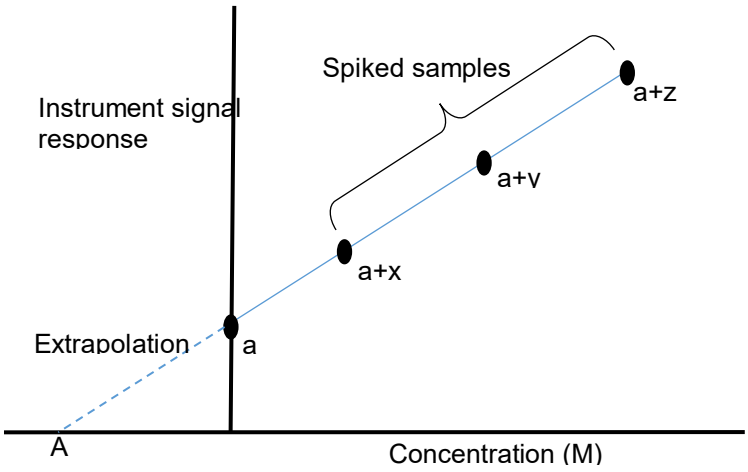

Figure 2.1.3: Standard addition method plot

Here, the response for a sample with matrix having unknown target compound is 'a.' The measurements after spiking increased amounts of known concentrations of target compound are a+x, a+y, and a+z. The extrapolated x intercept value: A, which is best approximated by dividing the y-intercept of the best fit line by the slope of the best fit line, can be used to determine the concentration of the target compound in the unknown (143).

2.2. Electrochemical sensor overview

Electrochemical biosensors measure the change in the current of a working electrode due to electrochemical oxidation or reduction of a biochemical reaction, and ideally, the current relates directly to the concentration of the chemical compound. A few advantages of electrochemical biosensors are fast response, high sensitivity, and use of low analyte volume. In addition to their

robustness and miniaturization, electrochemical biosensors offer advantages of low detection limit and wide linear response range. The three-electrode electrochemical cell consists of a working electrode, counter electrode, and reference electrode as shown in Fig 2.3. Current flows between the working and counter electrodes and the reference electrode is used to accurately measure the applied potential relative to a stable reference reaction. An electrochemical instrument that measures the voltage and current between these electrodes is known as potentiostat (64).

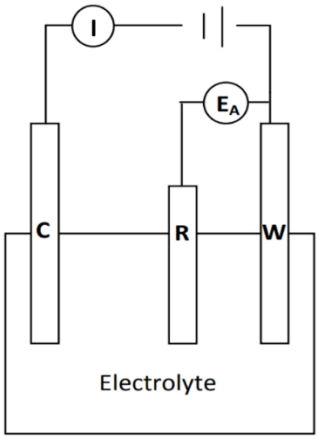

Figure 2.3: Schematic of the three-electrode cell electrochemical set-up configuration where C, R, and W are the counter, working, and reference electrodes, respectively. E_A is the applied voltage.

2.2.1 Working Electrode (WE)

The working electrode is where the potential is regulated by a potentiostat vs. the reference electrode and the current is measured. One of the most essential features of a working electrode is that it should exhibit favorable redox behavior with the analyte and reproducible electron transfer without undergoing electrode fouling. Working electrodes are often modified with nanomaterials in order to improve the surface area of the electrode, enhance the catalytic activity, and reduce or promote surface adsorption (65,66). Some typical materials for working electrodes are gold

nanoparticles/glassy carbon electrodes, carbon nanotubes/carbon paste electrode, and graphene oxide/platinum (67–69). In this thesis, nickel oxide thin film deposited on indium tin oxide substrate was used as a working electrode.

2.2.2 Reference Electrode (RE)

The reference electrode in an electrochemical cell needs to have an equilibrium potential that is well-defined and stable. It is a benchmark against which other electrodes' potentials in the cell can be measured. Thus, the applied potential is typically reported as "vs" a specified reference. The saturated calomel electrode (SCE) (70,71), standard hydrogen electrode (SHE) (72,73), and AgCl/Ag electrode (74,75) are all commonly used reference electrodes. In this thesis, Ag/AgCl reference electrode was selected because of its excellent stability, reversibility, and polarizability.

2.2.3 Counter Electrode (CE)

The counter electrode's function is to complete the electrical circuit. Counter electrode should allow fast electron transfer and not limit the rate of reaction occurring at the working electrode. Therefore, they should be manufactured from inert material such as carbon or platinum (76,77). The counter electrode should be a good electrical conductor, which is well known, if the counter electrode is not a good conductor, it means that a poor amount of current will pass at the counter electrode. In this regard, the surface area of the counter electrode is an important parameter. A large surface area is required to support the current generated by the working electrode to ensure no current limitations arise. CE should not contaminate the solution. In practice, there will likely be some electrochemical reaction at CE. The reaction products of platinum and carbon are usually gases (oxygen or hydrogen) that can be removed by bubbling air. In this thesis, platinum was used as a counter electrode.

2.3. Xanthine electrochemical biosensors

The advantages of electrochemical sensors such as fast response time, sensitivity, requirement of small analyte volume, have resulted in their wide usage for determining various biomarkers in recent years, including lactate, glucose, and xanthine (70,78,79). To develop a biosensor for such biomarkers, the enzymes lactate oxidase, glucose oxidase, and xanthine oxidase have been widely used. Enzymes (specific to its target substrate) are the natural biological catalyst which accelerates the rate of a chemical reaction within all living organisms. Electrodes immobilized with enzymes can interact with their target substrates in the presence of interfering compounds, producing a measurable signal which is proportional to the concentration of its target substrate. The first enzyme electrochemical sensor was developed to monitor glucose using glucose oxidase (GOx) (80). In the presence of glucose, GOx reduces oxygen to hydrogen peroxide and measures the decrease in oxygen concentration or the increase in hydrogen peroxide concentration as a result of the reaction. One of the limitation here was peroxide requirement for the high potential to generate current. Alternatively, an electron-transfer mediator which has fast electron kinetics, can carry electrons between enzyme and electrode surface at low potential. In order to shuttle electrons between the enzyme and electrode surface, the mediator must be able to cycle rapidly between its oxidized and reduced states (81). When enzyme come into contact with its target substrate, FAD (a cofactor of enzyme) is reduced to $FADH_2$. In an electrochemical biosensor, a $mediator_{ox}$ (such as $Ni(OH)_2$) regenerates FAD while reducing itself ($mediator_{red}$) at the same time. The $mediator_{red}$ then regenerates at the electrode surface, resulting in a measurable electric signal (79). The mediator can be readily regenerated at lower applied voltages, thus eliminating interference from background species (82). The introduction of an electron transfer mediator is therefore advantageous to achieve the highly desirable low limit of detection and fast electron transfer. In this thesis $Ni(OH)_2$/NiOOH was used as a mediator.

2.4. Enzyme immobilization techniques

Enzymatic biosensor consists of an enzyme which recognizes the target compound and selectively reacts with it, generating a chemical signal. Therefore, the enzymes should maintain their structural, functional, and biological properties when used in biosensors. Poorly immobilized biorecognition elements may be inactivated or leached away after several hours of use (83). For example, electrodes without or with weakly immobilized enzymes may still be able to detect the molecule of interest, but the current may be caused by interfering species or background signal. Enzymes are comprised of amino acids, which have different functional groups to bind the support and target compound through various types of interactions. A good enzyme-immobilized electrode can show a signal selectively for its corresponding substrate in the presence of interfering species. Therefore, selecting an appropriate immobilization approach on the surface of the transducer is necessary. The choice of an appropriate technique depends on the element of biorecognition, the transducer, the physiochemical environment and the properties of the analyte.

The supports or matrix on the electrodes are important in maintaining the structure of enzymes by forming covalent or hydrogen bonds with enzymes. In spite of the fact that there is no universal support suitable for all enzymes and applications, certain characteristics of the support material to be used should be considered, including high affinity for protein, availability of reactive functional groups, mechanical stability, non-toxicity, and biodegradability (84). Common supports include starch, collagen, ion exchange resins, active charcoal, silica, clay, aluminum oxide, titanium, nanoparticles, carbon nanotubes, agarose, or porous nanoparticles, as well as certain polymers (85–91). The key property of a support or matrix is the high surface area and a large number of pores that contribute to higher enzyme loading per unit mass. For instance, the enzymatic electrode was developed for sensing by immobilizing alcohol oxidase on a glassy carbon electrode/carbon

nanotube matrix. Alcohol converts to formaldehyde in presence of alcohol oxidase, while simultaneously converting reducing oxygen to hydrogen peroxide. The sensitivity and LOD were 282.82 $\mu A \cdot cm^{-2} \cdot mM^{-1}$ and 0.98 µM, respectively (92). Different enzyme immobilization techniques in biosensors are: (a) physical adsorption (93–95), (b) entrapment (96,97), (c) encapsulation (98,99), (d) covalent attachment (100–102), and (e) crosslinking (103,104).

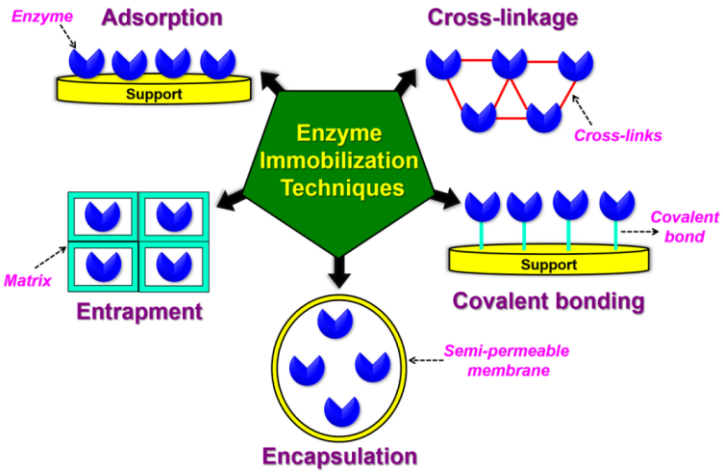

Figure 2.4: Enzyme immobilization techniques (55).

2.4.1. Physical adsorption

The physical adsorption technique is frequently used in enzymatic biosensors when a biorecognition element is immobilized on the outer surface of a solid using weak attractive forces such as Van der Waals force, electrostatic force, ionic bonding, or hydrogen bonding. This technique is commonly occurred by immersing the electrode surface into the enzyme solution for a fixed period. One example of a physical adsorption technique is by using reduced gold nanoparticles with a negatively charged ligand such as citrate. The resulting citrate layer imparts a negative charge which gets combined with positively charge amino acid residues, allowing enzymes in solution to be electrostatically adsorbed on the surface (105). The other popular metal

ions are Cu^{2+}, Co^{2+}, and Ni^{2+} (106). Physical adsorption method has several advantages, including its simple and cost-effective nature, non-destructiveness to bioreceptor activity, and requires no modification of biological materials. The disadvantage of this method is that it is sensitive to changes in pH, temperature, and ionic strength, has weak interactions, and low operational and storage stability.

2.4.2 Entrapment

In this method, enzymes are physically restricted within a confined space using covalent or non-covalent bonds that allow the substrate and products to pass through but retains the enzyme. Entrapment immobilization occurs via mixing the enzyme with a monomer solution, which is then polymerized by a chemical reaction. Here, enzymes are entrapped inside the 3D network of organic or inorganic materials. Polydimethylsiloxane, N-vinylformamide, gelatin, alginate, cellulose, acetate phthalate, modified polypropylene, and polyacrylamide are used as organic materials, whereas activated carbon and porous ceramic materials are used as inorganic materials (83,107–109). The immobilization of xanthine oxidase in a silica sol-gel thin film on CNT modified glassy carbon electrode has been achieved by this method, preserving the enzyme and allowing xanthine to pass through at the same time (72). The disadvantage of this method is poor contact of enzyme and substrate.

2.4.3 Encapsulation

The encapsulation technique involves enclosing enzymes with a semi-permeable membrane such as nitrocellulose or nylon (112,113). Encapsulation occurs in two ways: 1. phase separation of enzyme microdroplets within water-immiscible liquid phases, or 2. polymerization of a monomer at the interface between two immiscible substances (interfacial polymerization), which results in

the obscuration of the enzyme within the membrane. For instance, a large quantity of enzyme was stored in a three-dimensional HRP-encapsulated protein nanoparticle to develop an H_2O_2 sensor using TMB substrate (114). One of the main drawbacks of this method is that only small substrate molecules are able to cross the membrane.

2.4.4 Covalent binding

In this method, covalent bonds are formed between chemical groups in enzymes and chemical groups on the support. Chemical groups in the support that can form a covalent bond with enzymes are amino group, hydroxyl group, thiol group, and phenol rings (115). The mechanism of this technique is divided into two stages. a) the activation of the substrate using linker molecules such as thiol, b) the other end of the linker is connected with the enzyme. A covalent bond has several advantages, including a strong bond between the biorecognition element (enzyme) and support, and high resistance to environmental changes. One example of the covalent immobilization of glucose oxidase was demonstrated with a sol-gel carbon composite electrode. The composite consists of graphite powder, ferrocene, and an amino-methyl compound (1-ethyl-3-(3-dimethylaminopropyl)). The sol-gel composite electrode was soaked in phosphate buffer solution containing linker agents for 1.5 hours, then dipped in glucose oxidase solution for another 1.5 hours. The ferrocene acts as mediator and the amino groups on the sol-gel electrode is used to makes the covalent bond with the carboxylic acid groups on the enzyme. The enzymatic electrode was used to monitor glucose which showed the linearity of biosensor in the range of 0.1-27 mM and LOD 26 μM (116). One of the main drawbacks of this method is the use of harsh chemicals can lead to the loss of the functional conformation of enzyme.

2.4.5 Cross-linking

Cross-linking involves joining enzyme molecules to each other to form a large three-dimensional aggregates. A commonly used cross-linker is glutaraldehyde which contains two or more reactive ends to chemically attach to specific functional groups (such as amines) on proteins or other molecules (117). An enzymatic biosensor was prepared using cross linking glucose oxidase enzyme to glassy carbon electrode (GCE). GCE was first modified with CNT before coating the electrode surface with glucose oxidase. The developed enzyme electrode was then dried in air and kept in chamber saturated with the vapors of glutaraldehyde solution to avoid the enzyme leakage (118). The advantages of using this technique are the reduced enzyme leakage and good chemical binding. However, the disadvantage is that crosslinking reagents may denature or structurally modify the enzyme leading to the loss of catalytic properties.

2.5 Nanomaterials used in xanthine electrochemical biosensors

Non enzymatic electrochemical sensors often lack the selectivity needed for the sensing biomarkers with low concentrations. Hence, enzyme modified system is used which exhibits the advanced and successful biosensors because of the high catalytic activity and selective nature of enzymes. However, enzymatic electrochemical sensors may still have limited stability, low sensitivity, and high LOD. To overcome this challenge, nanomaterials have been incorporated onto the electrode surface. Nanomaterials are 1-100 nm in size and are extremely beneficial due to large surface-to-volume ratio which are responsible for significant increment in sensitivity and act as scaffold for effective enzyme immobilization (119). This makes nanomaterials a good choice to incorporate in enzymatic electrochemical sensors. Over the last few years, electrochemical biosensor platforms with the integration of nanostructured materials have tremendously been employed by captivating the benefit of easy-to-handle, cost effective, high sensitivity, and rapid

response. Nanomaterials play a very crucial role in the development of enzymatic electrochemical sensors, improving the sensor stability, sensitivity, and act as an efficient support material for effective enzyme loading. Nanomaterials modified electrodes also provide a large surface area with several active sites offering improved electrocatalytic activity. A variety of nanoparticles, such as graphene, metal oxides, and metal oxide frameworks, are widely incorporated into electrode modifications for XA biosensors to enhance sensitivity, to lower LOD, and to widen the linear range, as shown in Table 2.1. Although there are many different kinds of nanomaterials, they should be carefully chosen based on the effects desired.

Table 2.1: A list of xanthine oxidase (XO) electrochemical XA biosensors to monitor food freshness with different nanomaterials used in the fabrication process and their analytical performance

Electrode	Method	Nano materials	Detection limit (nM)	Linear range (μM)	Sensitivity	Ref.
XO/graphite rod	Amp	Not applicable	100	0.1-0.6	Not reported	(120)
XO/iron oxide nanoparticles (Fe_3O_4 NPs) /gold (Au)	Amp	Fe_3O_4 NPs	2500	400-2400	4.94 μA nM^{-1}	(37)

XO/zinc oxide nanoparticles-polypyrrole (ZnO-NPs-PPy/Platinum (Pt)	Amp	ZnO NPs	800	0.8-40	NR	(121)
XO/Cobalt oxide (Co_3O_4)/multiwalled carbonnanotube (MWCNT)/chitosan (CS)	Amp	Co_3O_4/MWCNTs	200	0.2-16	NR	(122)
XO/MWCNT/gold-polyphenylenediamine (Au-PPD)/glassy carbon electrode	DPV	MWCNT/Au-PPD/GCE	50	0.05-120	NR	(27)
XO/Titanium dioxide (TiO_2)/MWCNT	EIS	TiO_2/MWCNT	500	0.5-500	NR	(61)
Reduced graphene oxide (RGO)/ZnO/Zn foil	DPV	RGO/ZnO	1670	5-400	2.1 $\mu A\ \mu M^{-1}\ cm^{-2}$	(123)

Carbon nanomaterials such as graphene, carbon nanotubes, nanofibers, nanoribbons, nanodiamond, and nanospheres have received the most attention in recent years for sensing applications due to their excellent electroconductivity, mechanical strength, and chemical stability. However, carbon-based nanomaterials lack the functional groups required for the immobilization

of bioreceptors of the biosensors. Therefore, the formation of surface carboxyl, hydroxyl, amine, and thiol groups on its surface allows their binding to enzymes. The most commonly used carbon nanomaterials in biosensors are graphene (124–126) and carbon nanotubes (27,127,128).

Metal oxide nanoparticles (MONPs) are also of great interest to develop XA electrochemical biosensors as they not only exhibit high surface area, good biocompatibility, strong adsorption ability, and chemical stability, but also display rapid electron transfer kinetics. These nanoparticles are known for their unique ability to enhance electron transfer kinetics between electrode surface and enzymes, as well as for their intrinsic catalytic properties. For instance, an enzymatic XA biosensor based on ZnO was reported by Devi et al. (121). XO was immobilized by physisorption over a composite film made from ZnO nanoparticles/chitosan/carbon nanotubes/polyaniline, electrodeposited over a Pt electrode, resulting in a compatible environment for XO. The developed enzyme-based biosensor showed a linear range of 0.8 to 40 μM showing a good performance in detection of XA in fish meat. However, MONPs undergo high volume contraction and expansion during charging and discharging processes, which can destroy the conductive film of which they are a part.

Metal organic frameworks (MOFs) consist of metal-containing core units joined together by organic ligands (linkers) to form highly structured crystalline frameworks with persistent porosity. MOF structures have been widely used for many applications due to their high surface area, intrinsic catalytic activity, excellent thermal and chemical stability, optical and electrical properties, and adjustable chemical properties. These long networks can be built with different metal ions or clusters and a wide range of linkers, thereby allowing a limitless number of MOF combinations, and the materials have been reviewed in detail (129–132). Recently, Wang et al. reported Cu-MOF nanofibers incorporating XO for the monitoring of fish freshness. Cu-MOF

nanofibers served as a biocompatible matrix to immobilize XO which was suspended in sodium alginate and deposited on glassy carbon electrodes. The reported biosensor detects XA via differential pulse voltammetry in the range of 0.01-10 μM and was successfully implemented for its detection in fish.

The main challenges in XA sensors are slow electron transfer, small linear range, high response time and LOD, and low selectivity. The key factor to address these challenges is kinetics of the electron transfer between enzyme and electrode surface. The electron transfer rate between enzyme and electrode surface can be increased using mediator such as NiO nanoparticles (79). NiO nanoparticles possess good electrocatalytic properties and are available at low cost (133). High surface energy, a large fraction of surface atoms, and the order in which nanoparticles are arranged with the enzyme determine the amount of electron flow which enhances electron flow and sensing (134). Electrons can be monitored by the change in current, potential, or impedence; using chronoamperometry, cyclic voltammetry (CV), differential pulse voltammetry (DPV), chronoamperometry (CA) and electrochemical impedance spectroscopy (EIS).

Cyclic voltammetry: This is an electrochemical technique for measuring the current response of a redox active solution to a linearly cycled potential sweep between two set values. The voltage between the working and reference electrodes is linearly scanned by a potentiostat until it hits a pre-set limit, at which time it is swept back in the opposite way as shown in Fig 2.5. Depending on the direction of the ramping potential, the chemical either loses an electron (oxidation) or acquires an electron (reduction) during a scan. CV's main limitation is its incapability to detect low concentrations such as nM range (135).

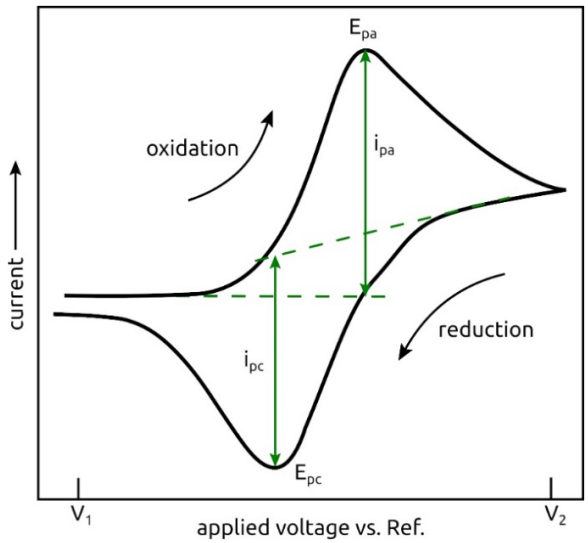

Figure 2.5: A generic cyclic voltammogram of a redox system. V_1: starting voltage, V_2: ending voltage; E_{pa}: anodic peak potential. E_{pc}: cathodic potential, i_{pa}: anodic current, i_{pc}: cathodic current (136).

One example showing CV technique for an enzymatic electrochemical sensor was demonstrated using XO/ZnO-Nps/polyppyrole /Pt electrode. The increase in the oxidation current with increase in xanthine (0.8-200 µM) resulted due to the H_2O_2 produced during enzymatic reaction with a detection limit of 0.8 µM (121).

Differential pulse voltammetry: In differential pulse voltammetry (DPV), small amplitude, short pulses are superimposed on a linear ramp. Current is measured before the application of the pulse (red arrows, Fig 2.6) and at the end of each pulse, and the difference between the currents is calculated which signifies the concentration compound of interest present in the solution. This procedure effectively reduces the background current, and thus this procedure results in a Faradaic current free of most capacitive current.

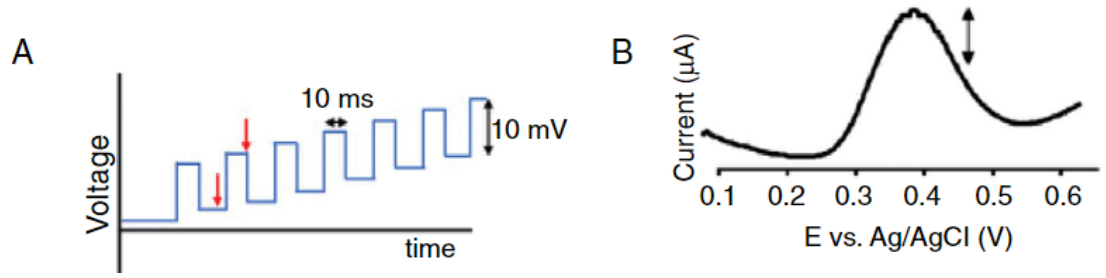

Figure 2.6: (A) Schematic waveform for DPV. Red arrow shows where the differential current is measured, at the end of each step. (B) DPV voltammogram, adapted with permission from ref (137).

A DPV-based enzymatic electrochemical sensor has been demonstrated using multiwall single walled carbon nanotubes doped with nanogold on a glassy carbon electrode to detect xanthine. Applied potential range was 0.3 to 1.0 V and the oxidative peak varies with the concentration of XA. Calibration curves showed linear range between 0.01 μM and 300 μM and a detection limit of 12 nM (27).

Chronoamperometry: In this technique, a potential step is applied to the electrode and the resulting current vs. time is observed. The current going through the cell is measured as a function of time after a pulse potential is supplied to a working electrode. Rises or reductions in the diffuse layers of the analyte at the surface of the working electrode cause changes in the current. This varies with the analyte concentration. Chronoamperometry gives high signal to noise ratio, resulting in an accurate measurement. In Fig 2.7, An enzymatic electrochemical sensor based on this technique was developed using chitosan-polyppyrole/gold-xanthine oxidase(Chi-PPy/Au-XO) which exhibited the linear range from 1 μM to 200 μM, low detection limit of 0.25 μM , and response time of 8 seconds.

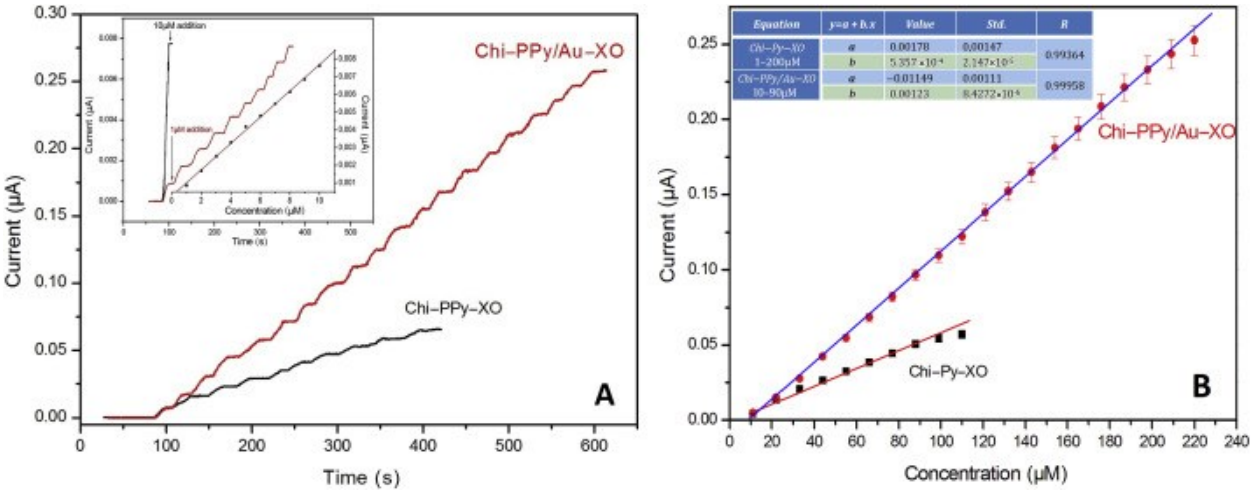

Figure 2.7: Chitosan-polyppyrole/gold-xanthine oxidase(Chi-PPy/Au-XO) enzymatic electrochemical sensor for xanthine detection (A) Chronoamperometric curve (B) The calibration plot for xanthine measurement (34).

Electrochemical impedance spectroscopy (EIS): Enzyme–electrode interfaces possess different resistive, capacitive, and inductive elements depending upon their interaction, which can be detected using EIS. It is a highly sensitive method for establishing the electrical response of chemical systems without causing any damage to them. An EIS system measures the time response of chemical systems using alternating current (AC) voltages of low amplitudes over a range of frequencies and records the impedance. The resultant data is then modeled and fit to an equivalent circuit to get charge transfer resistance which can be used to detect coverage of biorecognition element (in this case- enzyme) layer on electrode surface assemblies through charge transfer resistance.

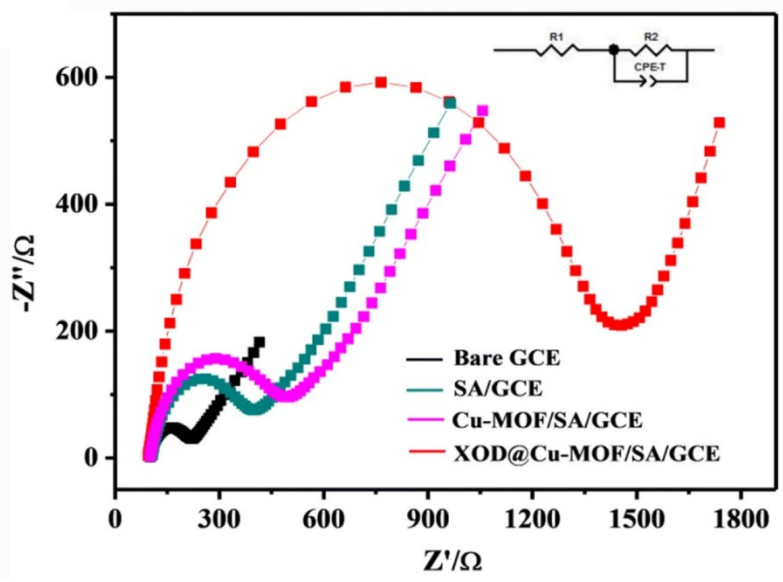

Figure 2.8: EIS of bare glassy carbon electrode (black), sodium alginate/glassy carbon electrode (olive line), Cu-metal organic framework /sodium alginate/glassy carbon electrode (magenta), and xanthine oxidase/ Cu-metal organic framework /sodium alginate/glassy carbon electrode in 5mM $[Fe(CN)_6]^{3-/4-}$, adapted with permission from ref (138).

Fig 2.8 shows an EIS technique used to study electron transfer properties and impedance changes of enzymatic (XO) electrochemical sensor. The diameter of the semicircle at higher frequencies corresponds to the charge transfer resistance. Increase in charge transfer resistance value indicates the presence of shielding layer which is successful immobilization of enzyme.

2.6 Uric acid colorimetric biosensors

The detection of uric acid is currently done by many standard analytical methods such as photometric (139), spectrophotometry, fluorometry, isoelectric focusing, electrokinetic processes, chromatography (47), weight based detections, capillary electrophoresis (CE) (140), chemiluminescence (CL), and electromagnetic sensing (141) techniques. All these analytical methods are well established and exhibit a large range of advantages such as reliability and

accuracy. Among all these techniques, colorimetric detection offers an inexpensive, easy-to-use technique, low cost, good performance, and visual detection (142). This can exhibit huge application prospects in practical applications and resource-limited regions. It, therefore, is more suitable for field analysis and point-of-care testing (POCT).

Colorimetric methods use color reagents to report the presence of an analyte or even measure its concentration. An example of a color reagent is 3,3`,5,5` tetramethylbenzidine (TMB), a noncarcinogenic chromogenic substrate that produces a blue end product after oxidation reaction. During the last few decades, the redox reaction of TMB for colorimetric detection has been used due to its inexpensive, safe, portable, easy to fabricate, user friendly, and biocompatible nature. The natural TMB is a colorless solution, which is oxidized by peroxide (H_2O_2) in presence of a catalyst (such as horseradish peroxidase) and turns into a blue colored solution (17). This blue colored solution becomes colorless when it encounters a reducing agent (a compound that loses an electron to another chemical species in chemical redox reaction) such as uric acid (UA). Higher the concentration of reducing agent leads to more colorless solution. This color change mechanism can be used to quantify reducing agents such as dopamine, glutathione, hydroquinone, uric acid etc.

A method used for the quantification of the color of a solution is to measure optical absorbance at a given wavelength by UV-VIS spectrophotometry. The absorbance is associated with concentration as given in equation 4.

$$A = \varepsilon L c = \log_{10}\left(\frac{I_0}{I}\right) = \log_{10}\left(\frac{1}{T}\right) = -\log_{10}(T) \qquad (4)$$

As mentioned previously, oxidized TMB is critical to read the color change on adding a reducing agent (UA). The color change can be observed visually and its quantitative information in terms

of absorbance can be read by UV-Vis spectrometer. However, blue colored oxidized TMB solution can not be attained without catalyzing the reaction between TMB and H_2O_2.

Relevant examples of conventional catalysts for the oxidation of TMB include enzyme such as horse radish peroxidase (HRP). It acts as catalyst for the reduction of peroxide. Upon reduction, the reduced compounds can then oxidize TMB, causing a color change to blue from colorless solution as shown in Fig 2.9.

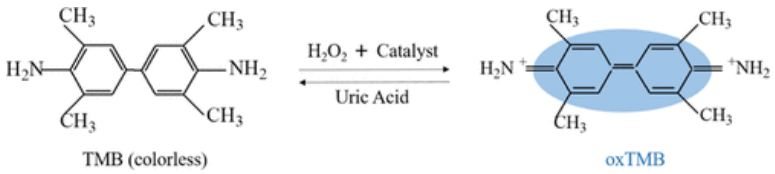

Figure 2.9: Reaction scheme for uric acid detection by the colorimetric redox reaction of TMB and H_2O_2 (143).

The obtained ox-TMB solution shows a change in absorbance with the concentration of uric acid. Chen and co-authors used this mechanism to develop a microfluidic paper-based device for colorimetric sensing of uric acid. In their work, the catalyst was urate oxidase and HRP enzyme. In the presence of oxygen, urate oxidase oxidizes uric acid to allantoin ($C_4H_6N_4O_3$) and H_2O_2. H_2O_2 can oxidizes TMB in presence of HRP. The system shows a response in 30 minutes with a LOD of 0.28 mM (144). However, enzymes as a catalyst have a few limitations for TMB reaction. First, obtainable LOD are too high for already available body fluids (such as sweat or saliva), which are easily accessible unlike blood. UA concentration in these biofluids lies in micromolar and nanomolar range. Second, on exposure to chemical denaturants, inhibitors, or relatively harsh environmental conditions, the enzyme structures unfolds (denatures) leading instability to the structure, which in turn results in a loss of their catalytic activity. Third, the high cost in

preparation, purification, and storage of natural enzymes also restricts their wide technological applications.

2.7 Nanozymes for peroxidase mimicking and colorimetric sensing of uric acid

Man-made enzymes or artificial enzymes can overcome most of the above-mentioned challenges(145). Artificial enzymes in the form of nanomaterials, known as nanozymes, have been explored to mimic enzymes. As an ideal candidate for artificial enzymes, nanozymes specifically refer to the nanomaterials with enzyme-mimetic catalytic activity, which can simulate the catalytic function of natural enzymes well in some important biochemical and chemical reactions. Since the first finding of intrinsic peroxidase-like activity (POX) of Fe_3O_4 nanoparticles in 2007, diverse nanozymes with intrinsic enzyme-like catalytic activities have been extensively explored, such as metal nanoparticles, carbon nanomaterials, and metal oxides (146–148). Compared to natural enzymes, these developed nanozymes have higher reaction stability and simple preparation. These unique merits enable the use of nanozymes in colorimetric sensing applications, as they can provide a series of simple and inexpensive devices and tools that are armed with simple signal color readout. For colorimetric sensing response, a number of organic indicators have been used as peroxidase or oxidase substrates, including 3, 3′, 5, 5′-tetramethylbenzydine (TMB), *o*-phenylenediamine (OPD) and 2, 2-azinobis-(3-ethylben-zothizoline-6-sulfonic acid (ABTS). OPD is carcinogenic and less sensitive than TMB, while ABTS is the least sensitive. In the presence of hydrogen peroxide, a peroxidase reaction with TMB, OPD, and ABTS yields blue, yellow-orange, and green products, respectively. UV-Vis spectroscopy can read these colors at 652 nm (blue), 492 nm (yellow-orange), and 405 nm (green).

One reason that nanoparticles make effective nanozyme catalysts is that nanomaterials have higher surface area to volume ratio than bulk materials. Increments in surface area increase the proportion of surface atoms with respect to the bulk. Such a substantial change in the ratio of surface atoms to interior atoms in nanoparticles leads to great changes in the physical and chemical properties of the material. High surface area nanoparticles used with TMB and H_2O_2 can catalyze the decomposition of peroxide in order to generate free radicals and produce blue colored solution with high absorbance, as was shown in Fig 2.9.

The use of nanoparticle based catalysts for UA sensing by TMB and peroxide reaction is favorable as high surface area nanoparticles even in small concentrations can catalyze TMB (141). In addition to this, nanoparticles are able to achieve a reasonable LOD for UA at room temperature for the reaction of TMB and hydrogen peroxide. For instance, Kumar et al. used gold nanoparticles to achieve LOD of 0.08 mM (141). Another research group targeted expanding the surface area of nanoparticles by incorporating graphene oxide and achieved a lower LOD of 0.01 mM (149). These studies give the indication towards the extended surface area, which played a major role in getting the intense blue color and low LOD.

Nanozyme-based strategies have been recently demonstrated that can effectively accelerate and advance the development of colorimetric sensors for biosensing events. However, several challenges remain in implementation of nanozymes. First, most of the reported nanozymes are dispersed in solution, making it difficult to recover and reuse. Second, the majority of existing nanozyme-based colorimetric assays are limited by the specificities and catalytic activities of nanozymes. It is therefore highly desirable to develop effective strategies to improve the performance and advance the practical application for nanozyme-based colorimetric sensors (150). Many efforts have demonstrated that several factors are closely related to the catalytic activity of

nanozymes, such as pH and temperature, size, morphology and composition (151). Based on these findings, various strategies were recently explored to tune the catalytic activity of nanozymes by focusing on the above factors, which greatly accelerated nanozymes-based colorimetric sensing applications such as quantitative detection of disease-specific biomarkers, food safety monitoring and environmental pollution detection (152–154). Several metalorganic frameworks (MOFs) and nanocrystals as peroxidase mimics are also being explored, and some of these high-surface-area catalysts are being used to detect UA colorimetrically. Researchers have used peroxidase-mimicking MOFs in the presence of TMB to detect H_2O_2, and nanoparticles and nanocrystals have also been used to mimic peroxidase for UA biosensing. For instance, Liu et al. employed peroxidase-mimicking MOFs in the presence of TMB to colorimetrically detect H_2O_2 produced during the interaction of uric acid with uricase, and other nanoparticles and nanocrystals have also been used to mimic peroxidase behavior for UA biosensing .

Nanomaterials are effective as nanozymes due to their high surface energy and high concentration of catalytically active sites from their large surface area. Modifying the surface can often enhance surface energy further, using methods such as the addition of surfactants, or doping with phosphorus, sulfur, and nitrogen atoms. For instance, N-doped MoS_2 exhibited higher peroxidase-like catalytic activity than undoped MoS_2 (22). Similarly, hydrothermal doping of MoO_2 nanobelts with N and S resulted in excellent electrocatalytic activity (155). In each case, the improved performance was attributed to improved charge transport as a result of increased electron density. However, a common downside of these nanomaterial-based systems is the difficulty in recovering the catalyst after use, which prohibits nanozyme catalysts from being reused. In addition to this, nanozymes also have lower concentrations of active sites per mass than natural enzymes, resulting in decreased enzyme-like activity (150).

Loading nanoparticles on a substrate can offer the freedom of reusability while still behaving as nanomaterials with high sensitivity, reusability, and non-tedious synthesis process. Therefore, further discussion on using nanomaterials in form of deposited films over a substrate is continued, which will have the properties of nanomaterials in order to provide them high sensitivity with the special property of reusability.

2.8 Michaelis Menten constant

The Michaelis Menten constant (K_m) is the amount of substrate required to half-saturate the enzyme or achieve half-maximum reaction rate (1/2 V_{max}). K_m shows the affinity of the catalyst for its substrate and used as a parameter to compare the behavior of different catalyst (enzyme/nanozymes).

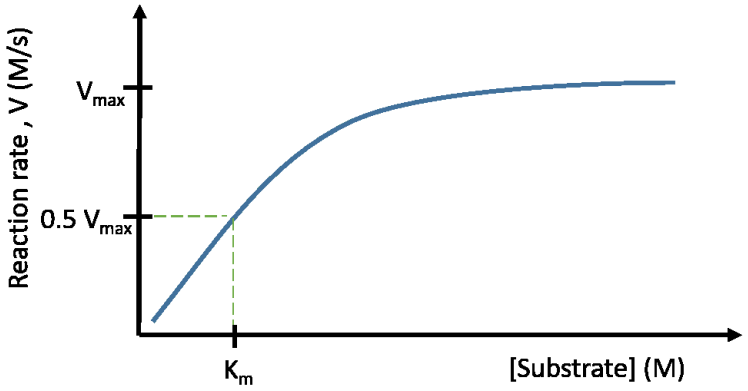

Figure 2.10: Michaelis Menten plot illustrating the effect of substrate concentration on reaction rate.

The smaller the value of K_m, the stronger the binding of the enzyme to the substrate. A substrate-enzyme catalyzed reaction has a direct relationship with reaction rate, until the enzyme reaches its limit and a steady state is reached (156). At this point, adding more substrate won't affect reaction

rate since all the enzyme's active sites are saturated with substrate molecules. Equation 5 describes the dependence of enzyme-catalyzed reaction rates on substrate concentration by using the Michaelis-Menten constant (K_m).

$$V = \frac{V_{max}[S]}{K_m + [S]} \qquad (5)$$

Here, V_{max} (unit=M/s) represents the maximum rate achieved by the enzyme-substrate reaction, occurred at saturated substrate concentration for a specific enzyme concentration. V is the reaction velocity (unit=M/s), measured for a range of substrate concentrations. K_m (unit=M) is the substrate concentration at which the reaction rate is half of V_{max}. A low K_m value indicates a large binding affinity. Thus the reaction will approach V_{max} more rapidly. A high K_m indicates that the enzyme does not bind as efficiently with the substrate, and V_{max} will only be reached if the substrate concentration is high enough to saturate the enzyme (156).

Glancing Angle Deposition (GLAD), a type of physical vapor deposition (PVD), is a technique which combines oblique angle deposition and substrate position control to yield nano-sized columnar films with controlled porosity and shapes (25). GLAD occurs in high vacuum chamber where the deposition flux is incident onto a substrate with a large angle with respect to surface normal. Nanocolumnar structures are produced by GLAD through the shadowing effect, while a column's shape is controlled by deposition angle and substrate rotation at different speeds. The morphology of the columns is determined by three parameters: the incident angle, the growth rate, and the rotational speed of the substrate. By changing these parameters, one can obtain the different morphology of the columns such as S-shape, zigzag shape, helical, and vertical columns (157). GLAD can not only control the growth of nanostructures but also exhibits many other advantages: 1. The porosity of the film can be controlled by changing the incident angle. 2. Wide variety of

evaporable materials can be deposited such as metals, inorganic materials, organic materials, and polymers. 3. The shape and in-plane alignments can be easily modified. 4. Natural formation of nanocolumns due to shadowing effect. 5. Film thickness can be easily controlled (158).

All of these advantages make the GLAD technique very promising for nanostructure fabrication using physical vapor deposition. In the next section, a brief review of this deposition method is given.

2.9 Physical Vapor Deposition

The process can be described into the following steps: (1) the materials to be deposited is vaporized in an evacuated chamber, (2) the vaporized material is transferred from its source to the substrate, and (3) the vaporized material condenses on the substrate to produce a thin film. Physical vapor deposition (PVD) methods are commonly used to deposit thin films with thicknesses ranging from a few nanometers to thousands of nanometers. This technology includes electron-beam evaporation, thermal evaporation, and laser ablation, among other deposition processes. In this thesis, an electron beam (e-beam) evaporation method (Fig 2.11) is used to fabricate nanostructured materials using GLAD technique where the source material can be evaporated using high energy electrons in the form of an intense beam. A hot filament causes the thermionic emission of electrons, which provides sufficient energy to evaporate source material.

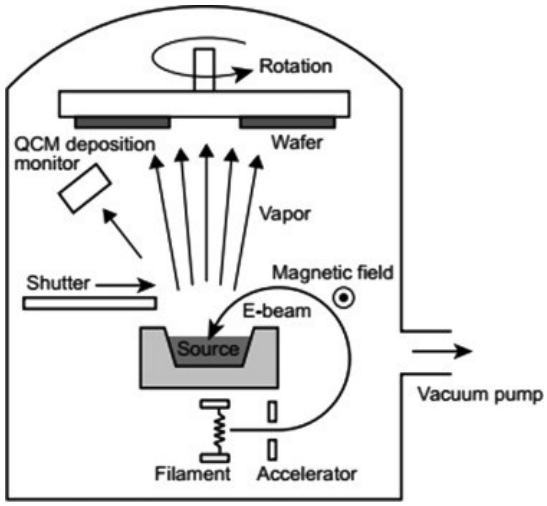

Figure 2.11: Schematic illustration of electron beam evaporation, adapted with permission from ref (159).

2.10 Glancing angle deposition (GLAD) technique

2.10.1 Apparatus

An electron beam evaporation source is situated at the base in a vacuum chamber which is usually kept at pressures ranging from 10^{-8} to 10^{-5} Torr during deposition. Electrons are thermionically emitted from filaments and accelerated by high voltages of roughly 6-9 kV. The resulting high kinetic energy electron beam is directed towards the source material where they lose energy after striking the source material. The kinetic energy of the electrons is transformed to thermal energy, which is used to melt or sublimate the source material and evaporate it. A schematic illustration of glancing angle deposition is shown in Fig 2.12, where two motors control the position of the substrate, which is held at a height above the source. Rotating about the α-axis changes the angle from which the incident flux reaches the substrate. As the source location changes, shadowing dynamics and column growth will also change, resulting into different morphologies of GLAD films. Further, GLAD films' morphologies can be controlled by rotation about the ϕ–axis which

changes the apparent location of the vapor source from the perspective of the growing columns. The quartz crystal microbalance monitors the deposition rate, so the computer-controlled motors can make precise movements and compensate their rotation speed accordingly.

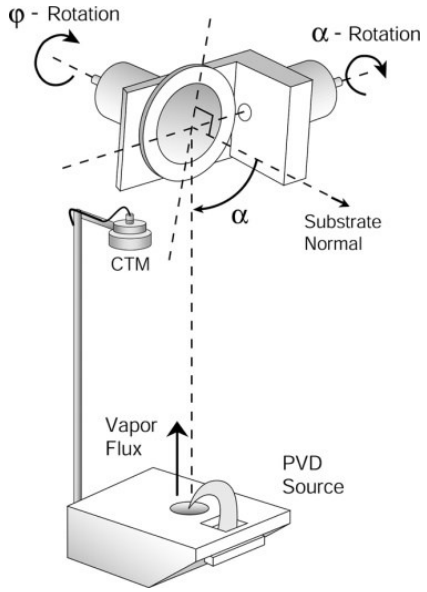

Figure 2.12: Schematic representation of glancing angle deposition technique, adapted with permission from ref (160).

Various researchers in the literature have employed different substrate movements to tailor the morphology of GLAD thin films. SEM images of thin films morphology that depicts some of the different morphologies which were obtained by tilting a substrate at a fixed angle while rotating the substrate during deposition, are shown in Fig 2.13.

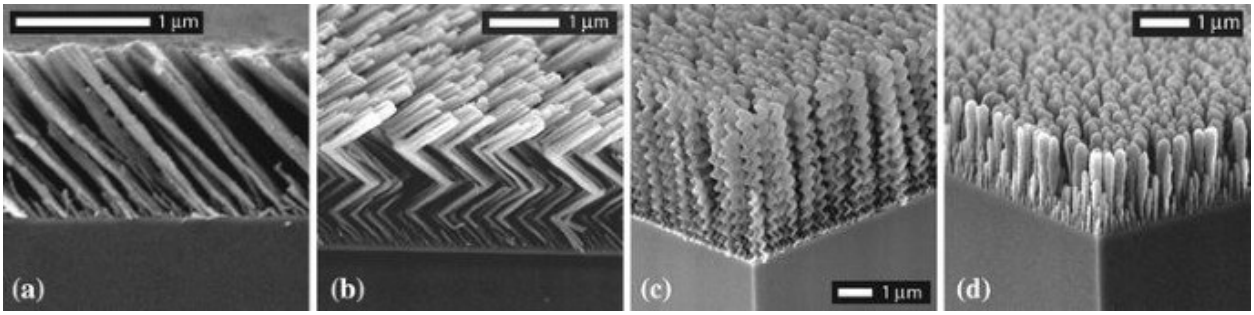

Figure 2.13: SEM images of GLAD nanostructured thin films. (a) The slanted film was fabricated by keeping constant α and φ. (b) Zig-zag film was fabricated by increasing φ between slanted posts. (c) Helical film was fabricated by rotating φ at a slow rate, high rate of φ will generate into vertical post structures (d), adapted with permission from ref (160).

2.10.2 Deposition principle

The steps needed to grow the film are condensation of the vapors of atomic or small molecular species on the growing surface (adsorption), surface diffusion of the reactants, reaction to form the film, coalescence of the reacted material into islands of atoms, and desorption (re-evaporation) of any product or unused reactant from the surface.

The interaction of the depositing material with the surface can form a structure on which subsequent depositing atoms nucleate and grow. The nucleus growth rate is determined by the balance between the arrival rate and the detachment probability of adatoms, which are the atoms landing on a substrate as illustrated in Fig 2.14. In a growing nucleus, the rate of adatom detachment from the substrate decreases, until eventually the nucleus reaches a critical size where the adatom attachment and detachment rates are balanced and the nucleus is stabilized. The critical nuclei present in this initial growth phase are not many times larger than the size of an atom, but after stabilization they rapidly grow to dominate the surface. The film grows and is further deposited as the critical nuclei absorb additional atoms, either through the attachment of diffusing adatoms or through direct condensation from the vapour phase.

When the substrate is tilted with an angle α compared to the target normal, the depositing particles nucleate on the substrate, but the region behind the nucleus does not receive any vapor since it is in the shadow of the nucleus. This phenomenon is known as the shadowing effect. As a result, a larger number of particles will be deposited onto the nuclei than in the shadowed area. This inequality increases as growth continues. As only the tops of the nuclei receive the depositing material, the nuclei will start developing columns, resulting in extremely porous structures tilted in the direction of the incident particles flux and forming an angle β with the substrate normal (β < α) (26).

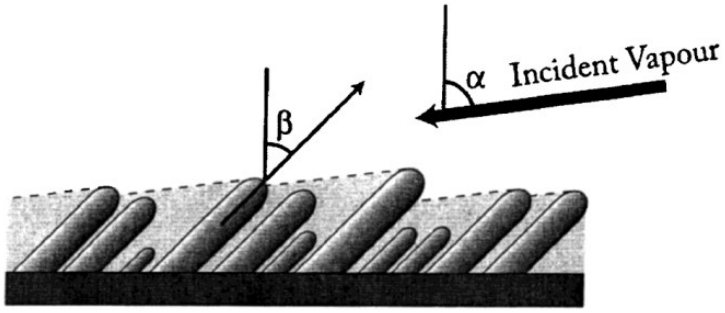

Figure 2.14: Schematic representation of the film growth process resulting in slanted post structures. Vapour flux impinging at an angle α is shadowed by already existing structures, which grow toward the incident vapor at an angle β, adapted with permission from ref (26).

2.10.3 GLAD based sensors

The high porosity, large surface area, controlled morphology, and ability to use varieties of PVD-compatible source materials make GLAD films ideal for sensing applications. In this section, we will read a brief overview on GLAD based optical, electrochemical, and mechanical sensors.

The interaction of light with GLAD film is sensitive to the dielectric constant of the surrounding medium. Through shifts in the optical absorption peak, molecules can be detected that absorb to

the GLAD film. This principle was used to develop Surface Enhanced Raman sensors and was used to detect bacteria as well as RNA strands (161,162).

Another interest in sensing field is GLAD film based electrochemical sensors which has gained massive attention in the last few years. GLAD thin film-based electrodes been used for immobilizing matrices in electrochemical biosensors, due to their high surface area scaffolds, fast electron transfer kinetics, non-toxicity, and excellent catalytic properties (163).

GLAD films were also used to develop a pressure sensor. In this technique, when a load (<1 MPa) is applied to the film, each column elastically deforms and contacts neighboring columns, resulting in a change in the conduction path through the film. This changes the film's electrical resistance which was measured by a two-point probe (164).

References

1. Califf RM. Biomarker definitions and their applications. Exp Biol Med [Internet]. 2018 Feb 6;243(3):213–21. Available from: http://journals.sagepub.com/doi/10.1177/1535370217750088
2. Cheng J, Gao R, Li H, Wu S, Fang J, Ma K, et al. Evaluating Potential Markers of Spoilage Foods Using a Metabolic Profiling Approach. Food Anal Methods [Internet]. 2015 May 18;8(5):1141–9. Available from: http://link.springer.com/10.1007/s12161-014-9999-z
3. Greiner J V., Glonek T. Intracellular ATP Concentration and Implication for Cellular Evolution. Biology (Basel) [Internet]. 2021 Nov 12;10(11):1166. Available from: https://www.mdpi.com/2079-7737/10/11/1166
4. Hagberg H, Andersson P, Lacarewicz J, Jacobson I, Butcher S, Sandberg M. Extracellular Adenosine, Inosine, Hypoxanthine, and Xanthine in Relation to Tissue Nucleotides and Purines in Rat Striatum During Transient Ischemia. J Neurochem [Internet]. 1987 Jul;49(1):227–31. Available from: https://onlinelibrary.wiley.com/doi/10.1111/j.1471-4159.1987.tb03419.x
5. Boll M, Fuchs G, Meier C, Trautwein A, El Kasmi A, Ragsdale SW, et al. Redox Centers of 4-Hydroxybenzoyl-CoA Reductase, a Member of the Xanthine Oxidase Family of Molybdenum-containing Enzymes. J Biol Chem [Internet]. 2001 Dec;276(51):47853–62. Available from: https://linkinghub.elsevier.com/retrieve/pii/S0021925819402925
6. Dervisevic M, Dervisevic E, Çevik E, Şenel M. Novel electrochemical xanthine biosensor based on chitosan–polypyrrole–gold nanoparticles hybrid bio-nanocomposite platform. J

Food Drug Anal [Internet]. 2017 Jul;25(3):510–9. Available from: https://linkinghub.elsevier.com/retrieve/pii/S1021949817300224
7. Khan MZH, Ahommed MS, Daizy M. Detection of xanthine in food samples with an electrochemical biosensor based on PEDOT:PSS and functionalized gold nanoparticles. RSC Adv [Internet]. 2020;10(59):36147–54. Available from: http://xlink.rsc.org/?DOI=D0RA06806C
8. Hlavay J, Haemmerli SD, Guilbault GG. Fibre-optic biosensor for hypoxanthine and xanthine based on a chemiluminescence reaction. Biosens Bioelectron [Internet]. 1994 Jan;9(3):189–95. Available from: https://linkinghub.elsevier.com/retrieve/pii/0956566394801215
9. Thandavan K, Gandhi S, Sethuraman S, Rayappan JBB, Krishnan UM. Development of electrochemical biosensor with nano-interface for xanthine sensing – A novel approach for fish freshness estimation. Food Chem [Internet]. 2013 Aug;139(1–4):963–9. Available from: https://linkinghub.elsevier.com/retrieve/pii/S0308814613001660
10. Kushiyama A, Nakatsu Y, Matsunaga Y, Yamamotoya T, Mori K, Ueda K, et al. Role of Uric Acid Metabolism-Related Inflammation in the Pathogenesis of Metabolic Syndrome Components Such as Atherosclerosis and Nonalcoholic Steatohepatitis. Mediators Inflamm [Internet]. 2016;2016:1–15. Available from: https://www.hindawi.com/journals/mi/2016/8603164/
11. de Oliveira EP, Burini RC. High plasma uric acid concentration: causes and consequences. Diabetol Metab Syndr [Internet]. 2012 Dec 4;4(1):12. Available from: https://dmsjournal.biomedcentral.com/articles/10.1186/1758-5996-4-12
12. Kim KY, Ralph Schumacher H, Hunsche E, Wertheimer AI, Kong SX. A literature review of the epidemiology and treatment of acute gout. Clin Ther [Internet]. 2003 Jun;25(6):1593–617. Available from: https://linkinghub.elsevier.com/retrieve/pii/S0149291803801583
13. Davis SN, Lastra-Gonzalez G. Diabetes and Low Blood Sugar (Hypoglycemia). J Clin Endocrinol Metab [Internet]. 2008 Aug;93(8):0–0. Available from: https://academic.oup.com/jcem/article-lookup/doi/10.1210/jcem.93.8.9993
14. Wu F, Huang Y, Li Q. Animal tissue-based chemiluminescence sensing of uric acid. Anal Chim Acta [Internet]. 2005 Apr;536(1–2):107–13. Available from: https://linkinghub.elsevier.com/retrieve/pii/S000326700401671X
15. Galbán J. Direct determination of uric acid in serum by a fluorometric-enzymatic method based on uricase. Talanta [Internet]. 2001 Jun 21;54(5):847–54. Available from: https://linkinghub.elsevier.com/retrieve/pii/S0039914001003356
16. Zhao S, Wang J, Ye F, Liu Y-M. Determination of uric acid in human urine and serum by capillary electrophoresis with chemiluminescence detection. Anal Biochem [Internet]. 2008 Jul;378(2):127–31. Available from: https://linkinghub.elsevier.com/retrieve/pii/S0003269708002236
17. Rocha DL, Rocha FRP. A flow-based procedure with solenoid micro-pumps for the spectrophotometric determination of uric acid in urine. Microchem J [Internet]. 2010 Jan;94(1):53–9. Available from: https://linkinghub.elsevier.com/retrieve/pii/S0026265X09001271
18. PERELLO J, SANCHIS P, GRASES F. Determination of uric acid in urine, saliva and calcium oxalate renal calculi by high-performance liquid chromatography/mass spectrometry. J Chromatogr B [Internet]. 2005 Sep 25;824(1–2):175–80. Available from: https://linkinghub.elsevier.com/retrieve/pii/S1570023205005015

19. Zhao FY, Wang ZH, Wang H, Zhao R, Ding MY. Determination of uric acid in human urine by ion chromatography with conductivity detector. Chinese Chem Lett [Internet]. 2011 Mar;22(3):342–5. Available from: https://linkinghub.elsevier.com/retrieve/pii/S1001841710004055
20. Dai X, Fang X, Zhang C, Xu R, Xu B. Determination of serum uric acid using high-performance liquid chromatography (HPLC)/isotope dilution mass spectrometry (ID-MS) as a candidate reference method. J Chromatogr B [Internet]. 2007 Oct;857(2):287–95. Available from: https://linkinghub.elsevier.com/retrieve/pii/S1570023207005454
21. Mabey D, Peeling RW, Ustianowski A, Perkins MD. Diagnostics for the developing world. Nat Rev Microbiol. 2004;2(3):231–40.
22. Huang X, Tan C, Yin Z, Zhang H. 25th Anniversary Article: Hybrid Nanostructures Based on Two-Dimensional Nanomaterials. Adv Mater [Internet]. 2014 Apr;26(14):2185–204. Available from: https://onlinelibrary.wiley.com/doi/10.1002/adma.201304964
23. Li X, Shan J, Zhang W, Su S, Yuwen L, Wang L. Recent Advances in Synthesis and Biomedical Applications of Two-Dimensional Transition Metal Dichalcogenide Nanosheets. Small [Internet]. 2017 Feb;13(5):1602660. Available from: https://onlinelibrary.wiley.com/doi/10.1002/smll.201602660
24. Su S, Chao J, Pan D, Wang L, Fan C. Electrochemical Sensors Using Two-Dimensional Layered Nanomaterials. Electroanalysis [Internet]. 2015 May;27(5):1062–72. Available from: https://onlinelibrary.wiley.com/doi/10.1002/elan.201400655
25. Ping J, Fan Z, Sindoro M, Ying Y, Zhang H. Recent Advances in Sensing Applications of Two-Dimensional Transition Metal Dichalcogenide Nanosheets and Their Composites. Adv Funct Mater [Internet]. 2017 May;27(19):1605817. Available from: https://onlinelibrary.wiley.com/doi/10.1002/adfm.201605817
26. Chimene D, Alge DL, Gaharwar AK. Two-Dimensional Nanomaterials for Biomedical Applications: Emerging Trends and Future Prospects. Adv Mater [Internet]. 2015 Dec;27(45):7261–84. Available from: https://onlinelibrary.wiley.com/doi/10.1002/adma.201502422
27. Mehrotra P. Biosensors and their applications – A review. J Oral Biol Craniofacial Res [Internet]. 2016 May;6(2):153–9. Available from: https://linkinghub.elsevier.com/retrieve/pii/S2212426815001323
28. Naresh V, Lee N. A Review on Biosensors and Recent Development of Nanostructured Materials-Enabled Biosensors. Sensors [Internet]. 2021 Feb 5;21(4):1109. Available from: https://www.mdpi.com/1424-8220/21/4/1109
29. Tetyana P, Morgan Shumbula P, Njengele-Tetyana Z. Biosensors: Design, Development and Applications. In: Nanopores [Internet]. IntechOpen; 2021. Available from: https://www.intechopen.com/books/nanopores/biosensors-design-development-and-applications
30. Singh RS, Singh T, Singh AK. Enzymes as Diagnostic Tools. In: Advances in Enzyme Technology [Internet]. Elsevier; 2019. p. 225–71. Available from: https://linkinghub.elsevier.com/retrieve/pii/B9780444641144000091
31. Al-Tamer YY, Hadi EA, Al-Badrani I eldin I. Sweat urea, uric acid and creatinine concentrations in uraemic patients. Urol Res [Internet]. 1997 Sep;25(5):337–40. Available from: http://link.springer.com/10.1007/BF01294662
32. De Acha N, Socorro-Leránoz AB, Elosúa C, Matías IR. Trends in the Design of Intensity-Based Optical Fiber Biosensors (2010–2020). Biosensors [Internet]. 2021 Jun 15;11(6):197. Available from: https://www.mdpi.com/2079-6374/11/6/197

33. Rogers JK, Taylor ND, Church GM. Biosensor-based engineering of biosynthetic pathways. Curr Opin Biotechnol [Internet]. 2016 Dec;42:84–91. Available from: https://linkinghub.elsevier.com/retrieve/pii/S0958166916300611
34. Narang J, Malhotra N, Singhal C, Pundir CS. Evaluation of Freshness of Fishes Using MWCNT/TiO2 Nanobiocomposites Based Biosensor. Food Anal Methods [Internet]. 2017 Feb 21;10(2):522–8. Available from: http://link.springer.com/10.1007/s12161-016-0594-3
35. Yadav SK, Singh J, Agrawal VV, Malhotra BD. Nanostructured nickel oxide film for application to fish freshness biosensor. Appl Phys Lett [Internet]. 2012 Jul 9;101(2):023703. Available from: http://aip.scitation.org/doi/10.1063/1.4736578
36. Lavín Á, Vicente J, Holgado M, Laguna M, Casquel R, Santamaría B, et al. On the Determination of Uncertainty and Limit of Detection in Label-Free Biosensors. Sensors [Internet]. 2018 Jun 26;18(7):2038. Available from: http://www.mdpi.com/1424-8220/18/7/2038
37. Sen S, Sarkar P. A novel third-generation xanthine biosensor with enzyme modified glassy carbon electrode using electrodeposited MWCNT and nanogold polymer composite film. RSC Adv [Internet]. 2015;5(116):95911–25. Available from: http://xlink.rsc.org/?DOI=C5RA18889J
38. Grieshaber D, MacKenzie R, Vörös J, Reimhult E. Electrochemical Biosensors - Sensor Principles and Architectures. Sensors [Internet]. 2008 Mar 7;8(3):1400–58. Available from: http://www.mdpi.com/1424-8220/8/3/1400
39. Son J, Buck EC, Riechers SL, Yu X-Y. Stamping Nanoparticles onto the Electrode for Rapid Electrochemical Analysis in Microfluidics. Micromachines [Internet]. 2021 Jan 6;12(1):60. Available from: https://www.mdpi.com/2072-666X/12/1/60
40. Maduraiveeran G, Jin W. Nanomaterials based electrochemical sensor and biosensor platforms for environmental applications. Trends Environ Anal Chem [Internet]. 2017 Jan;13:10–23. Available from: https://linkinghub.elsevier.com/retrieve/pii/S2214158817300132
41. Shen Y, Rao D, Sheng Q, Zheng J. Simultaneous voltammetric determination of hydroquinone and catechol by using a glassy carbon electrode modified with carboxy-functionalized carbon nanotubes in a chitosan matrix and decorated with gold nanoparticles. Microchim Acta [Internet]. 2017 Sep 29;184(9):3591–601. Available from: http://link.springer.com/10.1007/s00604-017-2392-z
42. Rao D, Sheng Q, Zheng J. Preparation of flower-like Pt nanoparticles decorated chitosan-grafted graphene oxide and its electrocatalysis of hydrazine. Sensors Actuators B Chem [Internet]. 2016 Nov;236:192–200. Available from: https://linkinghub.elsevier.com/retrieve/pii/S0925400516308462
43. Azab SM, Fekry AM. Electrochemical design of a new nanosensor based on cobalt nanoparticles, chitosan and MWCNT for the determination of daclatasvir: a hepatitis C antiviral drug. RSC Adv [Internet]. 2017;7(2):1118–26. Available from: http://xlink.rsc.org/?DOI=C6RA25826C
44. Boluda A, Casado C, Alonso B, García Armada M. Efficient Oxidase Biosensors Based on Bioelectrocatalytic Surfaces of Electrodeposited Ferrocenyl Polycyclosiloxanes—Pt Nanoparticles. Chemosensors [Internet]. 2021 Apr 15;9(4):81. Available from: https://www.mdpi.com/2227-9040/9/4/81
45. VEDRINE C. Amperometric tyrosinase based biosensor using an electrogenerated polythiophene film as an entrapment support. Talanta [Internet]. 2003 Mar;59(3):535–44.

Available from: https://linkinghub.elsevier.com/retrieve/pii/S0039914002005404
46. Button VLDSN. Electrodes for Biopotential Recording and Tissue Stimulation. In: Principles of Measurement and Transduction of Biomedical Variables [Internet]. Elsevier; 2015. p. 25–76. Available from: https://linkinghub.elsevier.com/retrieve/pii/B9780128007747000027
47. Zhang JXJ, Hoshino K. Electrical transducers: Electrochemical sensors and semiconductor molecular sensors. In: Molecular Sensors and Nanodevices [Internet]. Elsevier; 2019. p. 181–230. Available from: https://linkinghub.elsevier.com/retrieve/pii/B9780128148624000041
48. Sun C, Xu Q, Zou X, Cheng H, Lu X. A new method to determine AgCl(1% mol)/Ag electrode potential versus the standard chloride electrode potential in a LiCl-KCl eutectic. Electrochem commun [Internet]. 2021 Sep;130:107111. Available from: https://linkinghub.elsevier.com/retrieve/pii/S1388248121001958
49. Nguyen TSV, Huynh TM, To TD, Doan TCD, Dang CM. Ag/AgCl Film Electrodes Coated with Agarose Gel as Planar Reference Electrodes for Potentiometric Sensors. Univers J Mater Sci [Internet]. 2018 Nov;6(5):148–54. Available from: http://www.hrpub.org/journals/article_info.php?aid=7510
50. Chen X, Lu L, Gu D, Zhang X, Yu H, Chen F, et al. Chlorine management of a carbon counter electrode for high performance printable perovskite solar cells. J Mater Chem C [Internet]. 2021;9(27):8615–22. Available from: http://xlink.rsc.org/?DOI=D1TC00890K
51. Chen R, Yang C, Cai W, Wang H-Y, Miao J, Zhang L, et al. Use of Platinum as the Counter Electrode to Study the Activity of Nonprecious Metal Catalysts for the Hydrogen Evolution Reaction. ACS Energy Lett [Internet]. 2017 May 12;2(5):1070–5. Available from: https://pubs.acs.org/doi/10.1021/acsenergylett.7b00219
52. Saha T, Fang J, Mukherjee S, Knisely CT, Dickey MD, Velev OD. Osmotically Enabled Wearable Patch for Sweat Harvesting and Lactate Quantification. Micromachines [Internet]. 2021 Dec 4;12(12):1513. Available from: https://www.mdpi.com/2072-666X/12/12/1513
53. Mathew M, Sandhyarani N. A highly sensitive electrochemical glucose sensor structuring with nickel hydroxide and enzyme glucose oxidase. Electrochim Acta [Internet]. 2013 Oct;108:274–80. Available from: https://linkinghub.elsevier.com/retrieve/pii/S0013468613012784
54. Clark LC, Lyons C. ELECTRODE SYSTEMS FOR CONTINUOUS MONITORING IN CARDIOVASCULAR SURGERY. Ann N Y Acad Sci [Internet]. 2006 Dec 15;102(1):29–45. Available from: https://onlinelibrary.wiley.com/doi/10.1111/j.1749-6632.1962.tb13623.x
55. Batool R, Rhouati A, Nawaz MH, Hayat A, Marty JL. A Review of the Construction of Nano-Hybrids for Electrochemical Biosensing of Glucose. Biosensors [Internet]. 2019 Mar 25;9(1):46. Available from: https://www.mdpi.com/2079-6374/9/1/46
56. Pandey PC, Pandey G, Narayan RJ. Minimally Invasive Platforms in Biosensing. Front Bioeng Biotechnol [Internet]. 2020 Aug 31;8. Available from: https://www.frontiersin.org/article/10.3389/fbioe.2020.00894/full
57. Imam HT, Marr PC, Marr AC. Enzyme entrapment, biocatalyst immobilization without covalent attachment. Green Chem [Internet]. 2021;23(14):4980–5005. Available from: http://xlink.rsc.org/?DOI=D1GC01852C
58. Zdarta J, Meyer A, Jesionowski T, Pinelo M. A General Overview of Support Materials for Enzyme Immobilization: Characteristics, Properties, Practical Utility. Catalysts

[Internet]. 2018 Feb 24;8(2):92. Available from: http://www.mdpi.com/2073-4344/8/2/92
59. Pandey G, Munguambe DM, Tharmavaram M, Rawtani D, Agrawal YK. Halloysite nanotubes - An efficient 'nano-support' for the immobilization of α-amylase. Appl Clay Sci [Internet]. 2017 Feb;136:184–91. Available from: https://linkinghub.elsevier.com/retrieve/pii/S016913171630535X
60. Doonan C, Riccò R, Liang K, Bradshaw D, Falcaro P. Metal–Organic Frameworks at the Biointerface: Synthetic Strategies and Applications. Acc Chem Res [Internet]. 2017 Jun 20;50(6):1423–32. Available from: https://pubs.acs.org/doi/10.1021/acs.accounts.7b00090
61. Grigoras AG. Catalase immobilization—A review. Biochem Eng J [Internet]. 2017 Jan;117:1–20. Available from: https://linkinghub.elsevier.com/retrieve/pii/S1369703X16302972
62. Kim T-S, Patel SKS, Selvaraj C, Jung W-S, Pan C-H, Kang YC, et al. A highly efficient sorbitol dehydrogenase from Gluconobacter oxydans G624 and improvement of its stability through immobilization. Sci Rep [Internet]. 2016 Dec 16;6(1):33438. Available from: http://www.nature.com/articles/srep33438
63. Komiyama M, Yoshimoto K, Sisido M, Ariga K. Chemistry Can Make Strict and Fuzzy Controls for Bio-Systems: DNA Nanoarchitectonics and Cell-Macromolecular Nanoarchitectonics. Bull Chem Soc Jpn [Internet]. 2017 Sep 15;90(9):967–1004. Available from: http://www.journal.csj.jp/doi/10.1246/bcsj.20170156
64. Murata K, Akatsuka W, Tsujimura S. Bioelectrocatalytic Oxidation of Glucose on MgO-templated Mesoporous Carbon-modified Electrode. Chem Lett [Internet]. 2014 Jun 5;43(6):928–30. Available from: http://www.journal.csj.jp/doi/10.1246/cl.140189
65. Daneshjou S, Dabirmanesh B, Rahimi F, Khajeh K. Porous silicon nanoparticle as a stabilizing support for chondroitinase. Int J Biol Macromol [Internet]. 2017 Jan;94:852–8. Available from: https://linkinghub.elsevier.com/retrieve/pii/S0141813016321365
66. Fang Y, Umasankar Y, Ramasamy RP. A novel bi-enzyme electrochemical biosensor for selective and sensitive determination of methyl salicylate. Biosens Bioelectron [Internet]. 2016 Jul;81:39–45. Available from: https://linkinghub.elsevier.com/retrieve/pii/S0956566316300963
67. Jegannathan KR, Abang S, Poncelet D, Chan ES, Ravindra P. Production of Biodiesel Using Immobilized Lipase—A Critical Review. Crit Rev Biotechnol [Internet]. 2008 Jan 16;28(4):253–64. Available from: http://www.tandfonline.com/doi/full/10.1080/07388550802428392
68. Boscolo B, Trotta F, Ghibaudi E. High catalytic performances of Pseudomonas fluorescens lipase adsorbed on a new type of cyclodextrin-based nanosponges. J Mol Catal B Enzym [Internet]. 2010 Feb;62(2):155–61. Available from: https://linkinghub.elsevier.com/retrieve/pii/S1381117709002550
69. Ponvel KM, Lee D-G, Woo E-J, Ahn I-S, Lee C-H. Immobilization of lipase on surface modified magnetic nanoparticles using alkyl benzenesulfonate. Korean J Chem Eng [Internet]. 2009 Jan 28;26(1):127–30. Available from: http://link.springer.com/10.1007/s11814-009-0019-8
70. Yang G, Wu J, Xu G, Yang L. Improvement of catalytic properties of lipase from Arthrobacter sp. by encapsulation in hydrophobic sol–gel materials. Bioresour Technol [Internet]. 2009 Oct;100(19):4311–6. Available from: https://linkinghub.elsevier.com/retrieve/pii/S0960852409003472
71. Yilmaz E, Sezgin M. Enhancement of the Activity and Enantioselectivity of Lipase by Sol–Gel Encapsulation Immobilization onto β-cyclodextrin-Based Polymer. Appl

Biochem Biotechnol [Internet]. 2012 Apr 1;166(8):1927–40. Available from: http://link.springer.com/10.1007/s12010-012-9621-z
72. Cacicedo ML, Manzo RM, Municoy S, Bonazza HL, Islan GA, Desimone M, et al. Immobilized Enzymes and Their Applications. In: Advances in Enzyme Technology [Internet]. Elsevier; 2019. p. 169–200. Available from: https://linkinghub.elsevier.com/retrieve/pii/B9780444641144000078
73. Minteer SD. Cell-Free Biotechnologies. In: Biotechnology for Biofuel Production and Optimization [Internet]. Elsevier; 2016. p. 433–48. Available from: https://linkinghub.elsevier.com/retrieve/pii/B9780444634757000169
74. Liang Y-Y, Zhang L-M. Bioconjugation of Papain on Superparamagnetic Nanoparticles Decorated with Carboxymethylated Chitosan. Biomacromolecules [Internet]. 2007 May 1;8(5):1480–6. Available from: https://pubs.acs.org/doi/10.1021/bm061091g
75. Bai Y, Li Y, Lei L. Synthesis of a mesoporous functional copolymer bead carrier and its properties for glucoamylase immobilization. Appl Microbiol Biotechnol [Internet]. 2009 Jun 1;83(3):457–64. Available from: http://link.springer.com/10.1007/s00253-009-1864-4
76. Chiou S-H, Wu W-T. Immobilization of Candida rugosa lipase on chitosan with activation of the hydroxyl groups. Biomaterials [Internet]. 2004 Jan;25(2):197–204. Available from: https://linkinghub.elsevier.com/retrieve/pii/S0142961203004824
77. Heck T, Faccio G, Richter M, Thöny-Meyer L. Enzyme-catalyzed protein crosslinking. Appl Microbiol Biotechnol [Internet]. 2013 Jan 25;97(2):461–75. Available from: http://link.springer.com/10.1007/s00253-012-4569-z
78. Govardhan CP. Crosslinking of enzymes for improved stability and performance. Curr Opin Biotechnol [Internet]. 1999 Aug;10(4):331–5. Available from: https://linkinghub.elsevier.com/retrieve/pii/S0958166999800603
79. Goossens J, Sein H, Lu S, Radwanska M, Muyldermans S, Sterckx YG-J, et al. Functionalization of gold nanoparticles with nanobodies through physical adsorption. Anal Methods [Internet]. 2017;9(23):3430–40. Available from: http://xlink.rsc.org/?DOI=C7AY00854F
80. Lin P, Zhang Y, Ren H, Wang Y, Wang S, Fang B. Assembly of graphene oxide-formate dehydrogenase composites by nickel-coordination with enhanced stability and reusability. Eng Life Sci [Internet]. 2018 May;18(5):326–33. Available from: https://onlinelibrary.wiley.com/doi/10.1002/elsc.201700137
81. Zhang D, Hegab HE, Lvov Y, Dale Snow L, Palmer J. Immobilization of cellulase on a silica gel substrate modified using a 3-APTES self-assembled monolayer. Springerplus [Internet]. 2016 Dec 20;5(1):48. Available from: https://springerplus.springeropen.com/articles/10.1186/s40064-016-1682-y
82. Uddin KMA, Orelma H, Mohammadi P, Borghei M, Laine J, Linder M, et al. Retention of lysozyme activity by physical immobilization in nanocellulose aerogels and antibacterial effects. Cellulose [Internet]. 2017 Jul 5;24(7):2837–48. Available from: http://link.springer.com/10.1007/s10570-017-1311-0
83. de Alteriis E, Parascandola P, Pecorella MA, Scardi V. Entrapment of microbial cells within a gelatin matrix: A comparison of three procedures. Biotechnol Tech [Internet]. 1987 Jun;1(2):109–14. Available from: http://link.springer.com/10.1007/BF00159331
84. Gao Y, Shen C, Di J, Tu Y. Fabrication of amperometric xanthine biosensors based on direct chemistry of xanthine oxidase. Mater Sci Eng C [Internet]. 2009 Aug;29(7):2213–6. Available from: https://linkinghub.elsevier.com/retrieve/pii/S0928493109001568
85. Lates V, Marty J-L, Popescu IC. Determination of Antioxidant Capacity by Using

Xanthine Oxidase Bioreactor Coupled with Flow-through H2O2 Amperometric Biosensor. Electroanalysis [Internet]. 2010 Dec 22;n/a-n/a. Available from: https://onlinelibrary.wiley.com/doi/10.1002/elan.201000544
86. Isgrove FH, Williams RJH, Niven GW, Andrews AT. Enzyme immobilization on nylon–optimization and the steps used to prevent enzyme leakage from the support. Enzyme Microb Technol [Internet]. 2001 Feb;28(2–3):225–32. Available from: https://linkinghub.elsevier.com/retrieve/pii/S0141022900003124
87. Kumar A, Kanwar SS. Catalytic potential of a nitrocellulose membrane-immobilized lipase in aqueous and organic media. J Appl Polym Sci [Internet]. 2012 Jun 25;124(S1):E37–44. Available from: https://onlinelibrary.wiley.com/doi/10.1002/app.35434
88. Shin J-H, Lee M-J, Choi J-H, Song J, Kim T-H, Oh B-K. Electrochemical H2O2 biosensor based on horseradish peroxidase encapsulated protein nanoparticles with reduced graphene oxide-modified gold electrode. Nano Converg [Internet]. 2020 Dec 16;7(1):39. Available from: https://nanoconvergencejournal.springeropen.com/articles/10.1186/s40580-020-00249-0
89. Trevan MD. Enzyme Immobilization by Covalent Bonding. In: New Protein Techniques [Internet]. New Jersey: Humana Press; p. 495–510. Available from: http://link.springer.com/10.1385/0-89603-126-8:495
90. Yang X, Hua L, Gong H, Tan SN. Covalent immobilization of an enzyme (glucose oxidase) onto a carbon sol–gel silicate composite surface as a biosensing platform. Anal Chim Acta [Internet]. 2003 Feb;478(1):67–75. Available from: https://linkinghub.elsevier.com/retrieve/pii/S0003267002015076
91. Salem M, Mauguen Y, Prangé T. Revisiting glutaraldehyde cross-linking: the case of the Arg–Lys intermolecular doublet. Acta Crystallogr Sect F Struct Biol Cryst Commun [Internet]. 2010 Mar 1;66(3):225–8. Available from: http://scripts.iucr.org/cgi-bin/paper?S1744309109054037
92. Carpani I, Scavetta E, Tonelli D. Amperometric Glucose Biosensors Based on Glassy Carbon and SWCNT-Modified Glassy Carbon Electrodes. Electroanalysis [Internet]. 2008 Jan;20(1):84–90. Available from: https://onlinelibrary.wiley.com/doi/10.1002/elan.200704054
93. Curulli A. Nanomaterials in Electrochemical Sensing Area: Applications and Challenges in Food Analysis. Molecules [Internet]. 2020 Dec 7;25(23):5759. Available from: https://www.mdpi.com/1420-3049/25/23/5759
94. Favrod-Coune T, Broers B. Addiction to Caffeine and Other Xanthines. In: Textbook of Addiction Treatment: International Perspectives [Internet]. Milano: Springer Milan; 2015. p. 437–53. Available from: http://link.springer.com/10.1007/978-88-470-5322-9_18
95. Devi R, Thakur M, Pundir CS. Construction and application of an amperometric xanthine biosensor based on zinc oxide nanoparticles–polypyrrole composite film. Biosens Bioelectron [Internet]. 2011 Apr;26(8):3420–6. Available from: https://linkinghub.elsevier.com/retrieve/pii/S0956566311000388
96. Dalkiran B, Kaçar C, Erden PE, Kiliç E. Amperometric xanthine biosensors based on chitosan-Co3O4-multiwall carbon nanotube modified glassy carbon electrode. Sensors Actuators B Chem [Internet]. 2014 Sep;200:83–91. Available from: https://linkinghub.elsevier.com/retrieve/pii/S0925400514004262
97. Zhang X, Dong J, Qian X, Zhao C. One-pot synthesis of an RGO/ZnO nanocomposite on zinc foil and its excellent performance for the nonenzymatic sensing of xanthine. Sensors

Actuators B Chem [Internet]. 2015 Dec;221:528–36. Available from: https://linkinghub.elsevier.com/retrieve/pii/S092540051500814X
98. Raj MA, John SA. Simultaneous determination of uric acid, xanthine, hypoxanthine and caffeine in human blood serum and urine samples using electrochemically reduced graphene oxide modified electrode. Anal Chim Acta [Internet]. 2013 Apr;771:14–20. Available from: https://linkinghub.elsevier.com/retrieve/pii/S000326701300233X
99. Zhu D, Guo D, Zhang L, Tan L, Pang H, Ma H, et al. Non-enzymatic xanthine sensor of heteropolyacids doped ferrocene and reduced graphene oxide via one-step electrodeposition combined with layer-by-layer self-assembly technology. Sensors Actuators B Chem [Internet]. 2019 Feb;281:893–904. Available from: https://linkinghub.elsevier.com/retrieve/pii/S0925400518319282
100. Luo A, Lian Q, An Z, Li Z, Guo Y, Zhang D, et al. Simultaneous determination of uric acid, xanthine and hypoxanthine based on sulfonic groups functionalized nitrogen-doped graphene. J Electroanal Chem [Internet]. 2015 Nov;756:22–9. Available from: https://linkinghub.elsevier.com/retrieve/pii/S1572665715300679
101. Rahman MM, Marwani HM, Algethami FK, Asiri AM. Xanthine sensor development based on ZnO–CNT, ZnO–CB, ZnO–GO and ZnO nanoparticles: an electrochemical approach. New J Chem [Internet]. 2017;41(14):6262–71. Available from: http://xlink.rsc.org/?DOI=C7NJ00278E
102. Devi R, Yadav S, Pundir CS. Amperometric determination of xanthine in fish meat by zinc oxide nanoparticle/chitosan/multiwalled carbon nanotube/polyaniline composite film bound xanthine oxidase. Analyst [Internet]. 2012;137(3):754–9. Available from: http://xlink.rsc.org/?DOI=C1AN15838D
103. Kreno LE, Leong K, Farha OK, Allendorf M, Van Duyne RP, Hupp JT. Metal–Organic Framework Materials as Chemical Sensors. Chem Rev [Internet]. 2012 Feb 8;112(2):1105–25. Available from: https://pubs.acs.org/doi/10.1021/cr200324t
104. Furukawa H, Cordova KE, O'Keeffe M, Yaghi OM. The Chemistry and Applications of Metal-Organic Frameworks. Science (80-) [Internet]. 2013 Aug 30;341(6149). Available from: https://www.science.org/doi/10.1126/science.1230444
105. Xu Y, Li Q, Xue H, Pang H. Metal-organic frameworks for direct electrochemical applications. Coord Chem Rev [Internet]. 2018 Dec;376:292–318. Available from: https://linkinghub.elsevier.com/retrieve/pii/S001085451830290X
106. Fang X, Zong B, Mao S. Metal–Organic Framework-Based Sensors for Environmental Contaminant Sensing. Nano-Micro Lett [Internet]. 2018 Oct 13;10(4):64. Available from: http://link.springer.com/10.1007/s40820-018-0218-0
107. Salimi A, Sharifi E, Noorbakhsh A, Soltanian S. Direct electrochemistry and electrocatalytic activity of catalase immobilized onto electrodeposited nano-scale islands of nickel oxide. Biophys Chem [Internet]. 2007 Feb;125(2–3):540–8. Available from: https://linkinghub.elsevier.com/retrieve/pii/S0301462206003371
108. Hayat A, Catanante G, Marty J. Current Trends in Nanomaterial-Based Amperometric Biosensors. Sensors [Internet]. 2014 Dec 8;14(12):23439–61. Available from: http://www.mdpi.com/1424-8220/14/12/23439
109. Elgrishi N, Rountree KJ, McCarthy BD, Rountree ES, Eisenhart TT, Dempsey JL. A Practical Beginner's Guide to Cyclic Voltammetry. J Chem Educ [Internet]. 2018 Feb 13;95(2):197–206. Available from: https://pubs.acs.org/doi/10.1021/acs.jchemed.7b00361
110. Zhou Y. Investigation of nanostructured lithium-ion battery materials. Friedrich-Alexander-Universität Erlangen-Nürnberg; 2020.

111. Venton BJ, DiScenza DJ. Voltammetry. In: Electrochemistry for Bioanalysis [Internet]. Elsevier; 2020. p. 27–50. Available from: https://linkinghub.elsevier.com/retrieve/pii/B978012821203500004X
112. Wang Z, Ma B, Shen C, Lai O-M, Tan C-P, Cheong L-Z. Electrochemical Biosensing of Chilled Seafood Freshness by Xanthine Oxidase Immobilized on Copper-Based Metal–Organic Framework Nanofiber Film. Food Anal Methods [Internet]. 2019 Aug 6;12(8):1715–24. Available from: http://link.springer.com/10.1007/s12161-019-01513-8
113. Chen WC, Wu SY, Liu HP, Chang CH, Chen HY, Chen HY, et al. Identification of melamine/cyanuric acid-containing nephrolithiasis by infrared spectroscopy. J Clin Lab Anal. 2010;24(2):92–9.
114. Pavlíček V, Tůma P, Matějčková J, Samcová E. Very fast electrophoretic determination of creatinine and uric acid in human urine using a combination of two capillaries with different internal diameters. Electrophoresis. 2014;35(7):956–61.
115. Kumar A, Hens A, Arun RK, Chatterjee M, Mahato K, Layek K, et al. A paper based microfluidic device for easy detection of uric acid using positively charged gold nanoparticles. Analyst [Internet]. 2015;140(6):1817–21. Available from: http://xlink.rsc.org/?DOI=C4AN02333A
116. Jazayeri MH, Aghaie T, Avan A, Vatankhah A, Ghaffari MRS. Colorimetric detection based on gold nano particles (GNPs): An easy, fast, inexpensive, low-cost and short time method in detection of analytes (protein, DNA, and ion). Sens Bio-Sensing Res. 2018;20(May):1–8.
117. Harpaz D, Eltzov E, Ng TSE, Marks RS, Tok AIY. Enhanced Colorimetric Signal for Accurate Signal Detection in Paper-Based Biosensors. Diagnostics [Internet]. 2020 Jan 7;10(1):28. Available from: https://www.mdpi.com/2075-4418/10/1/28
118. Tripathi A, Harris KD, Elias AL. Peroxidase-Like Behavior of Ni Thin Films Deposited by Glancing Angle Deposition for Enzyme-Free Uric Acid Sensing. ACS Omega [Internet]. 2020 Apr 28;5(16):9123–30. Available from: https://pubs.acs.org/doi/10.1021/acsomega.9b04071
119. Chen X, Chen J, Wang F, Xiang X, Luo M, Ji X, et al. Determination of glucose and uric acid with bienzyme colorimetry on microfluidic paper-based analysis devices. Biosens Bioelectron [Internet]. 2012 May;35(1):363–8. Available from: https://linkinghub.elsevier.com/retrieve/pii/S095656631200187X
120. Liu F, He J, Zeng M, Hao J, Guo Q, Song Y, et al. Cu–hemin metal-organic frameworks with peroxidase-like activity as peroxidase mimics for colorimetric sensing of glucose. J Nanoparticle Res [Internet]. 2016 May 15;18(5):106. Available from: http://link.springer.com/10.1007/s11051-016-3416-z
121. Lin L, Song X, Chen Y, Rong M, Zhao T, Wang Y, et al. Intrinsic peroxidase-like catalytic activity of nitrogen-doped graphene quantum dots and their application in the colorimetric detection of H2O2 and glucose. Anal Chim Acta [Internet]. 2015 Apr;869:89–95. Available from: https://linkinghub.elsevier.com/retrieve/pii/S0003267015002020
122. Chen J, Xu F, Zhang Q, Li S. N-doped MoS2-nanoflowers as peroxidase-like nanozymes for total antioxidant capacity assay. Anal Chim Acta [Internet]. 2021 Oct;1180:338740. Available from: https://linkinghub.elsevier.com/retrieve/pii/S0003267021005663
123. Gao L, Zhuang J, Nie L, Zhang J, Zhang Y, Gu N, et al. Intrinsic peroxidase-like activity of ferromagnetic nanoparticles. Nat Nanotechnol [Internet]. 2007 Sep 26;2(9):577–83. Available from: http://www.nature.com/articles/nnano.2007.260

124. Kumar S, Bhushan P, Bhattacharya S. Development of a paper-based analytical device for colorimetric detection of uric acid using gold nanoparticles–graphene oxide (AuNPs–GO) conjugates. Anal Methods [Internet]. 2016;8(38):6965–73. Available from: http://xlink.rsc.org/?DOI=C6AY01926A
125. Huang L, Chen J, Gan L, Wang J, Dong S. Single-atom nanozymes. Sci Adv. 2019;5(5).
126. Das B, Franco J Lou, Logan N, Balasubramanian P, Kim M Il, Cao C. Nanozymes in Point-of-Care Diagnosis: An Emerging Futuristic Approach for Biosensing. Nano-Micro Lett [Internet]. 2021 Jan 13;13(1):193. Available from: https://link.springer.com/10.1007/s40820-021-00717-0
127. Mahmudunnabi RG, Farhana FZ, Kashaninejad N, Firoz SH, Shim Y-B, Shiddiky MJA. Nanozyme-based electrochemical biosensors for disease biomarker detection. Analyst [Internet]. 2020;145(13):4398–420. Available from: http://xlink.rsc.org/?DOI=D0AN00558D
128. Wang W, Gunasekaran S. Nanozymes-based biosensors for food quality and safety. TrAC Trends Anal Chem [Internet]. 2020 May;126:115841. Available from: https://linkinghub.elsevier.com/retrieve/pii/S0165993619306739
129. Wong ELS, Vuong KQ, Chow E. Nanozymes for Environmental Pollutant Monitoring and Remediation. Sensors [Internet]. 2021 Jan 8;21(2):408. Available from: https://www.mdpi.com/1424-8220/21/2/408
130. Feng L, Zhang L, Zhang S, Chen X, Li P, Gao Y, et al. Plasma-Assisted Controllable Doping of Nitrogen into MoS 2 Nanosheets as Efficient Nanozymes with Enhanced Peroxidase-Like Catalysis Activity. ACS Appl Mater Interfaces [Internet]. 2020 Apr 15;12(15):17547–56. Available from: https://pubs.acs.org/doi/10.1021/acsami.0c01789
131. Zhou W, Hou D, Sang Y, Yao S, Zhou J, Li G, et al. MoO2 nanobelts@nitrogen self-doped MoS2 nanosheets as effective electrocatalysts for hydrogen evolution reaction. J Mater Chem A [Internet]. 2014;2(29):11358–64. Available from: http://xlink.rsc.org/?DOI=c4ta01898b
132. Johnson KA, Goody RS. The Original Michaelis Constant: Translation of the 1913 Michaelis–Menten Paper. Biochemistry [Internet]. 2011 Oct 4;50(39):8264–9. Available from: https://pubs.acs.org/doi/10.1021/bi201284u
133. Sit JC, Vick D, Robbie K, Brett MJ. Thin Film Microstructure Control Using Glancing Angle Deposition by Sputtering. J Mater Res [Internet]. 1999 Apr;14(4):1197–9. Available from: http://link.springer.com/10.1557/JMR.1999.0162
134. Barranco A, Borras A, Gonzalez-Elipe AR, Palmero A. Perspectives on oblique angle deposition of thin films: From fundamentals to devices. Prog Mater Sci [Internet]. 2016 Mar;76:59–153. Available from: https://linkinghub.elsevier.com/retrieve/pii/S0079642515000705
135. Elias A, Brett M, Harris K, Bastiaansen C, Broer D. Three Techniques for Micropatterning Liquid Crystalline Polymers. Mol Cryst Liq Cryst [Internet]. 2007 Dec 12;477:137–51. Available from: http://www.tandfonline.com/doi/abs/10.1080/15421400701695687
136. Zhang JXJ, Hoshino K. Fundamentals of nano/microfabrication and scale effect. In: Molecular Sensors and Nanodevices [Internet]. Elsevier; 2019. p. 43–111. Available from: https://linkinghub.elsevier.com/retrieve/pii/B9780128148624000028
137. Steele JJ, Brett MJ. Nanostructure engineering in porous columnar thin films: recent advances. J Mater Sci Mater Electron [Internet]. 2007 Jan 8;18(4):367–79. Available from: http://link.springer.com/10.1007/s10854-006-9049-8

138. Hawkeye MM, Brett MJ. Glancing angle deposition: Fabrication, properties, and applications of micro- and nanostructured thin films. J Vac Sci Technol A Vacuum, Surfaces, Film [Internet]. 2007;25(5):1317. Available from: http://scitation.aip.org/content/avs/journal/jvsta/25/5/10.1116/1.2764082
139. Huh YS, Erickson D. Aptamer based surface enhanced Raman scattering detection of vasopressin using multilayer nanotube arrays. Biosens Bioelectron [Internet]. 2010 Jan 15;25(5):1240–3. Available from: https://linkinghub.elsevier.com/retrieve/pii/S0956566309005272
140. Chu H, Huang Y, Zhao Y. Silver Nanorod Arrays as a Surface-Enhanced Raman Scattering Substrate for Foodborne Pathogenic Bacteria Detection. Appl Spectrosc [Internet]. 2008 Aug 1;62(8):922–31. Available from: http://journals.sagepub.com/doi/10.1366/000370208785284330
141. Lin D, Harris KD, Chan NWC, Jemere AB. Nanostructured indium tin oxide electrodes immobilized with toll-like receptor proteins for label-free electrochemical detection of pathogen markers. Sensors Actuators B Chem [Internet]. 2018 Mar;257:324–30. Available from: https://linkinghub.elsevier.com/retrieve/pii/S0925400517320543
142. Kesapragada S V., Gall D. Anisotropic broadening of Cu nanorods during glancing angle deposition. Appl Phys Lett [Internet]. 2006 Nov 13;89(20):203121. Available from: http://aip.scitation.org/doi/10.1063/1.2388861
143. Hasegawa K, Minakata K, Suzuki M, Suzuki O. The standard addition method and its validation in forensic toxicology. Forensic Toxicology [Internet]. 2021 June;39:311-333. Avaialble from: https://doi.org/10.1007/s11419-021-00585-8
144. Gillissen B, Burkle L, Andre B, Kuhn C, Rentsch, Brandl B, Frommer WB, A new family of high-affinity transporters for adenine, cytosine, and purine derivativatives in Arabidopsis. Plant Cell [Internet]. 2000 Feb, 12(2): 291-300. Available from: 10.1105/tpc.12.2.291

Chapter 3: Amperometric determination of xanthine using nanostructured NiO electrodes loaded with xanthine oxidase[1]

Anuja Tripathi[1,2], Anastasia L. Elias[1], Abebaw B. Jemere[2], Kenneth D. Harris[2,3]

[1]Department of Chemical and Materials Engineering, University of Alberta, Donadeo Innovation Centre for Engineering, Edmonton, Alberta, T6G 1H9, Canada

[2]National Research Council Canada, Nanotechnology Research Centre, Edmonton, Alberta, T6G 2M9, Canada

[3]Department of Mechanical Engineering, University of Alberta, Edmonton, Alberta, T6G 1H9, Canada

---

3.1 Abstract

Nickel oxide (NiO) thin film electrodes prepared by glancing angle deposition (GLAD) were investigated for enzymatic electrochemical quantification of xanthine, a noted indicator of meat freshness. The large surface area of the macroporous GLAD NiO electrodes provided a suitable scaffold to successfully immobilize the enzyme xanthine oxidase (XO) via physisorption, and resulted in an enhanced amperometric signal in a reagent-free alkaline medium due to the surface bound redox probe ($Ni^{2+/3+}$). The immobilization of XO onto the GLAD NiO electrode was characterized by cyclic voltammetry, electrochemical impedance spectroscopy and x-ray photoelectron spectroscopy. Parameters affecting the performance of the enzymatic

[1] A version of this chapter has been submitted for publication as: Anuja Tripathi, Anastasia L. Elias, Abebaw B. Jemere, Kenneth D. Harris, Amperometric determination of xanthine using nanostructured NiO electrodes loaded with xanthine oxidase.

biosensor (such as the amount of immobilized XO, applied potential, temperature, and dissolved oxygen content) were examined and optimized. Under optimal conditions, the fabricated xanthine biosensor exhibited a rapid response (~7 s), wide dynamic range (0.1 μM – 650 μM), good reproducibility (relative standard deviation of ~4%, n=18), superior limit of detection (37 nM), and very high sensitivity (1.1 $\mu A \cdot \mu M^{-1} \cdot cm^{-2}$ in the low concentration range from 0.1-5 μM, and 0.3 $\mu A \cdot \mu M^{-1} \cdot cm^{-2}$ in the higher concentration range from 5-650 μM). The biosensor was also evaluated against a selection of potential interferents commonly found in fish samples (hypoxanthine, uric acid, glucose, and sodium benzoate), demonstrating good selectivity toward xanthine. A low Michaelis-Menten constant (K_m) of 0.4 mM for xanthine signifies the high affinity of the enzymatic sensor towards the target analyte. Measurements in real fish samples were also successfully performed, revealing strongly increased xanthine sensitivity in the presence of fish matrix (from 0.085 $\mu A\ \mu M^{-1}$ without fish extract to as much as 0.27 $\mu A\ \mu M^{-1}$).

KEYWORDS: xanthine, glancing angle deposition, food freshness sensing, biosensing, amperometry, nanostructured electrodes

3.2 Introduction

Fish and fishery products are easily perishable, undergoing rapid biochemical decomposition and microbiological spoilage.[1] Immediately following the death of fish, enzymatic degradation of adenosine triphosphate (ATP) begins, resulting in the formation of xanthine (3,7-dihydropurine-2,6-dione) as one of the major catabolites.[2] Because the concentration of xanthine increases with storage time, measuring xanthine concentration is considered as an important means to assess fish meat freshness.[3] High levels of xanthine in human biological fluids (≳4 μM in serum, ≳17 μM in

urine) have also been linked to increased risk of leukemia and kidney stones,[3] hence quantitative determination of xanthine is also of clinical importance. Classical analytical methods such as chromatography coupled with spectroscopy or mass spectrometry detections[4,5] and enzyme-linked immunosorbent assays[3] have high xanthine sensitivity and reliability. However, these techniques tend to be time-consuming, require skilled personnel, and are not suitable for in-field analysis. By comparison, biosensors (particularly electrochemical biosensors) can offer faster response times than other methods, and are relatively easy to miniaturize and inherently better-suited to in-field measurements.[3]

Enzymatic amperometric biosensors that utilize immobilized redox enzymes are attractive due to their high sensitivity, selectivity, rapid response time, low cost, and ease of integration, making them promising for inexpensive disposable sensors.[6] Xanthine oxidase (XO), for instance, specifically catalyzes the oxidation of xanthine to uric acid. Therefore, incorporating XO at the working electrode yields electrochemical sensors with selectivity for xanthine. The underlying electrode materials, however, also play a critical role in the construction of high performance electrochemical sensing platforms, and therefore, a variety of electrode materials including conducting polymers, metal and metal oxide nanoparticles, and graphenic nanomaterials, have been reported as efficient XO-immobilizing matrices for amperometric determination of xanthine in both food samples and clinical diagnosis.[3,7] In recent years, the surface-bound (Ni^{2+}/Ni^{3+}) redox pairs of nickel oxide (NiO) have attracted particular attention for the development of both enzymatic[8–10] and non-enzymatic amperometric biosensors[11,12] due to NiO's biocompatibility, conductivity, and electrocatalytic properties. The high isoelectric point (IEP) of NiO (pH 10.7) can aid in the electrostatic immobilization of enzymes with low IEP (pH 4.0±0.1 for XO); NiO electrodes have previously been used for enzymatic electrochemical determinations of glucose, urea, and xanthine.[8–10,13]

Nanostructured metal oxide electrodes, fabricated by chemical and physical deposition techniques, have received considerable attention as immobilizing matrices for electrochemical biosensors due to their high surface area and fast electron transfer kinetics.[10,14,15] One of the few methods for fabricating meso- and macro-porous metal and metal oxide electrodes with a high degree of control over morphological properties such as shape, porosity, density, and film thickness is the glancing angle deposition (GLAD). GLAD is a single-step physical vapor deposition technique that combines oblique angle deposition with precise substrate motion to create nanocolumnar structures with an open and accessible pore structure. These GLAD-derived nanostructures have been used as supports for protein and enzyme immobilization,[10,17,19] as well as electrodes for enzyme-free electrochemical determination of glucose and hydrogen peroxide.[11,12] They have also been integrated in microfluidic systems.[17]

In this work, we report the development of a highly sensitive and reagent-free amperometric biosensor for xanthine determination using XO immobilized on nanostructured NiO thin films formed by GLAD. These electrodes have a high specific surface area and well-defined porosity, and the response of the biosensors to micromolar concentrations of xanthine in the presence of known interfering compounds (including real-world fish samples) is optimized and studied in detail.

3.3 Materials and Methods

3.3.1 Chemicals and reagents

Xanthine (XA), uric acid, phosphate buffered saline (PBS), glucose, hypoxanthine, xanthine oxidase (XO) from bovine milk, potassium ferricyanide [$K_3Fe(CN)_6$], potassium ferrocyanide [$K_4Fe(CN)_6$], and potassium nitrate (KNO_3) were purchased from Sigma-Aldrich Canada (Oakville, ON). Sodium benzoate, sodium hydroxide (NaOH), and isopropanol (IPA) were

purchased from Fisher Scientific Canada (Toronto, ON). All chemicals were used without further purification. ITO coated glass substrates (8-12 Ω/□ for sensing, 15-30 Ω/□ for optimization) were purchased from Delta Technologies Limited (Loveland, CO, USA), and NiO pellets (2-3 mm, 99%) were obtained from Heeger Materials (Denver, CO, USA). High resistivity, ultrapure water (18.2 MΩ·cm) used for sample preparation was obtained using a Barnstead Nanopure Diamond water purification system (Fisher Scientific, Toronto, ON). Canned tuna fish (packaged in an airtight tin preventing microbial interactions) was purchased from a local supermarket. Stock solutions of xanthine, hypoxanthine, glucose, uric acid, and sodium benzoate were prepared in 0.1 M NaOH and were used the same day. (Caution! NaOH is corrosive and can irritate the skin. Wear appropriate protection.)

3.3.2 Fabrication of macroporous NiO electrodes

0.5 μm thick GLAD NiO films were deposited on ITO substrates using a previously published protocol.(177) Briefly, ITO substrates were first cleaned by successive 30 min sonication processes in soapy water, IPA, and deionized water. The electrodes were then dried in an N_2 stream and masked with Kapton tape (Caplinq, Ottawa, ON, Canada) to leave a 0.28 cm^2 circular area exposed on one side. The masked substrates were mounted on an aluminum plate using Kapton tape, and then loaded into a GLAD-enabled electron beam evaporation system (Kurt J. Lesker Company, Clairton, PA, USA), which was equipped with computer-controlled stepper motors for rotating and tilting the substrate holder. NiO pellets were placed in graphite crucible liners, and the vacuum chamber was evacuated to $<8\times10^{-7}$ Pa. During deposition, an e-beam emission current of 80 mA with a 6.5 kV accelerating voltage led to a NiO deposition rate of ~0.5 nm s^{-1} at deposition pressure of $\sim4\times10^{-5}$ Pa. Vertical post NiO films were deposited by fixing the deposition angle at 80° with respect to the substrate normal, and continuously rotating the substrates at a rate of one complete rotation for every 10 nm of film growth. For comparison purposes, NiO controls

were also prepared in a separate process. For these control samples, equivalent substrates, cleaning processes, deposition equipment, materials and substrate rotation rates were used, but the samples were coated with NiO using a near normal (0°) deposition angle to a thickness of 500 nm. For analysis by scanning electron microscopy (SEM, Hitachi S-4800, Japan), small pieces of (100) Si wafers were also included on the aluminum sample plate and coated with NiO in the same GLAD processes.

3.3.3 Preparation of enzyme-loaded electrodes

Prior to enzyme immobilization, GLAD NiO electrodes were first electrochemically activated by applying a potential between 0.0 V and +0.8 V in 0.1 M NaOH at a scan rate of 10 mV/s for 25 cycles, followed by rinsing in deionized water and air-drying at room temperature. To load the enzyme, 20 µl of 2 mg/ml XO (prepared in 0.01 M PBS buffer, pH 7.4) was pipetted onto the surface of the electrode, which was then placed in a humidified petri dish for four hours at room temperature. (20 µl of enzyme solution was sufficient to fully cover the exposed circular area of the electrode surface.) Subsequently, the enzyme-modified electrode was washed with PBS buffer to remove unbound enzyme. When not in use, the electrodes were kept at 4°C in PBS buffer. The modification of GLAD NiO electrodes by XO was characterized by cyclic voltammetry, electrochemical impedance spectroscopy (EIS) and x-ray photoelectron spectroscopy (AXIS 165 Spectrometer, Kratos Analytical Inc., Spring Valley, NY).

3.3.4 Electrochemical characterization

All electrochemical measurements were performed using a potentiostat (Reference 600, Gamry Instruments Inc., Warminster, PA, USA) in a 3-electrode configuration, with Ag/AgCl (3 M NaCl saturated solution) reference electrode (BASi, West Lafayette, IN, USA), a Pt coil counter electrode, and the NiO thin films used as the working electrode. Prior to electrochemical experiments, the working electrodes were activated by cycling in the potential window of 0.0 V to

+0.8 V for ~8 cycles in 0.1 M NaOH with a 10 mV/s scan rate. EIS was performed in a 0.1 M KNO_3 solution containing 1 mM $[Fe(CN)_6]^{3-/4-}$ redox couple. Chronoamperometry (CA) experiments were performed while the solution was magnetically stirred at ~ 200 RPM. With the exception of the optimization experiments, all CA tests were performed by applying +0.5 V (vs. Ag/AgCl) to an electrode immersed in a 50 ml 0.1 M NaOH solution that was saturated with oxygen (bubbled for one hour) at a temperature of 30 °C. Following an initial stabilization period of ~300 s, XA or interferent solutions (1 mM or 26 mM) were pipetted into the oxygen-saturated 0.1 M NaOH solution at intervals of 200 s. To generate the XA dose response curve for the biosensor, the first few injections were 5 µl, 20 µl, and 30 µl from 1 mM XA stock, followed by 40 µl, 50 µl, and 60 µl from 26 mM XA stock, and finally successive injections of 70 µl from 26 mM XA stock solution.

Enzymatic reaction kinetics were calculated from the CA experimental data by fitting against the Michaelis-Menten equation shown in equation (1),

$$\frac{1}{V} = \frac{K_m}{V_{max}}\left(\frac{1}{[XA]} + \frac{1}{K_m}\right) \qquad (1)$$

where, V is the reaction rate for the substrate concentration [XA], V_{max} is the maximum reaction rate at high concentration, and K_m is the Michaelis-Menten constant, representing the substrate concentration at which the reaction rate is half of the maximum value. The reaction rates were calculated based on their proportionality with the measured current (I) using: $V = I / (F \times v)$, where F, and v are the Faraday constant (F=96485.33 C/mol) and the volume of the electrochemical cell (i.e., 50 ml), respectively.

The areas under the anodic CV peaks for electrodes cycled in NaOH were used to calculate the surface coverage (Γ) of $NiOOH/Ni(OH)_2$ for the GLAD NiO and planar NiO electrodes using: Γ

= Q/nFA, where Q is integrated charge, n is number of electrons per redox process (i.e., 1), F is Faraday's constant, and A is the geometrical area of the electrodes (0.28 cm^2).

3.3.5 Fish sample preparation and analysis

Canned tuna fish was purchased from a local supermarket, and to minimize variation, the same product type was used for all experiments. The tuna extract was prepared based on an established procedure.[18,19] Briefly, fish meat was stored uncovered at room temperature, and 5 g samples were removed as needed (after 0 to 7 days of storage). Each 5 g sample was ground using a mortar and pestle and homogenized in 25 ml of PBS by stirring manually for ~60 s. The homogenous solution was then passed through cellulose filter paper (Whatman) with a pore size of 11 µm, and the collected filtrate was diluted 1:1 with 0.1 M NaOH and analyzed by CA at the experimentally optimized conditions. Distinct calibration plots were determined for each aged fish sample using the standard addition method. For each, 50 µl of the fish filtrate solution was first spiked into 50 ml of 0.1 M NaOH, and the change in CA current was recorded and plotted as the electrode response to zero added XA. The remainder of the points in each series were generated by spiking with fixed 50 µl volumes of 13 mM xanthine in 50 mM NaOH and recording the CA response. The data were fit by linear regression.

3.4 Results and Discussion

3.4.1 NiO electrode fabrication and characterization

Macroporous vertical post NiO films were deposited onto ITO-coated glass substrates by GLAD. The morphology of an electrode characterized using SEM is shown in Fig 1. Overall, the film structure consisted of loosely-packed, vertical columnar nanostructures that were 500 nm in height and separated from one another by gaps of 60-90 nm. This structure has been shown previously to massively amplify the surface area of the electrode (as compared with a flat surface),[14] providing

ample area for immobilization of large quantities of xanthine oxidase (XO). For biosensor applications requiring enzyme immobilization, macroporous (pore sizes of >50 nm) and mesoporous (pore sizes of 2 – 50 nm) surfaces are favored over microporous (pore size < 2 nm) surfaces as they correlate well with the diameter of enzymes.

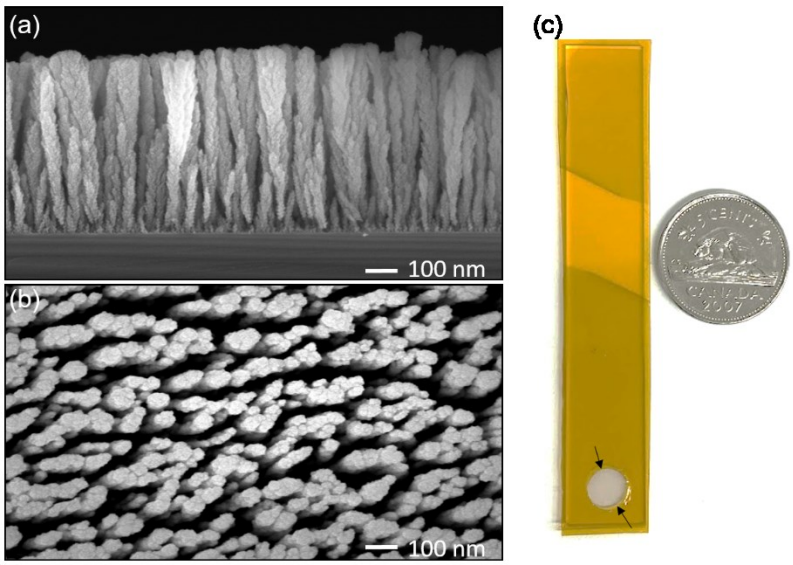

Figure 3.1: Scanning electron microscope images of GLAD NiO films on Si substrates. (a) cross-sectional view, (b) top view, and (c) image of electrode where the exposed circular part (surrounded by arrows) is a NiO GLAD film.

3.4.2 Immobilization of XO on GLAD NiO electrode

Prior to enzyme immobilization, the GLAD NiO electrodes were activated by cycling in 0.1 M NaOH until stable CV curves were obtained, and a representative series of CV curves taken during an activation process (25 cycles from 0 V to +0.8 V vs. Ag/AgCl) is depicted in Fig 3.2.

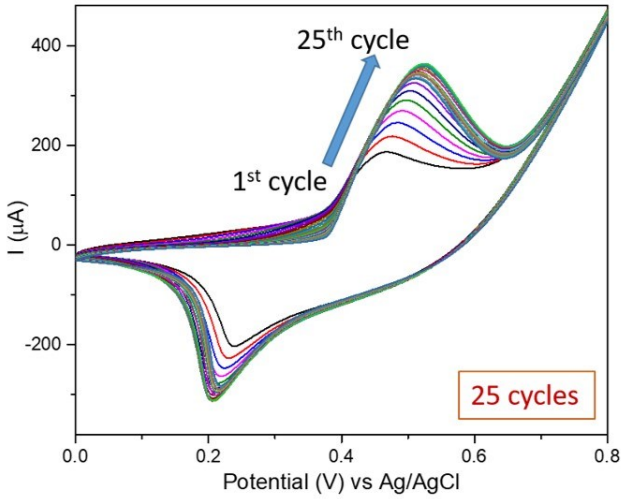

Figure 3.2: Electrochemical conditioning of the NiO electrode using cyclic voltammetry in 0.1 M NaOH from 0 to +0.8 V at 10 mV/s.

The peak currents increased from 160 µA to 360 µA during the 25 activation cycles, and there was no significant current increase for cycles >25. This increase in current was accompanied by a shift in the anodic and cathodic peak potentials, together with a visual change in the electrode's appearance from a cloudy grey color to a uniform black color. These changes can be attributed to progressive surface enrichment in $Ni(OH)_2$/NiOOH species, according to reactions (2-3) below.[12] The anodic sweep in alkaline media first converts NiO to nickel hydroxide, $Ni(OH)_2$, and scanning the electrode to higher potentials further oxidizes the electrode from Ni^{2+} to Ni^{3+} in the form of NiOOH:

$$2NiO + 4OH^- \longrightarrow 2Ni(OH)_2 + O_2 + 4e^- \quad (2)$$

$$Ni(OH)_2 + OH^- \rightleftharpoons NiOOH + H_2O + e^- \quad (3)$$

This activation process is crucial to generate the stable electrocatalytic $Ni(OH)_2$/NiOOH redox pair, which interchanges electrons during the cathodic and anodic sweeps. A series of CV curves

for an activated electrode taken at a range of scan rates from 10 mV/s to 150 mV/s is shown in Fig 3.3. From the CV curves of activated electrodes, we estimated the surface concentration, Γ (from $\Gamma = Q/nFA$), of the redox active Ni^{2+}/Ni^{3+} species to be $6.3 \pm 0.5 \times 10^{-7}$ mol cm^{-2}, which is similar to a previously reported value for a GLAD NiO electrode[11] and two orders of magnitude higher than a planar NiO electrode fabricated in a conventional (non-GLAD) thin film deposition process (data not shown). For an ideal surface-bound redox species, CV at slow scan rates results in oxidation/reduction peaks without separation, and peak currents that are proportional to scan rate.[12] The CV curves in Fig 3.3, however, show asymmetrical redox peaks even at low scan rates (ΔE = 0.164 V at 10 mV/s), indicating a quasi-reversible redox process at the Ni^{2+}/Ni^{3+} GLAD electrode. This deviation from ideality may be attributed to mechanisms we identified previously.[11] In the present work, the plot of peak potential *vs.* log(ν) shows both the anodic and cathodic potentials increased linearly ($R^2 > 0.99$, in the range of 40-150 mV/s). Using the Laviron method[20],we estimate electron transfer coefficients (α) of 0.74 and 0.35 for the anodic and cathodic processes, respectively. These values are similar to what has been reported for GLAD NiO electrodes fabricated on Ni substrates.[11] Since α is used to describe the symmetry between the forward and reverse electron transfer steps, these values indicate an asymmetric reaction favoring NiOOH.

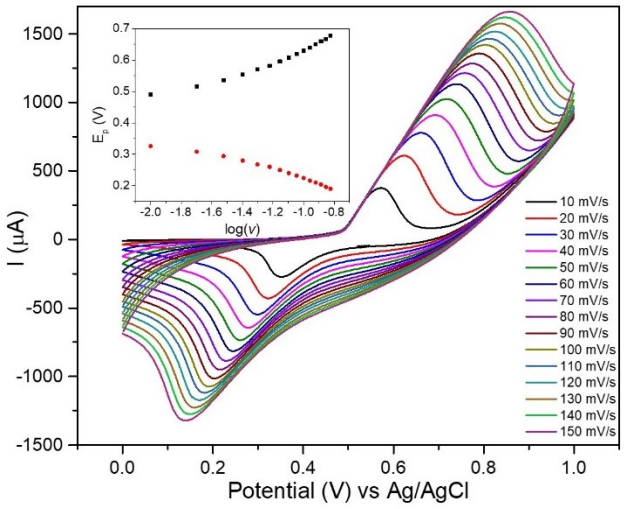

Figure 3.3: Cyclic voltammograms for NiOOH electrode in 0.1 M NaOH at varying scan rates ($_v$) from 10 mV/s to 150 mV/s. Inset: relationship between log (v) and peak potential (E_p) where anodic and cathodic peak potentials are in black and red, respectively.

The GLAD NiO nanocolumns are separated by significantly greater distances (60-90 nm) than the diameter of XO (~7.4 nm), and thus, we expect that when the electrodes are immersed in XO-containing solution, the enzyme will penetrate into the pore structure to interact with the columns. Because XO's isoelectric point is lower than the solution pH, the enzyme carries a negative charge, and we expect this property to encourage physisorption of XO at the positively-charged NiOOH surface. Therefore, XO was immobilized on the surface of activated NiO/NiOOH electrodes by applying a fixed volume of aqueous XO solution (20 µl) to the exposed electrode. Three XO concentrations were evaluated (1 mg/ml, 2 mg/ml, and 4 mg/ml), and in each case, weakly-bound XO was removed from the electrode by washing thoroughly with PBS solution (for 20-30s), leaving only immobilized XO on the surface. After this immobilization process, the electrodes were studied by CV, EIS, and XPS to understand the changes in electrical characteristics and chemical compositions of the modified electrodes. The CVs of freshly activated and XO-modified NiO/NiOOH electrodes (modified in a 2 mg/ml solution) are shown in Fig 3.4, and these CVs indicate that the peak oxidation and reduction currents decreased significantly after XO modification (the peak oxidation current decreased from 330 µA for the unmodified electrode to 260 µA for the XO-modified electrode), and the peak potential slightly shifted from 0.52 V to 0.48 V. The peak separation was found to be reduced, indicating the enhanced redox catalytic activity of the enzyme modified electrode. Similar trends were observed in previous studies of NiO-based enzymatic electrochemical sensors for xanthine and urea,[8,13] and based on these previous findings we attribute these changes to the adsorption of XO on the electrode surface.

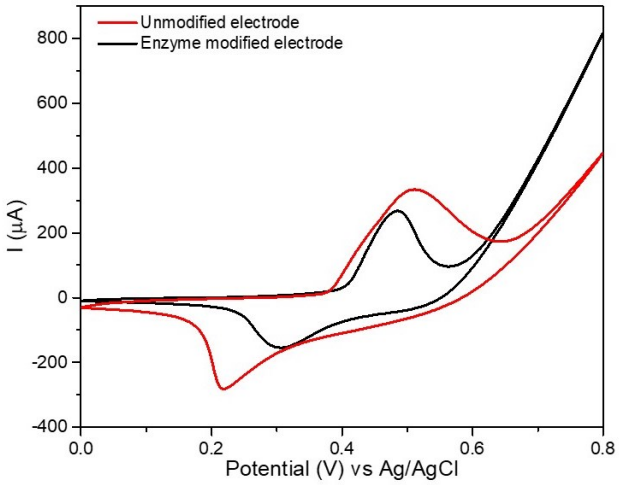

Figure 3.4: Cyclic voltammetry scans of unmodified NiOOH electrode (red) and XO-modified (2 mg/ml) ITO/$Ni(OH)_2$ electrode (black) in 0.1 M NaOH at 10 mV/s.

Interfacial properties of bare and XO-modified electrodes were also studied by EIS in the frequency range of 10^{-1} to 10^5 Hz, and the impedance responses of these electrodes in $[Fe(CN)_6]^{3-/4-}$ solution are shown in Fig 3.5. Each EIS spectrum can be modeled by a Randles circuit (Fig 3.5, inset), consisting of two resistive elements (series resistance, R_s, and charge transfer resistance, R_{ct}), a Warburg element (W), and a capacitor representing the double layer (C). The values of each element best fitting the EIS spectra for the three different concentrations are shown in Table 3.1. Warburg frequency specific parameter (Zw) can be calculated using Warburg coefficient (Aw): $Zw = Aw/\omega^{1/2} - Aw/\omega^{1/2}$. For the ITO substrate (spectrum not shown) and bare GLAD NiO electrode, R_{ct} was estimated to be 338 Ω and 420 Ω, respectively. Significantly higher R_{ct} values were determined for the XO modified electrodes: 1.2 kΩ, 3.5 kΩ, and 2.9 kΩ for GLAD NiO electrodes modified with 1 mg/ml, 2 mg/ml, and 4 mg/ml XO solutions, respectively. The increase in charge transfer resistance suggests the formation of an electrically-insulating barrier after the XO immobilization process, which impedes electron transfer between the redox probe and the

electrode surface. The maximal charge transfer resistance was observed for the electrode treated with the 2 mg/ml enzyme solution, implying that the most complete XO coverage was observed for this treatment, and no noticeable benefits were observed from higher enzyme concentration. Therefore, we used 2 mg/ml XO treatments in all subsequent studies.

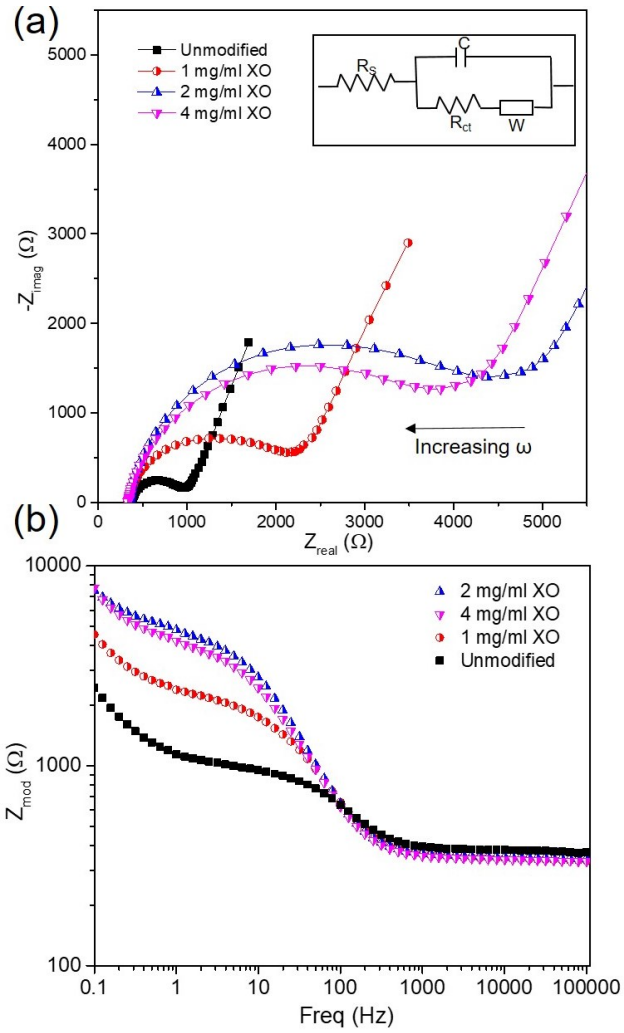

Figure 3.5: Electrochemical impedance characterization of bare and XO-modified GLAD NiO electrodes. (a) Nyquist plot and (b) Bode plot. Impedance was measured at frequencies (ω) of 0.1 Hz to 100 kHz using 1 mM $[Fe(CN)]^{3-/4-}$ prepared in 0.1 M KNO_3. Electrodes are either untreated with XO solution (black) or treated by immersion in 1 mg/ml (red), 2 mg/ml (blue), or 4 mg/ml (pink) XO solution for four hours at room temperature (inset: equivalent Randles circuit model, C: double-layer capacitance, W: Warburg impedance, R_s: electrolyte resistance, R_{ct}: charge transfer resistance).

Table 3.1: Best fitting elements from EIS spectra

Electrode	R_{ct} (Ω)	R_s (Ω)	C (nF)	A_W ($\Omega \cdot s^{-1/2}$)
Bare NiO	420	378	12.7	918
1 mg/ml enzyme modified NiO electrode	1.2×10^3	338	4.0	4958.7
2 mg/ml enzyme modified NiO electrode	3.5×10^3	349	1.4	2549.9
4 mg/ml enzyme modified NiO electrode	2.9×10^3	339	1.5	2675.4

To further confirm the XO modification of GLAD NiO electrodes, the surface chemical compositions of bare and XO-modified GLAD NiO electrodes were investigated by XPS, and the results are shown in Fig 3. In Fig 3(a), peaks located at 854.6 eV (with its associated satellite peak at 861.6 eV) and 856.3 eV are assigned to $Ni^{2+/3+}$ in oxides.[21,22] The peak at 873.5 eV (with its satellite peak at 879.4 eV) also indicates the presence of Ni^{2+} in the bare electrode.[23,24] For the XO-modified electrode, the $Ni^{2+/3+}$ peaks shift to slightly higher binding energies (now 855.6 eV with satellite at 862.5 eV), [25] and all Ni(2p) peaks were present with much lower intensity than for the bare electrode, which is consistent with the formation of a shielding layer over the electrode surface. Neither N nor S (Fig 3b and 3c) was observed in the bare electrode, which is consistent with a NiO surface without protein modification. The XO-modified electrode, on the other hand, exhibited an N(1s) peak at 399.9 eV (Fig 3b) corresponding to amines present in the protein structure. Normally, amine peaks are observed at higher binding energies around 401.9 eV, however, this reduced binding energy has been observed previously in the literature and attributed

to amine/amide interactions with metallic structures (which are consistent with our activated NiO electrodes).[26] In Fig 3c, peaks are also observed in the S(2p) spectrum for the XO-modified electrode (but not for the bare electrode) at 164.5 eV and 163.8 eV, and these are attributed to C-S-C and C-SH, respectively, which are expected within methionine and cysteine groups in the XO structure.[27] In Fig 3d, the spectra for the P(2p) regions are shown. A very small peak at ~133.6 eV (normally attributed to P-O)[28] is observed for the bare electrode, but because the peak intensity is low and the phosphorous source is unclear, we suspect this is the result of adventitious contamination before XPS characterization. After XO-modification, however, the P(2p) peak is much stronger, consistent with the phosphate residue in the active site of XO.[29,30] Overall, these XPS results support the electrochemical data shown above and confirm that an XO layer has been formed over the NiO GLAD electrode following treatment in XO solution.

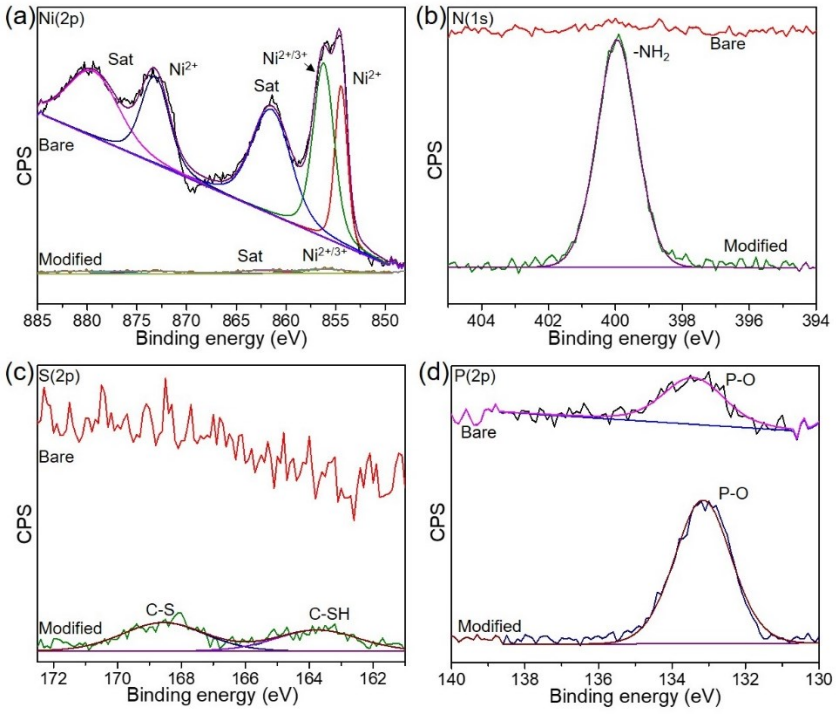

Figure 3.6: XPS spectra and fitting curves for bare and XO-modified NiO electrodes in the bindng energy regions associated with Ni (a), N (b), S (c), and P (d).

3.4.3 Xanthine response of XO-modified GLAD NiO electrodes

Xanthine oxidase is a homodimer containing one flavin adenine dinucleotide (FAD), one molybdenum cofactor (Moco), and two iron-sulfur centers in each of its two subunits.[31,32] Although aspects of the mechanism by which XO catalyzes XA oxidation remain uncertain, most proposed reaction schemes share some common features. The reaction requires XA binding to Moco and donation of its two electrons to the enzyme, thereby reducing Mo^{6+} to Mo^{4+}. The two electrons are then shuttled from the Moco to the FAD cofactor through the iron-sulfur centers, reducing FAD to $FADH_2$.[31,32] This reductive half reaction is summarized in reaction (4). Electrons are then transferred from the enzyme to NiOOH sites on the GLAD electrode surface according to reaction (5), yielding $Ni(OH)_2$ and reoxidizing the $XO(FADH_2)$ to its original XO(FAD) form. The $Ni(OH)_2$/NiOOH redox pair is a good substrate for XO's redox activity since it can efficiently exchange protons and electrons. To complete the reaction process, $Ni(OH)_2$ is reoxidized to NiOOH according to (6), and electrons originally resident within XA are released into the circuit for detection.

$$2XO(FAD) + 2XA + O_2 \longrightarrow 2XO(FADH_2) + 2\text{Uric acid} \quad (4)$$

$$XO(FADH_2) + 2NiOOH \longrightarrow XO(FAD) + 2Ni(OH)_2 \quad (5)$$

$$Ni(OH)_2 + OH^- \rightleftharpoons NiOOH + H_2O + e^- \quad (6)$$

The CV characteristics of the bare and XO-modified GLAD NiO electrodes as functions of XA concentration are presented in Fig 3.7 and 3.8, respectively. For the bare GLAD NiO electrodes (Fig 3.7), no current increase was observed when the electrode was exposed to XA at concentrations as high as 490 µM, suggesting that XA cannot be directly oxidized by the NiO GLAD electrode. However, for the XO-modified electrodes (Fig 3.8), we observed that the peak current slowly increased from 130 µA to 150 µA as the XA concentration was increased from 0 to

270 µM, indicating the enzyme catalyzed oxidation of xanthine and subsequent electronic transport between XO and GLAD NiO electrodes.

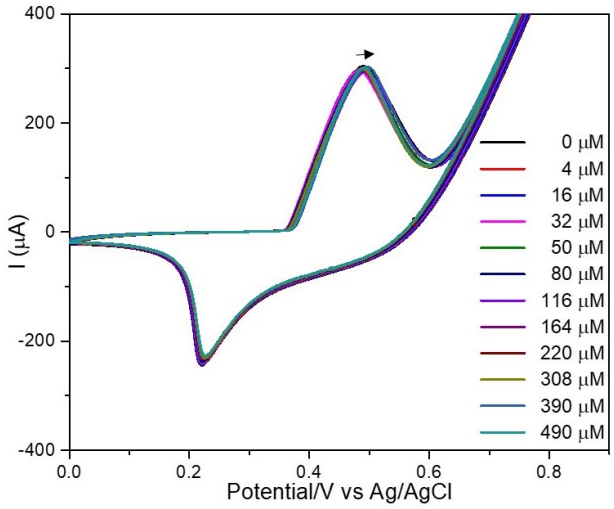

Figure 3.7: Cyclic voltammograms for an unmodified NiO/NiOOH electrode in 0.1 M NaOH solutions with various XA concentrations. The scan rate was 10 mV/s, and the arrow indicates the direction of increasing XA concentration.

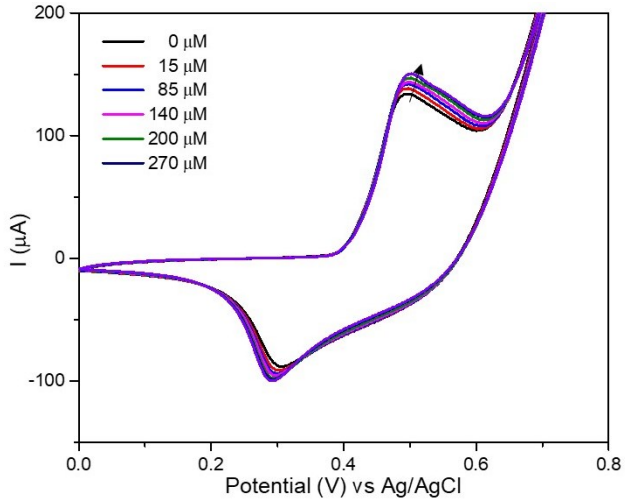

Figure 3.8: Cyclic voltammograms for the NiO/NiOOH electrode modified in 2 mg/ml XO solution in the presence of various XA concentrations. This experiment was performed in 0.1 M NaOH solution at 10 mV/s, and the arrow indicates the direction of increasing XA concentration.

3.4.4 Xanthine determination by chronoamperometry

As CA is generally considered more relevant than CV to real-world sensor implementations, we measured the CA response of XO-modified electrodes operating at a range of applied potentials (+0.4 V to +0.6 V vs. Ag/AgCl) to the addition of 78 µM xanthine. These results are shown in Fig 3.9. We found that the amperometric response increased for applied potentials from +0.40 V to +0.50 V, and then decreased with further potential increments. As a result, the XO-modified electrode's optimum operating potential was determined to be +0.50 V, which matches the peak potential found by CV in Fig 3.8.

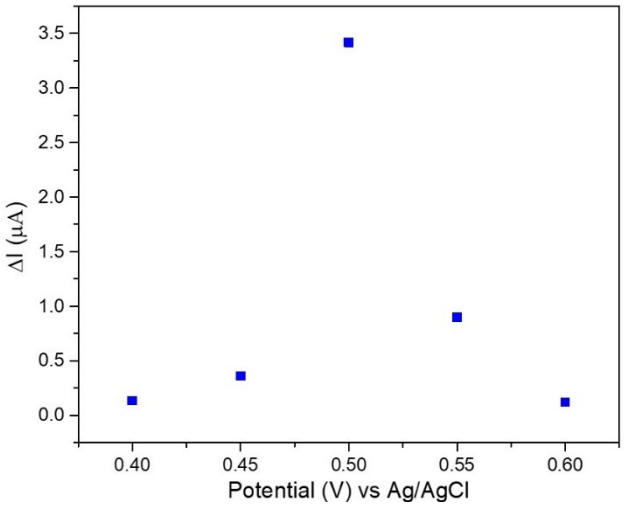

Figure 3.9: Change in chronoamperometry current produced for an XO-modified electrode in response to the addition of 78 µM XA at various cell potentials. The electrodes and electrolyte solution were at room temperature and no oxygen bubbling was employed.

It is well documented that both temperature and dissolved oxygen concentration can affect the performance of enzymatic reactions,[33] and therefore, the effects of temperature and oxygenation over the electrochemical responses of XO-modified electrodes were also studied. As shown in Fig 3.10, the XO-modified electrode's response to the addition of 265 µM XA gradually increased with

temperature from 20 to 37 °C, then dropped dramatically at higher temperatures. The decrease in amperometric response at higher temperatures (> 37 °C) could be due to a decrease in dissolved oxygen content of the solution or thermal deactivation of the enzyme,[34] but we also believe that delamination of GLAD NiO from the ITO substrate – which was observed at higher temperatures, and possibly arises from interfacial stress due to thermochemical processes involving NiO and NaOH – is also a factor. While the best response was achieved at 37 °C, we noted that sensors couldn't be used for more than a single experiment at this temperature due to NiO delamination, and this observation may also implicate the delamination process in the reduced CA performance at even higher temperatures. Therefore, 30 °C was selected for all further experiments.

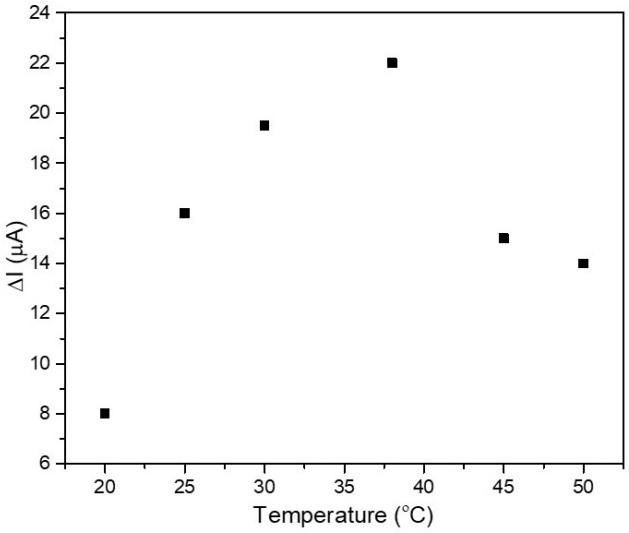

Figure 3.10: Change in chronoamperometry current produced for an XO-modified electrode at various temperatures in response to the addition of 265 μM XA. Electrodes were maintained at a constant applied potential of 0.50 V vs. Ag/AgCl in 0.1 M NaOH.

As shown in equation (4), dissolved oxygen is one of the substrates in the enzymatic oxidation of xanthine, and therefore, the effect of dissolved oxygen content on the sensor's amperometric response to XA was studied by bubbling oxygen into the NaOH solution for one hour. The data

depicted in Fig 3.11 and 3.12b show that the sensitivity of the sensor tested using an O_2 saturated solution at 30°C was found to be 6.5, 1.8 and 1.1 times higher than those of similarly-prepared sensors tested in ambient solution at room temperature, O_2 saturated solution at room temperature, and ambient solution at 30°C, respectively. Thus, O_2 saturated NaOH solution at 30°C was used in all subsequent studies.

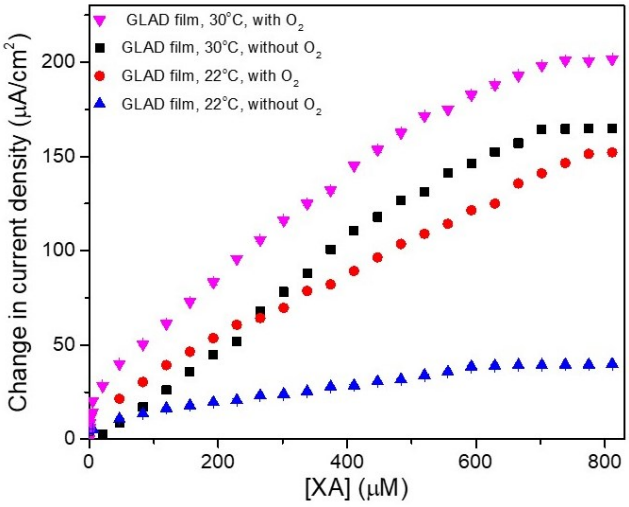

Figure 3.11: Calibration curves for electrode responses to added XA using a GLAD film at 30°C in oxygenated solution (pink triangles), without oxygenation at 30°C (black squares), a GLAD film at 22°C in an oxygen saturated solution (red circles), and a GLAD film at 22°C without oxygenation (blue triangles).

The CA response of the XO-immobilized GLAD NiO electrode as increasing concentrations of XA are added to an oxygen-saturated solution at 30°C is presented in Fig 3.12a. With each XA addition, the XO-immobilized electrode responded rapidly by reaching 95% of the steady-state current within ~7.5 s, which indicates a relatively fast response in comparison to previously reported values (30 s and 15 s).[35,8] In Fig 3.12b, current density is plotted vs. XA concentration, with each data point representing a mean value from three independent XO sensors fabricated and tested under the optimized conditions. Two linear regions with distinct slopes were observed in

the 0.1-5 μM (slope = 0.3 μA/μM, R^2 = 0.942) and 5-650 μM (slope = 0.085 μA/μM, R^2 = 0.995) ranges. In the literature, similar dose response curves with two or even three distinct linear regions have been reported for amperometric determination of XA using XO modified electrodes,[36,37] which was ascribed to the nature of the interaction of the XO redox center with the electrode surfaces. Using the sensitivity (slope) of the sensor in the lower concentration range (0.3 μA/μM), we calculated a theoretical limit of detection (LOD, which is 3σ/slope, where σ is the standard deviation for the lowest measured concentration) of 37 nM XA.

To better demonstrate the effect of the massive surface area enhancement induced by the GLAD process, we compared the enzymatic electrochemical sensor performance of the NiO GLAD electrode to that of a 500 nm thick, planar NiO film deposited on ITO-coated glass without a GLAD process. As shown in Fig 3.12b, the GLAD NiO-based sensor yielded far superior sensitivity (0.3 μA/μM) compared to the flat NiO-based enzymatic sensor (0.01 μA/μM). The high sensitivity of the GLAD NiO-based XA sensor is attributed to the high surface area of the GLAD electrode and the associated increase in immobilized XO. The greater sensitivity of the GLAD-based sensor is also consistent with previous reports of proteins (including enzymes) immobilized on GLAD NiO and ITO electrodes leading to high sensitivity electrochemical biosensors.[13,14,38] In the literature, a variety of nanomaterials and nanostructured thin films have been modified with XO for the electrochemical determination of XA; the performance of a variety of such sensors is summarized in Table 3.2. Our sensor compares favorably displaying very wide linear range, high sensitivity and a sub-μM detection limit.

In order to understand the affinity of the XO-modified GLAD NiO electrode for XA, Michaelis-Menten kinetics were studied by measuring the CA current responses as a function of time for various XA concentrations (10 μM – 104 μM) as shown in Fig 3.12c. When the potential is applied

at t = 0, the current immediately increases to a large value, then declines until a diffusion-limited steady state is reached. Both the steady state current and the time required to attain equilibrium generally increase with substrate concentration. The Lineweaver-Burk plot in Fig 3.12d was used to determine V_{max} (0.8 µM/s) and K_m (0.4 mM). The low apparent K_m value indicates the immobilized enzyme has a high affinity for XA compared to most of the literature reported sensors, as shown in Table 3.2. It is, however, important to note that these studies used various XO functionalization materials and methods to fabricate enzyme modified electrodes, and as such direct comparison of K_m values is difficult.

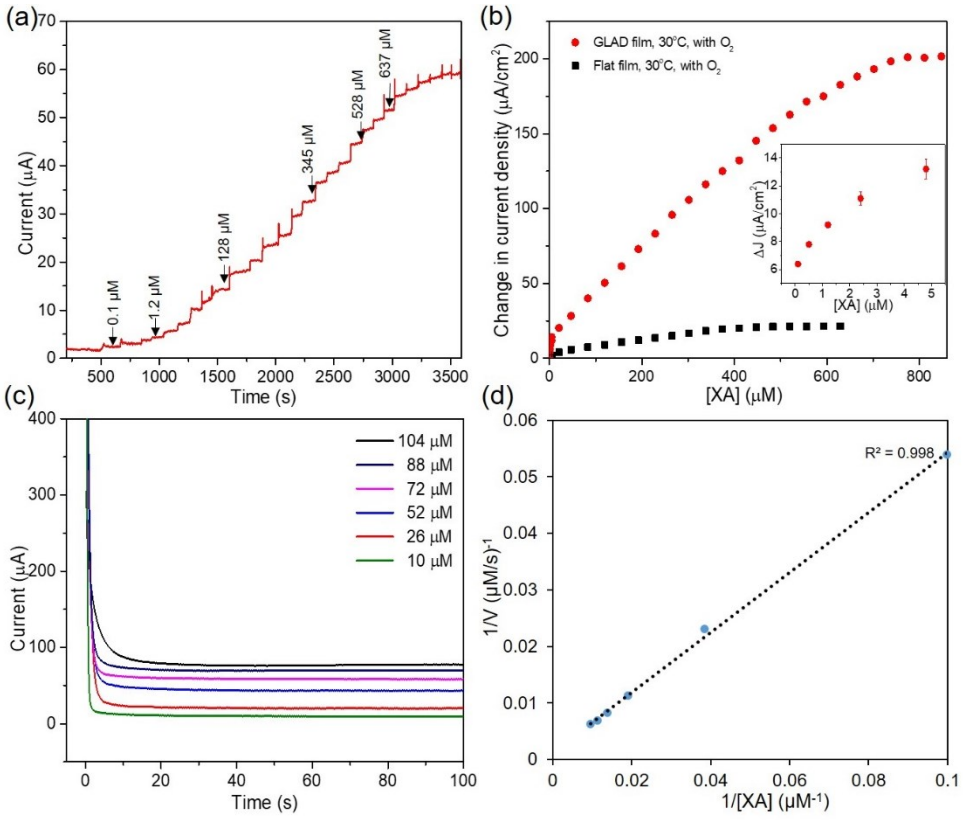

Figure 3.12: (a) Chronoamperometry response recorded for an enzyme modified electrode at an applied potential of 0.5 V during successive additions of XA in 0.1 M NaOH solution. (b) Calibration curves for electrode response to XA using GLAD (red circles) and planar (black squares) NiO electrodes at 30°C in an oxygen saturated solution. Error bars showing the standard deviation of the three measurements are also included, but they are smaller than the data points themselves (inset: zoomed-in view of the low concentration region up to 5 µM) (c)

Chronoamperometric response curves for XO-modified GLAD NiO electrodes in different concentrations of XA. (d) Lineweaver-Burk plot for XO-modified NiO electrode using different concentrations of XA.

Table 3.2: Comparison of the analytical performances of various XA sensors. Amp: amperometric, DPV: differential pulse voltammetry, EIS: impedance spectroscopy, CV: cyclic voltammetry, NR: not reported.

Electrode	Sensing method	K_m	LOD	Linear range	Sensitivity	Reference
XO/MNP-PAMAM-PtNP/rGO-CMC/GCE	Amp	NR	13 nM	0.05-12 µM	0.1 µA μM^{-1} cm^{-2}	[39]
P(GMA-co-VFc)/REGO-Fe_3O_4	Amp	NR	170 nM	2-36 µM	0.17 µA M^{-1}	[19]
XO-AuNPs	Amp	NR	720 nM	2-37.3 µM	0.1 µA μM^{-1} cm^{-2}	[40]
XO-SWCNH	Amp	NR	610 nM	1.5-35.4 µM	0.2 µA μM^{-1} cm^{-2}	[40]

XO/fMWCNT/Au-PPD/GCE	DPV	NR	12 nM	0.01-300 μM	140.0 μA μM^{-1} cm^{-2}	[41]
XO/TiO_2/MWCNT	EIS	NR	500 nM	0.5-500 μM	NR	[35]
XO/MWCNT/CF	Amp	NR	750 nM	10-135 μM	1.2 μA μM^{-1} cm^{-2}	[42]
XO/NiO	CV	0.03 mM	2.98 μM	10-200 μM	0.62 μA μM^{-1} cm^{-2}	[8]
XO/graphite	Amp	0.3 mM	NR	45-80 μM	0.26 μA μM^{-1}	[43]
XO/chitosan/graphene/Co_3O_4 NPs	Amp	0.17 mM	200 nM	5×10^{-4} - 8×10^{-2} mM	6.58 μA mM^{-1}	[44]
XO/ $CuPtCl_6$	Amp	1.11 mM	100 nM	6×10^{-7} - 2×10^{-4} M	NR	[45]
XO/PVF/PtNPs	Amp	3.4 mM	130 nM	0.43 × 10^{-3} –	68.8 μA mM^{-1} cm^{-2}	[46]

				2.84 mM		
XO/NiO GLAD film	Amp	0.4 mM	37 nM	0.1-650 µM	1.1 µA μM^{-1} cm^{-2}	This work

3.4.5 Interference study

To determine the selectivity of the sensor, the CA response to equivalent concentrations (47 µM) of xanthine and four potentially interfering substances (hypoxanthine, glucose, sodium benzoate, and uric acid) was compared, and the resulting data is shown in Fig 3.13. The sensor's initial response to xanthine was an increase of 8 µA, which agrees with the previously developed calibration curve (Fig 3.4b). Similar to other electrochemical xanthine sensors in the literature,[47] we observed an appreciable current response (2 µA, i.e., 25% of the response to xanthine) upon the addition of hypoxanthine, but no interference whatsoever was observed in the presence of glucose, sodium benzoate or uric acid. This indicates good selectivity for the intended analyte. Interestingly, the sensor's response to the second dose of XA was 83% of the response to the first injection, which may be due to accumulation of the interfering compounds on the electrode surface.

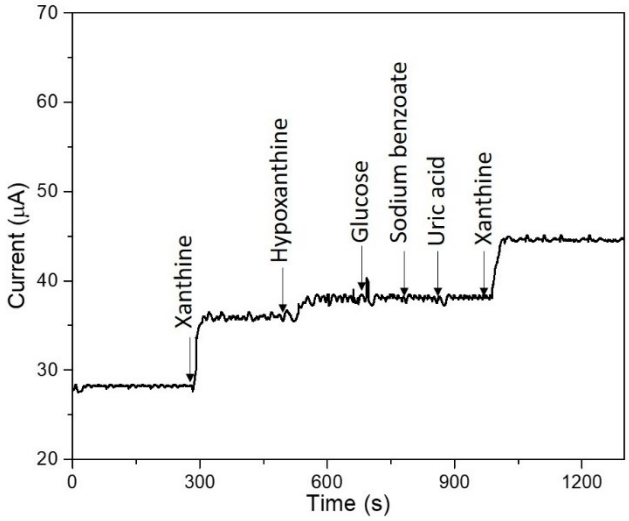

Figure 3.13: Chronoamperometry response recorded for an XO-modified electrode at an applied potential of 0.5 V vs. Ag/AgCl during additions of 47 μM xanthine, hypoxanthine, glucose, sodium benzoate, and uric acid.

3.4.6 Reproducibility and storage stability

To test the reproducibility of the sensor signal, an XO-modified GLAD NiO electrode was subjected to repeated injections of 450 μM XA at 200 s intervals. The CA current changes are plotted in Fig 3.14a against the number of measurements. Two additional values were removed after failing to meet the 95% level of confidence from the Q test. The relative standard deviation (%RSD) obtained over the 18 measurements using the same electrode was found to be 4%, indicating the high reproducibility of the XO-modified electrode's response towards XA. The %RSD of the change in current of three independent XO sensors measured over a concentration range of 0.1 – 650 μM XA was <7%, indicating good reproducibility of the sensor's fabrication.

The stability of the biosensor was tested by recording the current response for the same electrode to equivalent sensing cycles over a period of twelve days. In each test, the conditions were the same (20 μM XA, 0.1 M NaOH, CA at +0.5 V vs. Ag/AgCl), and between tests the electrode was

rinsed and stored for recovery at 4°C in PBS solution at pH 7.4. Before taking measurements, the electrode was reactivated by cycling 5 times in 0.1 M NaOH. The responses are shown in Fig 3.14(b). After an initial 22% loss of signal on day 2, similar current responses were obtained on the second and fifth days. However, the sensor retained only 53% of its initial response on day 12, which might be due to loss of enzyme and enzyme activity as well as compromised adhesion between NiO and ITO substrate due to the repeated redox cycles occurring during reactivation and CA measurements.

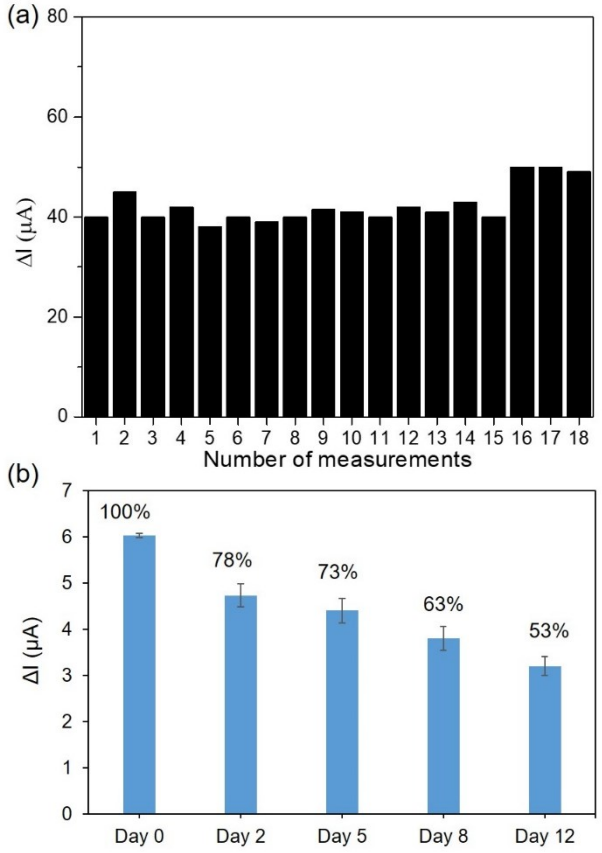

Figure 3.14: (a) XO-modified electrode responses to eighteen consecutive additions of 450 μM XA in 0.1 M NaOH. Measurements were performed in a continuous process without removal from the electrochemical cell. (b) Relative change in CA current for XO-modified electrodes in response to additions of 20 μM xanthine in independent experiments performed over 12 days. After each measurement, these electrodes were rinsed and stored at 4°C in pH 7.4 PBS then reactivated by CV prior to each test.

3.4.7 Determination of xanthine concentration in real fish samples

The developed sensor was tested with tuna fish extracts obtained from fish samples stored at room temperature and processed as indicated in the experimental section. Calibration plots for the sensor operating in the presence of these fish extracts were generated according to the standard addition method, and they are shown in Fig 3.15. In these datasets, the sensor responses to the initial introduction of fish extract (50 µl fish extract solution into 50 ml of 0.1 M NaOH while recording CA current at +0.5 V vs. Ag/AgCl) are represented by the initial points at [XA] = 0 µM, and the remaining points are responses to additions of 50 µl aliquots of 13 mM XA. For fresh fish extract (i.e., Day 0), the data followed the regression equation $I = (0.12\ \mu A\ \mu M^{-1})\ [XA] + 0.6\ \mu A$ with an $R^2 = 0.997$. We note that the slope of this calibration curve increased by 41% with respect to the corresponding data for the sensor operating in NaOH alone (i.e., Fig 3.4b), indicating that the device's sensitivity to XA has increased substantially in the presence of fish extract. This effect is further observed for sensor responses to aged samples where XA sensitivities of 0.25, 0.26 and 0.27 $\mu A\ \mu M^{-1}$ were measured for sensors operating in the presence of fish samples aged 2, 4 and 7 days, respectively. We can offer no conclusive explanation for this effect at present, noting that the fish extract includes many solubilized compounds, and some combination may expedite enzyme turnover or modify the electrical double layer.

Based on the negative intercept of the regression equation, the xanthine concentration in the fresh fish extract (i.e., Day 0) was estimated to be 5.2 µM (±0.09 µM). This value roughly matches other reports of XA concentrations measured in fresh fish, where values ranged from ~2.2 nM to 5 µM,[34,48–50] but it is important to note that our experiment measures concentration after dilution in the electrochemical cell, and experimental conditions may vary widely between studies. For the

samples aged 2, 4 and 7 days, we measured increasing XA concentrations of 9.9 µM (±0.14 µM), 17.3 µM (±0.25 µM), and 32.2 µM (±0.45 µM), respectively. This increasing XA concentration results from purine nucleotide breakdown during the degradation of fish meat, as seen in previous studies.[51,52,45,48]

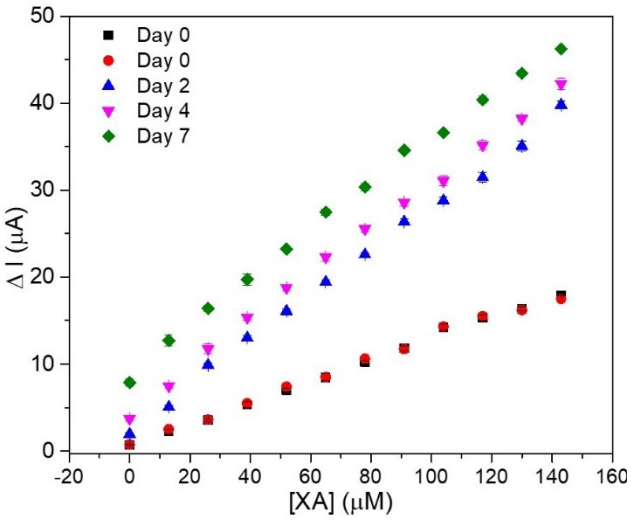

Figure 3.15: Chronoamperometry responses for XO-modified NiO/NiOOH electrodes exposed to various concentrations of XA in the presence of fish extracts. The experiments were performed at 30°C in 0.1 M NaOH with oxygenation and at a CA potential of +0.5 V vs. Ag/AgCl. The data points at [XA] = 0 µM indicate the electrode response to the addition of fish extract, with the age of the fish sample indicated in the legend. Two distinct symbol types (red circle, black squares) are used for fresh fish extract with the two data sets representing experiments performed weeks apart using different batches of fresh fish. Within each dataset, the plotted data points are averages from three different electrodes.

Overall, we have established that nanocolumnar NiO thin films deposited by the GLAD technique can be functionalized with XO to create a high-performance sensor for xanthine quantification. The sensors rapidly respond to variations in xanthine concentration and exhibit higher sensitivity and lower limits of detection than many previously-established systems. Excellent reproducibility and limited response to interfering species were also observed, although we believe the electrochemical activation process (in which the NiO surface is converted to NiOOH) may limit

the ability of the devices to perform repeated experiments over longer periods. Importantly, we also showed that the sensor was able to quantify xanthine in fish samples purchased at a local grocery store, and we measured markedly increased xanthine sensitivity (from 0.085 $\mu A\ \mu M^{-1}$ without fish extract to as much as 0.27 $\mu A\ \mu M^{-1}$ for aged fish) during measurements of these real-world samples. While the increased sensitivity is beneficial, the variation in response to different matrices would also prevent a real-world sensor from measuring the XA concentration in an unknown sample by simply recording CA current and comparing against a calibration curve. Instead, the real-world sensor would incorporate an XA reservoir and implement the complete standard addition method to determine the unknown XA concentration.

Acknowledgements

The authors are thankful to Paul Conception for SEM imaging, Natasha Singer for early xanthine detection experiments using a different materials system, and the University of Alberta for supporting the nanoFAB facility. Financial support from the Natural Sciences and Engineering Research Council of Canada is greatly acknowledged.

References

(1) Ghaly A. E.; Dave D.; Budge S.; Brooks M. S. Fish Spoilage Mechanisms and Preservation Techniques: Review. *Am. J. Appl. Sci.* **2010**, *7* (7), 859–877. https://doi.org/10.3844/ajassp.2010.859.877.

(2) Hong, H.; Regenstein, J. M.; Luo, Y. The Importance of ATP-Related Compounds for the Freshness and Flavor of Post-Mortem Fish and Shellfish Muscle: A Review. *Crit. Rev. Food Sci. Nutr.* **2015**, 00–00. https://doi.org/10.1080/10408398.2014.1001489.

(3) Pundir, C. S.; Devi, R. Biosensing Methods for Xanthine Determination: A Review. *Enzyme Microb. Technol.* **2014**, *57*, 55–62. https://doi.org/10.1016/j.enzmictec.2013.12.006.

(4) Lu, J.-J.; Jia, B.-J.; Yang, L.; Zhang, W.; Dong, X.; Li, P.; Chen, J. Ultra-High Performance Liquid Chromatography with Ultraviolet and Tandem Mass Spectrometry for Simultaneous Determination of Metabolites in Purine Pathway of Rat Plasma. *J. Chromatogr. B* **2016**, *1036–1037*, 84–92. https://doi.org/10.1016/j.jchromb.2016.09.023.

(5) Logotheti, M.; Theochari, K.; Kostakis, M.; Pasias, I. N.; Thomaidis, N. S. Development and Validation of a HILIC-UV Method for the Determination of Nucleotides in Fish Samples. *Food Chem.* **2018**, *248*, 70–77. https://doi.org/10.1016/j.foodchem.2017.12.040.

(6) Monteiro, T.; Almeida, M. G. Electrochemical Enzyme Biosensors Revisited: Old Solutions for New Problems. *Crit. Rev. Anal. Chem.* **2019**, *49* (1), 44–66. https://doi.org/10.1080/10408347.2018.1461552.

(7) Franceschelli, L.; Berardinelli, A.; Dabbou, S.; Ragni, L.; Tartagni, M. Sensing Technology for Fish Freshness and Safety: A Review. *Sensors* **2021**, *21* (4), 1373. https://doi.org/10.3390/s21041373.

(8) Yadav, S. K.; Singh, J.; Agrawal, V. V.; Malhotra, B. D. Nanostructured Nickel Oxide Film for Application to Fish Freshness Biosensor. *Appl. Phys. Lett.* **2012**, *101* (2), 023703. https://doi.org/10.1063/1.4736578.

(9) Mathew, M.; Sandhyarani, N. A Highly Sensitive Electrochemical Glucose Sensor Structuring with Nickel Hydroxide and Enzyme Glucose Oxidase. *Electrochim. Acta* **2013**, *108*, 274–280. https://doi.org/10.1016/j.electacta.2013.07.010.

(10) Tyagi, M.; Tomar, M.; Gupta, V. Glad Assisted Synthesis of NiO Nanorods for Realization of Enzymatic Reagentless Urea Biosensor. *Biosens. Bioelectron.* **2014**, *52*, 196–201. https://doi.org/10.1016/j.bios.2013.08.020.

(11) Singer, N.; Pillai, R. G.; Johnson, A. I. D.; Harris, K. D.; Jemere, A. B. Nanostructured Nickel Oxide Electrodes for Non-Enzymatic Electrochemical Glucose Sensing. *Microchim. Acta* **2020**, *187* (4), 196. https://doi.org/10.1007/s00604-020-4171-5.

(12) Salazar, P.; Rico, V.; González-Elipe, A. R. Non-Enzymatic Hydrogen Peroxide Detection at NiO Nanoporous Thin Film- Electrodes Prepared by Physical Vapor Deposition at Oblique Angles. *Electrochim. Acta* **2017**, *235*, 534–542. https://doi.org/10.1016/j.electacta.2017.03.087.

(13) Tyagi, M.; Tomar, M.; Gupta, V. NiO Nanoparticle-Based Urea Biosensor. *Biosens. Bioelectron.* **2013**, *41*, 110–115. https://doi.org/10.1016/j.bios.2012.07.062.

(14) Lin, D.; Harris, K. D.; Chan, N. W. C.; Jemere, A. B. Nanostructured Indium Tin Oxide Electrodes Immobilized with Toll-like Receptor Proteins for Label-Free Electrochemical Detection of Pathogen Markers. *Sensors Actuators B Chem.* **2018**, *257*, 324–330. https://doi.org/10.1016/j.snb.2017.10.140.

(15) Fu, K.; Seo, J.; Kesler, V.; Maganzini, N.; Wilson, B. D.; Eisenstein, M.; Murmann, B.;

Soh, H. T. Accelerated Electron Transfer in Nanostructured Electrodes Improves the Sensitivity of Electrochemical Biosensors. *Adv. Sci.* **2021**, *8* (23), 2102495. https://doi.org/10.1002/advs.202102495.

(16) Arora, K.; Tomar, M.; Gupta, V. Highly Sensitive and Selective Uric Acid Biosensor Based on RF Sputtered NiO Thin Film. *Biosens. Bioelectron.* **2011**. https://doi.org/10.1016/j.bios.2011.09.026.

(17) Bezuidenhout, L. W.; Nazemifard, N.; Jemere, A. B.; Harrison, D. J.; Brett, M. J. Microchannels Filled with Diverse Micro- and Nanostructures Fabricated by Glancing Angle Deposition. *Lab Chip* **2011**, *11* (9), 1671. https://doi.org/10.1039/c0lc00721h.

(18) Nakatani, H. S.; Santos, L. V. dos; Pelegrine, C. P.; Gomes, S. T. M.; Matsushita, M.; Souza, N. E. de; Visentaine, J. V. Biosensor Based on Xanthine Oxidase for Monitoring Hypoxanthine in Fish Meat. *Am. J. Biochem. Biotechnol.* **2005**, *1* (2), 85–89. https://doi.org/10.3844/ajbbsp.2005.85.89.

(19) Dervisevic, M.; Custiuc, E.; Çevik, E.; Durmus, Z.; Şenel, M.; Durmus, A. Electrochemical Biosensor Based on REGO/Fe3O4 Bionanocomposite Interface for Xanthine Detection in Fish Sample. *Food Control* **2015**, *57*, 402–410. https://doi.org/10.1016/j.foodcont.2015.05.001.

(20) Eckermann, A. L.; Feld, D. J.; Shaw, J. A.; Meade, T. J. Electrochemistry of Redox-Active Self-Assembled Monolayers. *Coord. Chem. Rev.* **2010**, *254* (15–16), 1769–1802. https://doi.org/10.1016/j.ccr.2009.12.023.

(21) Tripathi, A.; Harris, K. D.; Elias, A. L. High Surface Area Nitrogen-Functionalized Ni Nanozymes for Efficient Peroxidase-like Catalytic Activity. *PLoS One* **2021**, *16* (10), e0257777. https://doi.org/10.1371/journal.pone.0257777.

(22) Grosvenor, A. P.; Biesinger, M. C.; Smart, R. S. C.; McIntyre, N. S. New Interpretations of XPS Spectra of Nickel Metal and Oxides. *Surf. Sci.* **2006**, *600* (9), 1771–1779. https://doi.org/10.1016/j.susc.2006.01.041.

(23) Tripathi, A.; Harris, K. D.; Elias, A. L. Peroxidase-Like Behavior of Ni Thin Films Deposited by Glancing Angle Deposition for Enzyme-Free Uric Acid Sensing. *ACS Omega* **2020**, *5* (16), 9123–9130. https://doi.org/10.1021/acsomega.9b04071.

(24) Mao, F.; Liu, P. F.; Yang, P.; Gu, J.; Yang, H. G. One-Step Coating of Commercial Ni Nanoparticles with a Ni, N-Co-Doped Carbon Shell towards Efficient Electrocatalysts for CO 2 Reduction. *Chem. Commun.* **2020**, *56* (54), 7495–7498. https://doi.org/10.1039/D0CC02188A.

(25) Zheng, X.; Zhang, Y.; Liu, H.; Fu, D.; Chen, J.; Wang, J.; Zhong, C.; Deng, Y.; Han, X.; Hu, W. In Situ Fabrication of Heterostructure on Nickel Foam with Tuned Composition for Enhancing Water-Splitting Performance. *Small* **2018**, *14* (50), 1803666. https://doi.org/10.1002/smll.201803666.

(26) Ramanathan, T.; Fisher, F. T.; Ruoff, R. S.; Brinson, L. C. Amino-Functionalized Carbon Nanotubes for Binding to Polymers and Biological Systems. *Chem. Mater.* **2005**, *17* (6), 1290–1295. https://doi.org/10.1021/cm048357f.

(27) Radhakrishnan, K.; Panneerselvam, P.; Marieeswaran, M. A Green Synthetic Route for the Surface-Passivation of Carbon Dots as an Effective Multifunctional Fluorescent Sensor for the Recognition and Detection of Toxic Metal Ions from Aqueous Solution. *Anal. Methods* **2019**, *11* (4), 490–506. https://doi.org/10.1039/C8AY02451K.

(28) Li, R.; Wei, Z.; Gou, X.; Xu, W. Phosphorus-Doped Graphene Nanosheets as Efficient Metal-Free Oxygen Reduction Electrocatalysts. *RSC Adv.* **2013**, *3* (25), 9978.

https://doi.org/10.1039/c3ra41079j.
(29) Davis, M. D.; Edmondson, D. E.; Muller, F. 31P Nuclear Magnetic Resonance and Chemical Studies of the Phosphorus Residues in Bovine Milk Xanthine Oxidase. *Eur. J. Biochem.* **1984**, *145* (2), 237–243. https://doi.org/10.1111/j.1432-1033.1984.tb08544.x.
(30) Johnson, J. L.; London, R. E.; Rajagopalan, K. V. Covalently Bound Phosphate Residues in Bovine Milk Xanthine Oxidase and in Glucose Oxidase from Aspergillus Niger: A Reevaluation. *Proc. Natl. Acad. Sci. U. S. A.* **1989**, *86* (17), 6493–6497. https://doi.org/10.1073/pnas.86.17.6493.
(31) Ribeiro, P. M. G.; Fernandes, H. S.; Maia, L. B.; Sousa, S. F.; Moura, J. J. G.; Cerqueira, N. M. F. S. A. The Complete Catalytic Mechanism of Xanthine Oxidase: A Computational Study. *Inorg. Chem. Front.* **2021**, *8* (2), 405–416. https://doi.org/10.1039/D0QI01029D.
(32) Berry, C. E.; Hare, J. M. Xanthine Oxidoreductase and Cardiovascular Disease: Molecular Mechanisms and Pathophysiological Implications. *J. Physiol.* **2004**, *555* (3), 589–606. https://doi.org/10.1113/jphysiol.2003.055913.
(33) Arslan, F.; Yaşar, A.; Kılıç, E. An Amperometric Biosensor for Xanthine Determination Prepared from Xanthine Oxidase Immobilized in Polypyrrole Film. *Artif. Cells, Blood Substitutes, Biotechnol.* **2006**, *34* (1), 113–128. https://doi.org/10.1080/10731190500430289.
(34) Dervisevic, M.; Dervisevic, E.; Çevik, E.; Şenel, M. Novel Electrochemical Xanthine Biosensor Based on Chitosan–Polypyrrole–Gold Nanoparticles Hybrid Bio-Nanocomposite Platform. *J. Food Drug Anal.* **2017**, *25* (3), 510–519. https://doi.org/10.1016/j.jfda.2016.12.005.
(35) Narang, J.; Malhotra, N.; Singhal, C.; Pundir, C. S. Evaluation of Freshness of Fishes Using MWCNT/TiO2 Nanobiocomposites Based Biosensor. *Food Anal. Methods* **2017**, *10* (2), 522–528. https://doi.org/10.1007/s12161-016-0594-3.
(36) Dervisevic, M.; Custiuc, E.; Çevik, E.; Şenel, M. Construction of Novel Xanthine Biosensor by Using Polymeric Mediator/MWCNT Nanocomposite Layer for Fish Freshness Detection. *Food Chem.* **2015**, *181*, 277–283. https://doi.org/10.1016/j.foodchem.2015.02.104.
(37) Saadaoui, M.; Sánchez, A.; Díez, P.; Raouafi, N.; Pingarrón, J. M.; Villalonga, R. Amperometric Xanthine Biosensors Using Glassy Carbon Electrodes Modified with Electrografted Porous Silica Nanomaterials Loaded with Xanthine Oxidase. *Microchim. Acta* **2016**, *183* (6), 2023–2030. https://doi.org/10.1007/s00604-016-1840-5.
(38) Renault, C.; Andrieux, C. P.; Tucker, R. T.; Brett, M. J.; Balland, V.; Limoges, B. Unraveling the Mechanism of Catalytic Reduction of O 2 by Microperoxidase-11 Adsorbed within a Transparent 3D-Nanoporous ITO Film. *J. Am. Chem. Soc.* **2012**, *134* (15), 6834–6845. https://doi.org/10.1021/ja301193s.
(39) Borisova, B.; Sánchez, A.; Jiménez-Falcao, S.; Martín, M.; Salazar, P.; Parrado, C.; Pingarrón, J. M.; Villalonga, R. Reduced Graphene Oxide-Carboxymethylcellulose Layered with Platinum Nanoparticles/PAMAM Dendrimer/Magnetic Nanoparticles Hybrids. Application to the Preparation of Enzyme Electrochemical Biosensors. *Sensors Actuators B Chem.* **2016**, *232*, 84–90. https://doi.org/10.1016/j.snb.2016.02.106.
(40) Zhang, L.; Lei, J.; Zhang, J.; Ding, L.; Ju, H. Amperometric Detection of Hypoxanthine and Xanthine by Enzymatic Amplification Using a Gold Nanoparticles–Carbon Nanohorn Hybrid as the Carrier. *Analyst* **2012**, *137* (13), 3126. https://doi.org/10.1039/c2an35284b.

(41) Sen, S.; Sarkar, P. A Novel Third-Generation Xanthine Biosensor with Enzyme Modified Glassy Carbon Electrode Using Electrodeposited MWCNT and Nanogold Polymer Composite Film. *RSC Adv.* **2015**, *5* (116), 95911–95925. https://doi.org/10.1039/C5RA18889J.
(42) Torres, A. C.; Ghica, M. E.; Brett, C. M. A. Design of a New Hypoxanthine Biosensor: Xanthine Oxidase Modified Carbon Film and Multi-Walled Carbon Nanotube/Carbon Film Electrodes. *Anal. Bioanal. Chem.* **2013**, *405* (11), 3813–3822. https://doi.org/10.1007/s00216-012-6631-1.
(43) Horozova, E. G.; Dimcheva, N. D.; Jordanova, Z. J. Study of Xanthine Oxidase Immobilized Electrode Based on Modified Graphite. *Zeitschrift für Naturforsch. C* **2000**, *55* (1–2), 60–65. https://doi.org/10.1515/znc-2000-1-212.
(44) Dalkıran, B.; Erden, P. E.; Kılıç, E. Construction of an Electrochemical Xanthine Biosensor Based on Graphene/Cobalt Oxide Nanopartiles/Chitosan Composite for Fish Freshness Detection. *J. Turkish Chem. Soc. Sect. A Chem.* **2017**, *4* (1), 23–44. https://doi.org/10.18596/jotcsa.54485.
(45) Pei, J.; Li, X. Xanthine and Hypoxanthine Sensors Based on Xanthine Oxidase Immobilized on a CuPtCl6 Chemically Modified Electrode and Liquid Chromatography Electrochemical Detection. *Anal. Chim. Acta* **2000**, *414* (1–2), 205–213. https://doi.org/10.1016/S0003-2670(00)00775-3.
(46) Baş, S. Z.; Gülce, H.; Yıldız, S. Amperometric Xanthine Biosensors Based on Electrodeposition of Platinum on Polyvinylferrocenium Coated Pt Electrode. *J. Mol. Catal. B Enzym.* **2011**, *72* (3–4), 282–288. https://doi.org/10.1016/j.molcatb.2011.06.017.
(47) Wang, Z.; Ma, B.; Shen, C.; Lai, O.-M.; Tan, C.-P.; Cheong, L.-Z. Electrochemical Biosensing of Chilled Seafood Freshness by Xanthine Oxidase Immobilized on Copper-Based Metal–Organic Framework Nanofiber Film. *Food Anal. Methods* **2019**, *12* (8), 1715–1724. https://doi.org/10.1007/s12161-019-01513-8.
(48) Khan, M. Z. H.; Ahommed, M. S.; Daizy, M. Detection of Xanthine in Food Samples with an Electrochemical Biosensor Based on PEDOT:PSS and Functionalized Gold Nanoparticles. *RSC Adv.* **2020**, *10* (59), 36147–36154. https://doi.org/10.1039/D0RA06806C.
(49) Garg, D.; Verma, N. Fibre-Optic Biosensor for the Detection of Xanthine for the Evaluation of Meat Freshness. *J. Phys. Conf. Ser.* **2020**, *1531* (1), 012098. https://doi.org/10.1088/1742-6596/1531/1/012098.
(50) Thandavan, K.; Gandhi, S.; Sethuraman, S.; Rayappan, J. B. B.; Krishnan, U. M. Development of Electrochemical Biosensor with Nano-Interface for Xanthine Sensing – A Novel Approach for Fish Freshness Estimation. *Food Chem.* **2013**, *139* (1–4), 963–969. https://doi.org/10.1016/j.foodchem.2013.02.008.
(51) Sahyar, B. Y.; Kaplan, M.; Ozsoz, M.; Celik, E.; Otles, S. Electrochemical Xanthine Detection by Enzymatic Method Based on Ag Doped ZnO Nanoparticles by Using Polypyrrole. *Bioelectrochemistry* **2019**, *130*, 107327. https://doi.org/10.1016/j.bioelechem.2019.107327.
(52) Joon, A.; Ahlawat, J.; Aggarwal, V.; Jaiwal, R.; Pundir, C. S. An Improved Amperometric Determination of Xanthine with Xanthine Oxidase Nanoparticles for Testing of Fish Meat Freshness. *Sens. Bio-Sensing Res.* **2021**, *33*, 100437. https://doi.org/10.1016/j.sbsr.2021.100437.
(53) Devi, R.; Yadav, S.; Pundir, C. S. Amperometric Determination of Xanthine in Fish Meat

by Zinc Oxide Nanoparticle/Chitosan/Multiwalled Carbon Nanotube/Polyaniline Composite Film Bound Xanthine Oxidase. *Analyst* **2012**, *137* (3), 754–759. https://doi.org/10.1039/C1AN15838D.

Chapter 4: Peroxidase-like behavior of Ni thin films deposited by glancing angle deposition for enzyme-free uric acid sensing[2]

Anuja Tripathi[1], Kenneth D. Harris[2,3], Anastasia L. Elias[1]

Department of Chemical and Materials Engineering, University of Alberta, Donadeo Innovation Centre for Engineering, Edmonton, Alberta, T6G 1H9, Canada

[2]National Research Council Canada, Nanotechnology Research Centre, Edmonton, Alberta, T6G 2M9, Canada

[3]Department of Mechanical Engineering, University of Alberta, Edmonton, Alberta, T6G 1H9, Canada

---

4.1 Abstract

We present a nanozyme-based biosensor fabricated from nanostructured Ni films deposited onto a silicon wafer by glancing angle deposition (GLAD) for enzyme-free colorimetric monitoring of uric acid (UA), a biomarker for gout, high blood pressure, heart disease and kidney disease. The helically-structured Ni GLAD nanozymes exhibit excellent peroxidase-like activity to accelerate the oxidation reaction of colorless 3, 3′, 5, 5′-tetramethylbenzidine (TMB) to a blue product, oxidized TMB (oxTMB), mediated by H_2O_2. In the presence of UA, oxTMB is reduced, decreasing the optical absorbance by an amount determined by the concentration of UA in the solution. The nanozyme not only mimics peroxidase but also possesses the notable qualities of reusability,

[2] A version of this chapter has been published as Anuja Tripathi, Kenneth D. Harris, Anastasia L. Elias, *ACS Omega*, 2020, 5, 16, 912-9130.

simple operation and reliability, making it environment-friendly and suitable for on-demand analysis. We optimized essential working parameters (pH, TMB concentration, and H_2O_2 concentration) to maximize the initial color change of the TMB solution. The catalytic activity of this nanozyme was compared with conventional nanofilms using Michaelis-Menten theory. Based on this, enzyme-free biosensors were developed for colorimetric detection of UA, providing a wide detection range and a limit of detection (3.3 μM) suitable for measurements of UA concentration in sweat. Furthermore, interference from glucose and urea were studied so as to explore the potential of the biosensor for use in clinical diagnosis of UA biomarkers.

KEYWORDS: Peroxidase mimicking, glancing angle deposition, colorimetric sensors, nanozymes

4.2 Introduction

Uric acid (UA) is an important biomarker of human health, given that it is implicated in a range of medical conditions such as gout, arthritis, kidney stones, heart diseases and renal failure (1). Gout, for example, is a prevalent and painful disease caused by uric acid buildup in joints (2). At high concentration, UA forms crystals, which deposit in the affected joints and cause tissue damage (3). The UA concentration *in vivo* is directly related to the incidence rate of gout (and the other conditions mentioned above), and thus, the assessment of UA levels in serum plays an important role in early diagnosis and therapy (4–6). Most current clinical methods are based on the analysis of blood samples, as the UA concentration in blood is relatively high: 155-357 μM in adult females and 208-428 μM in adult males (7). However, less invasive testing — such as the analysis of sweat — would reduce the need for collection of blood samples. As the UA

concentration in sweat is much lower than in blood in the range of 18-35 µM, which requires quantification methods with high sensitivity and low operating range (8).

In the literature, various methods for the detection and quantification of UA concentration in human serum samples have been described, including chemiluminescence, chromatographic, electrochemical, and spectroscopic/colorimetric techniques (3,9–12). Among these techniques, colorimetric detection has begun to attract massive attention over the last few decades due to its potential for simplified operation and user friendliness. The convenience of colorimetric sensing could ultimately lead to deployment outside a medical environment and/or operation by individuals with more limited training (13). Techniques for colorimetric detection of UA have previously been demonstrated. For instance, Mason *et al.* used horseradish peroxidase (HRP) to catalyze the oxidation of 3, 3', 5, 5'-tetramethylbenzidine (TMB) with H_2O_2. TMB is a chromogen (colorless in the reduced form and blue in the oxidized form) which can be easily observed with the naked eye or by UV-Vis spectroscopy (14). The TMB oxidation reaction and its distinctive color change are reversed in the presence of UA, and therefore, the reaction mechanism has been used to sense UA (3,5). In this sensing scheme (Scheme 1), the catalyst is a critical element that facilitates the decomposition of hydrogen peroxide to generate active oxygen species or free radicals, which further react with colorless TMB to form the blue-colored oxTMB compound. When UA is added to this oxTMB solution, the oxTMB is reduced, and the blue color fades.

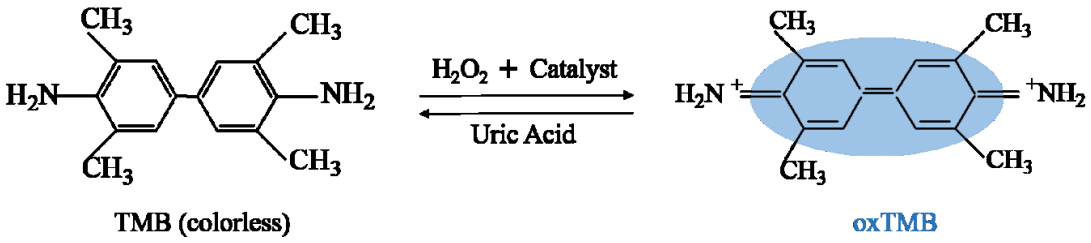

Scheme1. Reaction scheme for colorimetric detection of uric acid using TMB and a catalyst.

Throughout the literature, the initial oxidation of TMB is generally done through a natural peroxidase-based catalyst, however, these natural enzymes often require well-controlled storage conditions (temperature, pH, purity, etc.), which may result in poor stability and shelf-life (15–17). Nanoparticles used as "artificial enzymes" or "nanozymes" have also been investigated, and they have been shown to possess remarkably improved stability under harsh working conditions, and well as efficient catalytic activity at low concentration (17–19). For instance, Kumar *et al.* used gold nanoparticles as a catalyst to accelerate the TMB oxidation reaction for UA sensing, and Sanjay *et al.* expanded the catalytic surface area and reduced the limit of detection (LOD) by incorporating graphene oxide (3, 5). These studies suggest that the extended surface area of the catalyst plays an important role in increasing the absorbance of oxTMB. As a result, metal-organic frameworks (MOFs) and nanocrystals (such as MIL-53 (Fe), $ZnFe_2O_4$, etc.) are also being explored as peroxidase mimics, and some of these high surface area catalysts have been used for the colorimetric detection of UA. For example, Rongxin *et al.* used peroxidase-mimicking MOFs in the presence of TMB to colorimetrically detect H_2O_2 generated during the reaction of uric acid with uricase, and other nanoparticles and nanocrystals have also been used to mimic the behavior of peroxidase for UA biosensing (18,20–22). Among these high surface area nanozymes, Ni has begun to attract considerable attention due to its excellent catalytic activity, high stability, low cost and ease of preparation (23). One common drawback among these nanomaterial-based systems, however, is the difficulty in recovering the catalyst after use, which prevents the re-use of nanozyme catalysts (22, 23).

The effectiveness of nanomaterials as catalysts results from the their large specific surface area, which results in a high concentration of catalytically-active sites (26). One method of producing surface-anchored materials with very high surface area is glancing angle deposition (GLAD).

GLAD is a physical vapor deposition technique that exploits atomic shadowing and dynamic motion control to engineer nanostructures with high surface area and controlled porosity (27–29). During GLAD, vapor flux is incident onto the substrate at glancing angles (>70°) with respect to the surface normal. The thin films fabricated by GLAD tend to be porous in nature with wide gaps separating nanosized columns, and as a result, they also tend to have high internal porosity. In previous work it has also been shown that the nanostructures may have a fine, fibrous structure, such as the Si helices deposited at 83° shown in reference (30). By employing dynamic substrate motion, the GLAD technique also enables the fabrication of peculiarly-shaped nanostructures including vertical columns, zigzags, and helices. These GLAD films have been reported in a wide range of applications such as photocatalysis, solar cells, microfluidics, and electrical sensors, and NiO GLAD films in particular have been demonstrated previously as catalysts in a reagent-less, amperometric biosensor for urea (29–31).

For the first time, we report the TMB-based colorimetric detection of UA using helical Ni nanofilms deposited onto a silicon surface by GLAD as a catalyst. As these nanofilms consist of surface-anchored helical structures, we expect that they can be easily recovered after use and reused. In this work, we first optimize the conditions (reactant concentration, pH, etc.) of the TMB oxidation reaction in the presence of the helical Ni catalyst. Next, we compare the catalytic activity of the nanostructured films to a flat Ni reference sample. Finally, we investigate the use of this system for the detection of uric acid at physiologically relevant concentrations. The selectivity, limit of detection, and re-usability of the GLAD film are also characterized.

4.3 Experimental

4.3.1 Reagents and materials

3, 3', 5, 5'-tetramethylbenzidine tablets (TMB, T5525), 30% hydrogen peroxide (H_2O_2), phosphate citrate buffer, sodium hydroxide, dimethylformamide (DMF), uric acid (UA), urea and glucose were purchased from Sigma Aldrich (St. Louis, MO, USA) and used as received. Deionized water of conductivity 0.055 μS was used throughout this work.

4.3.2 Fabrication of GLAD films and characterization

The Ni GLAD films were deposited on clean silicon wafers by electron beam evaporation (see Taschuk et al. for an in-depth description of the process) (29). The base pressure prior to deposition was $<2x10^{-6}$ Torr, and the pressure during deposition was roughly $1x10^{-5}$ Torr. The deposition angle between the incident vapor flux and the substrate normal was set to $\alpha = 78°$, and during deposition, the substrate was rotated at a rate of one complete revolution for every 100 nm of film growth. The final thickness of the Ni GLAD film was 610 nm as measured on a cleaved sample in a cross-sectional view by scanning electron microscopy (SEM, Hitachi S-4800). X-ray photoelectron spectroscopy (XPS, Kratos AXIS Ultra) was used to analyze the surface composition of the GLAD film. In this technique, samples were irradiated with a monochromatic Al K_α source ($h\upsilon = 1486.71$ eV), and the pressure of the analysis chamber was below $5x10^{-10}$ Torr during all measurements. XPS spectra were corrected for charge effects against the C (1s) peak at 284.8 eV.

4.3.3 Colorimetric measurements

TMB solutions were prepared by dissolving the appropriate mass of TMB tablets in a 9:1 v/v mixture of phosphate citrate buffer and DMF followed by constant stirring at 700 rpm for 40

minutes at room temperate (21°C). Solutions of UA of various concentrations were prepared by dissolving UA powder in 0.01 M NaOH and stirring at room temperature (21°C) for one hour.

UA-free test solutions (for the optimization of light absorption) were prepared by combining 500 µL of TMB solution (prepared at concentrations from 0.4 mM to 1.6 mM and pH values from 3 to 9) with H_2O_2 solution (at concentrations from 0.1 M to 0.34 M). These solutions were then brought into contact with 0.5 cm^2 of the catalytic Ni film for 15 min, during which time the solution was stirred at 1100 rpm. (Care was taken to ensure that no contact occurred between the magnetic stir bar and the catalytic film.) The catalytic film was removed prior to UV-Vis measurement. UA-sensing test solutions were prepared by combining 100 µL of the appropriate UA solution, 500 µL of 1.6 mM TMB solution, and 15 µL of 0.29 M H_2O_2 solution, and then adding one piece of catalytic Ni film (0.5 cm^2) and incubating at room temperature (21°C) for 15 minutes. The catalytic film was removed immediately prior to UV-Vis measurement, and the total volume of the test solutions (without the Ni film) was 0.615 mL. Prior to reuse, films were gently rinsed with deionized water, acetone, isopropyl alcohol, and then again with deionized water. To prevent damaging the surface of the film, the silicon substrates were always handled by the edges using plastic tweezers.

Light absorbance of both UA-free reference solutions and UA-sensing solutions was measured by UV-Vis spectroscopy (Jasco V-630 spectrophotometer) from 500 nm to 750 nm, at a scanning rate of 120 nm/min. A cuvette filled with only phosphate citrate buffer was used as a blank. The limit of detection (LOD) was calculated based on the formula $LOD = 3\sigma/m$, where σ is the standard deviation of the absorbance measurement of the blank (calculated based on four measurements of independent samples), and m is the slope of the absorbance vs. UA concentration curve at low concentration.

4.3.4 Optical measurement of catalytic activity

Catalytic activity was measured by monitoring the evolution of absorbance at 652 nm and fitting to the Michaelis-Menten equation:(51)

$$\frac{1}{V} = \left(\frac{Km}{Vmax}\right)\left(\frac{1}{[S]} + \frac{1}{Km}\right) \qquad (1)$$

In this equation, V is the reaction rate, V_{max} is the maximal reaction rate, [S] is the concentration of TMB, and K_m is the Michaelis-Menten constant. The concentrations and reaction rates were extracted from the absorbance data according to Beer-Lambert's law, $A = \varepsilon l[S]$, where A is the absorbance at 652 nm, $\varepsilon = 3.9 \times 10^4\ M^{-1}\ cm^{-1}$ is the absorbance coefficient for oxTMB, and l is the path length (i.e., 1 cm) (52).

4.4 Results and Discussion

4.4.1 Fabrication and characterization of GLAD films

Two separate types of Ni thin films deposited on silicon surfaces were studied as peroxidase-mimicking catalysts for the oxidation of TMB: a nanostructured helical thin film deposited by the GLAD technique, and, as a control sample, a flat Ni film deposited at a conventional, near-normal deposition angle (~0°). The GLAD film was deposited at an oblique angle of 78°, which was selected as a compromise between maximum surface area and maximum accessibility of the interior pore structure. Surface area generally peaks for lower deposition angles in the 60°-70° range, however, for this range of angles, the separation between neighboring nanocolumns can be quite small, which potentially limits diffusion of reactants into the interior (32). At greater

deposition angles, the nanocolumns become increasingly separated reducing both the diffusion barrier and the surface area (33).

High resolution SEM images of the two catalytic films, the GLAD film and the flat film, are presented in Fig 4.1. The conventional flat Ni film (Fig 4.1a and 4.1b) is 150 nm thick, and while some surface roughness is apparent, there are no obvious voids present in the film. The GLAD structure (Fig 4.1c and 4.1d) is much different; analysis of the images leads to a thickness estimate of 610 nm, and the helical character of the film is clear. 10-30 nm spaces are observed between the individual columnar structures, which is significantly larger than all reactants and should allow diffusion into the interior of the GLAD structure.

To analyze the composition of the Ni GLAD film, x-ray photoelectron spectroscopy (XPS) was performed, and the binding energy regions associated with Ni and C are shown in Fig 4.2(a) and 4.2(b). The Ni (2p) spectrum exhibits peaks for metallic Ni (at 852.2 eV and 869.5 eV), but higher energy peaks are also observed for Ni^{2+} at 855 eV and 872.8 eV (together with their associated satellite peaks at 860.7 eV and 879.2 eV) (32, 33) These higher energy peaks likely arise as a result of spontaneous oxidation of the Ni surface following deposition, and they indicate that nickel oxide species may be present at the catalytically-active surfaces (36). In the C (1s) spectrum (Fig 4.2b), the peaks at 284.8 eV and 287.2 eV are respectively attributed to C-C and C-O from adventitious carbon adsorbed on the Ni surface (37).

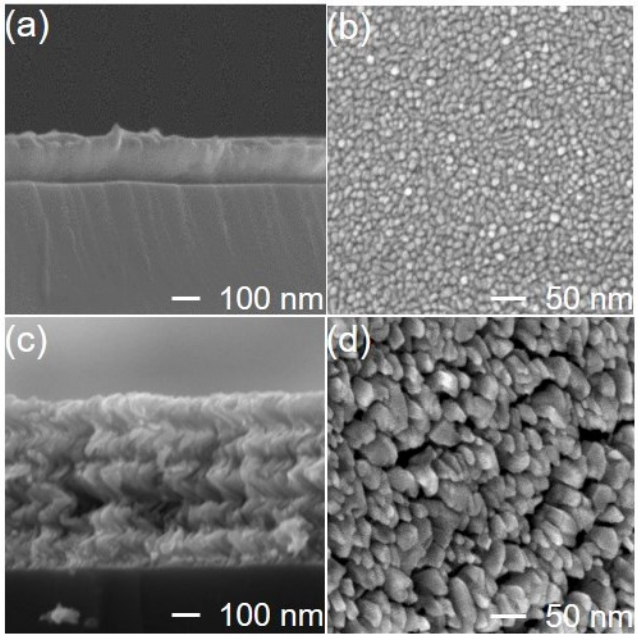

Figure 4.1: SEM images of the flat (a-b) and GLAD (c-d) catalytic Ni films. Cross-sectional views are shown in (a) and (c), and top views are shown in (b) and (d).

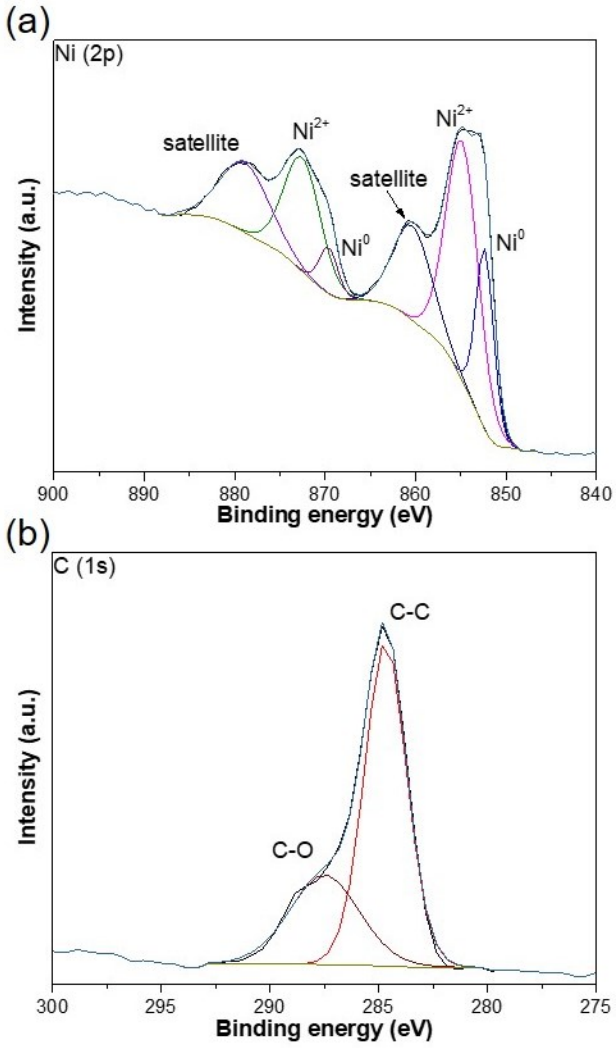

Figure 4.2: High resolution XPS data for the Ni GLAD film in the binding energy regions associated with (a) Ni and (b) C.

4.4.2 Optimization of the TMB oxidation conditions

Given the absence of information on Ni GLAD films as TMB oxidation catalysts, we first attempted to optimize the TMB oxidation conditions in the absence of uric acid to maximize the absorbance at 652 nm. We adjusted the TMB concentration, H_2O_2 concentration and solution pH, and the results of these experiments are presented in Fig 4.3. In each case, the UV-Vis spectra were recorded after 15 minutes of contact with the catalytic GLAD Ni film.

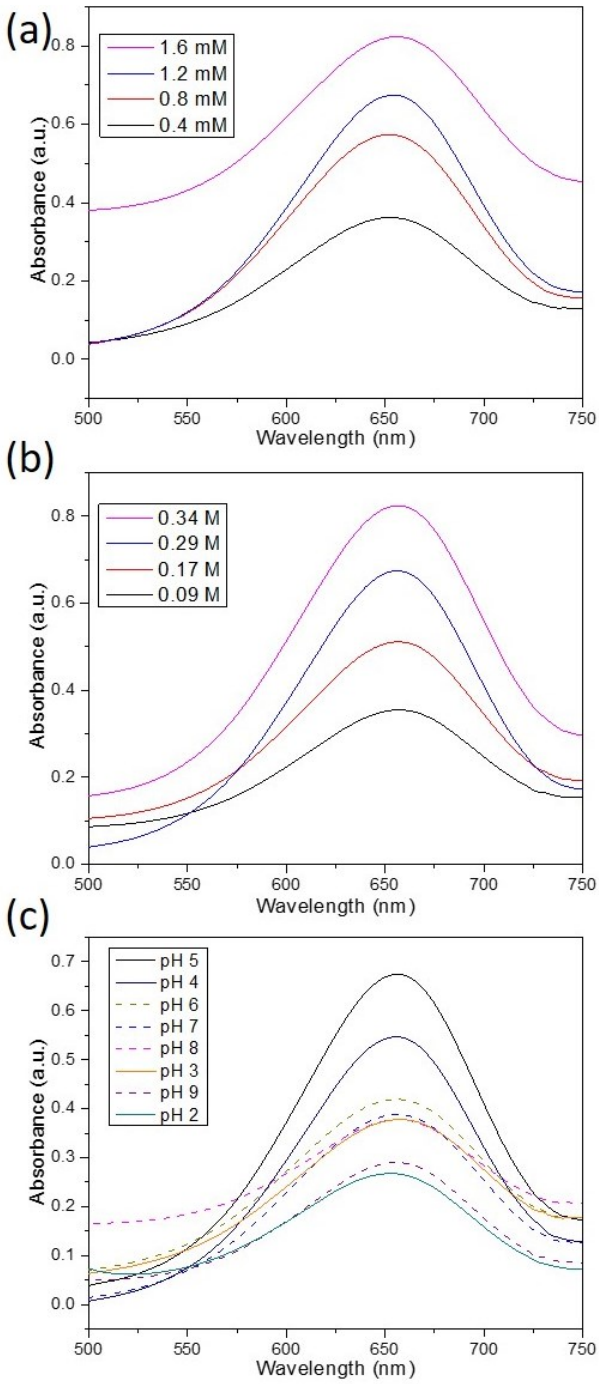

Figure 4.3: Representative UV-Vis absorbance spectra for TMB solutions oxidized in the absence of uric acid: (a) the TMB concentration is varied at a fixed pH (pH 5) and H_2O_2 concentration (0.29 M); (b) the H_2O_2 concentration is varied at a fixed pH (pH 5) and TMB concentration (1.2 mM); and (c) the pH is varied at fixed TMB and H_2O_2 concentrations (1.2 mM and 0.29 M, respectively). Spectra were recorded after 15 minutes of contact time with the Ni GLAD film, which was removed before measurement.

In its oxidized form, the chromogenic reagent TMB appears blue in solution, and thus, increasing the TMB concentration in the reaction mixture was expected to lead to greater absorbance at 652 nm. This effect is observed in Fig 4.3a, where increasing the concentration was found to increase the light absorption. We also found that the standard deviation of absorption measurements decreased for greater TMB concentrations (Fig 4.4a), and therefore, we fixed the TMB concentration to 1.6 mM in all subsequent experiments.

In Fig 4.3b, absorbance changes in response to variations in H_2O_2 concentration are shown. As hydroxyl radicals are known to oxidize TMB, greater H_2O_2 concentrations were expected to result in more strongly absorbing oxTMB solutions; this effect is observed in Fig 4.3b. The peak absorbance and standard deviation are shown in Fig 4.4b.

Fixing the TMB concentration at 1.2 mM and the H_2O_2 concentration at 0.29 M, we found that pH had a large influence over oxidation of the TMB. Fig 4.3(c) shows that lower pH values lead to dramatically increased absorption at 652 nm, with the highest absorbance measured at pH 5. The breakdown of hydrogen peroxide at low pH leads to the formation of $OH\cdot$ radicals which likely promote TMB oxidation and lead to increased absorbance (38). Earlier studies of enzyme-catalyzed TMB oxidation have described a tendency of oxTMB to further oxidize into diimine at pH values below 4.(39) We also observed a reduced absorption for all pH values below pH 5, and because of this, we fixed pH 5 as our optimum, and all subsequent experiments were performed at pH 5.

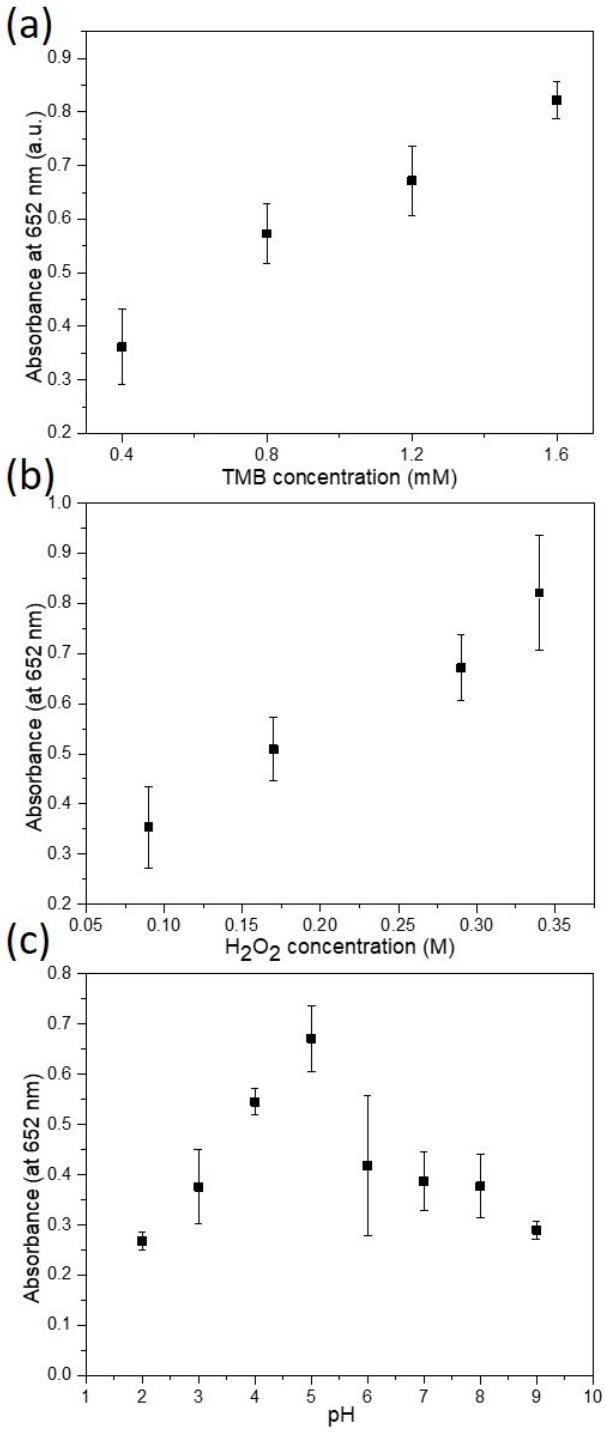

Figure 4.4: Peak absorbance at 652 nm for TMB solutions oxidized in the absence of uric acid: (a) the TMB concentration is varied at a fixed pH (pH 5) and H_2O_2 concentration (0.29 M); (b) the H_2O_2 concentration is varied at a fixed pH (pH 5) and TMB concentration (1.2 mM); and (c) the pH is varied at fixed TMB and H_2O_2 concentrations (1.2 mM and 0.29 M, respectively). Spectra

were recorded after 15 minutes of contact time with the Ni GLAD film, which was removed before measurement.

4.4.3 Peroxidase-like catalytic activity

In order to demonstrate the increased catalytic activity of the GLAD film, the oxidation of TMB was compared for flat and GLAD Ni films as well as a catalyst-free solution. Fig 4.5 shows UV-Vis spectra recorded for optimized 1.6 mM TMB solutions at pH 5 after 15 minutes in the presence of 0.29 M H_2O_2 and the catalytic Ni films. The catalyst-free solution (without either Ni film) has a relatively featureless UV-Vis spectrum with a gentle curve; by eye, the solution appeared colorless. On the other hand, for the flat Ni film, a relatively small peak (0.19 a.u.) is observed, and a faint blue color could be seen in solution. For the nanostructured nickel GLAD films, a dramatically increased absorption peak is observed at 652 nm (0.82 a.u.), and the solution appeared blue. This enzyme-like activity of the Ni films may originate from the Ni^{2+} ions present at the surface of the films (40). Using the Beer-Lambert equation, we can estimate the oxTMB concentrations of the solutions oxidized in the presence of flat and GLAD catalytic films to be 4.8 μM and 21 μM, respectively. The concentration achieved using the flat film is considerably lower than for the GLAD film, and thus we can conclude that the catalytic effect of the GLAD film is much stronger than that of the flat films for this reaction. This may be closely related to the high surface area of GLAD pillars and the associated high concentration of catalytically-active sites (41). These qualities of GLAD films have previously been shown to promote enhanced analyte sensitivity in systems such as indium tin oxide (ITO) columns modified with toll-like receptors for pathogen identification or ITO columns modified with recombinant hemoglobin I for H_2S detection (42,43).

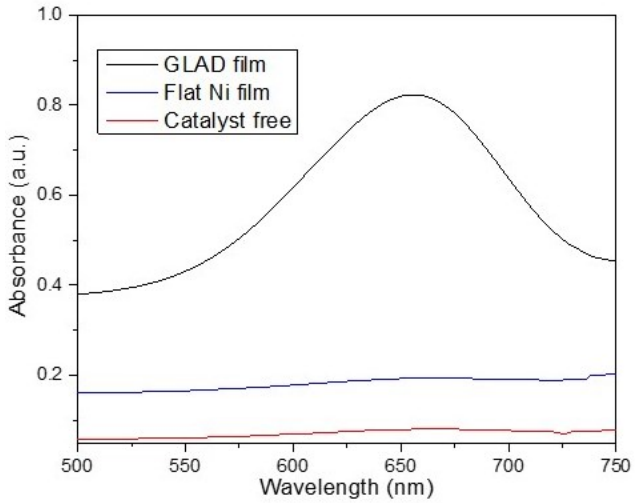

Figure 4.5: Comparison of absorbance spectra for aqueous solutions of 1.6 mM TMB as oxidized by a GLAD Ni film (black line), a flat Ni film (blue line) and a catalyst free solution (blue line) in the presence of 0.29 M H_2O_2 at pH 5. The areas of the catalyst films were both 0.5 cm^2, and the total volume of solution was 515 µL.

To further evaluate the performance of the catalytic films, the reaction kinetics were also studied and modelled using the Michaelis-Menten equation. Fig 4.6 describes the relationship between the rate of TMB conversion, V, and the TMB concentration, [S], for GLAD and flat Ni films. At low concentrations, the reaction rate increases linearly with TMB concentration ($R^2 = 0.996$); however, beyond a certain TMB concentration, the density of catalytically-active sites becomes the limiting factor and the reaction rate saturates. Using Equation 1, the Michaelis-Menten constant, K_m, which describes the substrate concentration when the reaction rate is half of the maximum reaction rate, was estimated to be 1.07 mM for the Ni GLAD film and 2.38 mM for the flat Ni film. The lower value is desirable as it indicates that the GLAD catalyst has greater affinity for TMB than its flat counterpart. Comparing these kinetic parameters to values obtained for other catalysts (see Table 4.1), it is clear that GLAD films exhibit good catalytic behavior for the oxidation of TMB in the presence of H_2O_2.

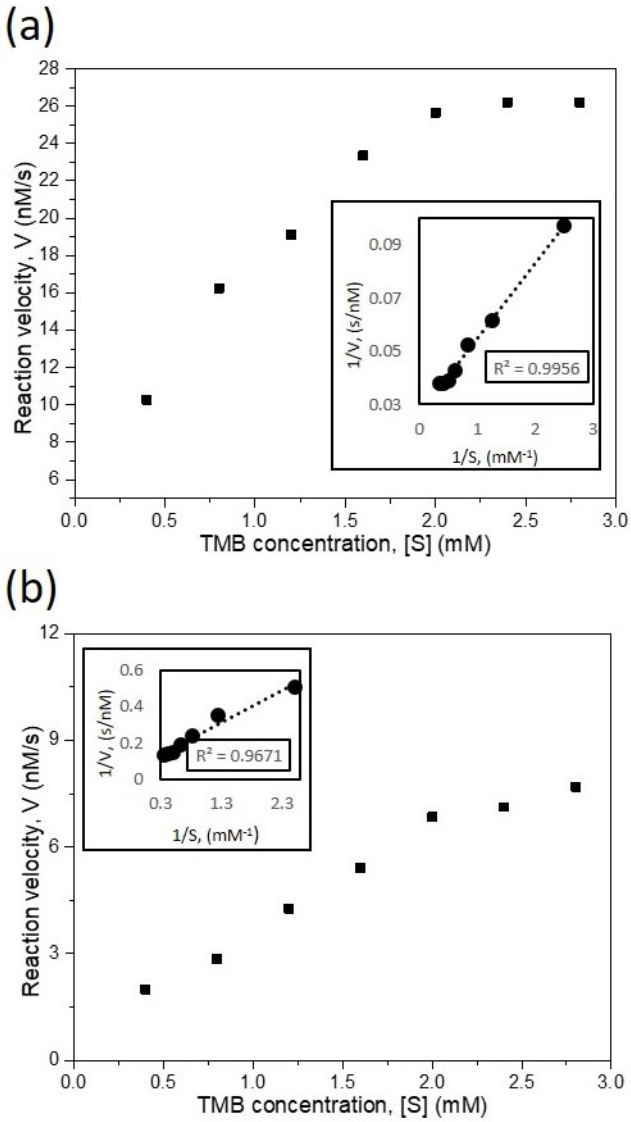

Figure 4.6: TMB conversion rate vs. concentration for TMB in the presence of (a) the GLAD film and (b) the flat Ni film.

Table 4.1: K_m values for different peroxidase mimicking materials.

Catalyst	K_m (mM)	Ref.
Hemin	5.23	(44)

HRP	0.43	(11,44)
CuS nanoparticles	0.21	(11)
Ni GLAD film	1.07	This work
Ni flat film	2.38	This work

4.4.4 Reusability of catalytic GLAD film

The reusability of the GLAD films was evaluated by recording absorbance spectra after consecutive TMB/H_2O_2 reactions. Each reaction cycle was performed for 15 minutes in the presence of the same Ni GLAD film, and after every measurement, the catalytic film was removed from solution, rinsed, and immersed in a fresh TMB/H_2O_2 solution before the next data point was collected. Precise handling and washing of the GLAD films with organic solvents after each use was important to ensure repeatability. As depicted in Fig 4.7, the absorbance of the oxTMB solutions after each reaction cycle was relatively constant (0.82 ± 0.03) indicating that the GLAD films can be reliably reused without a reaction terminating agent (45). This suggests that the GLAD catalyst may be more environmentally friendly and economically efficient than other technologies, and possibly easier to implement in the field.

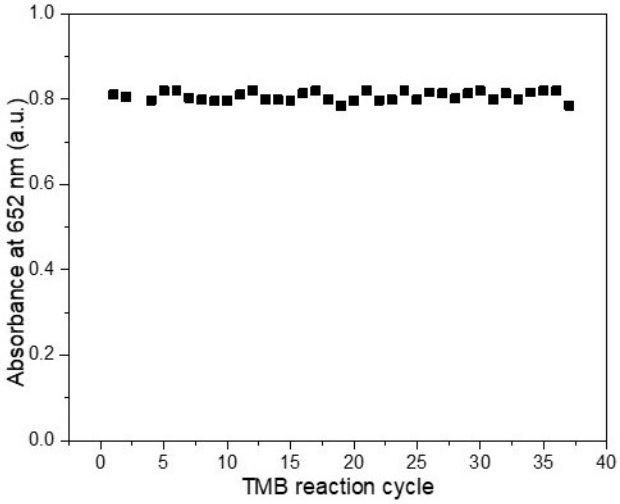

Figure 4.7: Absorbance of optimized oxTMB solutions at 652 nm. For every data point, a fresh solution (1.6 mM TMB, 0.29 M H_2O_2, pH 5) was prepared and left in the presence of the same 0.5 cm^2 Ni GLAD film for 15 min. After 15 min, the absorbance was measured and the solution discarded.

4.4.5 Colorimetric sensing of uric acid

UA biosensors were comprised of 515 µL of oxTMB/H_2O_2 solution, which was initially blue in color (absorbance of 0.82 a.u.). 100 µL of UA solution was then added at concentrations of 0 µM to 594 µM, resulting in a final volume of 615 µL. The biosensor operates based on the UA-activated suppression of the TMB color reaction; as shown in Fig 4.8(a), the higher the concentration of UA that was added, the lighter in color the solution became. In the UV-Vis spectra shown in Fig 4.8(b), the absorbance peak at 652 nm decreases with increasing UA concentration. Notably, UA concentrations as low as 1.5 µM were found to have an observable effect on the UV-Vis spectra. In the figures, the original concentration of the added UA is reported on the x-axis rather than the diluted values (which take into account the volume of the oxidized TMB and H_2O_2) because these represent the concentrations of UA in the actual test samples. For example, when

solutions containing 0 μM UA were added to the oxTMB/H_2O_2, the absorbance decreased from 0.821 to 0.812 due to the effect of the dilution.

The effect of the UA concentration over absorbance at 652 nm is shown in Fig 4.8(c), and a non-linear response was observed. In the low concentration end of the curve (0-6 μM), however, a fairly linear response was noted ($R^2 = 0.98$). The achieved limit of detection (LOD), 3.3 μM, was calculated using 3σ/slope within this low concentration range, and this value is lower than the UA concentration found in sweat (18-35 μM) (8).

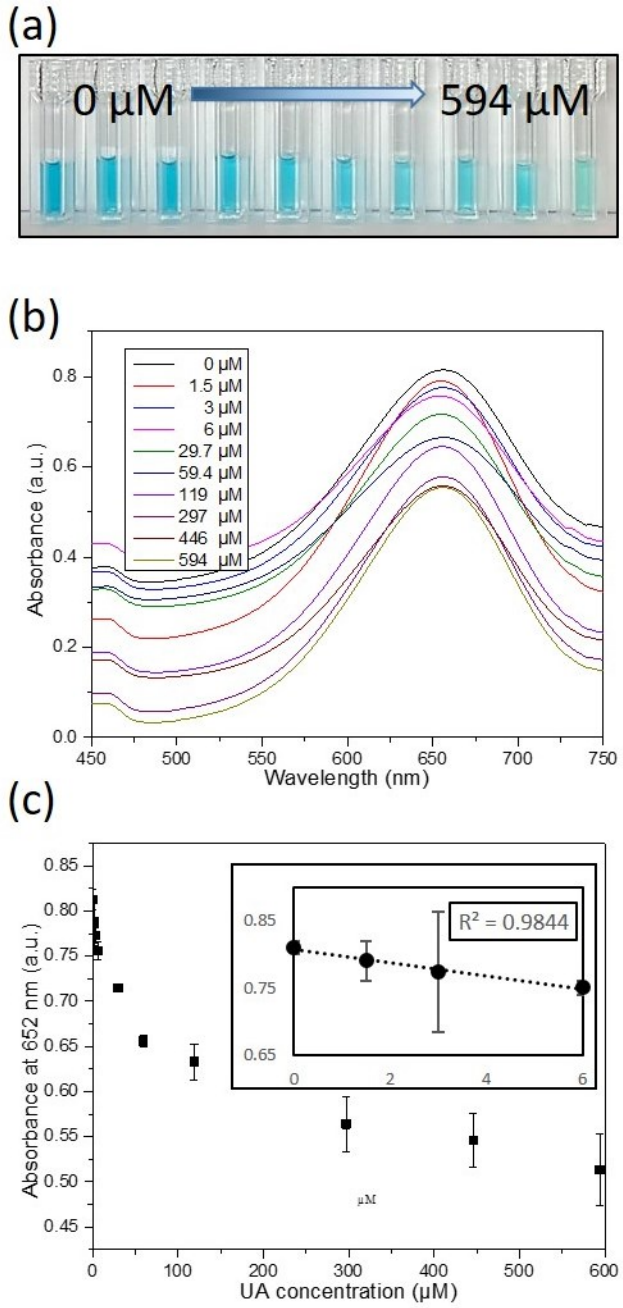

Figure 4.8: (a) Images of oxidized 1.6 mM TMB solutions, reduced via addition of UA solutions of various concentrations. (b) UV-Vis absorption spectra of the samples shown in (a). (c) Response curve for UA concentrations from 0 µM to 594 µM (Inset: zoomed in view of the low concentration region up to 6 µM).

To investigate the specificity of the biosensor, the response of the oxTMB solution to urea and glucose — which are also found in sweat — was characterized. In Fig 4.9, the GLAD Ni sensor's responses to equal concentrations (446 μM) of glucose, urea and UA are presented. As depicted, the change in absorbance is the greatest in response to UA, however, the addition of either glucose or urea also strongly suppresses the absorbance at 652 nm. Because these substances are found in high concentrations in sweat (22 mM for urea, and 1 mM for glucose), the data indicate that interference is likely to complicate the quantification of UA concentration based on the TMB mechanism (8,46). Because the TMB redox process is not unique to our sensing platform, other TMB-based sensor systems are also quite likely to suffer from these interference issues. One approach that could potentially be taken in the future to mitigate interference would be to use membrane separators to ensure that only UA reaches the sensor. Additional interferents such as Na^+, Cl^-, and Fe^{3+} should also be taken into account.

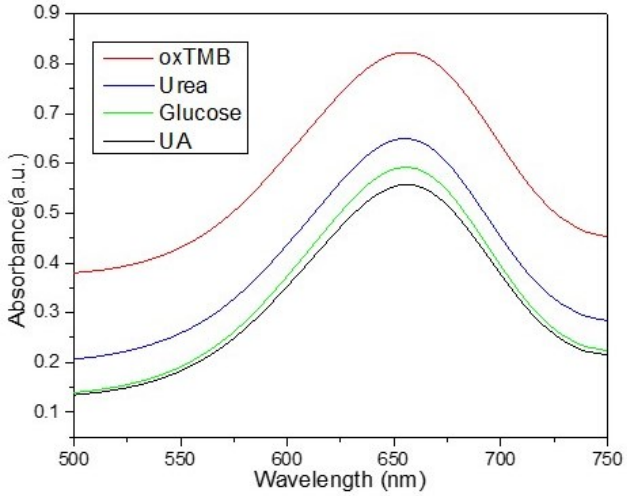

Figure 4.9: Comparison of absorbance spectra for oxTMB solutions before (red) and after the addition of 446 μM of urea (blue), glucose (green), or UA (black).

4.5 Conclusions

In summary, we have fabricated helically-structured Ni nanofilms on silicon substrates using GLAD, and we found that these films exhibited peroxidase-like activity to catalyze the oxidation of TMB. We utilized this colorimetric TMB/oxTMB reaction to form uric acid sensors that were able to achieve a low LOD (3.3 μM) and were sensitive throughout the entire clinically-relevant range (15-500 μM). The advantages of on-demand analysis, good recyclability, excellent analytical performance and visual detection, as well as the lack of natural enzymes and terminating agents, suggest GLAD-based sensors may be a promising tool for UA detection. However, we also conducted an interference study for TMB-based uric acid sensors, and we found that in addition to UA-sensitivity, the TMB-centered system also responds to several common metabolites (specifically, glucose and urea). The fact that colorimetric nanozyme/TMB-based sensor for other analytes including glucose, cysteine, and ascorbic acid have been demonstrated underscores the lack of specificity of this process (47–50). Care must therefore be taken to mitigate interference effects, particularly when working with complex biological samples such as blood or sweat.

Despite this limitation, glancing angle deposition is a versatile technique that can be used to fabricate nanostructured-thin films from wide range of materials, including precious metals, transition metals, oxides, and carbon (i.e., materials that can be evaporated). In this work, we have shown that helical nickel films exhibit enhanced catalytic activity for TMB oxidation; nanostructured thin films deposited by GLAD could potentially be used as nanozymes in reactions beyond TMB oxidation. To realize the full potential of GLAD films as reusable catalysts, the effects of the many tailorable physical properties must be explored.

References

1. Klinenberg JR. Current Concepts of Hyperuricemia and Gout. Calif Med. 1969;110(3):231–44.

2. Kaneko K, Aoyagi Y, Fukuuchi T, Inazawa K, Yamaoka N. Total Purine and Purine Base Content of Common Foodstuffs for Facilitating Nutritional Therapy for Gout and Hyperuricemia. Biol Pharm Bull [Internet]. 2014;37(5):709–21. Available from: https://www.jstage.jst.go.jp/article/bpb/37/5/37_b13-00967/_article

3. Kumar A, Hens A, Arun RK, Chatterjee M, Mahato K, Layek K, et al. A paper based microfluidic device for easy detection of uric acid using positively charged gold nanoparticles. Analyst [Internet]. 2015;140(6):1817–21. Available from: http://xlink.rsc.org/?DOI=C4AN02333A

4. Benn CL, Dua P, Gurrell R, Loudon P, Pike A, Storer RI, et al. Physiology of Hyperuricemia and Urate-Lowering Treatments. Front Med [Internet]. 2018 May 31;5:1–28. Available from: https://www.frontiersin.org/article/10.3389/fmed.2018.00160/full

5. Kumar S, Bhushan P, Bhattacharya S. Development of a paper-based analytical device for colorimetric detection of uric acid using gold nanoparticles–graphene oxide (AuNPs–GO) conjugates. Anal Methods [Internet]. 2016;8(38):6965–73. Available from: http://xlink.rsc.org/?DOI=C6AY01926A

6. El Ridi R, Tallima H. Physiological functions and pathogenic potential of uric acid: A review. J Adv Res [Internet]. 2017 Sep;8(5):487–93. Available from: https://linkinghub.elsevier.com/retrieve/pii/S2090123217300346

7. Desideri G, Castaldo G, Lombardi A, Mussap M, Testa A, Pontremoli R, et al. Is it time to revise the normal range of serum uric acid levels? Eur Rev Med Pharmacol Sci. 2014;18(9):1295–306.

8. Huang CT, Chen ML, Huang LL, Mao IF. Uric acid and urea in human sweat. Chin J Physiol. 2002;45(3):109–15.

9. Dong X. Study on Detection Methods for Uric Acid in Biological Samples. Int J Pharm Sci Res. 2017;8(2):925–9.

10. Dai X, Fang X, Zhang C, Xu R, Xu B. Determination of serum uric acid using high-performance liquid chromatography (HPLC)/isotope dilution mass spectrometry (ID-MS) as a candidate reference method. J Chromatogr B [Internet]. 2007 Oct;857(2):287–95. Available from: https://linkinghub.elsevier.com/retrieve/pii/S1570023207005454

11. Wang X, Tang CL, Liu JJ, Zhang H-Z, Wang J. Ultra-small CuS Nanoparticles as Peroxidase Mimetics for Sensitive and Colorimetric Detection of Uric Acid in Human Serum. Chinese J Anal Chem [Internet]. 2018;46(5):e1825–31. Available from: http://dx.doi.org/10.1016/S1872-2040(17)61083-1

12. Lakshmi D, Whitcombe MJ, Davis F, Sharma PS, Prasad BB. Electrochemical Detection of Uric Acid in Mixed and Clinical Samples: A Review. Electroanalysis [Internet]. 2011 Feb;23(2):305–20. Available from: https://onlinelibrary.wiley.com/doi/10.1002/elan.201000525

13. Zhou W, Gao X, Liu D, Chen X. Gold Nanoparticles for In Vitro Diagnostics. Chem Rev [Internet]. 2015 Oct 14;115(19):10575–636. Available from: https://pubs.acs.org/doi/10.1021/acs.chemrev.5b00100

14. Josephy PD, Eling T, Mason RP. The horseradish peroxidase-catalyzed oxidation of 3,5,3',5'-tetramethylbenzidine. Free radical and charge-transfer complex intermediates. J Biol Chem. 1982;257(7):3669–75.

15. Njagi JI, Kagwanja SM. Interfaces and Interphases in Analytical Chemistry [Internet]. Helburn R, Vitha MF, editors. Interfaces and Interphases in Analytical Chemistry. Washington, DC: American Chemical Society; 2011. 225–247 p. (ACS Symposium Series; vol. 1062). Available from: https://pubs.acs.org/doi/book/10.1021/bk-2011-1062

16. Caves MS, Derham BK, Jezek J, Freedman RB. Thermal Inactivation of Uricase (Urate Oxidase): Mechanism and Effects of Additives. Biochemistry [Internet]. 2013 Jan 22;52(3):497–507. Available from: https://pubs.acs.org/doi/10.1021/bi301334w

17. Çete S, Yaşar A, Arslan F. An Amperometric Biosensor for Uric Acid Determination Prepared from Uricase Immobilized in Polypyrrole Film. Artif Cells, Blood Substitutes, Biotechnol [Internet]. 2006 Jan 11;34(3):367–80. Available from: http://www.tandfonline.com/doi/full/10.1080/10731190600684116

18. Zhuang QQ, Lin ZH, Jiang YC, Deng HH, He S Bin, Su LT, et al. Peroxidase-like activity of nanocrystalline cobalt selenide and its application for uric acid detection. Int J Nanomedicine. 2017;12:3295–302.

19. Wu J, Li S, Wei H. Integrated nanozymes: facile preparation and biomedical applications. Chem Commun [Internet]. 2018;54(50):6520–30. Available from: http://xlink.rsc.org/?DOI=C8CC01202D

20. Lu J, Xiong Y, Liao C, Ye F. Colorimetric detection of uric acid in human urine and serum based on peroxidase mimetic activity of MIL-53(Fe). Anal Methods [Internet]. 2015;7(23):9894–9. Available from: http://xlink.rsc.org/?DOI=C5AY02240A

21. Liu X, Qi W, Wang Y, Su R, He Z. A facile strategy for enzyme immobilization with highly stable hierarchically porous metal–organic frameworks. Nanoscale [Internet]. 2017;9(44):17561–70. Available from: http://xlink.rsc.org/?DOI=C7NR06019J

22. Lu H-F, Li J-Y, Zhang M-M, Wu D, Zhang Q-L. A highly selective and sensitive colorimetric uric acid biosensor based on Cu(II)-catalyzed oxidation of 3,3′,5,5′-tetramethylbenzidine. Sensors Actuators B Chem [Internet]. 2017 Jun;244:77–83. Available from: http://dx.doi.org/10.1016/j.snb.2016.12.127

23. Wang X, Cao W, Qin L, Lin T, Chen W, Lin S, et al. Boosting the Peroxidase-Like

Activity of Nanostructured Nickel by Inducing Its 3+ Oxidation State in LaNiO3 Perovskite and Its Application for Biomedical Assays. Theranostics [Internet]. 2017;7(8):2277–86. Available from: http://www.thno.org/v07p2277.htm

24. Tripathi A. Parametric Studies of In-house Resin for Hardness Removal. Emerg Trends Chem Eng. 2014;1(3):34–9.

25. He Y, Qi F, Niu X, Zhang W, Zhang X, Pan J. Uricase-free on-demand colorimetric biosensing of uric acid enabled by integrated CoP nanosheet arrays as a monolithic peroxidase mimic. Anal Chim Acta [Internet]. 2018;1021:113–20. Available from: https://doi.org/10.1016/j.aca.2018.02.073

26. Eskandarloo H, Zaferani M, Kierulf A, Abbaspourrad A. Shape-controlled fabrication of TiO2 hollow shells toward photocatalytic application. Appl Catal B Environ [Internet]. 2018 Jul;227:519–29. Available from: https://doi.org/10.1016/j.apcatb.2018.01.059

27. Barranco A, Borras A, Gonzalez-Elipe AR, Palmero A. Perspectives on oblique angle deposition of thin films: From fundamentals to devices. Prog Mater Sci [Internet]. 2016 Mar;76:59–153. Available from: https://linkinghub.elsevier.com/retrieve/pii/S0079642515000705

28. Hawkeye MM, Brett MJ. Glancing angle deposition: Fabrication, properties, and applications of micro- and nanostructured thin films. J Vac Sci Technol A Vacuum, Surfaces, Film [Internet]. 2007;25(5):1317. Available from: http://scitation.aip.org/content/avs/journal/jvsta/25/5/10.1116/1.2764082

29. Taschuk MT, Hawkeye MM, Brett MJ. Glancing Angle Deposition [Internet]. Third Edit. Handbook of Deposition Technologies for Films and Coatings. Elsevier Ltd.; 2010. 621–678 p. Available from: http://dx.doi.org/10.1016/B978-0-8155-2031-3.00013-2

30. Malac M, Egerton RF. Observations of the microscopic growth mechanism of pillars and helices formed by glancing-angle thin-film deposition. J Vac Sci Technol A Vacuum, Surfaces, Film [Internet]. 2001 Jan;19(1):158–66. Available from: http://avs.scitation.org/doi/10.1116/1.1326940

31. Tyagi M, Tomar M, Gupta V. Glad assisted synthesis of NiO nanorods for realization of enzymatic reagentless urea biosensor. Biosens Bioelectron [Internet]. 2014 Feb;52:196–201. Available from: https://linkinghub.elsevier.com/retrieve/pii/S0956566313005617

32. Krause KM, Taschuk MT, Harris KD, Rider DA, Wakefield NG, Sit JC, et al. Surface Area Characterization of Obliquely Deposited Metal Oxide Nanostructured Thin Films. Langmuir [Internet]. 2010 Mar 16;26(6):4368–76. Available from: https://pubs.acs.org/doi/10.1021/la903444e

33. Harris KD, Vick D, Smy T, Brett MJ. Column angle variations in porous chevron thin films. J Vac Sci Technol A Vacuum, Surfaces, Film. 2002;20(6):2062.

34. Valdés-Martínez OU, Santolalla-Vargas CE, Santes V, de los Reyes JA, Pawelec B, Fierro JLG. Influence of calcination on metallic dispersion and support interactions for

NiRu/TiO2 catalyst in the hydrodeoxygenation of phenol. Catal Today [Internet]. 2019;329:149–55. Available from: https://doi.org/10.1016/j.cattod.2018.11.007

35. Li H, Ren C, Zhang R, Li R, Xu S, Wang L, et al. One–step Synthesis of MnO/Ni Nanoparticles Anchored on Porous Nitrogen–doped Carbons from Melamine Foam and Electrocatalytic Study towards Oxygen Reduction Reaction. ChemistrySelect. 2017;2(15):4234–40.

36. Chao Y, Zheng J, Zhang H, Ma Y, Li F, Tan Y, et al. Constructing Film Photocatalyst with Abundant Interfaces between CdS and Ni3S2 Nanosheets for Efficient Photocatalytic Hydrogen Production. Energy Technol [Internet]. 2018 Nov;6(11):2132–8. Available from: http://doi.wiley.com/10.1002/ente.201800180

37. Morais A, Alves JPC, Lima FAS, Lira-Cantu M, Nogueira AF. Enhanced photovoltaic performance of inverted hybrid bulk-heterojunction solar cells using TiO2 /Reduced graphene oxide films as electron transport layers. J Photonics Energy [Internet]. 2015 Mar 12;5(1):057408. Available from: http://photonicsforenergy.spiedigitallibrary.org/article.aspx?doi=10.1117/1.JPE.5.057408

38. Chen L, Li X, Zhang J, Fang J, Huang Y, Wang P, et al. Production of Hydroxyl Radical via the Activation of Hydrogen Peroxide by Hydroxylamine. Environ Sci Technol. 2015;49(17):10373–9.

39. Lou D, Tian Y, Zhang Y, Yin J, Yang T, He C, et al. Peroxidase-Like Activity of Gold Nanoparticles and Their Gold Staining Enhanced ELISA Application. J Nanosci Nanotechnol. 2017;18(2):951–8.

40. Hengne AM, Samal AK, Enakonda LR, Harb M, Gevers LE, Anjum DH, et al. Ni–Sn-Supported ZrO 2 Catalysts Modified by Indium for Selective CO 2 Hydrogenation to Methanol. ACS Omega [Internet]. 2018 Apr 30;3(4):3688–701. Available from: https://pubs.acs.org/doi/10.1021/acsomega.8b00211

41. Sit JC, Broer DJ, Brett MJ. Optical devices fabricated from porous thin films embedded with liquid crystals. In: International Electron Devices Meeting 1999 Technical Digest (Cat No99CH36318) [Internet]. IEEE; 1999. p. 123–6. Available from: http://ieeexplore.ieee.org/document/823861/

42. Lin D, Harris KD, Chan NWC, Jemere AB. Nanostructured indium tin oxide electrodes immobilized with toll-like receptor proteins for label-free electrochemical detection of pathogen markers. Sensors Actuators B Chem [Internet]. 2018 Mar;257:324–30. Available from: https://linkinghub.elsevier.com/retrieve/pii/S0925400517320543

43. Dulac M, Melet A, Harris KD, Limoges B, Galardon E, Balland V. An optical H2S biosensor based on the chemoselective Hb-I protein tethered to a transparent, high surface area nanocolumnar electrode. Sensors Actuators B Chem [Internet]. 2019 Jul;290:326–35. Available from: https://linkinghub.elsevier.com/retrieve/pii/S0925400519304903

44. Zhang L, Fan C, Liu M, Liu F, Bian S, Du S, et al. Biominerized gold-Hemin@MOF composites with peroxidase-like and gold catalysis activities: A high-throughput

colorimetric immunoassay for alpha-fetoprotein in blood by ELISA and gold-catalytic silver staining. Sensors Actuators B Chem [Internet]. 2018 Aug;266:543–52. Available from: https://linkinghub.elsevier.com/retrieve/pii/S0925400518306518

45. Frey A, Meckelein B, Externest D, Schmidt MA. A stable and highly sensitive 3,3′,5,5′-tetramethylbenzidine-based substrate reagent for enzyme-linked immunosorbent assays. J Immunol Methods [Internet]. 2000 Jan;233(1–2):47–56. Available from: https://linkinghub.elsevier.com/retrieve/pii/S0022175999001660

46. Lee H, Song C, Hong YS, Kim MS, Cho HR, Kang T, et al. Wearable/Disposable sweat-based glucose monitoring device with multistage transdermal drug delivery module. Sci Adv [Internet]. 2017 Mar 8;3(3):e1601314. Available from: http://advances.sciencemag.org/lookup/doi/10.1126/sciadv.1601314

47. Liang M, Yan X. Nanozymes: From New Concepts, Mechanisms, and Standards to Applications. Acc Chem Res [Internet]. 2019 Aug 20;52(8):2190–200. Available from: https://pubs.acs.org/doi/10.1021/acs.accounts.9b00140

48. Lee P-C, Li N-S, Hsu Y-P, Peng C, Yang H-W. Direct glucose detection in whole blood by colorimetric assay based on glucose oxidase-conjugated graphene oxide/MnO 2 nanozymes. Analyst [Internet]. 2019;144(9):3038–44. Available from: http://xlink.rsc.org/?DOI=C8AN02440E

49. Ray C, Dutta S, Sarkar S, Sahoo R, Roy A, Pal T. Intrinsic peroxidase-like activity of mesoporous nickel oxide for selective cysteine sensing. J Mater Chem B [Internet]. 2014 Jul 18;2(36):6097. Available from: http://xlink.rsc.org/?DOI=C4TB00968A

50. Zhong M, Chi M, Ma F, Zhu Y, Wang C, Lu X. Dual Responsive Enzyme Mimicking of Ternary Polyaniline–MnO 2 –Pd Nanowires and Its Application in Colorimetric Biosensing. ACS Sustain Chem Eng [Internet]. 2018 Dec 3;6(12):16482–92. Available from: https://pubs.acs.org/doi/10.1021/acssuschemeng.8b03567

51. Satterfield CN. Chemical reaction engineering, Octave Levenspiel, Wiley, New York(1972). AIChE J [Internet]. third. 1973 Jan;19(1):21–2. Available from: http://scholar.google.com/scholar?hl=en&btnG=Search&q=intitle:chemical+reaction+engineering#0

52. Liu Y, Zhu G, Yang J, Yuan A, Shen X. Peroxidase-like catalytic activity of Ag3PO4 nanocrystals prepared by a colloidal route. PLoS One. 2014;9(10):3–9.

Chapter 5. High surface area nitrogen-functionalized Ni nanozymes for efficient peroxidase-like catalytic activity[3]

Anuja Tripathi[1, 2], Kenneth D. Harris[1, 3], Anastasia L. Elias[2,*]

[1]National Research Council Canada, Nanotechnology Research Centre, Edmonton, 11421 Saskatchewan Dr. NW, Edmonton, T6G 2M9, Canada

[2]Department of Chemical and Materials Engineering, University of Alberta, Edmonton, T6G 2R3, Canada

[3]Department of Mechanical Engineering, University of Alberta, Edmonton, T6G 1H9, Canada

---

5.1 Abstract

N-functionalization is an effective means of improving the catalytic performances of nanozymes. In the present work, plasma-assisted nitrogen (N) modification of nanocolumnar Ni GLAD films was performed using an ammonia (NH_3) plasma, resulting in an improvement in the peroxidase-like catalytic performance of the porous, nanostructured Ni films. The plasma-treated nanozymes were characterized by TEM, SEM, XRD, and XPS, revealing a nitrogen-rich surface composition. Increased surface wettability was observed after ammonia plasma treatment, and the resulting N-functionalized Ni GLAD films presented dramatically enhanced peroxidase-like catalytic activity. The optimal time for plasma treatment was determined to be 120 s; when used to catalyze the oxidation of the colorimetric substrate TMB in the presence of H_2O_2, Ni films subjected to 120 s

[3] A version of this chapter has been published as Anuja Tripathi, Kenneth D. Harris, Anastasia L. Elias, PloS ONE, 2021, 16(10): e0257777

of plasma treatment yielded a much higher maximum reaction velocity (3.7×10^{-8} M/s vs 2.3×10^{-8} M/s) and lower Michaelis-Menten coefficient (0.17 mM vs 0.23 mM) than pristine Ni films with the same physical parameters. Additionally, we demonstrated the application of the nanozyme in a gravity-driven, continuous catalytic reaction device. Such a controllable plasma treatment strategy may open a new door toward surface-functionalized nanozymes with improved catalytic performance and potential applications in flow-driven point of care devices.

Keywords: plasma treatment, nitrogen functionalization, nanozyme, GLAD thin films, peroxidase activity, microfluidics

5.2 Introduction

Enzymes are complex biological structures that play key roles in metabolic activities and catalyze numerous biological reactions with excellent catalytic activity, efficiency, and selectivity. These natural enzymes, however, also generally require well-controlled reaction conditions (temperature, pH, purity, etc.) (1), and outside of the human body, precisely controlling these operation and storage conditions can be very difficult, which limits commercial applications (2). As an alternative, artificial enzymes known as "nanozymes" are nanomaterials with enzyme-like characteristics (3,4). Nanozymes have attracted enormous research interest in recent years for their unique advantages (low cost, tunable catalytic activity, stability under a wide range of conditions, and ease of mass production), which make them candidates for applications in biosensing, tissue engineering, therapeutics, and environmental protection (5,6).

Peroxidase is an important natural enzyme assisting in a wide range of physiological reaction pathways (7,8). Since the first evidence of ferromagnetic peroxidase mimetics was reported in

2007 (9), various nanomaterials have been identified that possess intrinsic peroxidase-like activity. These include graphene oxide (10), gold nanoparticles (11), and metal-organic frameworks (MOFs) (12). One reason that nanomaterials are effective as nanozymes stems from their large specific surface area, which results in both a high surface energy and concentration of catalytically active sites (13). Surface energy can often be further enhanced by surface modification, utilizing methods such as the introduction of surfactants, or doping of various atoms such as phosphorus, sulfur, and nitrogen (14). For instance, electrocatalytic performance was improved by chemical vapor deposition of N functionalized carbon nanotube cups for glucose and H_2O_2 detection, and hydrothermal doping with N and S on MoO_2 nanobelts for hydrogen evolution reaction (15,16). In each case, the improved performance was attributed to improved charge transport as a result of increased surface electron density. Several challenges, however, remain in the implementation of both peroxidase-like nanozymes and other types of nanozymes. First, most of the reported nanozymes are nanomaterials dispersed in solution, rendering the materials hard to recover and reuse. Second, nanozymes tend to have lower densities of active sites by mass than natural enzymes, resulting in reduced enzyme-like activity (17,18). Solving either of these challenges would lead to more practical nanozyme materials.

Numerous research groups (including our own) have examined the use of high-surface area thin films deposited by glancing angle deposition (GLAD) as catalytic materials (13,19,20). GLAD is a physical vapor deposition technique that uses atomic shadowing and dynamic motion control to create nanostructures with a large surface area and controlled porosity (21). During GLAD, vapor flux is incident upon the substrate at glancing angles (>70° with respect to the surface normal). The porous nanosized columnar thin films fabricated by GLAD are separated by wide gaps and possess high internal porosity (22). By employing dynamic substrate motion, the GLAD technique

also enables the fabrication of modified nanostructures with different shapes such as vertical columns, zigzags, helices, and slanted posts (20,23). As they possess an enormous internal surface area that is easily accessible to ambient species, these GLAD-based structures have previously been employed as biosensors for various substrates (21,23,24). In our own previous work, we demonstrated the peroxidase-like behavior of helically-structured Ni GLAD films using TMB as a substrate. This process is illustrated in Scheme 1, where the oxidation of colorless TMB (the substrate) into blue oxTMB (the product) occurs in the presence of H_2O_2 and the peroxidase-like catalyst (13). In this previous work, the oxTMB product was further used as an optical sensor for uric acid (UA).

In the present work, we aim to improve the GLAD-based nanozymes' peroxidase-like activity through nitridization of these nanostructured films. Inspired by the above-mentioned work on surface modification, we deposit nanocolumnar Ni GLAD films and then N-functionalize these films in an NH_3 plasma. In a plasma treatment, energetic species bombard the target surface, causing topographical changes and incorporating various surface functional groups (25). Plasma treatment has emerged as a simple, rapid, and highly efficient tool for the green preparation and surface modification of nanomaterials, with the merits of low energy consumption and chemical waste-free yield (14). We utilize the plasma-modified and pristine Ni films to catalyze the oxidation of TMB by H_2O_2, and we show that the N-functionalized films present enhanced catalytic reaction rates. We demonstrate significantly improved catalytic performance parameters that are among the best in the literature for monometallic, surface-functionalized nanozymes. To further demonstrate the utility of the Ni nanozyme, we also assemble a simple gravity-driven continuous reaction device capable of converting TMB to oxTMB (as shown in Scheme 1). The device layout demonstrates a simple GLAD-based thin film architecture that leads toward

integration into portable, point of care devices for disease diagnostics. This device structure represents a step toward the introduction of nanozyme structures in real-world applications.

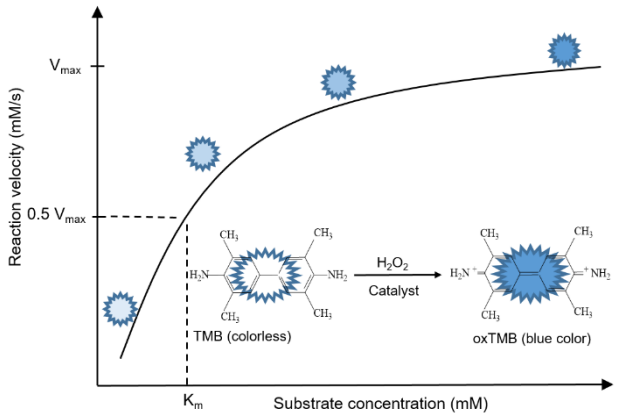

Scheme 1. Kinetic curve for peroxidase-like reaction using TMB as a substrate

5.3 Materials and Methods

5.3.1 Reagents

3,3',5,5'-Tetramethyl benzidine (TMB), hydrogen peroxide, isopropanol (IPA), dimethyl formamide (DMF), and phosphate citrate buffer (pH 5) were purchased from Sigma-Aldrich. Deionized water (0.055 µS) was used throughout this work. All chemicals were of analytical grade and were used as received without further purification.

5.3.2 Preparation of N-functionalized thin films

Ni thin films were deposited on piranha cleaned silicon wafers by electron beam evaporation. The base pressure prior to deposition was $<2\times10^{-6}$ Torr, and the pressure during the deposition was roughly 1×10^{-5} Torr. The deposition angle between the incident vapor flux and the substrate normal was 80°, and during deposition, the substrate was rotated at a rate of one complete revolution for

every 100 nm of film growth. Ammonia plasma treatment was performed in an instrument primarily intended for plasma-enhanced chemical vapor deposition: a Trion Orion PECVD. The films were exposed to a 220 W RF ammonia plasma at a temperature of 350°C. The ammonia flow rate was 20 sccm, and the operating pressure was kept at 400 mT. Plasma-free thermal treatment at 350 °C was also performed in the Trion Orion PECVD. Oxygen plasma treatment was executed in a Trion RIE at room temperature. The films were exposed to a 100 W RF oxygen plasma. The oxygen flow rate was 98 sccm and the operating pressure was 100 mT. The so-obtained thin films were stored at room temperature before use.

5.3.3 Apparatus

High-resolution scanning electron microscopy (SEM) was performed using a Hitachi S5500, and high-resolution transmission electron microscopy (HRTEM) was performed using a Hitachi H-9500 instrument. X-ray photoelectron spectroscopy (XPS, Kratos AXXIS Ultra) was used to analyze the surface composition of the GLAD film. Samples were irradiated with a monochromatic Al Kα source ($h\nu$ = 1486.71 eV), and the pressure of the analysis chamber was below 5×10^{-10} Torr during the elemental analysis. The phase compositions of the prepared materials were determined by X-ray powder diffractometry (Rigaku XRD Ultima IV). The diffraction patterns of samples were recorded in the range of 2θ=10-80° using a Cu radiation source with fixed power (40 kV, 44 mA). Contact angles of purified water droplets on Ni GLAD films were monitored using a First Ten Angstroms contact angle goniometer (FTA-200).

5.3.4 Measurements of peroxidase-like catalytic performances

Colorimetric investigations of the peroxidase-like catalytic performances were conducted using the chromogenic TMB-H_2O_2 reaction in phosphate citrate buffer (pH5). For the basic reaction,

0.7±0.02 cm^2 of Ni film was immersed in 525 µl of solution containing 0.4 mM TMB and 470 mM H_2O_2. Contact was maintained for 15 minutes, then the film was removed, and the absorbance spectra recorded. For optimization of the catalytic reaction conditions, the parameters were varied as noted in the accompanying text with all other conditions fixed as above.

5.3.5 Studies of Michaelis-Menten kinetics

The studies of the steady-state catalysis kinetics were performed at a fixed concentration of 470 mM H_2O_2 and varying concentrations of TMB. The absorbance values were recorded at 652 nm, and the kinetic catalysis parameters were obtained by linear fitting of the Lineweaver-Burk double-reciprocal plot. The Michaelis-Menten constant (K_m) and the maximal reaction velocity (V_{max}) were extracted from:

$$\frac{1}{V} = \frac{K_m}{V_{max}[TMB]} + \frac{1}{V_{max}}$$

where, V is the initial reaction velocity, and [TMB] refers to the substrate concentration.

5.4 Results and Discussion

5.4.1 Fabrication and characterization of pristine and nitrogen-functionalized Ni films

Nanocolumnar Ni films were deposited on Si substrates by GLAD and treated with NH_3 plasma for different lengths of time to yield N-functionalized Ni GLAD films. The morphologies of these Ni films were investigated by SEM (Fig 5.1a,b), and in all cases, a vertical columnar structure with large intercolumn distance was observed. No significant morphology changes were identified by

SEM following plasma treatment (Fig 5.2), indicating that the plasma processing does not strongly affect the film morphology and associated surface area. The nanocolumnar Ni films were approximately 600 nm thick with intercolumnar spacing of 90-120 nm. As will be relevant below, these intercolumnar distances are significantly larger than all chemical reactants and should allow diffusion into the interior of the GLAD structures.

The pristine and plasma-modified Ni films were also analyzed by high-resolution transmission electron microscopy (HRTEM, Fig 5.1c-f), and little structural variation was noted following plasma processing. Interplanar spacings of ~0.20 nm were measured for both pristine and plasma-modified films, which is close to the accepted value for (111) planes in face-centered cubic (FCC) Ni crystallites. This suggests that both films include FCC Ni crystallites, but due to the nature of this analysis technique, it does not necessarily indicate that this is the only – or even the most prevalent – crystal phase present.

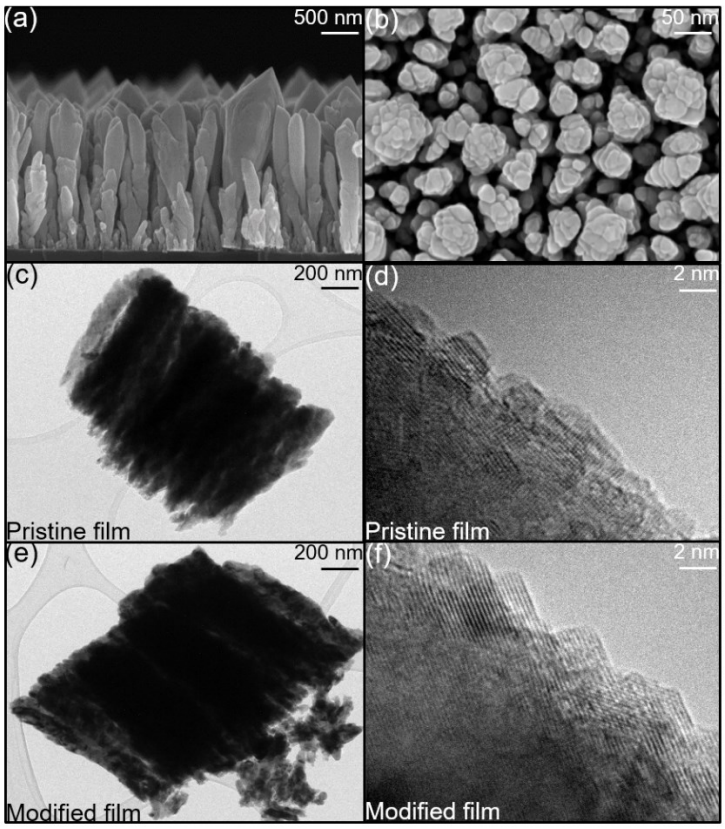

Figure 5.1: (a,b) SEM images of the pristine GLAD Ni film including cross-sectional (a) and top (b) views. (c-f) HRTEM images of pristine (c,d) and NH_3 plasma treated (120 s) (e,f) Ni GLAD film.

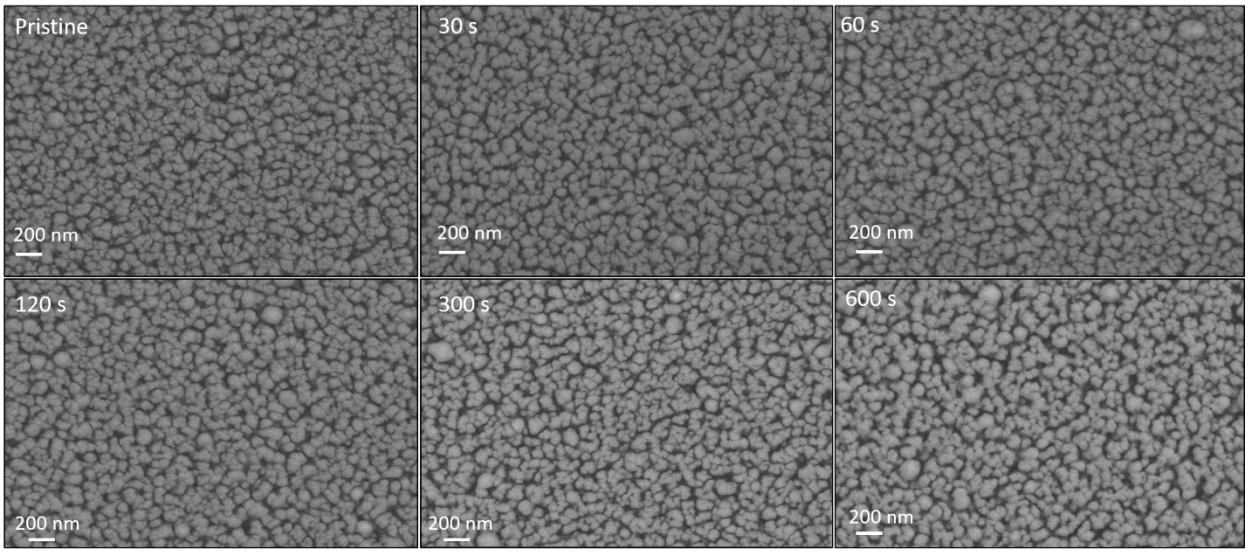

Figure 5.2: SEM images of pristine and N-functionalized Ni films

The crystal phase structure of the Ni films was investigated by x-ray diffractometry (XRD), and the spectra for both pristine and plasma-treated Ni films are shown in Fig 5.3. The spectrum for the pristine Ni film generally suggests a non-uniform, semi-crystalline structure with mixed phases. Diffraction peaks at 44.4°, 51.6° and 76.2° correspond to the (111), (200) and (220) planes, respectively, for FCC Ni (JCPDS card no. 00-001-1258) (28), while the peak at 58.1° suggests the (012) plane of HCP Ni (JCPDS card no. 45-1027) (29), and the peak at 56.7° suggests the (202) plane for Ni_2O_3 (JCPDS card no. 14-0481) (30). All of these peaks are retained in the diffractogram for the NH_3 plasma-treated film, and three additional peaks attributed to NiO (111), (200) and (220) planes are now observed at 37.3°, 43.4° and 62.9° (JCPDS card no. 22-1189) (31). This new crystal phase likely arises as a result of the high temperature processing, but it is clear from the overall XRD pattern that the entire structure has not transitioned to this new phase. Overall, this XRD data suggests complex, non-equilibrium structures incorporating both Ni and NiO_x, and this is true for both the pristine and plasma-modified films.

In addition, we note that each of the peaks originally observed in the pristine Ni film has shifted to slightly smaller 2θ positions (by approximately 0.3°), potentially indicating lattice strain from O or N atom insertion (26).

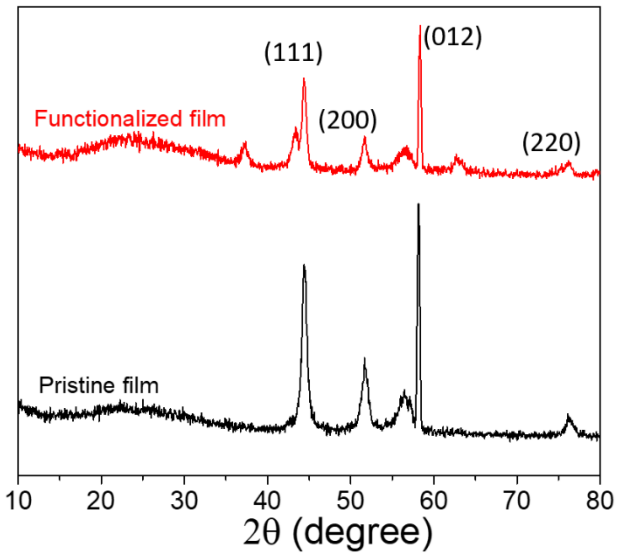

Figure 5.3: XRD spectra for (black) pristine Ni film and (red) N-functionalized Ni film. The N-functionalized film was treated for 120 s in NH_3 plasma.

The surface chemical composition and elemental valence states of the pristine and plasma-modified Ni films were also investigated by X-ray photoelectron spectroscopy (XPS), and the results are shown in Fig 5.4. Pronounced peaks for Ni are present for both pristine and plasma-treated films (Fig 5.4a,b), but N could only be distinguished in the plasma-treated samples (Fig 5.4d). In Fig 5.4a, peaks located at 852.1 eV and 853.6 eV indicate that metallic Ni^0 is present (32), and Ni(2p) peaks at 855.5eV, 860.6 eV, and 872.1 eV (with its satellite peak present at 879.2 eV) also confirm the presence of Ni^{2+} on the pristine Ni films, likely in the form of NiO (33). The same peaks are also observed for the Ni films after exposure to NH_3 plasma (Fig 5.4b), however, the peaks have shifted to slightly higher binding energies. Ni^0 is observed at 852.3 eV and 854.2 eV, and Ni^{2+} at 855.9 eV, 861.1 eV and 872.8 eV (with its satellite peak at 879.6 eV) (34). This small shift may indicate that a fraction of the bound oxygen has been replaced with more electronegative nitrogen species.

Additional evidence for this effect is found in the N(1s) spectra in Fig 5.4c,d. No N(1s) signal was found for the pristine Ni film (Fig 5.4c), but after NH_3 plasma treatment, strong peaks located at 397.6 eV, 398.6 eV, and 403.2 eV are visible in the XPS spectrum (Fig 5.4d), which can be assigned to adsorbed ammonia in the forms of NH (NH_{ads}), N^{3-} ions (N^{3-}), and molecular nitrogen (N_2), respectively (35,36). Based on the N(1s) XPS spectra of the plasma-treated films (Fig 5.4e), we found that the fraction of nitrogen atoms present as NH_{ads} was at a minimum for films treated for 120s, while the fraction of N^{3-} ions was at a maximum. As nitrogen has a more negative valence state than oxygen, the incorporation of N^{3-} leads to oxygen (O^{2-}) displacement. Overall, these results suggest nitrogen doping within the Ni/NiO crystalline lattices (37,38).

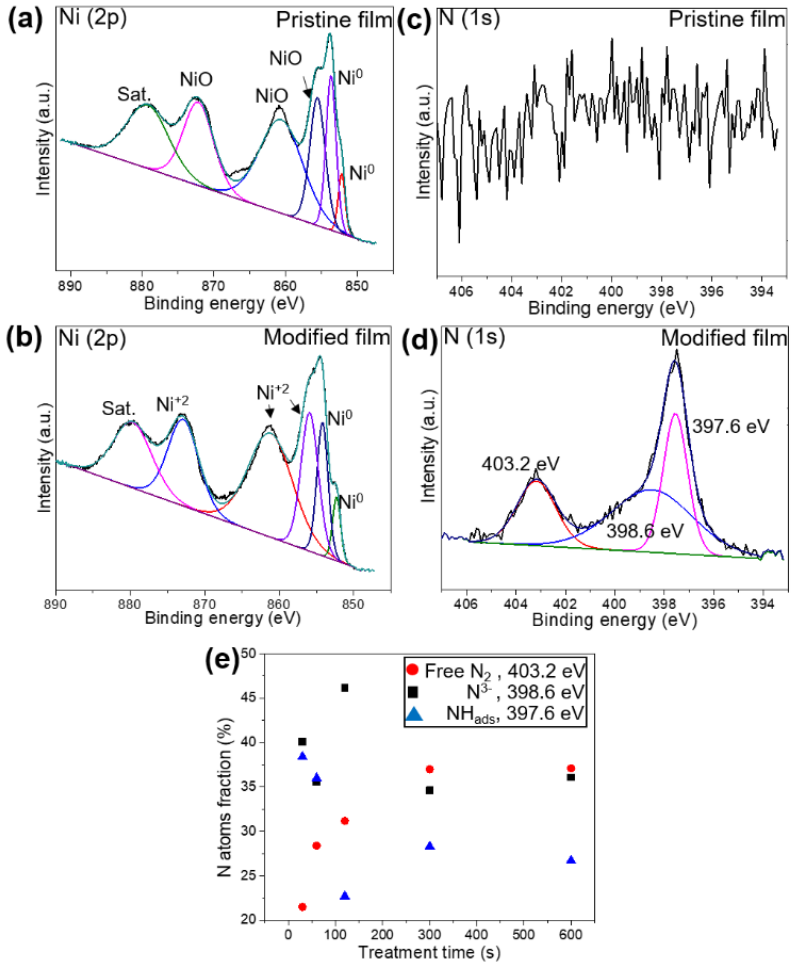

Figure 5.4: XPS spectra for pristine (a,c) and nitrogen-functionalized (b,d) Ni films in the binding energy regions associated with Ni(2p) (a,b) and N(1s) (c,d). In (b,d), the GLAD Ni films have been treated with NH_3 plasma for 120 s. In (e), the fraction of nitrogen atoms present as adsorbed ammonia (NH_{ads}), N^{3-} ions (N^{3-}), and molecular nitrogen (N_2), are plotted versus NH_3 plasma treatment time.

5.4.2 Plasma assisted enhancement of catalysis performances

The peroxidase-like catalytic activity of N-functionalized and pristine Ni GLAD thin films was investigated by exposing the catalytic Ni films to TMB solutions for 15 minutes at room temperature and pH 5 in the presence of 470 mM H_2O_2, thereby oxidizing the TMB (causing the color of the solution to change from colorless to blue). The data supporting the choice of these

conditions is provided in Fig 5.5, and a brief description of the rationale follows. Both H_2O_2 concentration and contact time between the TMB solution and catalytic film play vital roles in the formation of oxTMB solutions (13), as reflected by the strong correlations between each of these parameters and the absorbance at 652 nm (Fig 5.5a-c). Notably, we did not observe considerable oxidation of TMB by either N-functionalized or pristine films in the absence of H_2O_2, indicating that the films do not exhibit oxidase-like activity. 470 mM H_2O_2 was fixed as per previously reported literature for similar TMB concentrations (34,39), and in this literature, excess H_2O_2 in the TMB+H_2O_2 reaction was avoided to prevent two-electron conversion of oxTMB into the yellow colored diimine form (36). We fixed the contact time at 15 minutes as increasing the time further did not substantially increase the absorbance. Room temperature was chosen both for simplicity as well as producing the optimum absorbance (40), and pH 5 was chosen based on our previous work (13) and its physiological relevance to study peroxidase mimicking behavior (41). It should also be noted that the reaction rates vary with the thickness and area of the GLAD Ni film (Fig 5.6), so these values were kept consistent throughout the study, i.e. 0.7 cm^2 film area with 600 nm Ni thickness.

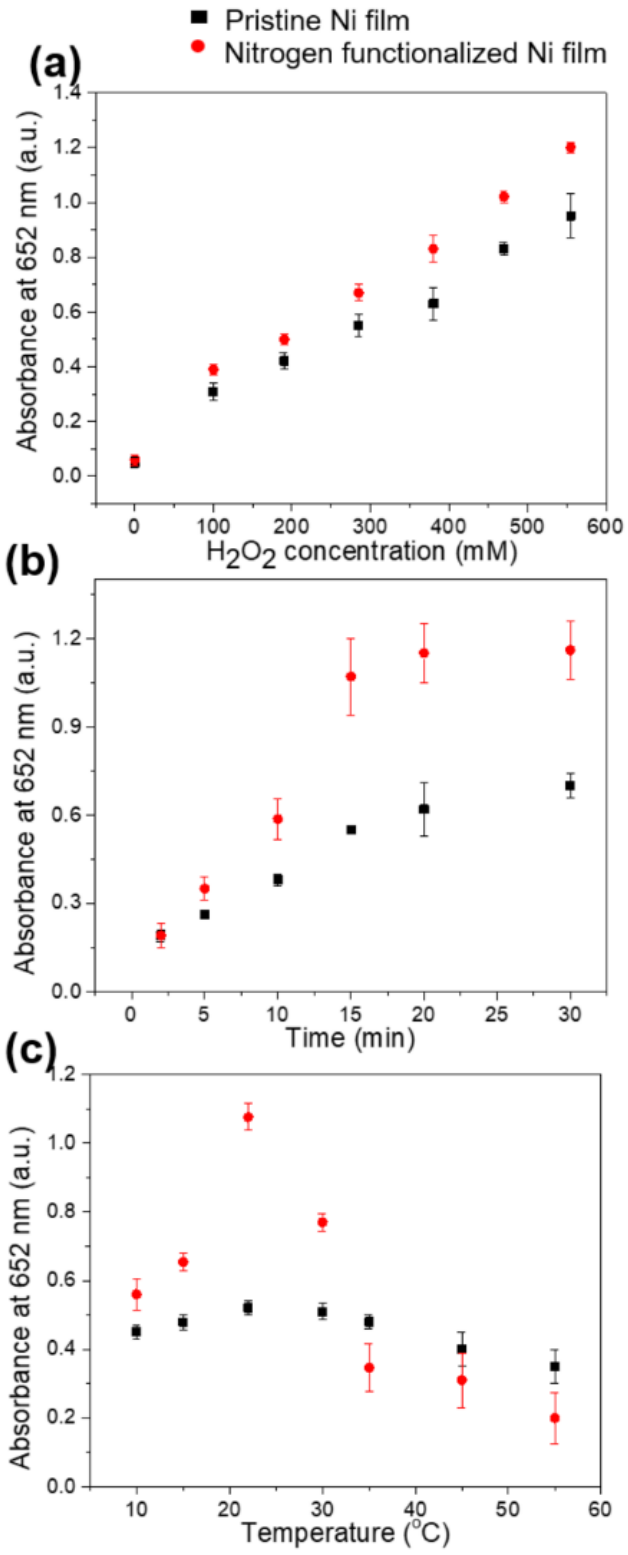

Figure 5.5: Optimal reaction conditions for peroxidase-like activity

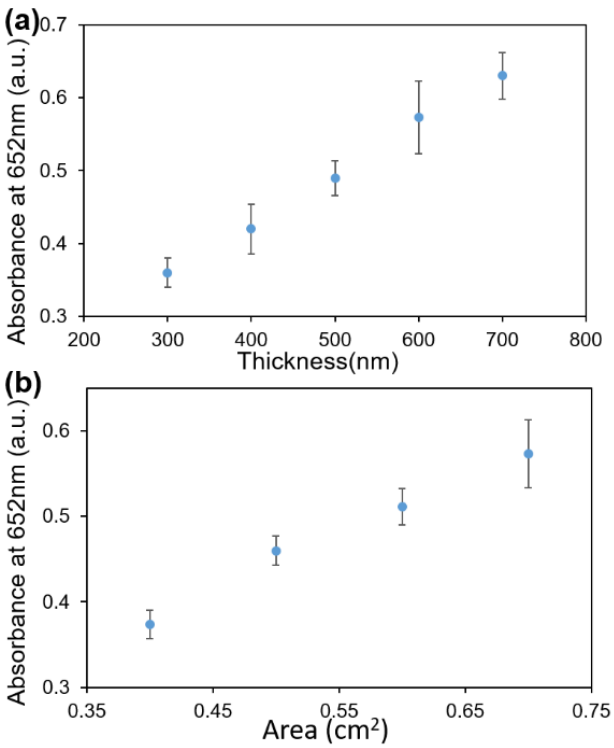

Figure 5.6: Effect of thickness and area of Ni films on absorbance

Fig 5.7a shows that the absorbance at 652 nm increased to a maximum after 120 s of NH_3 plasma treatment, then declined with additional exposure. The absorbance of solutions exposed to control films, prepared by exposing Ni GLAD films to either an oxygen plasma or to a high temperature (350 °C), plasma free-environment (black squares and blue triangles, respectively, in Fig 5.7a), differed little from the absorbance of solutions exposed to pristine Ni films, suggesting that incorporation of nitrogen is responsible for the increased absorption. This behavior is consistent with previous work from Feng et al., who showed that a 2 min NH_3 plasma treatment of MoS_2 films led to 3-fold greater catalytic activity than pristine MoS_2 (14).

The peroxidase-like performance of plasma treated films and pristine thin films were compared with varying concentrations of TMB. In its oxidized form, the chromogenic reagent TMB appears

blue in solution (detectable at 652 nm by UV-Vis), and thus increasing the TMB concentration in the reaction mixture was expected to lead to greater absorbance at 652 nm. This effect was observed in Fig 5.7b. Lesser absorbance changes were observed beyond 0.4 mM, and thus 0.4 mM TMB became a standard throughout this research study.

In terms of mechanism, the catalytic surface of the nanozyme plays an important role in the oxidation of the substrate (the TMB) and the reduction of the H_2O_2. Lone pair electrons from the adsorbed TMB are transferred to the peroxide via the catalyst, forming water (14,42–45). Studies from the literature on metallic nanozymes have showed that an increase in both electron density and conductivity occur during this process (46,47). In the literature, nitridation of a variety of metallic nanozymes has led to an enhancement in peroxidase-like activity (14,42–45). The enhanced catalytic activity of N-modified materials have been attributed to numerous factors: the strong electron affinity of the N atoms to the TMB lone electron pairs (for carbon nanotube cups) (15), an increase in defect states (in MoS_2 nanoflowers) (43), increased wettability of the surface (14). Comparing the contact angles for pristine and modified films (Table 5.1) is also revealing. Reduced contact angles were observed for plasma-treated films with respect to the pristine, as-deposited films (0 s plasma treatment), suggesting the incorporation of polar surface groups and possibly improving the ability of the redox species (i.e., TMB and H_2O_2) to access the catalytic surfaces. Additional factors mentioned above may also contribute to the enhanced catalytic activity of the N-modified films.

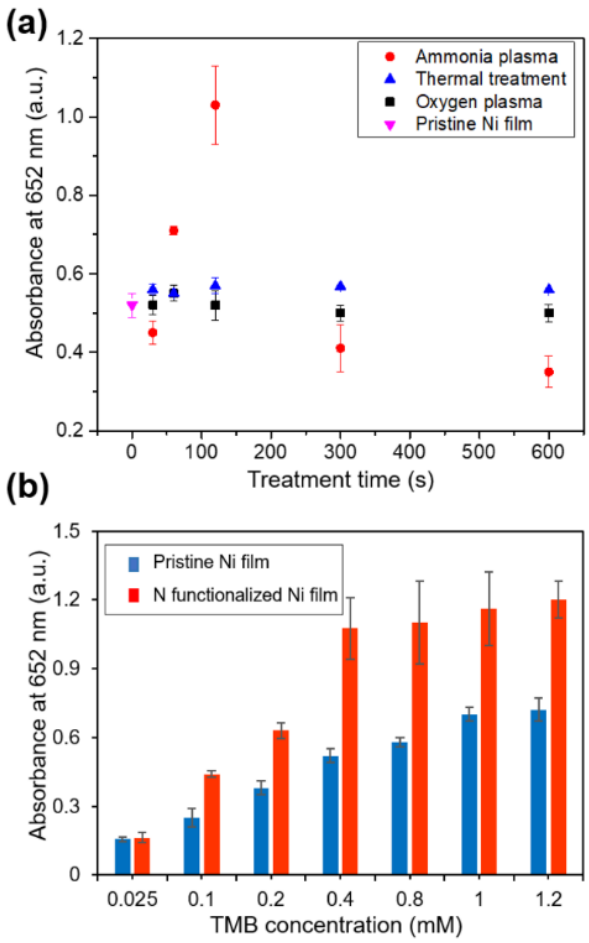

Figure 5.7: (a) Comparison of absorbance at 652 nm for equivalent TMB solutions oxidized by Ni GLAD films that were exposed to ammonia plasmas (red circles), oxygen plasmas (black squares) and plasma-free thermal treatments at 350 °C (blue triangles) for various lengths of time. The original reaction solutions were always 525 µl (0.4 mM TMB and 470 mM H_2O_2), and the oxidation process was allowed to proceed for 15 minutes. (b) Comparison of absorbance at 652 nm for pristine Ni films and N-functionalized Ni films exposed for 120s to different concentrations of TMB.

Table 5.1: Contact angles of water droplets on ammonia and oxygen plasma-treated Ni film for different treatment time

Treatment time (s)	**Contact angle (°)**

	O_2 plasma	NH_3 plasma
0	39.4	43.3
30	15.5	37.0
60	11.4	42.1
120	9.6	26.6
300	8.6	41.8
600	8.6	33.4

5.3.3 Kinetic studies of the peroxidase-like reaction

Kinetic studies were carried out to compare the catalytic performances of N-functionalized and pristine Ni films using the TMB substrate, with the results shown in Fig 5.8. The kinetic properties of nanozymes vary with the concentration of substrate (reactant) present, as described by Michaelis-Menten kinetics. At low substrate concentrations the reaction rate (V) is linearly related to the substrate concentration [TMB], and the reaction exhibits first-order kinetics. At high concentrations, the rate of reaction (V_{max}) is limited by the availability of active sites on the catalyst, and thus follows zero-order kinetics (i.e. V is independent of substrate concentration). The Michaelis-Menten constant K_m describes the substrate concentration at which the rate of reaction is half of V_{max}, and is indicative of the affinity of the substrate for the catalyst. An effective catalyst exhibits a high V_{max} and low K_m value, indicating that the catalytic reaction can occur at a high rate over a useful range of substrate concentrations.

The Michaelis-Menten kinetic parameters were obtained by fitting the absorbance values for the catalytic reaction products versus time with varying concentrations of TMB. In Fig 5.8, the reaction rates for N-functionalized thin films generally exceed those for the pristine thin film, suggesting enhanced peroxidase-mimicking behavior. Accordingly, the kinetic parameters including the maximal reaction velocity (V_{max}) and Michaelis-Menten coefficient (K_m) for the N-functionalized film (3.7×10^{-8} M/s and 0.17 mM) are superior to those of the pristine film (2.3×10^{-8} M/s and 0.23 mM) showing that the catalytic properties have been enhanced. For comparison, the K_m and V_{max} values of a variety of nanozymes from the literature (evaluated using TMB) are shown in Table 5.2. Direct comparison of different materials is difficult as testing is done under different conditions, and enzymatic activity varies with both pH and temperature. The pH of our studies was set at 5 (to avoid damaging the nanozyme film) and the temperature at 22 ℃ (to simplify the process). Varying these parameters will lead to different reaction kinetics. The surface-anchored GLAD film, which has the outstanding advantage of reusability, also leads to imperfect side-by-side comparisons with the solution-dispersed nanozymes. Nonetheless, our materials have competitive V_{max} values and lower K_m values as compared with other nanozymes. Notably, the K_m value for the N-functionalized film is considerably lower than all other literature reports for similar chromogenic TMB-H_2O_2 oxidation systems, showing that the N-functionalized thin film has a high tendency to bind to its TMB substrate, resulting in higher response.

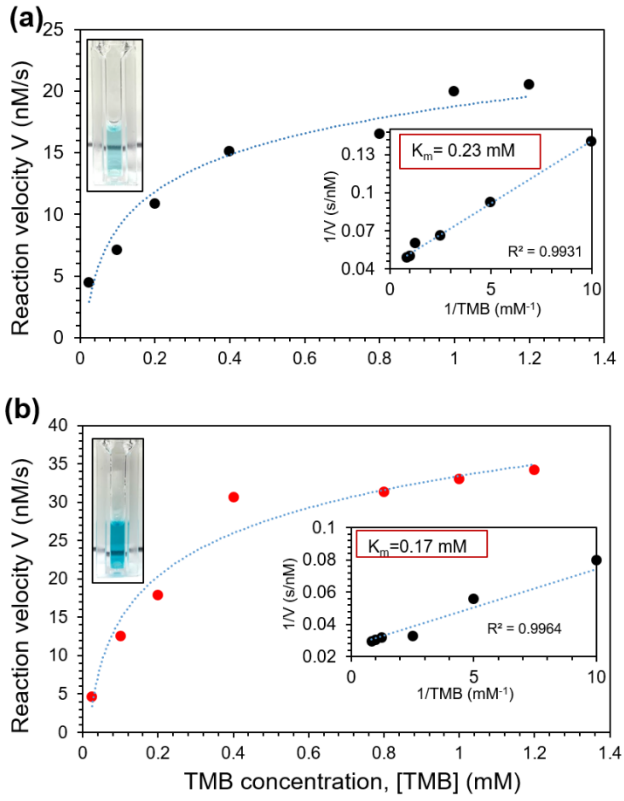

Figure 5.8. TMB conversion rate vs TMB concentration. (a) pristine Ni film, and (b) NH_3 plasma modified Ni film for 120s

Table 5.2: Km values for different peroxidase-mimicking materials

Catalyst	**K_m(mM)**	**V_{max} (10^{-8} M s^{-1})**	**Ref**
MIL-53 (Fe)	1.08	3.12	(48)
MoS_2 NPs	0.52	5.16	(49)
MoS_2-$Pt_{74}Ag_{26}$	25.71	7.29	(50)

GO-Fe_3O_4	0.43	13.08	(51)
Hemin-graphene	5.10	4.5	(52)
Hemin	4.84	4.6	(52)
Au-NPs/graphene	0.14	7.1±0.1	(53)
N-doped graphene quantum dots	11.19	0.38	(54)
HRP	0.43	10	(9)
MoS_2	0.82	1.16	(14)
Ni helical GLAD film	1.07	2.6	(13)
N-doped MoS_2	0.79	1.79	(14)
Ni nanocolumnar GLAD film	0.23	2.3	This work
N-functionalized Ni nanocolumnar GLAD film	0.17	3.7	This work

5.4.4 Application of GLAD-based nanozyme for continuous catalytic reaction

Various types of analysis techniques such as colorimetry, fluorescence, electrochemical sensing, chemiluminescence, and surface-enhanced Raman spectroscopy have been implemented in point-of-care diagnostic (POC) devices, including immunostrips and microfluidic devices (37,55). Some advances have been made for detection through strip-based tests, commonly known as lateral flow

based assays. Lateral flow based assays are an advantageous diagnostic test configuration with features including less time consumption, easy operation, stability, low cost for POC devices, and smaller sample volumes (56), however, immobilizing enzymes on POC devices without compromising their function remains a challenge (57–59). Self-driven flow over GLAD film-based nanozymes could be a unique fit for POC diagnostic platforms due to their excellent peroxidase-like activity, reusability (as shown in our previous work (13)), and high stability under a variety of storage conditions.

In Fig 5.9, we present a simple gravity-assisted device for continuous catalytic reaction on N functionalized GLAD films, and we adapt the device to function as a sensor for uric acid (UA), which is an important biomarker of human health conditions such as gout, arthritis, heart diseases, and kidney stones. As noted above, GLAD Ni catalysts facilitate the decomposition of hydrogen peroxide to generate oxygen species and form the blue-colored oxTMB from colorless TMB solution. In our previous work (13), when UA was added to the oxTMB solution, the blue color faded in proportion to UA concentration. Here, we adapted this system to demonstrate a gravity-driven device as a UA sensor by combining various concentrations of dilute UA with the TMB/H_2O_2 reagent mixture. We used 170 µl of 0.4 mM TMB, 170 µl of 470 mM H_2O_2, and 160 µl of UA solution (500 µl in total), and the combined solutions traveled across a catalytic GLAD Ni film because the substrate tilted at an angle of 30°. The flow was complete in ~3 minutes, and no external power source was required. As demonstrated in the supplementary movie (with 0 mM UA concentration), the colorless reactants became blue after traversing the reaction substrate. We found that this blue oxTMB solution could be wicked into cellulose paper or collected by pipette for additional analysis, and the initially colorless TMB solution (0.08 a.u.) reached a much stronger absorbance (0.51 a.u.) due to the ongoing oxidation reaction.

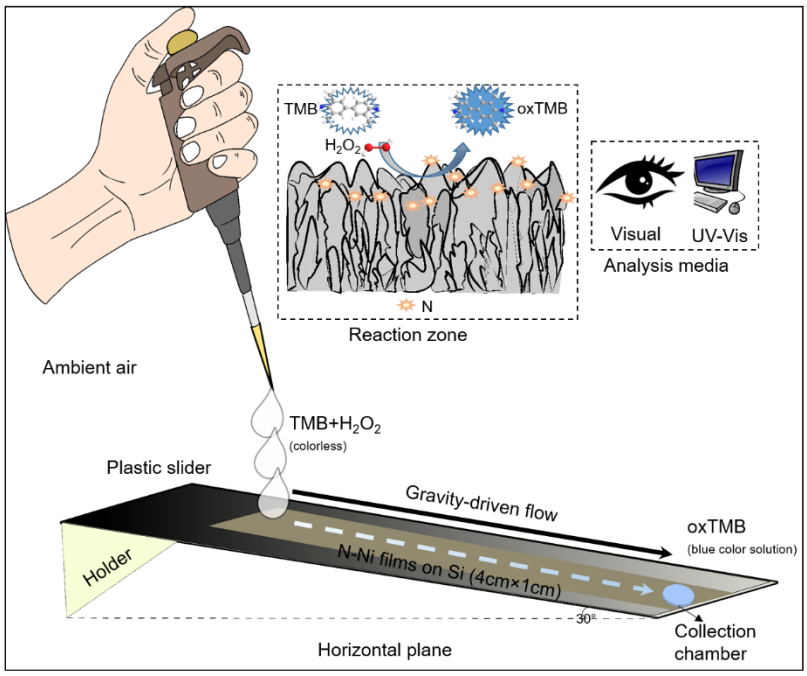

Figure 5.9: Schematic representation of gravity assisted flow device

After the three component solution traverses the device, we expected higher concentrations of UA to lead to lower absorbance solutions collected at the outlet. In Fig 5.10, we provide the calibration data, and it can be noted that as the UA concentration increases from 0 µM to 3.5 µM, the solution absorbance decreases from 0.47 to 0.24 with an R^2 value of 0.97. In this configuration, the limit of detection (LOD) that was achieved was 0.98 µM (calculated as 3σ/slope). No external power sources were required, and the solutions were all generated from the same plasma-treated Ni thin film, demonstrating reusability and opening the way toward potential application in colorimetric sensors.

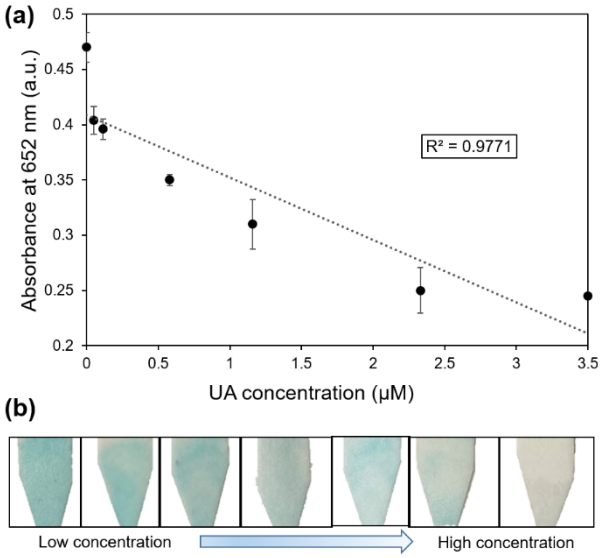

Figure 5.10: (a) Response of the gravity-driven device to variations in UA concentration from 0 μM to 3.5 μM. (b) Photographs show respective solutions collected on filter paper

5.5 Conclusions

An effective, environmentally-friendly GLAD film-based biosensor was improved using a simple ammonia-plasma treatment process. The resulting surface-mounted nanozymes presented dramatically enhanced catalytic performance (with respect to untreated pristine counterparts) depending on the plasma treatment conditions. SEM, TEM, XRD, and XPS analysis results revealed that the plasma treatment introduced N-rich surface species, and greatly increased surface wettability was observed, allowing easier access for reactants. Although the exact catalysis mechanism may be further explored, the enhanced catalytic performance parameters demonstrated for a reusable nanozyme may open the door towards electrochemical and colorimetric sensors for environmental monitoring, food safety, and biomedical analysis. The demonstration of continuous catalytic activity (via gravity-driven flow across the film) represents one additional step toward these real-world applications, particularly for integration in flow-driven point of care devices.

Acknowledgments

The authors thank Dr. Ravin Narain for providing access to the UV-vis equipment. We also thank both Paul Concepcion and Dr. Jian Chen for SEM and TEM imaging, respectively.

References

1. Torng W, Altman RB. High precision protein functional site detection using 3D convolutional neural networks. Valencia A, editor. Bioinformatics. 2019 May 1;35(9):1503–12. Available from: https://academic.oup.com/bioinformatics/article/35/9/1503/5104336

2. Daniel RM, Dines M, Petach HH. The denaturation and degradation of stable enzymes at high temperatures. Biochem J. 1996 Jul 1;317(1):1–11. Available from: https://portlandpress.com/biochemj/article/317/1/1/31738/The-denaturation-and-degradation-of-stable-enzymes

3. Wu, J.; Wang X.; Wang Q.; Lou Z.; Li S.; Zhu Y.; Qin L.; Wei H. Nanomaterials with enzyme-like characteristics (nanozymes): next-generation artificial enzymes (II). Chem Soc Rev. 2019;48(4):1004–76.

4. Jiang B, Duan D, Gao L, Zhou M, Fan K, Tang Y, et al. Standardized assays for determining the catalytic activity and kinetics of peroxidase-like nanozymes. Nat Protoc. 2018 Jul 2;13(7):1506–20. Available from: http://www.nature.com/articles/s41596-018-0001-1

5. Wang X, Tang CL, Liu JJ, Zhang HZ, Wang J. Ultra-small CuS Nanoparticles as Peroxidase Mimetics for Sensitive and Colorimetric Detection of Uric Acid in Human Serum. Chinese J Anal Chem. 2018 May;46(5):e1825–31. Available from: https://linkinghub.elsevier.com/retrieve/pii/S1872204017610831

6. Golchin J, Golchin K, Alidadian N, Ghaderi S, Eslamkhah S, Eslamkhah M, et al. Nanozyme applications in biology and medicine: an overview. Artif Cells, Nanomedicine, Biotechnol. 2017 Aug 18;45(6):1069–76. Available from: https://www.tandfonline.com/doi/full/10.1080/21691401.2017.1313268

7. Khan AA, Rahmani AH, Aldebasi YH, Aly SM. Biochemical and Pathological Studies on Peroxidases –An Updated Review. Glob J Health Sci. 2014 May 13;6(5). Available from: http://ccsenet.org/journal/index.php/gjhs/article/view/35689

8. Everse J, Coates PW. Role of peroxidases in Parkinson disease: a hypothesis. Free Radic Biol Med. 2005 May;38(10):1296–310. Available from: https://linkinghub.elsevier.com/retrieve/pii/S0891584905000365

9. Gao L, Zhuang J, Nie L, Zhang J, Zhang Y, Gu N, et al. Intrinsic peroxidase-like activity of ferromagnetic nanoparticles. Nat Nanotechnol. 2007 Sep 26;2(9):577–83. Available

from: http://www.nature.com/articles/nnano.2007.260

10. Song Y, Qu K, Zhao C, Ren J, Qu X. Graphene Oxide: Intrinsic Peroxidase Catalytic Activity and Its Application to Glucose Detection. Adv Mater. 2010 Mar 5;22(19):2206–10. Available from: http://doi.wiley.com/10.1002/adma.200903783

11. Huang JY, Lin HT, Chen TH, Chen CA, Chang HT, Chen CF. Signal Amplified Gold Nanoparticles for Cancer Diagnosis on Paper-Based Analytical Devices. ACS Sensors. 2018 Jan 26;3(1):174–82. Available from: https://pubs.acs.org/doi/10.1021/acssensors.7b00823

12. Liu F, He J, Zeng M, Hao J, Guo Q, Song Y, et al. Cu–hemin metal-organic frameworks with peroxidase-like activity as peroxidase mimics for colorimetric sensing of glucose. J Nanoparticle Res. 2016 May 15;18(5):106. Available from: http://link.springer.com/10.1007/s11051-016-3416-z

13. Tripathi A, Harris KD, Elias AL. Peroxidase-Like Behavior of Ni Thin Films Deposited by Glancing Angle Deposition for Enzyme-Free Uric Acid Sensing. ACS Omega. 2020 Apr 28;5(16):9123–30. Available from: https://pubs.acs.org/doi/10.1021/acsomega.9b04071

14. Feng L, Zhang L, Zhang S, Chen X, Li P, Gao Y, et al. Plasma-Assisted Controllable Doping of Nitrogen into MoS_2 Nanosheets as Efficient Nanozymes with Enhanced Peroxidase-Like Catalysis Activity. ACS Appl Mater Interfaces. 2020 Apr 15;12(15):17547–56. Available from: https://pubs.acs.org/doi/10.1021/acsami.0c01789

15. Tang Y, Allen BL, Kauffman DR, Star A. Electrocatalytic Activity of Nitrogen-Doped Carbon Nanotube Cups. J Am Chem Soc. 2009 Sep 23;131(37):13200–1. Available from: https://pubs.acs.org/doi/10.1021/ja904595t

16. Zhou W, Hou D, Sang Y, Yao S, Zhou J, Li G, et al. MoO_2 nanobelts@nitrogen self-doped MoS_2 nanosheets as effective electrocatalysts for hydrogen evolution reaction. J Mater Chem A. 2014;2(29):11358–64. Available from: http://xlink.rsc.org/?DOI=c4ta01898b

17. Huang L, Chen J, Gan L, Wang J, Dong S. Single-atom nanozymes. Sci Adv. 2019;5(5).

18. Bae G, Kim H, Choi H, Jeong P, Kim DH, Kwon HC, et al. Quantification of Active Site Density and Turnover Frequency: From Single-Atom Metal to Nanoparticle Electrocatalysts. JACS Au. 2021 May 24;1(5):586–97. Available from: https://pubs.acs.org/doi/10.1021/jacsau.1c00074

19. Grüner C, Reeck P, Jacobs P-P, Liedtke S, Lotnyk A, Rauschenbach B. Gold coated metal nanostructures grown by glancing angle deposition and pulsed electroplating. Phys Lett A. 2018 May;382(19):1287–90. Available from: https://linkinghub.elsevier.com/retrieve/pii/S0375960118302536

20. Hawkeye MM, Brett MJ. Glancing angle deposition: Fabrication, properties, and

applications of micro- and nanostructured thin films. J Vac Sci Technol A Vacuum, Surfaces, Film. 2007;25(5):1317. Available from: http://scitation.aip.org/content/avs/journal/jvsta/25/5/10.1116/1.2764082

21. Singer N, Pillai RG, Johnson AID, Harris KD, Jemere AB. Nanostructured nickel oxide electrodes for non-enzymatic electrochemical glucose sensing. Microchim Acta. 2020 Apr 3;187(4):196. Available from: http://link.springer.com/10.1007/s00604-020-4171-5

22. Barranco A, Borras A, Gonzalez-Elipe AR, Palmero A. Perspectives on oblique angle deposition of thin films: From fundamentals to devices. Prog Mater Sci. 2016 Mar;76:59–153. Available from: https://linkinghub.elsevier.com/retrieve/pii/S0079642515000705

23. Lin D, Harris KD, Chan NWC, Jemere AB. Nanostructured indium tin oxide electrodes immobilized with toll-like receptor proteins for label-free electrochemical detection of pathogen markers. Sensors Actuators B Chem. 2018 Mar;257:324–30. Available from: https://linkinghub.elsevier.com/retrieve/pii/S0925400517320543

24. Dulac M, Melet A, Harris KD, Limoges B, Galardon E, Balland V. An optical H_2S biosensor based on the chemoselective Hb-I protein tethered to a transparent, high surface area nanocolumnar electrode. Sensors Actuators B Chem. 2019 Jul;290:326–35. Available from: https://linkinghub.elsevier.com/retrieve/pii/S0925400519304903

25. Vohrer U. Interfacial engineering of functional textiles for biomedical applications. In: R. Shishoo, editor. Plasma Technologies for Textiles. 1st ed. Woodhead Publishing; 2007. p. 202–27. Available from: https://linkinghub.elsevier.com/retrieve/pii/B9781845690731500081

26. Li G, Wu X, Guo H, Guo Y, Chen H, Wu Y, et al. Plasma Transforming $Ni(OH)_2$ Nanosheets into Porous Nickel Nitride Sheets for Alkaline Hydrogen Evolution. ACS Appl Mater Interfaces [Internet]. 2020 Feb 5;12(5):5951–7. Available from: https://pubs.acs.org/doi/10.1021/acsami.9b20887

27. Meftah A, Gharibshahi E, Soltani N, Yunus W, Saion E. Structural, Optical and Electrical Properties of PVA/PANI/Nickel Nanocomposites Synthesized by Gamma Radiolytic Method. Polymers (Basel). 2014 Sep 24;6(9):2435–50. Available from: http://www.mdpi.com/2073-4360/6/9/2435

28. Chandrabhan Shende R, Muruganathan M, Mizuta H, Akabori M, Sundara R. Chemical Simultaneous Synthesis Strategy of Two Nitrogen-Rich Carbon Nanomaterials for All-Solid-State Symmetric Supercapacitor. ACS Omega. 2018 Dec 31;3(12):17276–86. Available from: https://pubs.acs.org/doi/10.1021/acsomega.8b02835

29. Han M, Liu Q, He J, Song Y, Xu ZCS and MP of C and HPNN, Zhu JM. Controllable Synthesis and Magnetic Properties of Cubic and Hexagonal Phase Nickel Nanocrystals. Adv Mater. 2007 Apr 20;19(8):1096–100. Available from: https://onlinelibrary.wiley.com/doi/10.1002/adma.200601460

30. Barrientos L, Rodriguez - Llamazares S, Merchani J, Jara P, Yutronic N, Lavayen V.

Unveiling the structure of Ni/Ni oxide nanoparticles system. J Chil Chem Soc. 2009 Dec;54(4). Available from: http://www.scielo.cl/scielo.php?script=sci_arttext&pid=S0717-97072009000400014&lng=en&nrm=iso&tlng=en

31. Nazir S, Bano S, Munir S, Fahad Al-Ajmi M, Afzal M, Mazhar K. “Smart” nickel oxide based core-shell nanoparticles for combined chemo and photodynamic cancer therapy. Int J Nanomedicine. 2016 Jul;Volume 11:3159–66. Available from: https://www.dovepress.com/quotsmartquot-nickel-oxide-based-corendashshell-nanoparticles-for-comb-peer-reviewed-article-IJN

32. Hengne AM, Samal AK, Enakonda LR, Harb M, Gevers LE, Anjum DH, et al. Ni–Sn-Supported ZrO_2 Catalysts Modified by Indium for Selective CO_2 Hydrogenation to Methanol. ACS Omega. 2018 Apr 30;3(4):3688–701. Available from: https://pubs.acs.org/doi/10.1021/acsomega.8b00211

33. Karki V, Debnath AK, Kumar S, Bhattacharya D. Synthesis of co-sputter deposited Ni–Ti thin alloy films and their compositional characterization using depth sensitive techniques. Thin Solid Films. 2020 Mar;697:137800. Available from: https://linkinghub.elsevier.com/retrieve/pii/S004060902030016X

34. Tanaka S, Masud MK, Kaneti YV, Shiddiky MJA, Fatehmulla A, Aldhafiri AM, et al. Enhanced Peroxidase Mimetic Activity of Porous Iron Oxide Nanoflakes. ChemNanoMat. 2019 Apr 4;5(4):506–13. Available from: https://onlinelibrary.wiley.com/doi/abs/10.1002/cnma.201800487

35. Smirnov A, Hausner D, Laffers R, Strongin DR, Schoonen MA. Abiotic ammonium formation in the presence of Ni-Fe metals and alloys and its implications for the Hadean nitrogen cycle. Geochem Trans. 2008 Dec 19;9(1):5. Available from: https://geochemicaltransactions.biomedcentral.com/articles/10.1186/1467-4866-9-5

36. Josephy PD, Eling T, Mason RP. The horseradish peroxidase-catalyzed oxidation of 3,5,3’,5’-tetramethylbenzidine. Free radical and charge-transfer complex intermediates. J Biol Chem. 1982;257(7):3669–75.

37. Carrell C, Kava A, Nguyen M, Menger R, Munshi Z, Call Z, et al. Beyond the lateral flow assay: A review of paper-based microfluidics. Microelectron Eng. 2019 Feb;206:45–54. Available from: https://linkinghub.elsevier.com/retrieve/pii/S0167931718305069

38. Song HJ, Shin HJ, Chung Y, Lee JC, Lee MK. X-ray absorption and photoelectron spectroscopic study of plasma-nitrided SiO_2 film. J Appl Phys. 2005 Jun;97(11):113711. Available from: http://aip.scitation.org/doi/10.1063/1.1927283

39. Sun J, Li C, Qi Y, Guo S, Liang X. Optimizing Colorimetric Assay Based on V_2O_5 Nanozymes for Sensitive Detection of H_2O_2 and Glucose. Sensors. 2016 Apr 22;16(4):584. Available from: http://www.mdpi.com/1424-8220/16/4/584

40. Trawczyńska I. New Method of Determining Kinetic Parameters for Decomposition of

Hydrogen Peroxide by Catalase. Catalysts. 2020 Mar 12;10(3):323. Available from: https://www.mdpi.com/2073-4344/10/3/323

41. Lian J, Liu P, Jin C, Shi Z, Luo X, Liu Q. Perylene diimide-functionalized CeO_2 nanocomposite as a peroxidase mimic for colorimetric determination of hydrogen peroxide and glutathione. Microchim Acta. 2019 Jun 6;186(6):332. Available from: http://link.springer.com/10.1007/s00604-019-3439-0

42. Gao L, Fan K, Yan X. Iron Oxide Nanozyme: A Multifunctional Enzyme Mimetic for Biomedical Applications. Theranostics. 2017;7(13):3207–27. Available from: http://www.thno.org/v07p3207.htm

43. Chen J, Xu F, Zhang Q, Li S. N-doped MoS_2-nanoflowers as peroxidase-like nanozymes for total antioxidant capacity assay. Anal Chim Acta. 2021 Oct;1180:338740. Available from: https://linkinghub.elsevier.com/retrieve/pii/S0003267021005663

44. Lou Z, Zhao S, Wang Q, Wei H. N-Doped Carbon As Peroxidase-Like Nanozymes for Total Antioxidant Capacity Assay. Anal Chem. 2019 Dec 3;91(23):15267–74. Available from: https://pubs.acs.org/doi/10.1021/acs.analchem.9b04333

45. Bao Y-W, Hua X-W, Ran H-H, Zeng J, Wu F-G. Metal-doped carbon nanoparticles with intrinsic peroxidase-like activity for colorimetric detection of H_2O_2 and glucose. J Mater Chem B. 2019;7(2):296–304. Available from: http://xlink.rsc.org/?DOI=C8TB02404A

46. Cui M, Zhou J, Zhao Y, Song Q. Facile synthesis of iridium nanoparticles with superior peroxidase-like activity for colorimetric determination of H_2O_2 and xanthine. Sens. Actuators. B. 2016 Nov 27;243(2017):203-210. Available from: https://linkinghub.elsevier.com/retrieve/pii/S0925400516319438

47. Ju P, Xiang Y, Xiang Z, Wang M, Zhao Y, Zhang D, et al. BiOI hierarchical nanoflowers as novel robust peroxidase mimetics for colorimetric detection of H_2O_2. RSC Adv. 2016;6(21):17483–93. Available from: http://xlink.rsc.org/?DOI=C6RA00368K

48. Ai L, Li L, Zhang C, Fu J, Jiang J. MIL-53(Fe): A Metal-Organic Framework with Intrinsic Peroxidase-Like Catalytic Activity for Colorimetric Biosensing. Chem - A Eur J. 2013 Nov 4;19(45):15105–8. Available from: http://doi.wiley.com/10.1002/chem.201303051

49. Lin T, Zhong L, Guo L, Fu F, Chen G. Seeing diabetes: visual detection of glucose based on the intrinsic peroxidase-like activity of MoS_2 nanosheets. Nanoscale. 2014;6(20):11856–62. Available from: http://xlink.rsc.org/?DOI=C4NR03393K

50. Cai S, Han Q, Qi C, Lian Z, Jia X, Yang R, et al. $Pt_{74}Ag_{26}$ nanoparticle-decorated ultrathin MoS_2 nanosheets as novel peroxidase mimics for highly selective colorimetric detection of H_2O_2 and glucose. Nanoscale. 2016;8(6):3685–93. Available from: http://xlink.rsc.org/?DOI=C5NR08038J

51. Dong Y, Zhang H, Rahman ZU, Su L, Chen X, Hu J, et al. Graphene oxide–Fe_3O_4

magnetic nanocomposites with peroxidase-like activity for colorimetric detection of glucose. Nanoscale [Internet]. 2012;4(13):3969. Available from: http://xlink.rsc.org/?DOI=c2nr12109c

52. Guo Y, Deng L, Li J, Guo S, Wang E, Dong S. Hemin−Graphene Hybrid Nanosheets with Intrinsic Peroxidase-like Activity for Label-free Colorimetric Detection of Single-Nucleotide Polymorphism. ACS Nano. 2011 Feb 22;5(2):1282–90. Available from: https://pubs.acs.org/doi/10.1021/nn1029586

53. Liu M, Zhao H, Chen S, Yu H, Quan X. Stimuli-responsive peroxidase mimicking at a smart graphene interface. Chem Commun. 2012;48(56):7055. Available from: http://xlink.rsc.org/?DOI=c2cc32406g

54. Lin L, Song X, Chen Y, Rong M, Zhao T, Wang Y, et al. Intrinsic peroxidase-like catalytic activity of nitrogen-doped graphene quantum dots and their application in the colorimetric detection of H_2O_2 and glucose. Anal Chim Acta. 2015 Apr;869:89–95. Available from: https://linkinghub.elsevier.com/retrieve/pii/S0003267015002020

55. Omidfar K, Khorsand B, Larijani B. Development of a new sensitive immunostrip assay based on mesoporous silica and colloidal Au nanoparticles. Mol Biol Rep. 2012 Feb 21;39(2):1253–9. Available from: http://link.springer.com/10.1007/s11033-011-0856-5

56. Liu Y, Zhan L, Qin Z, Sackrison J, Bischof JC. Ultrasensitive and Highly Specific Lateral Flow Assays for Point-of-Care Diagnosis. ACS Nano. 2021 Mar 23;15(3):3593–611. Available from: https://pubs.acs.org/doi/10.1021/acsnano.0c10035

57. Reis C, Sousa E, Serpa J, Oliveira R, Oliveira R, Santos J. Design of immobilized enzyme biocatalysts: Drawbacks and opportunities. Quim Nova. 2019 July; 42(7):1-16 Available from: https://www.scielo.br/j/qn/a/cBRd9MXMLCQSry9bXwrNtNc/?lang=en

58. Christodouleas DC, Kaur B, Chorti P. From Point-of-Care Testing to eHealth Diagnostic Devices (eDiagnostics). ACS Cent Sci. 2018 Dec 26;4(12):1600–16. Available from: https://pubs.acs.org/doi/10.1021/acscentsci.8b00625

59. Mohamad NR, Marzuki NHC, Buang NA, Huyop F, Wahab RA. An overview of technologies for immobilization of enzymes and surface analysis techniques for immobilized enzymes. Biotechnol Biotechnol Equip. 2015 Mar 4;29(2):205–20. Available from: http://www.tandfonline.com/doi/abs/10.1080/13102818.2015.1008192

Chapter 6: Summary and Future work

This thesis focused on the fabrication of surface-anchored nanostructured thin film using the glancing angle deposition (GLAD) technique for its application in electrochemical and colorimetric biosensors. The GLAD film demonstrated high catalytic activity, reusability, recoverability, and satisfactory storage conditions, resulting in an efficient biosensor compared to a flat film-based biosensor.

Nanoparticles used as artificial enzymes or nanozymes exhibited remarkable stability and efficient catalytic conditions at harsh working conditions. However, the solution-dispersed nanozymes possessed a lack of recoverability, which prevents the reuse of nanozyme catalysts. Overall, the entire thesis can be categorized into three different areas:

1. Macroporous NiO GLAD thin film for enzymatic electrochemical sensing of xanthine (Chapter 3).
2. Peroxidase-like behavior of Ni thin films deposited by glancing angle deposition for enzyme-free uric acid sensing (Chapter 4).
3. High surface area nitrogen-functionalized Ni nanozymes for efficient peroxidase-like catalytic activity (Chapter 5).

Xanthine is one of the last metabolites created by purine decomposition. Its concentration increases with time. In chapter 3 of this thesis, an enzymatic electrochemical biosensor was developed using a mesoporous vertical post NiO GLAD film deposited on an ITO substrate. High surface area NiO GLAD film possessed high electrocatalytic activity and can be used as a scaffold to immobilize xanthine oxidase enzyme to selectively react with xanthine, which is a marker for food freshness.

One of the novel aspects of this work was fabricating an electrochemical sensor with GLAD-deposited NiO electrodes to monitor xanthine concentration. With the help of a bioreceptor (enzyme) and nanostructured electrodes, I developed an electrochemical biosensor of quick response and high selectivity for xanthine against common biological compounds found in fish meat. The developed enzymatic electrochemical sensor under optimum conditions outperforms the non-enzymatic electrochemical sensor in terms of detection limits, repeatability, sensitivity, and selectivity. The work has significantly contributed to understanding the effect of enzyme immobilized nanostructured electrodes on the electrochemical sensor and was further used on real fish samples to monitor spoilage with storage time. The obtained concentration of evolved XA in fish meat suggests the applicability of sensors to detect fish spoilage for consumers. The work presented here is a significant step towards developing a fast and sensitive platform for providing early warnings before fish meat spoils.

Chapter 4 of this thesis describes the first reusable Ni GLAD nanozymes deposited on silicon substrates using the GLAD technique. The high surface energy of Ni GLAD film was taken into account to mimic enzyme (horseradish peroxidase) which demonstrated efficient catalytic activity, recoverability, and freedom to reuse it. Ni GLAD films showed a peroxidase-like activity in catalyzing colorless TMB and H_2O_2 reaction to yield oxidized blue TMB. This color change is reversed in presence of uric acid, and therefore the reaction mechanism could be used to sense uric acid. The GLAD-based colorimetric sensor showed on-demand analysis, excellent analytical performance, and visual detection, as well as the lack of natural enzymes. Additionally, an interference study for TMB-based uric acid sensors was also conducted and found that the system responds to several common metabolites (specifically, glucose and urea).

Chapter 5 presented a simple ammonia-plasma treatment method for enhancing the catalytic activity of GLAD film-based colorimetric biosensor. Different strategies for enhancing the surface energy of Ni GLAD film were also investigated, in order to mimic the enzyme efficiently. In comparison to pristine counterparts (without plasma treatment), surface-mounted nanozymes showed dramatically improved catalytic efficiency. Plasma treatment led to a large accumulation of N-rich surface species, which enhanced the wettability of catalyst surface, making it easier for reactants to reach the active sites. Furthermore, I also demonstrated continuous catalytic activity via gravity-driven flow as another step toward real-world applications, particularly integration in flow-driven point-of-care and microfluidic devices.

6.1 Future directions

The different studies in this thesis open the opportunity to expand the present findings in this Ph.D. work. Continuation of this work could progress in several directions. Some of them could include:

An exciting avenue to investigate the enzyme-like catalytic activities using films with different thickness, porosity, compositions, and morphologies. In addition to peroxidase, the oxidase enzyme is also involved in catalytic activity in the human body, such as catalyzing dissolved oxygen to produce free radicals, which may be identified with a colorimetric dye such as TMB/ABTS. One of the efficient ways may be designing new compositions of surface-treated nanozyme to mimic oxidase by decomposing dissolved oxygen to free radicals. For example, carbon based nanozymes may mimic oxidase and peroxidase.

GLAD thin films are used in different sectors such as biosensors. However, understanding their actual catalytic and sensing mechanism remains an ultimate goal. To solve this, fabricating GLAD films for fast electron transport employing metals and metal oxides doping could be promising in the future. The actual sensing mechanisms can be studied through a combination of theoretical calculations and analytical methods to study changes in electronic properties at the microlevel. The model for theoretical calculation can be generated from the crystallographic data originated from XRD and XPS. Theoretical calculation can be used to find (a) the transition states between reactant and product, and (b) activation energy required between reactant and product. This will provide insight into the nature of catalytic activities of GLAD thin films and will help to understand the actual sensing mechanism.

The current findings reported in the thesis are directed toward understanding the NiO mechanism for sensing applications, which are focused on achieving low sample handling and high throughput. Although the reported NiO biosensors discussed in this thesis contribute to understand the fundamentals, translation of such devices into routine diagnostics practices is still a long way away. Future work could focus on the demonstration of sensitive and selective biomarker detection in a natural biological buffer for the practical application of these devices in the biosensor industry.

Bibliography

A bibliography of all the works cited in the thesis is listed below.

Ishangulyyev R, Kim S, Lee S. Understanding Food Loss and Waste—Why Are We Losing and Wasting Food? Foods [Internet]. 2019 Jul 29;8(8):297. Available from: https://www.mdpi.com/2304-8158/8/8/297

Gibbons A. Disgusted by spoiled food? You may be protecting yourself from disease. Science (80-) [Internet]. 2021 Feb 15; Available from: https://www.sciencemag.org/news/2021/02/disgusted-spoiled-food-you-may-be-protecting-yourself-disease

Mustafa F, Andreescu S. Chemical and Biological Sensors for Food-Quality Monitoring and Smart Packaging. Foods [Internet]. 2018 Oct 16;7(10):168. Available from: https://www.mdpi.com/2304-8158/7/10/168

Falohun T, McShane MJ. An Optical Urate Biosensor Based on Urate Oxidase and Long-Lifetime Metalloporphyrins. Sensors [Internet]. 2020 Feb 11;20(4):959. Available from: https://www.mdpi.com/1424-8220/20/4/959

Vashist S. Point-of-Care Diagnostics: Recent Advances and Trends. Biosensors [Internet]. 2017 Dec 18;7(4):62. Available from: http://www.mdpi.com/2079-6374/7/4/62

Dodero A, Escher A, Bertucci S, Castellano M, Lova P. Intelligent Packaging for Real-Time Monitoring of Food-Quality: Current and Future Developments. Appl Sci [Internet]. 2021 Apr 15;11(8):3532. Available from: https://www.mdpi.com/2076-3417/11/8/3532

Jin B, Li Z, Zhao G, Ji J, Chen J, Yang Y, et al. Upconversion fluorescence-based paper disc for multiplex point-of-care testing in water quality monitoring. Anal Chim Acta [Internet]. 2022 Feb;1192:339388. Available from: https://linkinghub.elsevier.com/retrieve/pii/S0003267021012149

Rasmi Y, Li X, Khan J, Ozer T, Choi JR. Emerging point-of-care biosensors for rapid diagnosis of COVID-19: current progress, challenges, and future prospects. Anal Bioanal Chem [Internet]. 2021 Jul 18;413(16):4137–59. Available from: https://link.springer.com/10.1007/s00216-021-03377-6

Land KJ, Boeras DI, Chen X-S, Ramsay AR, Peeling RW. REASSURED diagnostics to inform disease control strategies, strengthen health systems and improve patient outcomes. Nat Microbiol [Internet]. 2019 Jan 13;4(1):46–54. Available from: http://www.nature.com/articles/s41564-018-0295-3

Wang X, Li F, Guo Y. Recent Trends in Nanomaterial-Based Biosensors for Point-of-Care Testing. Front Chem [Internet]. 2020 Oct 16;8. Available from: https://www.frontiersin.org/article/10.3389/fchem.2020.586702/full

Bucur B, Purcarea C, Andreescu S, Vasilescu A. Addressing the Selectivity of Enzyme Biosensors: Solutions and Perspectives. Sensors [Internet]. 2021 Apr 26;21(9):3038. Available from: https://www.mdpi.com/1424-8220/21/9/3038

Navaee A, Salimi A. Enzyme-based electrochemical biosensors. In: Electrochemical Biosensors [Internet]. Elsevier; 2019. p. 167–211. Available from: https://linkinghub.elsevier.com/retrieve/pii/B9780128164914000073

Cho I-H, Kim DH, Park S. Electrochemical biosensors: perspective on functional nanomaterials for on-site analysis. Biomater Res [Internet]. 2020 Dec 4;24(1):6. Available from: https://biomaterialsres.biomedcentral.com/articles/10.1186/s40824-019-0181-y

Caves MS, Derham BK, Jezek J, Freedman RB. Thermal Inactivation of Uricase (Urate Oxidase): Mechanism and Effects of Additives. Biochemistry [Internet]. 2013 Jan 22;52(3):497–507. Available from: https://pubs.acs.org/doi/10.1021/bi301334w

Çete S, Yaşar A, Arslan F. An Amperometric Biosensor for Uric Acid Determination Prepared from Uricase Immobilized in Polypyrrole Film. Artif Cells, Blood Substitutes, Biotechnol [Internet]. 2006 Jan 11;34(3):367–80. Available from: http://www.tandfonline.com/doi/full/10.1080/10731190600684116

Zhu D, Liu B, Wei G. Two-Dimensional Material-Based Colorimetric Biosensors: A Review. Biosensors [Internet]. 2021 Jul 31;11(8):259. Available from: https://www.mdpi.com/2079-6374/11/8/259

Harpaz D, Eltzov E, Ng TSE, Marks RS, Tok AIY. Enhanced Colorimetric Signal for Accurate Signal Detection in Paper-Based Biosensors. Diagnostics [Internet]. 2020 Jan 7;10(1):28. Available from: https://www.mdpi.com/2075-4418/10/1/28

Njagi JI, Kagwanja SM. The Interface in Biosensing: Improving Selectivity and Sensitivity. In 2011. p. 225–47. Available from: https://pubs.acs.org/doi/abs/10.1021/bk-2011-1062.ch011

Zhang R, Yan X, Fan K. Nanozymes Inspired by Natural Enzymes. Accounts Mater Res [Internet]. 2021 Jul 23;2(7):534–47. Available from: https://pubs.acs.org/doi/10.1021/accountsmr.1c00074

Wu J, Li S, Wei H. Integrated nanozymes: facile preparation and biomedical applications. Chem Commun [Internet]. 2018;54(50):6520–30. Available from: http://xlink.rsc.org/?DOI=C8CC01202D

Park H, Kim G, Seo Y, Yoon Y, Min J, Park C, et al. Improving Biosensors by the Use of Different Nanomaterials: Case Study with Microcystins as Target Analytes. Biosensors [Internet]. 2021 Dec 20;11(12):525. Available from: https://www.mdpi.com/2079-6374/11/12/525

Feng L, Zhang L, Zhang S, Chen X, Li P, Gao Y, et al. Plasma-Assisted Controllable Doping of Nitrogen into MoS 2 Nanosheets as Efficient Nanozymes with Enhanced Peroxidase-Like Catalysis Activity. ACS Appl Mater Interfaces [Internet]. 2020 Apr

15;12(15):17547–56. Available from: https://pubs.acs.org/doi/10.1021/acsami.0c01789

Dervisevic M, Dervisevic E, Şenel M. Recent progress in nanomaterial-based electrochemical and optical sensors for hypoxanthine and xanthine. A review. Microchim Acta [Internet]. 2019 Dec 6;186(12):749. Available from: http://link.springer.com/10.1007/s00604-019-3842-6

Wu, J.; Wang X.; Wang Q.; Lou Z.; Li S.; Zhu Y.; Qin L.; Wei H. Nanomaterials with enzyme-like characteristics (nanozymes): next-generation artificial enzymes (II). Chem Soc Rev. 2019;48(4):1004–76.

Sit JC, Vick D, Robbie K, Brett MJ. Thin Film Microstructure Control Using Glancing Angle Deposition by Sputtering. J Mater Res [Internet]. 1999 Apr;14(4):1197–9. Available from: http://link.springer.com/10.1557/JMR.1999.0162

Hawkeye MM, Brett MJ. Glancing angle deposition: Fabrication, properties, and applications of micro- and nanostructured thin films. J Vac Sci Technol A Vacuum, Surfaces, Film [Internet]. 2007;25(5):1317. Available from: http://scitation.aip.org/content/avs/journal/jvsta/25/5/10.1116/1.2764082

Sen S, Sarkar P. A novel third-generation xanthine biosensor with enzyme modified glassy carbon electrode using electrodeposited MWCNT and nanogold polymer composite film. RSC Adv [Internet]. 2015;5(116):95911–25. Available from: http://xlink.rsc.org/?DOI=C5RA18889J

Kushiyama A, Nakatsu Y, Matsunaga Y, Yamamotoya T, Mori K, Ueda K, et al. Role of Uric Acid Metabolism-Related Inflammation in the Pathogenesis of Metabolic Syndrome Components Such as Atherosclerosis and Nonalcoholic Steatohepatitis. Mediators Inflamm [Internet]. 2016;2016:1–15. Available from: https://www.hindawi.com/journals/mi/2016/8603164/

Califf RM. Biomarker definitions and their applications. Exp Biol Med [Internet]. 2018 Feb 6;243(3):213–21. Available from: http://journals.sagepub.com/doi/10.1177/1535370217750088

Cheng J, Gao R, Li H, Wu S, Fang J, Ma K, et al. Evaluating Potential Markers of Spoilage Foods Using a Metabolic Profiling Approach. Food Anal Methods [Internet]. 2015 May 18;8(5):1141–9. Available from: http://link.springer.com/10.1007/s12161-014-9999-z
Greiner J V., Glonek T. Intracellular ATP Concentration and Implication for Cellular Evolution. Biology (Basel) [Internet]. 2021 Nov 12;10(11):1166. Available from: https://www.mdpi.com/2079-7737/10/11/1166

Hagberg H, Andersson P, Lacarewicz J, Jacobson I, Butcher S, Sandberg M. Extracellular Adenosine, Inosine, Hypoxanthine, and Xanthine in Relation to Tissue Nucleotides and Purines in Rat Striatum During Transient Ischemia. J Neurochem [Internet]. 1987 Jul;49(1):227–31. Available from: https://onlinelibrary.wiley.com/doi/10.1111/j.1471-4159.1987.tb03419.x

Boll M, Fuchs G, Meier C, Trautwein A, El Kasmi A, Ragsdale SW, et al. Redox Centers of 4-Hydroxybenzoyl-CoA Reductase, a Member of the Xanthine Oxidase Family of Molybdenum-containing Enzymes. J Biol Chem [Internet]. 2001 Dec;276(51):47853–62. Available from: https://linkinghub.elsevier.com/retrieve/pii/S0021925819402925

Dervisevic M, Dervisevic E, Çevik E, Şenel M. Novel electrochemical xanthine biosensor based on chitosan–polypyrrole–gold nanoparticles hybrid bio-nanocomposite platform. J Food Drug Anal [Internet]. 2017 Jul;25(3):510–9. Available from: https://linkinghub.elsevier.com/retrieve/pii/S1021949817300224

Khan MZH, Ahommed MS, Daizy M. Detection of xanthine in food samples with an electrochemical biosensor based on PEDOT:PSS and functionalized gold nanoparticles. RSC Adv [Internet]. 2020;10(59):36147–54. Available from: http://xlink.rsc.org/?DOI=D0RA06806C

Hlavay J, Haemmerli SD, Guilbault GG. Fibre-optic biosensor for hypoxanthine and xanthine based on a chemiluminescence reaction. Biosens Bioelectron [Internet]. 1994 Jan;9(3):189–95. Available from: https://linkinghub.elsevier.com/retrieve/pii/0956566394801215

Thandavan K, Gandhi S, Sethuraman S, Rayappan JBB, Krishnan UM. Development of electrochemical biosensor with nano-interface for xanthine sensing – A novel approach for fish freshness estimation. Food Chem [Internet]. 2013 Aug;139(1–4):963–9. Available from: https://linkinghub.elsevier.com/retrieve/pii/S0308814613001660

Kushiyama A, Nakatsu Y, Matsunaga Y, Yamamotoya T, Mori K, Ueda K, et al. Role of Uric Acid Metabolism-Related Inflammation in the Pathogenesis of Metabolic Syndrome Components Such as Atherosclerosis and Nonalcoholic Steatohepatitis. Mediators Inflamm [Internet]. 2016;2016:1–15. Available from: https://www.hindawi.com/journals/mi/2016/8603164/

de Oliveira EP, Burini RC. High plasma uric acid concentration: causes and consequences. Diabetol Metab Syndr [Internet]. 2012 Dec 4;4(1):12. Available from: https://dmsjournal.biomedcentral.com/articles/10.1186/1758-5996-4-12

Kim KY, Ralph Schumacher H, Hunsche E, Wertheimer AI, Kong SX. A literature review of the epidemiology and treatment of acute gout. Clin Ther [Internet]. 2003 Jun;25(6):1593–617. Available from: https://linkinghub.elsevier.com/retrieve/pii/S0149291803801583

Davis SN, Lastra-Gonzalez G. Diabetes and Low Blood Sugar (Hypoglycemia). J Clin Endocrinol Metab [Internet]. 2008 Aug;93(8):0–0. Available from: https://academic.oup.com/jcem/article-lookup/doi/10.1210/jcem.93.8.9993

Wu F, Huang Y, Li Q. Animal tissue-based chemiluminescence sensing of uric acid. Anal Chim Acta [Internet]. 2005 Apr;536(1–2):107–13. Available from: https://linkinghub.elsevier.com/retrieve/pii/S000326700401671X

Galbán J. Direct determination of uric acid in serum by a fluorometric-enzymatic method based on uricase. Talanta [Internet]. 2001 Jun 21;54(5):847–54. Available from: https://linkinghub.elsevier.com/retrieve/pii/S0039914001003356

Zhao S, Wang J, Ye F, Liu Y-M. Determination of uric acid in human urine and serum by capillary electrophoresis with chemiluminescence detection. Anal Biochem [Internet]. 2008 Jul;378(2):127–31. Available from: https://linkinghub.elsevier.com/retrieve/pii/S0003269708002236

Rocha DL, Rocha FRP. A flow-based procedure with solenoid micro-pumps for the spectrophotometric determination of uric acid in urine. Microchem J [Internet]. 2010 Jan;94(1):53–9. Available from: https://linkinghub.elsevier.com/retrieve/pii/S0026265X09001271

PERELLO J, SANCHIS P, GRASES F. Determination of uric acid in urine, saliva and calcium oxalate renal calculi by high-performance liquid chromatography/mass spectrometry. J Chromatogr B [Internet]. 2005 Sep 25;824(1–2):175–80. Available from: https://linkinghub.elsevier.com/retrieve/pii/S1570023205005015

Zhao FY, Wang ZH, Wang H, Zhao R, Ding MY. Determination of uric acid in human urine by ion chromatography with conductivity detector. Chinese Chem Lett [Internet]. 2011 Mar;22(3):342–5. Available from: https://linkinghub.elsevier.com/retrieve/pii/S1001841710004055

Dai X, Fang X, Zhang C, Xu R, Xu B. Determination of serum uric acid using high-performance liquid chromatography (HPLC)/isotope dilution mass spectrometry (ID-MS) as a candidate reference method. J Chromatogr B [Internet]. 2007 Oct;857(2):287–95. Available from: https://linkinghub.elsevier.com/retrieve/pii/S1570023207005454

Mabey D, Peeling RW, Ustianowski A, Perkins MD. Diagnostics for the developing world. Nat Rev Microbiol. 2004;2(3):231–40.

Huang X, Tan C, Yin Z, Zhang H. 25th Anniversary Article: Hybrid Nanostructures Based on Two-Dimensional Nanomaterials. Adv Mater [Internet]. 2014 Apr;26(14):2185–204. Available from: https://onlinelibrary.wiley.com/doi/10.1002/adma.201304964

Li X, Shan J, Zhang W, Su S, Yuwen L, Wang L. Recent Advances in Synthesis and Biomedical Applications of Two-Dimensional Transition Metal Dichalcogenide Nanosheets. Small [Internet]. 2017 Feb;13(5):1602660. Available from: https://onlinelibrary.wiley.com/doi/10.1002/smll.201602660

Su S, Chao J, Pan D, Wang L, Fan C. Electrochemical Sensors Using Two-Dimensional Layered Nanomaterials. Electroanalysis [Internet]. 2015 May;27(5):1062–72. Available from: https://onlinelibrary.wiley.com/doi/10.1002/elan.201400655

Ping J, Fan Z, Sindoro M, Ying Y, Zhang H. Recent Advances in Sensing Applications of Two-Dimensional Transition Metal Dichalcogenide Nanosheets and Their Composites. Adv Funct Mater [Internet]. 2017 May;27(19):1605817. Available from: https://onlinelibrary.wiley.com/doi/10.1002/adfm.201605817

Chimene D, Alge DL, Gaharwar AK. Two-Dimensional Nanomaterials for Biomedical Applications: Emerging Trends and Future Prospects. Adv Mater [Internet]. 2015 Dec;27(45):7261–84. Available from: https://onlinelibrary.wiley.com/doi/10.1002/adma.201502422

Mehrotra P. Biosensors and their applications – A review. J Oral Biol Craniofacial Res [Internet]. 2016 May;6(2):153–9. Available from: https://linkinghub.elsevier.com/retrieve/pii/S2212426815001323

Naresh V, Lee N. A Review on Biosensors and Recent Development of Nanostructured Materials-Enabled Biosensors. Sensors [Internet]. 2021 Feb 5;21(4):1109. Available from: https://www.mdpi.com/1424-8220/21/4/1109

Tetyana P, Morgan Shumbula P, Njengele-Tetyana Z. Biosensors: Design, Development and Applications. In: Nanopores [Internet]. IntechOpen; 2021. Available from: https://www.intechopen.com/books/nanopores/biosensors-design-development-and-applications

Singh RS, Singh T, Singh AK. Enzymes as Diagnostic Tools. In: Advances in Enzyme Technology [Internet]. Elsevier; 2019. p. 225–71. Available from: https://linkinghub.elsevier.com/retrieve/pii/B9780444641144000091

Al-Tamer YY, Hadi EA, Al-Badrani I eldin I. Sweat urea, uric acid and creatinine concentrations in uraemic patients. Urol Res [Internet]. 1997 Sep;25(5):337–40. Available from: http://link.springer.com/10.1007/BF01294662

De Acha N, Socorro-Leránoz AB, Elosúa C, Matías IR. Trends in the Design of Intensity-Based Optical Fiber Biosensors (2010–2020). Biosensors [Internet]. 2021 Jun 15;11(6):197. Available from: https://www.mdpi.com/2079-6374/11/6/197

Rogers JK, Taylor ND, Church GM. Biosensor-based engineering of biosynthetic pathways. Curr Opin Biotechnol [Internet]. 2016 Dec;42:84–91. Available from: https://linkinghub.elsevier.com/retrieve/pii/S0958166916300611

Narang J, Malhotra N, Singhal C, Pundir CS. Evaluation of Freshness of Fishes Using MWCNT/TiO2 Nanobiocomposites Based Biosensor. Food Anal Methods [Internet]. 2017 Feb 21;10(2):522–8. Available from: http://link.springer.com/10.1007/s12161-016-0594-3

Yadav SK, Singh J, Agrawal VV, Malhotra BD. Nanostructured nickel oxide film for application to fish freshness biosensor. Appl Phys Lett [Internet]. 2012 Jul 9;101(2):023703. Available from: http://aip.scitation.org/doi/10.1063/1.4736578

Lavín Á, Vicente J, Holgado M, Laguna M, Casquel R, Santamaría B, et al. On the Determination of Uncertainty and Limit of Detection in Label-Free Biosensors. Sensors [Internet]. 2018 Jun 26;18(7):2038. Available from: http://www.mdpi.com/1424-8220/18/7/2038

Sen S, Sarkar P. A novel third-generation xanthine biosensor with enzyme modified glassy carbon electrode using electrodeposited MWCNT and nanogold polymer composite film. RSC Adv [Internet]. 2015;5(116):95911–25. Available from: http://xlink.rsc.org/?DOI=C5RA18889J

Grieshaber D, MacKenzie R, Vörös J, Reimhult E. Electrochemical Biosensors - Sensor Principles and Architectures. Sensors [Internet]. 2008 Mar 7;8(3):1400–58. Available from: http://www.mdpi.com/1424-8220/8/3/1400

Son J, Buck EC, Riechers SL, Yu X-Y. Stamping Nanoparticles onto the Electrode for Rapid Electrochemical Analysis in Microfluidics. Micromachines [Internet]. 2021 Jan 6;12(1):60. Available from: https://www.mdpi.com/2072-666X/12/1/60

Maduraiveeran G, Jin W. Nanomaterials based electrochemical sensor and biosensor platforms for environmental applications. Trends Environ Anal Chem [Internet]. 2017 Jan;13:10–23. Available from: https://linkinghub.elsevier.com/retrieve/pii/S2214158817300132

Shen Y, Rao D, Sheng Q, Zheng J. Simultaneous voltammetric determination of hydroquinone and catechol by using a glassy carbon electrode modified with carboxy-functionalized carbon nanotubes in a chitosan matrix and decorated with gold nanoparticles. Microchim Acta [Internet]. 2017 Sep 29;184(9):3591–601. Available from: http://link.springer.com/10.1007/s00604-017-2392-z

Rao D, Sheng Q, Zheng J. Preparation of flower-like Pt nanoparticles decorated chitosan-grafted graphene oxide and its electrocatalysis of hydrazine. Sensors Actuators B Chem [Internet]. 2016 Nov;236:192–200. Available from: https://linkinghub.elsevier.com/retrieve/pii/S0925400516308462

Azab SM, Fekry AM. Electrochemical design of a new nanosensor based on cobalt nanoparticles, chitosan and MWCNT for the determination of daclatasvir: a hepatitis C antiviral drug. RSC Adv [Internet]. 2017;7(2):1118–26. Available from: http://xlink.rsc.org/?DOI=C6RA25826C

Boluda A, Casado C, Alonso B, García Armada M. Efficient Oxidase Biosensors Based on Bioelectrocatalytic Surfaces of Electrodeposited Ferrocenyl Polycyclosiloxanes—Pt Nanoparticles. Chemosensors [Internet]. 2021 Apr 15;9(4):81. Available from: https://www.mdpi.com/2227-9040/9/4/81

VEDRINE C. Amperometric tyrosinase based biosensor using an electrogenerated

polythiophene film as an entrapment support. Talanta [Internet]. 2003 Mar;59(3):535–44. Available from: https://linkinghub.elsevier.com/retrieve/pii/S0039914002005404

Button VLDSN. Electrodes for Biopotential Recording and Tissue Stimulation. In: Principles of Measurement and Transduction of Biomedical Variables [Internet]. Elsevier; 2015. p. 25–76. Available from: https://linkinghub.elsevier.com/retrieve/pii/B9780128007747000027

Zhang JXJ, Hoshino K. Electrical transducers: Electrochemical sensors and semiconductor molecular sensors. In: Molecular Sensors and Nanodevices [Internet]. Elsevier; 2019. p. 181–230. Available from: https://linkinghub.elsevier.com/retrieve/pii/B9780128148624000041

Sun C, Xu Q, Zou X, Cheng H, Lu X. A new method to determine AgCl(1% mol)/Ag electrode potential versus the standard chloride electrode potential in a LiCl-KCl eutectic. Electrochem commun [Internet]. 2021 Sep;130:107111. Available from: https://linkinghub.elsevier.com/retrieve/pii/S1388248121001958

Nguyen TSV, Huynh TM, To TD, Doan TCD, Dang CM. Ag/AgCl Film Electrodes Coated with Agarose Gel as Planar Reference Electrodes for Potentiometric Sensors. Univers J Mater Sci [Internet]. 2018 Nov;6(5):148–54. Available from: http://www.hrpub.org/journals/article_info.php?aid=7510

Chen X, Lu L, Gu D, Zhang X, Yu H, Chen F, et al. Chlorine management of a carbon counter electrode for high performance printable perovskite solar cells. J Mater Chem C [Internet]. 2021;9(27):8615–22. Available from: http://xlink.rsc.org/?DOI=D1TC00890K

Chen R, Yang C, Cai W, Wang H-Y, Miao J, Zhang L, et al. Use of Platinum as the Counter Electrode to Study the Activity of Nonprecious Metal Catalysts for the Hydrogen Evolution Reaction. ACS Energy Lett [Internet]. 2017 May 12;2(5):1070–5. Available from: https://pubs.acs.org/doi/10.1021/acsenergylett.7b00219

Saha T, Fang J, Mukherjee S, Knisely CT, Dickey MD, Velev OD. Osmotically Enabled Wearable Patch for Sweat Harvesting and Lactate Quantification. Micromachines [Internet]. 2021 Dec 4;12(12):1513. Available from: https://www.mdpi.com/2072-666X/12/12/1513

Mathew M, Sandhyarani N. A highly sensitive electrochemical glucose sensor structuring with nickel hydroxide and enzyme glucose oxidase. Electrochim Acta [Internet]. 2013 Oct;108:274–80. Available from: https://linkinghub.elsevier.com/retrieve/pii/S0013468613012784

Clark LC, Lyons C. ELECTRODE SYSTEMS FOR CONTINUOUS MONITORING IN CARDIOVASCULAR SURGERY. Ann N Y Acad Sci [Internet]. 2006 Dec 15;102(1):29–45. Available from: https://onlinelibrary.wiley.com/doi/10.1111/j.1749-6632.1962.tb13623.x

Batool R, Rhouati A, Nawaz MH, Hayat A, Marty JL. A Review of the Construction of Nano-Hybrids for Electrochemical Biosensing of Glucose. Biosensors [Internet]. 2019 Mar 25;9(1):46. Available from: https://www.mdpi.com/2079-6374/9/1/46

Pandey PC, Pandey G, Narayan RJ. Minimally Invasive Platforms in Biosensing. Front Bioeng Biotechnol [Internet]. 2020 Aug 31;8. Available from: https://www.frontiersin.org/article/10.3389/fbioe.2020.00894/full

Imam HT, Marr PC, Marr AC. Enzyme entrapment, biocatalyst immobilization without covalent attachment. Green Chem [Internet]. 2021;23(14):4980–5005. Available from: http://xlink.rsc.org/?DOI=D1GC01852C

Zdarta J, Meyer A, Jesionowski T, Pinelo M. A General Overview of Support Materials for Enzyme Immobilization: Characteristics, Properties, Practical Utility. Catalysts [Internet]. 2018 Feb 24;8(2):92. Available from: http://www.mdpi.com/2073-4344/8/2/92

Pandey G, Munguambe DM, Tharmavaram M, Rawtani D, Agrawal YK. Halloysite nanotubes - An efficient 'nano-support' for the immobilization of α-amylase. Appl Clay Sci [Internet]. 2017 Feb;136:184–91. Available from: https://linkinghub.elsevier.com/retrieve/pii/S016913171630535X

Doonan C, Riccò R, Liang K, Bradshaw D, Falcaro P. Metal–Organic Frameworks at the Biointerface: Synthetic Strategies and Applications. Acc Chem Res [Internet]. 2017 Jun 20;50(6):1423–32. Available from: https://pubs.acs.org/doi/10.1021/acs.accounts.7b00090

Grigoras AG. Catalase immobilization—A review. Biochem Eng J [Internet]. 2017 Jan;117:1–20. Available from: https://linkinghub.elsevier.com/retrieve/pii/S1369703X16302972

Kim T-S, Patel SKS, Selvaraj C, Jung W-S, Pan C-H, Kang YC, et al. A highly efficient sorbitol dehydrogenase from Gluconobacter oxydans G624 and improvement of its stability through immobilization. Sci Rep [Internet]. 2016 Dec 16;6(1):33438. Available from: http://www.nature.com/articles/srep33438

Komiyama M, Yoshimoto K, Sisido M, Ariga K. Chemistry Can Make Strict and Fuzzy Controls for Bio-Systems: DNA Nanoarchitectonics and Cell-Macromolecular Nanoarchitectonics. Bull Chem Soc Jpn [Internet]. 2017 Sep 15;90(9):967–1004. Available from: http://www.journal.csj.jp/doi/10.1246/bcsj.20170156

Murata K, Akatsuka W, Tsujimura S. Bioelectrocatalytic Oxidation of Glucose on MgO-templated Mesoporous Carbon-modified Electrode. Chem Lett [Internet]. 2014 Jun 5;43(6):928–30. Available from: http://www.journal.csj.jp/doi/10.1246/cl.140189

Daneshjou S, Dabirmanesh B, Rahimi F, Khajeh K. Porous silicon nanoparticle as a stabilizing support for chondroitinase. Int J Biol Macromol [Internet]. 2017 Jan;94:852–8.

Available from: https://linkinghub.elsevier.com/retrieve/pii/S0141813016321365

Fang Y, Umasankar Y, Ramasamy RP. A novel bi-enzyme electrochemical biosensor for selective and sensitive determination of methyl salicylate. Biosens Bioelectron [Internet]. 2016 Jul;81:39–45. Available from: https://linkinghub.elsevier.com/retrieve/pii/S0956566316300963

Jegannathan KR, Abang S, Poncelet D, Chan ES, Ravindra P. Production of Biodiesel Using Immobilized Lipase—A Critical Review. Crit Rev Biotechnol [Internet]. 2008 Jan 16;28(4):253–64. Available from: http://www.tandfonline.com/doi/full/10.1080/07388550802428392

Boscolo B, Trotta F, Ghibaudi E. High catalytic performances of Pseudomonas fluorescens lipase adsorbed on a new type of cyclodextrin-based nanosponges. J Mol Catal B Enzym [Internet]. 2010 Feb;62(2):155–61. Available from: https://linkinghub.elsevier.com/retrieve/pii/S1381117709002550

Ponvel KM, Lee D-G, Woo E-J, Ahn I-S, Lee C-H. Immobilization of lipase on surface modified magnetic nanoparticles using alkyl benzenesulfonate. Korean J Chem Eng [Internet]. 2009 Jan 28;26(1):127–30. Available from: http://link.springer.com/10.1007/s11814-009-0019-8

Yang G, Wu J, Xu G, Yang L. Improvement of catalytic properties of lipase from Arthrobacter sp. by encapsulation in hydrophobic sol–gel materials. Bioresour Technol [Internet]. 2009 Oct;100(19):4311–6. Available from: https://linkinghub.elsevier.com/retrieve/pii/S0960852409003472

Yilmaz E, Sezgin M. Enhancement of the Activity and Enantioselectivity of Lipase by Sol–Gel Encapsulation Immobilization onto β-cyclodextrin-Based Polymer. Appl Biochem Biotechnol [Internet]. 2012 Apr 1;166(8):1927–40. Available from: http://link.springer.com/10.1007/s12010-012-9621-z

Cacicedo ML, Manzo RM, Municoy S, Bonazza HL, Islan GA, Desimone M, et al. Immobilized Enzymes and Their Applications. In: Advances in Enzyme Technology [Internet]. Elsevier; 2019. p. 169–200. Available from: https://linkinghub.elsevier.com/retrieve/pii/B9780444641144000078

Minteer SD. Cell-Free Biotechnologies. In: Biotechnology for Biofuel Production and Optimization [Internet]. Elsevier; 2016. p. 433–48. Available from: https://linkinghub.elsevier.com/retrieve/pii/B9780444634757000169

Liang Y-Y, Zhang L-M. Bioconjugation of Papain on Superparamagnetic Nanoparticles Decorated with Carboxymethylated Chitosan. Biomacromolecules [Internet]. 2007 May 1;8(5):1480–6. Available from: https://pubs.acs.org/doi/10.1021/bm061091g

Bai Y, Li Y, Lei L. Synthesis of a mesoporous functional copolymer bead carrier and its

properties for glucoamylase immobilization. Appl Microbiol Biotechnol [Internet]. 2009 Jun 1;83(3):457–64. Available from: http://link.springer.com/10.1007/s00253-009-1864-4

Chiou S-H, Wu W-T. Immobilization of Candida rugosa lipase on chitosan with activation of the hydroxyl groups. Biomaterials [Internet]. 2004 Jan;25(2):197–204. Available from: https://linkinghub.elsevier.com/retrieve/pii/S0142961203004824

Heck T, Faccio G, Richter M, Thöny-Meyer L. Enzyme-catalyzed protein crosslinking. Appl Microbiol Biotechnol [Internet]. 2013 Jan 25;97(2):461–75. Available from: http://link.springer.com/10.1007/s00253-012-4569-z

Govardhan CP. Crosslinking of enzymes for improved stability and performance. Curr Opin Biotechnol [Internet]. 1999 Aug;10(4):331–5. Available from: https://linkinghub.elsevier.com/retrieve/pii/S0958166999800603

Goossens J, Sein H, Lu S, Radwanska M, Muyldermans S, Sterckx YG-J, et al. Functionalization of gold nanoparticles with nanobodies through physical adsorption. Anal Methods [Internet]. 2017;9(23):3430–40. Available from: http://xlink.rsc.org/?DOI=C7AY00854F

Lin P, Zhang Y, Ren H, Wang Y, Wang S, Fang B. Assembly of graphene oxide-formate dehydrogenase composites by nickel-coordination with enhanced stability and reusability. Eng Life Sci [Internet]. 2018 May;18(5):326–33. Available from: https://onlinelibrary.wiley.com/doi/10.1002/elsc.201700137

Zhang D, Hegab HE, Lvov Y, Dale Snow L, Palmer J. Immobilization of cellulase on a silica gel substrate modified using a 3-APTES self-assembled monolayer. Springerplus [Internet]. 2016 Dec 20;5(1):48. Available from: https://springerplus.springeropen.com/articles/10.1186/s40064-016-1682-y

Uddin KMA, Orelma H, Mohammadi P, Borghei M, Laine J, Linder M, et al. Retention of lysozyme activity by physical immobilization in nanocellulose aerogels and antibacterial effects. Cellulose [Internet]. 2017 Jul 5;24(7):2837–48. Available from: http://link.springer.com/10.1007/s10570-017-1311-0

de Alteriis E, Parascandola P, Pecorella MA, Scardi V. Entrapment of microbial cells within a gelatin matrix: A comparison of three procedures. Biotechnol Tech [Internet]. 1987 Jun;1(2):109–14. Available from: http://link.springer.com/10.1007/BF00159331

Gao Y, Shen C, Di J, Tu Y. Fabrication of amperometric xanthine biosensors based on direct chemistry of xanthine oxidase. Mater Sci Eng C [Internet]. 2009 Aug;29(7):2213–6. Available from: https://linkinghub.elsevier.com/retrieve/pii/S0928493109001568

Lates V, Marty J-L, Popescu IC. Determination of Antioxidant Capacity by Using Xanthine Oxidase Bioreactor Coupled with Flow-through H2O2 Amperometric Biosensor. Electroanalysis [Internet]. 2010 Dec 22;n/a-n/a. Available from: https://onlinelibrary.wiley.com/doi/10.1002/elan.201000544

Isgrove FH, Williams RJH, Niven GW, Andrews AT. Enzyme immobilization on nylon–optimization and the steps used to prevent enzyme leakage from the support. Enzyme Microb Technol [Internet]. 2001 Feb;28(2–3):225–32. Available from: https://linkinghub.elsevier.com/retrieve/pii/S0141022900003124

Kumar A, Kanwar SS. Catalytic potential of a nitrocellulose membrane-immobilized lipase in aqueous and organic media. J Appl Polym Sci [Internet]. 2012 Jun 25;124(S1):E37–44. Available from: https://onlinelibrary.wiley.com/doi/10.1002/app.35434

Shin J-H, Lee M-J, Choi J-H, Song J, Kim T-H, Oh B-K. Electrochemical H2O2 biosensor based on horseradish peroxidase encapsulated protein nanoparticles with reduced graphene oxide-modified gold electrode. Nano Converg [Internet]. 2020 Dec 16;7(1):39. Available from: https://nanoconvergencejournal.springeropen.com/articles/10.1186/s40580-020-00249-0

Trevan MD. Enzyme Immobilization by Covalent Bonding. In: New Protein Techniques [Internet]. New Jersey: Humana Press; p. 495–510. Available from: http://link.springer.com/10.1385/0-89603-126-8:495

Yang X, Hua L, Gong H, Tan SN. Covalent immobilization of an enzyme (glucose oxidase) onto a carbon sol–gel silicate composite surface as a biosensing platform. Anal Chim Acta [Internet]. 2003 Feb;478(1):67–75. Available from: https://linkinghub.elsevier.com/retrieve/pii/S0003267002015076

Salem M, Mauguen Y, Prangé T. Revisiting glutaraldehyde cross-linking: the case of the Arg–Lys intermolecular doublet. Acta Crystallogr Sect F Struct Biol Cryst Commun [Internet]. 2010 Mar 1;66(3):225–8. Available from: http://scripts.iucr.org/cgi-bin/paper?S1744309109054037

Carpani I, Scavetta E, Tonelli D. Amperometric Glucose Biosensors Based on Glassy Carbon and SWCNT-Modified Glassy Carbon Electrodes. Electroanalysis [Internet]. 2008 Jan;20(1):84–90. Available from: https://onlinelibrary.wiley.com/doi/10.1002/elan.200704054

Curulli A. Nanomaterials in Electrochemical Sensing Area: Applications and Challenges in Food Analysis. Molecules [Internet]. 2020 Dec 7;25(23):5759. Available from: https://www.mdpi.com/1420-3049/25/23/5759

Favrod-Coune T, Broers B. Addiction to Caffeine and Other Xanthines. In: Textbook of Addiction Treatment: International Perspectives [Internet]. Milano: Springer Milan; 2015. p. 437–53. Available from: http://link.springer.com/10.1007/978-88-470-5322-9_18

Devi R, Thakur M, Pundir CS. Construction and application of an amperometric xanthine biosensor based on zinc oxide nanoparticles–polypyrrole composite film. Biosens Bioelectron [Internet]. 2011 Apr;26(8):3420–6. Available from: https://linkinghub.elsevier.com/retrieve/pii/S0956566311000388

Dalkiran B, Kaçar C, Erden PE, Kiliç E. Amperometric xanthine biosensors based on chitosan-Co3O4-multiwall carbon nanotube modified glassy carbon electrode. Sensors Actuators B Chem [Internet]. 2014 Sep;200:83–91. Available from: https://linkinghub.elsevier.com/retrieve/pii/S0925400514004262

Zhang X, Dong J, Qian X, Zhao C. One-pot synthesis of an RGO/ZnO nanocomposite on zinc foil and its excellent performance for the nonenzymatic sensing of xanthine. Sensors Actuators B Chem [Internet]. 2015 Dec;221:528–36. Available from: https://linkinghub.elsevier.com/retrieve/pii/S092540051500814X

Raj MA, John SA. Simultaneous determination of uric acid, xanthine, hypoxanthine and caffeine in human blood serum and urine samples using electrochemically reduced graphene oxide modified electrode. Anal Chim Acta [Internet]. 2013 Apr;771:14–20. Available from: https://linkinghub.elsevier.com/retrieve/pii/S000326701300233X

Zhu D, Guo D, Zhang L, Tan L, Pang H, Ma H, et al. Non-enzymatic xanthine sensor of heteropolyacids doped ferrocene and reduced graphene oxide via one-step electrodeposition combined with layer-by-layer self-assembly technology. Sensors Actuators B Chem [Internet]. 2019 Feb;281:893–904. Available from: https://linkinghub.elsevier.com/retrieve/pii/S0925400518319282

Luo A, Lian Q, An Z, Li Z, Guo Y, Zhang D, et al. Simultaneous determination of uric acid, xanthine and hypoxanthine based on sulfonic groups functionalized nitrogen-doped graphene. J Electroanal Chem [Internet]. 2015 Nov;756:22–9. Available from: https://linkinghub.elsevier.com/retrieve/pii/S1572665715300679

Rahman MM, Marwani HM, Algethami FK, Asiri AM. Xanthine sensor development based on ZnO–CNT, ZnO–CB, ZnO–GO and ZnO nanoparticles: an electrochemical approach. New J Chem [Internet]. 2017;41(14):6262–71. Available from: http://xlink.rsc.org/?DOI=C7NJ00278E

Devi R, Yadav S, Pundir CS. Amperometric determination of xanthine in fish meat by zinc oxide nanoparticle/chitosan/multiwalled carbon nanotube/polyaniline composite film bound xanthine oxidase. Analyst [Internet]. 2012;137(3):754–9. Available from: http://xlink.rsc.org/?DOI=C1AN15838D

Kreno LE, Leong K, Farha OK, Allendorf M, Van Duyne RP, Hupp JT. Metal–Organic Framework Materials as Chemical Sensors. Chem Rev [Internet]. 2012 Feb 8;112(2):1105–25. Available from: https://pubs.acs.org/doi/10.1021/cr200324t

Furukawa H, Cordova KE, O'Keeffe M, Yaghi OM. The Chemistry and Applications of Metal-Organic Frameworks. Science (80-) [Internet]. 2013 Aug 30;341(6149). Available from: https://www.science.org/doi/10.1126/science.1230444

Xu Y, Li Q, Xue H, Pang H. Metal-organic frameworks for direct electrochemical

applications. Coord Chem Rev [Internet]. 2018 Dec;376:292–318. Available from: https://linkinghub.elsevier.com/retrieve/pii/S001085451830290X

Fang X, Zong B, Mao S. Metal–Organic Framework-Based Sensors for Environmental Contaminant Sensing. Nano-Micro Lett [Internet]. 2018 Oct 13;10(4):64. Available from: http://link.springer.com/10.1007/s40820-018-0218-0

Salimi A, Sharifi E, Noorbakhsh A, Soltanian S. Direct electrochemistry and electrocatalytic activity of catalase immobilized onto electrodeposited nano-scale islands of nickel oxide. Biophys Chem [Internet]. 2007 Feb;125(2–3):540–8. Available from: https://linkinghub.elsevier.com/retrieve/pii/S0301462206003371

Hayat A, Catanante G, Marty J. Current Trends in Nanomaterial-Based Amperometric Biosensors. Sensors [Internet]. 2014 Dec 8;14(12):23439–61. Available from: http://www.mdpi.com/1424-8220/14/12/23439

Elgrishi N, Rountree KJ, McCarthy BD, Rountree ES, Eisenhart TT, Dempsey JL. A Practical Beginner's Guide to Cyclic Voltammetry. J Chem Educ [Internet]. 2018 Feb 13;95(2):197–206. Available from: https://pubs.acs.org/doi/10.1021/acs.jchemed.7b00361

Zhou Y. Investigation of nanostructured lithium-ion battery materials. Friedrich-Alexander-Universität Erlangen-Nürnberg; 2020.
Venton BJ, DiScenza DJ. Voltammetry. In: Electrochemistry for Bioanalysis [Internet]. Elsevier; 2020. p. 27–50. Available from: https://linkinghub.elsevier.com/retrieve/pii/B978012821203500004X

Wang Z, Ma B, Shen C, Lai O-M, Tan C-P, Cheong L-Z. Electrochemical Biosensing of Chilled Seafood Freshness by Xanthine Oxidase Immobilized on Copper-Based Metal–Organic Framework Nanofiber Film. Food Anal Methods [Internet]. 2019 Aug 6;12(8):1715–24. Available from: http://link.springer.com/10.1007/s12161-019-01513-8

Chen WC, Wu SY, Liu HP, Chang CH, Chen HY, Chen HY, et al. Identification of melamine/cyanuric acid-containing nephrolithiasis by infrared spectroscopy. J Clin Lab Anal. 2010;24(2):92–9.

Pavlíček V, Tůma P, Matějčková J, Samcová E. Very fast electrophoretic determination of creatinine and uric acid in human urine using a combination of two capillaries with different internal diameters. Electrophoresis. 2014;35(7):956–61.

Kumar A, Hens A, Arun RK, Chatterjee M, Mahato K, Layek K, et al. A paper based microfluidic device for easy detection of uric acid using positively charged gold nanoparticles. Analyst [Internet]. 2015;140(6):1817–21. Available from: http://xlink.rsc.org/?DOI=C4AN02333A

Jazayeri MH, Aghaie T, Avan A, Vatankhah A, Ghaffari MRS. Colorimetric detection based on gold nano particles (GNPs): An easy, fast, inexpensive, low-cost and short time

method in detection of analytes (protein, DNA, and ion). Sens Bio-Sensing Res. 2018;20(May):1–8.

Harpaz D, Eltzov E, Ng TSE, Marks RS, Tok AIY. Enhanced Colorimetric Signal for Accurate Signal Detection in Paper-Based Biosensors. Diagnostics [Internet]. 2020 Jan 7;10(1):28. Available from: https://www.mdpi.com/2075-4418/10/1/28

Tripathi A, Harris KD, Elias AL. Peroxidase-Like Behavior of Ni Thin Films Deposited by Glancing Angle Deposition for Enzyme-Free Uric Acid Sensing. ACS Omega [Internet]. 2020 Apr 28;5(16):9123–30. Available from: https://pubs.acs.org/doi/10.1021/acsomega.9b04071

Chen X, Chen J, Wang F, Xiang X, Luo M, Ji X, et al. Determination of glucose and uric acid with bienzyme colorimetry on microfluidic paper-based analysis devices. Biosens Bioelectron [Internet]. 2012 May;35(1):363–8. Available from: https://linkinghub.elsevier.com/retrieve/pii/S095656631200187X

Liu F, He J, Zeng M, Hao J, Guo Q, Song Y, et al. Cu–hemin metal-organic frameworks with peroxidase-like activity as peroxidase mimics for colorimetric sensing of glucose. J Nanoparticle Res [Internet]. 2016 May 15;18(5):106. Available from: http://link.springer.com/10.1007/s11051-016-3416-z

Lin L, Song X, Chen Y, Rong M, Zhao T, Wang Y, et al. Intrinsic peroxidase-like catalytic activity of nitrogen-doped graphene quantum dots and their application in the colorimetric detection of H2O2 and glucose. Anal Chim Acta [Internet]. 2015 Apr;869:89–95. Available from: https://linkinghub.elsevier.com/retrieve/pii/S0003267015002020

Chen J, Xu F, Zhang Q, Li S. N-doped MoS2-nanoflowers as peroxidase-like nanozymes for total antioxidant capacity assay. Anal Chim Acta [Internet]. 2021 Oct;1180:338740. Available from: https://linkinghub.elsevier.com/retrieve/pii/S0003267021005663

Gao L, Zhuang J, Nie L, Zhang J, Zhang Y, Gu N, et al. Intrinsic peroxidase-like activity of ferromagnetic nanoparticles. Nat Nanotechnol [Internet]. 2007 Sep 26;2(9):577–83. Available from: http://www.nature.com/articles/nnano.2007.260

Kumar S, Bhushan P, Bhattacharya S. Development of a paper-based analytical device for colorimetric detection of uric acid using gold nanoparticles–graphene oxide (AuNPs–GO) conjugates. Anal Methods [Internet]. 2016;8(38):6965–73. Available from: http://xlink.rsc.org/?DOI=C6AY01926A

Huang L, Chen J, Gan L, Wang J, Dong S. Single-atom nanozymes. Sci Adv. 2019;5(5).
Das B, Franco J Lou, Logan N, Balasubramanian P, Kim M Il, Cao C. Nanozymes in Point-of-Care Diagnosis: An Emerging Futuristic Approach for Biosensing. Nano-Micro Lett [Internet]. 2021 Jan 13;13(1):193. Available from: https://link.springer.com/10.1007/s40820-021-00717-0

Mahmudunnabi RG, Farhana FZ, Kashaninejad N, Firoz SH, Shim Y-B, Shiddiky MJA. Nanozyme-based electrochemical biosensors for disease biomarker detection. Analyst [Internet]. 2020;145(13):4398–420. Available from: http://xlink.rsc.org/?DOI=D0AN00558D

Wang W, Gunasekaran S. Nanozymes-based biosensors for food quality and safety. TrAC Trends Anal Chem [Internet]. 2020 May;126:115841. Available from: https://linkinghub.elsevier.com/retrieve/pii/S0165993619306739

Wong ELS, Vuong KQ, Chow E. Nanozymes for Environmental Pollutant Monitoring and Remediation. Sensors [Internet]. 2021 Jan 8;21(2):408. Available from: https://www.mdpi.com/1424-8220/21/2/408

Feng L, Zhang L, Zhang S, Chen X, Li P, Gao Y, et al. Plasma-Assisted Controllable Doping of Nitrogen into MoS 2 Nanosheets as Efficient Nanozymes with Enhanced Peroxidase-Like Catalysis Activity. ACS Appl Mater Interfaces [Internet]. 2020 Apr 15;12(15):17547–56. Available from: https://pubs.acs.org/doi/10.1021/acsami.0c01789

Zhou W, Hou D, Sang Y, Yao S, Zhou J, Li G, et al. MoO2 nanobelts@nitrogen self-doped MoS2 nanosheets as effective electrocatalysts for hydrogen evolution reaction. J Mater Chem A [Internet]. 2014;2(29):11358–64. Available from: http://xlink.rsc.org/?DOI=c4ta01898b

Johnson KA, Goody RS. The Original Michaelis Constant: Translation of the 1913 Michaelis–Menten Paper. Biochemistry [Internet]. 2011 Oct 4;50(39):8264–9. Available from: https://pubs.acs.org/doi/10.1021/bi201284u

Sit JC, Vick D, Robbie K, Brett MJ. Thin Film Microstructure Control Using Glancing Angle Deposition by Sputtering. J Mater Res [Internet]. 1999 Apr;14(4):1197–9. Available from: http://link.springer.com/10.1557/JMR.1999.0162

Barranco A, Borras A, Gonzalez-Elipe AR, Palmero A. Perspectives on oblique angle deposition of thin films: From fundamentals to devices. Prog Mater Sci [Internet]. 2016 Mar;76:59–153. Available from: https://linkinghub.elsevier.com/retrieve/pii/S0079642515000705

Elias A, Brett M, Harris K, Bastiaansen C, Broer D. Three Techniques for Micropatterning Liquid Crystalline Polymers. Mol Cryst Liq Cryst [Internet]. 2007 Dec 12;477:137–51. Available from: http://www.tandfonline.com/doi/abs/10.1080/15421400701695687

Zhang JXJ, Hoshino K. Fundamentals of nano/microfabrication and scale effect. In: Molecular Sensors and Nanodevices [Internet]. Elsevier; 2019. p. 43–111. Available from: https://linkinghub.elsevier.com/retrieve/pii/B9780128148624000028

Steele JJ, Brett MJ. Nanostructure engineering in porous columnar thin films: recent advances. J Mater Sci Mater Electron [Internet]. 2007 Jan 8;18(4):367–79. Available from: http://link.springer.com/10.1007/s10854-006-9049-8

Hawkeye MM, Brett MJ. Glancing angle deposition: Fabrication, properties, and applications of micro- and nanostructured thin films. J Vac Sci Technol A Vacuum, Surfaces, Film [Internet]. 2007;25(5):1317. Available from: http://scitation.aip.org/content/avs/journal/jvsta/25/5/10.1116/1.2764082

Huh YS, Erickson D. Aptamer based surface enhanced Raman scattering detection of vasopressin using multilayer nanotube arrays. Biosens Bioelectron [Internet]. 2010 Jan 15;25(5):1240–3. Available from: https://linkinghub.elsevier.com/retrieve/pii/S0956566309005272

Chu H, Huang Y, Zhao Y. Silver Nanorod Arrays as a Surface-Enhanced Raman Scattering Substrate for Foodborne Pathogenic Bacteria Detection. Appl Spectrosc [Internet]. 2008 Aug 1;62(8):922–31. Available from: http://journals.sagepub.com/doi/10.1366/000370208785284330

Lin D, Harris KD, Chan NWC, Jemere AB. Nanostructured indium tin oxide electrodes immobilized with toll-like receptor proteins for label-free electrochemical detection of pathogen markers. Sensors Actuators B Chem [Internet]. 2018 Mar;257:324–30. Available from: https://linkinghub.elsevier.com/retrieve/pii/S0925400517320543

Kesapragada S V., Gall D. Anisotropic broadening of Cu nanorods during glancing angle deposition. Appl Phys Lett [Internet]. 2006 Nov 13;89(20):203121. Available from: http://aip.scitation.org/doi/10.1063/1.2388861

Ghaly A. E.; Dave D.; Budge S.; Brooks M. S. Fish Spoilage Mechanisms and Preservation Techniques: Review. *Am. J. Appl. Sci.* **2010**, *7* (7), 859–877. https://doi.org/10.3844/ajassp.2010.859.877.

Hong, H.; Regenstein, J. M.; Luo, Y. The Importance of ATP-Related Compounds for the Freshness and Flavor of Post-Mortem Fish and Shellfish Muscle: A Review. *Crit. Rev. Food Sci. Nutr.* **2015**, 00–00. https://doi.org/10.1080/10408398.2014.1001489.

Pundir, C. S.; Devi, R. Biosensing Methods for Xanthine Determination: A Review. *Enzyme Microb. Technol.* **2014**, *57*, 55–62. https://doi.org/10.1016/j.enzmictec.2013.12.006.

Lu, J.-J.; Jia, B.-J.; Yang, L.; Zhang, W.; Dong, X.; Li, P.; Chen, J. Ultra-High Performance Liquid Chromatography with Ultraviolet and Tandem Mass Spectrometry for Simultaneous Determination of Metabolites in Purine Pathway of Rat Plasma. *J. Chromatogr. B* **2016**, *1036–1037*, 84–92. https://doi.org/10.1016/j.jchromb.2016.09.023.

Logotheti, M.; Theochari, K.; Kostakis, M.; Pasias, I. N.; Thomaidis, N. S. Development and Validation of a HILIC-UV Method for the Determination of Nucleotides in Fish Samples. *Food Chem.* **2018**, *248*, 70–77. https://doi.org/10.1016/j.foodchem.2017.12.040.

Monteiro, T.; Almeida, M. G. Electrochemical Enzyme Biosensors Revisited: Old Solutions for New Problems. *Crit. Rev. Anal. Chem.* **2019**, *49* (1), 44–66.

https://doi.org/10.1080/10408347.2018.1461552.

Franceschelli, L.; Berardinelli, A.; Dabbou, S.; Ragni, L.; Tartagni, M. Sensing Technology for Fish Freshness and Safety: A Review. *Sensors* **2021**, *21* (4), 1373. https://doi.org/10.3390/s21041373.

Yadav, S. K.; Singh, J.; Agrawal, V. V.; Malhotra, B. D. Nanostructured Nickel Oxide Film for Application to Fish Freshness Biosensor. *Appl. Phys. Lett.* **2012**, *101* (2), 023703. https://doi.org/10.1063/1.4736578.

Mathew, M.; Sandhyarani, N. A Highly Sensitive Electrochemical Glucose Sensor Structuring with Nickel Hydroxide and Enzyme Glucose Oxidase. *Electrochim. Acta* **2013**, *108*, 274–280. https://doi.org/10.1016/j.electacta.2013.07.010.

Tyagi, M.; Tomar, M.; Gupta, V. Glad Assisted Synthesis of NiO Nanorods for Realization of Enzymatic Reagentless Urea Biosensor. *Biosens. Bioelectron.* **2014**, *52*, 196–201. https://doi.org/10.1016/j.bios.2013.08.020.

Singer, N.; Pillai, R. G.; Johnson, A. I. D.; Harris, K. D.; Jemere, A. B. Nanostructured Nickel Oxide Electrodes for Non-Enzymatic Electrochemical Glucose Sensing. *Microchim. Acta* **2020**, *187* (4), 196. https://doi.org/10.1007/s00604-020-4171-5.

Salazar, P.; Rico, V.; González-Elipe, A. R. Non-Enzymatic Hydrogen Peroxide Detection at NiO Nanoporous Thin Film- Electrodes Prepared by Physical Vapor Deposition at Oblique Angles. *Electrochim. Acta* **2017**, *235*, 534–542. https://doi.org/10.1016/j.electacta.2017.03.087.

Tyagi, M.; Tomar, M.; Gupta, V. NiO Nanoparticle-Based Urea Biosensor. *Biosens. Bioelectron.* **2013**, *41*, 110–115. https://doi.org/10.1016/j.bios.2012.07.062.

Lin, D.; Harris, K. D.; Chan, N. W. C.; Jemere, A. B. Nanostructured Indium Tin Oxide Electrodes Immobilized with Toll-like Receptor Proteins for Label-Free Electrochemical Detection of Pathogen Markers. *Sensors Actuators B Chem.* **2018**, *257*, 324–330. https://doi.org/10.1016/j.snb.2017.10.140.

Fu, K.; Seo, J.; Kesler, V.; Maganzini, N.; Wilson, B. D.; Eisenstein, M.; Murmann, B.; Soh, H. T. Accelerated Electron Transfer in Nanostructured Electrodes Improves the Sensitivity of Electrochemical Biosensors. *Adv. Sci.* **2021**, *8* (23), 2102495. https://doi.org/10.1002/advs.202102495.

Arora, K.; Tomar, M.; Gupta, V. Highly Sensitive and Selective Uric Acid Biosensor Based on RF Sputtered NiO Thin Film. *Biosens. Bioelectron.* **2011**. https://doi.org/10.1016/j.bios.2011.09.026.

Bezuidenhout, L. W.; Nazemifard, N.; Jemere, A. B.; Harrison, D. J.; Brett, M. J. Microchannels Filled with Diverse Micro- and Nanostructures Fabricated by Glancing

Angle Deposition. *Lab Chip* **2011**, *11* (9), 1671. https://doi.org/10.1039/c0lc00721h.

Nakatani, H. S.; Santos, L. V. dos; Pelegrine, C. P.; Gomes, S. T. M.; Matsushita, M.; Souza, N. E. de; Visentaine, J. V. Biosensor Based on Xanthine Oxidase for Monitoring Hypoxanthine in Fish Meat. *Am. J. Biochem. Biotechnol.* **2005**, *1* (2), 85–89. https://doi.org/10.3844/ajbbsp.2005.85.89.

Dervisevic, M.; Custiuc, E.; Çevik, E.; Durmus, Z.; Şenel, M.; Durmus, A. Electrochemical Biosensor Based on REGO/Fe3O4 Bionanocomposite Interface for Xanthine Detection in Fish Sample. *Food Control* **2015**, *57*, 402–410. https://doi.org/10.1016/j.foodcont.2015.05.001.

Eckermann, A. L.; Feld, D. J.; Shaw, J. A.; Meade, T. J. Electrochemistry of Redox-Active Self-Assembled Monolayers. *Coord. Chem. Rev.* **2010**, *254* (15–16), 1769–1802. https://doi.org/10.1016/j.ccr.2009.12.023.

Tripathi, A.; Harris, K. D.; Elias, A. L. High Surface Area Nitrogen-Functionalized Ni Nanozymes for Efficient Peroxidase-like Catalytic Activity. *PLoS One* **2021**, *16* (10), e0257777. https://doi.org/10.1371/journal.pone.0257777.

Grosvenor, A. P.; Biesinger, M. C.; Smart, R. S. C.; McIntyre, N. S. New Interpretations of XPS Spectra of Nickel Metal and Oxides. *Surf. Sci.* **2006**, *600* (9), 1771–1779. https://doi.org/10.1016/j.susc.2006.01.041.

Tripathi, A.; Harris, K. D.; Elias, A. L. Peroxidase-Like Behavior of Ni Thin Films Deposited by Glancing Angle Deposition for Enzyme-Free Uric Acid Sensing. *ACS Omega* **2020**, *5* (16), 9123–9130. https://doi.org/10.1021/acsomega.9b04071.

Mao, F.; Liu, P. F.; Yang, P.; Gu, J.; Yang, H. G. One-Step Coating of Commercial Ni Nanoparticles with a Ni, N-Co-Doped Carbon Shell towards Efficient Electrocatalysts for CO 2 Reduction. *Chem. Commun.* **2020**, *56* (54), 7495–7498. https://doi.org/10.1039/D0CC02188A.

Zheng, X.; Zhang, Y.; Liu, H.; Fu, D.; Chen, J.; Wang, J.; Zhong, C.; Deng, Y.; Han, X.; Hu, W. In Situ Fabrication of Heterostructure on Nickel Foam with Tuned Composition for Enhancing Water-Splitting Performance. *Small* **2018**, *14* (50), 1803666. https://doi.org/10.1002/smll.201803666.

Ramanathan, T.; Fisher, F. T.; Ruoff, R. S.; Brinson, L. C. Amino-Functionalized Carbon Nanotubes for Binding to Polymers and Biological Systems. *Chem. Mater.* **2005**, *17* (6), 1290–1295. https://doi.org/10.1021/cm048357f.

Radhakrishnan, K.; Panneerselvam, P.; Marieeswaran, M. A Green Synthetic Route for the Surface-Passivation of Carbon Dots as an Effective Multifunctional Fluorescent Sensor for the Recognition and Detection of Toxic Metal Ions from Aqueous Solution. *Anal. Methods* **2019**, *11* (4), 490–506. https://doi.org/10.1039/C8AY02451K.

Li, R.; Wei, Z.; Gou, X.; Xu, W. Phosphorus-Doped Graphene Nanosheets as Efficient Metal-Free Oxygen Reduction Electrocatalysts. *RSC Adv.* **2013**, *3* (25), 9978. https://doi.org/10.1039/c3ra41079j.

Davis, M. D.; Edmondson, D. E.; Muller, F. 31P Nuclear Magnetic Resonance and Chemical Studies of the Phosphorus Residues in Bovine Milk Xanthine Oxidase. *Eur. J. Biochem.* **1984**, *145* (2), 237–243. https://doi.org/10.1111/j.1432-1033.1984.tb08544.x.

Johnson, J. L.; London, R. E.; Rajagopalan, K. V. Covalently Bound Phosphate Residues in Bovine Milk Xanthine Oxidase and in Glucose Oxidase from Aspergillus Niger: A Reevaluation. *Proc. Natl. Acad. Sci. U. S. A.* **1989**, *86* (17), 6493–6497. https://doi.org/10.1073/pnas.86.17.6493.

Ribeiro, P. M. G.; Fernandes, H. S.; Maia, L. B.; Sousa, S. F.; Moura, J. J. G.; Cerqueira, N. M. F. S. A. The Complete Catalytic Mechanism of Xanthine Oxidase: A Computational Study. *Inorg. Chem. Front.* **2021**, *8* (2), 405–416. https://doi.org/10.1039/D0QI01029D.

Berry, C. E.; Hare, J. M. Xanthine Oxidoreductase and Cardiovascular Disease: Molecular Mechanisms and Pathophysiological Implications. *J. Physiol.* **2004**, *555* (3), 589–606. https://doi.org/10.1113/jphysiol.2003.055913.

Arslan, F.; Yaşar, A.; Kılıç, E. An Amperometric Biosensor for Xanthine Determination Prepared from Xanthine Oxidase Immobilized in Polypyrrole Film. *Artif. Cells, Blood Substitutes, Biotechnol.* **2006**, *34* (1), 113–128. https://doi.org/10.1080/10731190500430289.

Dervisevic, M.; Dervisevic, E.; Çevik, E.; Şenel, M. Novel Electrochemical Xanthine Biosensor Based on Chitosan–Polypyrrole–Gold Nanoparticles Hybrid Bio-Nanocomposite Platform. *J. Food Drug Anal.* **2017**, *25* (3), 510–519. https://doi.org/10.1016/j.jfda.2016.12.005.

Narang, J.; Malhotra, N.; Singhal, C.; Pundir, C. S. Evaluation of Freshness of Fishes Using MWCNT/TiO2 Nanobiocomposites Based Biosensor. *Food Anal. Methods* **2017**, *10* (2), 522–528. https://doi.org/10.1007/s12161-016-0594-3.

Dervisevic, M.; Custiuc, E.; Çevik, E.; Şenel, M. Construction of Novel Xanthine Biosensor by Using Polymeric Mediator/MWCNT Nanocomposite Layer for Fish Freshness Detection. *Food Chem.* **2015**, *181*, 277–283. https://doi.org/10.1016/j.foodchem.2015.02.104.

Saadaoui, M.; Sánchez, A.; Díez, P.; Raouafi, N.; Pingarrón, J. M.; Villalonga, R. Amperometric Xanthine Biosensors Using Glassy Carbon Electrodes Modified with Electrografted Porous Silica Nanomaterials Loaded with Xanthine Oxidase. *Microchim. Acta* **2016**, *183* (6), 2023–2030. https://doi.org/10.1007/s00604-016-1840-5.

Renault, C.; Andrieux, C. P.; Tucker, R. T.; Brett, M. J.; Balland, V.; Limoges, B. Unraveling the Mechanism of Catalytic Reduction of O 2 by Microperoxidase-11 Adsorbed within a Transparent 3D-Nanoporous ITO Film. *J. Am. Chem. Soc.* **2012**, *134* (15), 6834–6845. https://doi.org/10.1021/ja301193s.

Borisova, B.; Sánchez, A.; Jiménez-Falcao, S.; Martín, M.; Salazar, P.; Parrado, C.; Pingarrón, J. M.; Villalonga, R. Reduced Graphene Oxide-Carboxymethylcellulose Layered with Platinum Nanoparticles/PAMAM Dendrimer/Magnetic Nanoparticles Hybrids. Application to the Preparation of Enzyme Electrochemical Biosensors. *Sensors Actuators B Chem.* **2016**, *232*, 84–90. https://doi.org/10.1016/j.snb.2016.02.106.

Zhang, L.; Lei, J.; Zhang, J.; Ding, L.; Ju, H. Amperometric Detection of Hypoxanthine and Xanthine by Enzymatic Amplification Using a Gold Nanoparticles–Carbon Nanohorn Hybrid as the Carrier. *Analyst* **2012**, *137* (13), 3126. https://doi.org/10.1039/c2an35284b.

Sen, S.; Sarkar, P. A Novel Third-Generation Xanthine Biosensor with Enzyme Modified Glassy Carbon Electrode Using Electrodeposited MWCNT and Nanogold Polymer Composite Film. *RSC Adv.* **2015**, *5* (116), 95911–95925. https://doi.org/10.1039/C5RA18889J.

Torres, A. C.; Ghica, M. E.; Brett, C. M. A. Design of a New Hypoxanthine Biosensor: Xanthine Oxidase Modified Carbon Film and Multi-Walled Carbon Nanotube/Carbon Film Electrodes. *Anal. Bioanal. Chem.* **2013**, *405* (11), 3813–3822. https://doi.org/10.1007/s00216-012-6631-1.

Horozova, E. G.; Dimcheva, N. D.; Jordanova, Z. J. Study of Xanthine Oxidase Immobilized Electrode Based on Modified Graphite. *Zeitschrift für Naturforsch. C* **2000**, *55* (1–2), 60–65. https://doi.org/10.1515/znc-2000-1-212.

Dalkıran, B.; Erden, P. E.; Kılıç, E. Construction of an Electrochemical Xanthine Biosensor Based on Graphene/Cobalt Oxide Nanopartiles/Chitosan Composite for Fish Freshness Detection. *J. Turkish Chem. Soc. Sect. A Chem.* **2017**, *4* (1), 23–44. https://doi.org/10.18596/jotcsa.54485.

Pei, J.; Li, X. Xanthine and Hypoxanthine Sensors Based on Xanthine Oxidase Immobilized on a CuPtCl6 Chemically Modified Electrode and Liquid Chromatography Electrochemical Detection. *Anal. Chim. Acta* **2000**, *414* (1–2), 205–213. https://doi.org/10.1016/S0003-2670(00)00775-3.

Baş, S. Z.; Gülce, H.; Yıldız, S. Amperometric Xanthine Biosensors Based on Electrodeposition of Platinum on Polyvinylferrocenium Coated Pt Electrode. *J. Mol. Catal. B Enzym.* **2011**, *72* (3–4), 282–288. https://doi.org/10.1016/j.molcatb.2011.06.017.

Wang, Z.; Ma, B.; Shen, C.; Lai, O.-M.; Tan, C.-P.; Cheong, L.-Z. Electrochemical Biosensing of Chilled Seafood Freshness by Xanthine Oxidase Immobilized on Copper-Based Metal–Organic Framework Nanofiber Film. *Food Anal. Methods* **2019**, *12* (8), 1715–

1724. https://doi.org/10.1007/s12161-019-01513-8.

Khan, M. Z. H.; Ahommed, M. S.; Daizy, M. Detection of Xanthine in Food Samples with an Electrochemical Biosensor Based on PEDOT:PSS and Functionalized Gold Nanoparticles. *RSC Adv.* **2020**, *10* (59), 36147–36154. https://doi.org/10.1039/D0RA06806C.

Garg, D.; Verma, N. Fibre-Optic Biosensor for the Detection of Xanthine for the Evaluation of Meat Freshness. *J. Phys. Conf. Ser.* **2020**, *1531* (1), 012098. https://doi.org/10.1088/1742-6596/1531/1/012098.

Thandavan, K.; Gandhi, S.; Sethuraman, S.; Rayappan, J. B. B.; Krishnan, U. M. Development of Electrochemical Biosensor with Nano-Interface for Xanthine Sensing – A Novel Approach for Fish Freshness Estimation. *Food Chem.* **2013**, *139* (1–4), 963–969. https://doi.org/10.1016/j.foodchem.2013.02.008.

Sahyar, B. Y.; Kaplan, M.; Ozsoz, M.; Celik, E.; Otles, S. Electrochemical Xanthine Detection by Enzymatic Method Based on Ag Doped ZnO Nanoparticles by Using Polypyrrole. *Bioelectrochemistry* **2019**, *130*, 107327. https://doi.org/10.1016/j.bioelechem.2019.107327.

Joon, A.; Ahlawat, J.; Aggarwal, V.; Jaiwal, R.; Pundir, C. S. An Improved Amperometric Determination of Xanthine with Xanthine Oxidase Nanoparticles for Testing of Fish Meat Freshness. *Sens. Bio-Sensing Res.* **2021**, *33*, 100437. https://doi.org/10.1016/j.sbsr.2021.100437.

Devi, R.; Yadav, S.; Pundir, C. S. Amperometric Determination of Xanthine in Fish Meat by Zinc Oxide Nanoparticle/Chitosan/Multiwalled Carbon Nanotube/Polyaniline Composite Film Bound Xanthine Oxidase. *Analyst* **2012**, *137* (3), 754–759. https://doi.org/10.1039/C1AN15838D.

Klinenberg JR. Current Concepts of Hyperuricemia and Gout. Calif Med. 1969;110(3):231–44.

Kaneko K, Aoyagi Y, Fukuuchi T, Inazawa K, Yamaoka N. Total Purine and Purine Base Content of Common Foodstuffs for Facilitating Nutritional Therapy for Gout and Hyperuricemia. Biol Pharm Bull [Internet]. 2014;37(5):709–21. Available from: https://www.jstage.jst.go.jp/article/bpb/37/5/37_b13-00967/_article

Kumar A, Hens A, Arun RK, Chatterjee M, Mahato K, Layek K, et al. A paper based microfluidic device for easy detection of uric acid using positively charged gold nanoparticles. Analyst [Internet]. 2015;140(6):1817–21. Available from: http://xlink.rsc.org/?DOI=C4AN02333A

Benn CL, Dua P, Gurrell R, Loudon P, Pike A, Storer RI, et al. Physiology of Hyperuricemia and Urate-Lowering Treatments. Front Med [Internet]. 2018 May 31;5:1–28. Available from: https://www.frontiersin.org/article/10.3389/fmed.2018.00160/full

Kumar S, Bhushan P, Bhattacharya S. Development of a paper-based analytical device for colorimetric detection of uric acid using gold nanoparticles–graphene oxide (AuNPs–GO) conjugates. Anal Methods [Internet]. 2016;8(38):6965–73. Available from: http://xlink.rsc.org/?DOI=C6AY01926A

El Ridi R, Tallima H. Physiological functions and pathogenic potential of uric acid: A review. J Adv Res [Internet]. 2017 Sep;8(5):487–93. Available from: https://linkinghub.elsevier.com/retrieve/pii/S2090123217300346

Desideri G, Castaldo G, Lombardi A, Mussap M, Testa A, Pontremoli R, et al. Is it time to revise the normal range of serum uric acid levels? Eur Rev Med Pharmacol Sci. 2014;18(9):1295–306.

Huang CT, Chen ML, Huang LL, Mao IF. Uric acid and urea in human sweat. Chin J Physiol. 2002;45(3):109–15.

Dong X. Study on Detection Methods for Uric Acid in Biological Samples. Int J Pharm Sci Res. 2017;8(2):925–9.

Dai X, Fang X, Zhang C, Xu R, Xu B. Determination of serum uric acid using high-performance liquid chromatography (HPLC)/isotope dilution mass spectrometry (ID-MS) as a candidate reference method. J Chromatogr B [Internet]. 2007 Oct;857(2):287–95. Available from: https://linkinghub.elsevier.com/retrieve/pii/S1570023207005454

Wang X, Tang CL, Liu JJ, Zhang H-Z, Wang J. Ultra-small CuS Nanoparticles as Peroxidase Mimetics for Sensitive and Colorimetric Detection of Uric Acid in Human Serum. Chinese J Anal Chem [Internet]. 2018;46(5):e1825–31. Available from: http://dx.doi.org/10.1016/S1872-2040(17)61083-1

Lakshmi D, Whitcombe MJ, Davis F, Sharma PS, Prasad BB. Electrochemical Detection of Uric Acid in Mixed and Clinical Samples: A Review. Electroanalysis [Internet]. 2011 Feb;23(2):305–20. Available from: https://onlinelibrary.wiley.com/doi/10.1002/elan.201000525

Zhou W, Gao X, Liu D, Chen X. Gold Nanoparticles for In Vitro Diagnostics. Chem Rev [Internet]. 2015 Oct 14;115(19):10575–636. Available from: https://pubs.acs.org/doi/10.1021/acs.chemrev.5b00100

Josephy PD, Eling T, Mason RP. The horseradish peroxidase-catalyzed oxidation of 3,5,3',5'-tetramethylbenzidine. Free radical and charge-transfer complex intermediates. J Biol Chem. 1982;257(7):3669–75.

Njagi JI, Kagwanja SM. Interfaces and Interphases in Analytical Chemistry [Internet]. Helburn R, Vitha MF, editors. Interfaces and Interphases in Analytical Chemistry. Washington, DC: American Chemical Society; 2011. 225–247 p. (ACS Symposium Series; vol. 1062). Available from: https://pubs.acs.org/doi/book/10.1021/bk-2011-1062

Caves MS, Derham BK, Jezek J, Freedman RB. Thermal Inactivation of Uricase (Urate Oxidase): Mechanism and Effects of Additives. Biochemistry [Internet]. 2013 Jan

22;52(3):497–507. Available from: https://pubs.acs.org/doi/10.1021/bi301334w

Çete S, Yaşar A, Arslan F. An Amperometric Biosensor for Uric Acid Determination Prepared from Uricase Immobilized in Polypyrrole Film. Artif Cells, Blood Substitutes, Biotechnol [Internet]. 2006 Jan 11;34(3):367–80. Available from: http://www.tandfonline.com/doi/full/10.1080/10731190600684116

Zhuang QQ, Lin ZH, Jiang YC, Deng HH, He S Bin, Su LT, et al. Peroxidase-like activity of nanocrystalline cobalt selenide and its application for uric acid detection. Int J Nanomedicine. 2017;12:3295–302.

Wu J, Li S, Wei H. Integrated nanozymes: facile preparation and biomedical applications. Chem Commun [Internet]. 2018;54(50):6520–30. Available from: http://xlink.rsc.org/?DOI=C8CC01202D

Lu J, Xiong Y, Liao C, Ye F. Colorimetric detection of uric acid in human urine and serum based on peroxidase mimetic activity of MIL-53(Fe). Anal Methods [Internet]. 2015;7(23):9894–9. Available from: http://xlink.rsc.org/?DOI=C5AY02240A

Liu X, Qi W, Wang Y, Su R, He Z. A facile strategy for enzyme immobilization with highly stable hierarchically porous metal–organic frameworks. Nanoscale [Internet]. 2017;9(44):17561–70. Available from: http://xlink.rsc.org/?DOI=C7NR06019J

Lu H-F, Li J-Y, Zhang M-M, Wu D, Zhang Q-L. A highly selective and sensitive colorimetric uric acid biosensor based on Cu(II)-catalyzed oxidation of 3,3′,5,5′-tetramethylbenzidine. Sensors Actuators B Chem [Internet]. 2017 Jun;244:77–83. Available from: http://dx.doi.org/10.1016/j.snb.2016.12.127

Wang X, Cao W, Qin L, Lin T, Chen W, Lin S, et al. Boosting the Peroxidase-Like Activity of Nanostructured Nickel by Inducing Its 3+ Oxidation State in LaNiO3 Perovskite and Its Application for Biomedical Assays. Theranostics [Internet]. 2017;7(8):2277–86. Available from: http://www.thno.org/v07p2277.htm

Tripathi A. Parametric Studies of In-house Resin for Hardness Removal. Emerg Trends Chem Eng. 2014;1(3):34–9.

He Y, Qi F, Niu X, Zhang W, Zhang X, Pan J. Uricase-free on-demand colorimetric biosensing of uric acid enabled by integrated CoP nanosheet arrays as a monolithic peroxidase mimic. Anal Chim Acta [Internet]. 2018;1021:113–20. Available from: https://doi.org/10.1016/j.aca.2018.02.073

Eskandarloo H, Zaferani M, Kierulf A, Abbaspourrad A. Shape-controlled fabrication of TiO2 hollow shells toward photocatalytic application. Appl Catal B Environ [Internet]. 2018 Jul;227:519–29. Available from: https://doi.org/10.1016/j.apcatb.2018.01.059

Barranco A, Borras A, Gonzalez-Elipe AR, Palmero A. Perspectives on oblique angle deposition of thin films: From fundamentals to devices. Prog Mater Sci [Internet]. 2016 Mar;76:59–153. Available from: https://linkinghub.elsevier.com/retrieve/pii/S0079642515000705

Hawkeye MM, Brett MJ. Glancing angle deposition: Fabrication, properties, and applications of micro- and nanostructured thin films. J Vac Sci Technol A Vacuum, Surfaces, Film [Internet]. 2007;25(5):1317. Available from: http://scitation.aip.org/content/avs/journal/jvsta/25/5/10.1116/1.2764082

Taschuk MT, Hawkeye MM, Brett MJ. Glancing Angle Deposition [Internet]. Third Edit. Handbook of Deposition Technologies for Films and Coatings. Elsevier Ltd.; 2010. 621–678 p. Available from: http://dx.doi.org/10.1016/B978-0-8155-2031-3.00013-2

Malac M, Egerton RF. Observations of the microscopic growth mechanism of pillars and helices formed by glancing-angle thin-film deposition. J Vac Sci Technol A Vacuum, Surfaces, Film [Internet]. 2001 Jan;19(1):158–66. Available from: http://avs.scitation.org/doi/10.1116/1.1326940

Tyagi M, Tomar M, Gupta V. Glad assisted synthesis of NiO nanorods for realization of enzymatic reagentless urea biosensor. Biosens Bioelectron [Internet]. 2014 Feb;52:196–201. Available from: https://linkinghub.elsevier.com/retrieve/pii/S0956566313005617

Krause KM, Taschuk MT, Harris KD, Rider DA, Wakefield NG, Sit JC, et al. Surface Area Characterization of Obliquely Deposited Metal Oxide Nanostructured Thin Films. Langmuir [Internet]. 2010 Mar 16;26(6):4368–76. Available from: https://pubs.acs.org/doi/10.1021/la903444e

Harris KD, Vick D, Smy T, Brett MJ. Column angle variations in porous chevron thin films. J Vac Sci Technol A Vacuum, Surfaces, Film. 2002;20(6):2062.

Valdés-Martínez OU, Santolalla-Vargas CE, Santes V, de los Reyes JA, Pawelec B, Fierro JLG. Influence of calcination on metallic dispersion and support interactions for NiRu/TiO2 catalyst in the hydrodeoxygenation of phenol. Catal Today [Internet]. 2019;329:149–55. Available from: https://doi.org/10.1016/j.cattod.2018.11.007

Li H, Ren C, Zhang R, Li R, Xu S, Wang L, et al. One–step Synthesis of MnO/Ni Nanoparticles Anchored on Porous Nitrogen–doped Carbons from Melamine Foam and Electrocatalytic Study towards Oxygen Reduction Reaction. ChemistrySelect. 2017;2(15):4234–40.

Chao Y, Zheng J, Zhang H, Ma Y, Li F, Tan Y, et al. Constructing Film Photocatalyst with Abundant Interfaces between CdS and Ni3S2 Nanosheets for Efficient Photocatalytic Hydrogen Production. Energy Technol [Internet]. 2018 Nov;6(11):2132–8. Available from: http://doi.wiley.com/10.1002/ente.201800180

Morais A, Alves JPC, Lima FAS, Lira-Cantu M, Nogueira AF. Enhanced photovoltaic performance of inverted hybrid bulk-heterojunction solar cells using TiO2 /Reduced graphene oxide films as electron transport layers. J Photonics Energy [Internet]. 2015 Mar 12;5(1):057408. Available from: http://photonicsforenergy.spiedigitallibrary.org/article.aspx?doi=10.1117/1.JPE.5.057408

Chen L, Li X, Zhang J, Fang J, Huang Y, Wang P, et al. Production of Hydroxyl Radical via the Activation of Hydrogen Peroxide by Hydroxylamine. Environ Sci Technol.

2015;49(17):10373–9.

Lou D, Tian Y, Zhang Y, Yin J, Yang T, He C, et al. Peroxidase-Like Activity of Gold Nanoparticles and Their Gold Staining Enhanced ELISA Application. J Nanosci Nanotechnol. 2017;18(2):951–8.

Hengne AM, Samal AK, Enakonda LR, Harb M, Gevers LE, Anjum DH, et al. Ni–Sn-Supported ZrO 2 Catalysts Modified by Indium for Selective CO 2 Hydrogenation to Methanol. ACS Omega [Internet]. 2018 Apr 30;3(4):3688–701. Available from: https://pubs.acs.org/doi/10.1021/acsomega.8b00211

Sit JC, Broer DJ, Brett MJ. Optical devices fabricated from porous thin films embedded with liquid crystals. In: International Electron Devices Meeting 1999 Technical Digest (Cat No99CH36318) [Internet]. IEEE; 1999. p. 123–6. Available from: http://ieeexplore.ieee.org/document/823861/

Lin D, Harris KD, Chan NWC, Jemere AB. Nanostructured indium tin oxide electrodes immobilized with toll-like receptor proteins for label-free electrochemical detection of pathogen markers. Sensors Actuators B Chem [Internet]. 2018 Mar;257:324–30. Available from: https://linkinghub.elsevier.com/retrieve/pii/S0925400517320543

Dulac M, Melet A, Harris KD, Limoges B, Galardon E, Balland V. An optical H2S biosensor based on the chemoselective Hb-I protein tethered to a transparent, high surface area nanocolumnar electrode. Sensors Actuators B Chem [Internet]. 2019 Jul;290:326–35. Available from: https://linkinghub.elsevier.com/retrieve/pii/S0925400519304903

Zhang L, Fan C, Liu M, Liu F, Bian S, Du S, et al. Biominerized gold-Hemin@MOF composites with peroxidase-like and gold catalysis activities: A high-throughput colorimetric immunoassay for alpha-fetoprotein in blood by ELISA and gold-catalytic silver staining. Sensors Actuators B Chem [Internet]. 2018 Aug;266:543–52. Available from: https://linkinghub.elsevier.com/retrieve/pii/S0925400518306518

Frey A, Meckelein B, Externest D, Schmidt MA. A stable and highly sensitive 3,3′,5,5′-tetramethylbenzidine-based substrate reagent for enzyme-linked immunosorbent assays. J Immunol Methods [Internet]. 2000 Jan;233(1–2):47–56. Available from: https://linkinghub.elsevier.com/retrieve/pii/S0022175999001660

Lee H, Song C, Hong YS, Kim MS, Cho HR, Kang T, et al. Wearable/Disposable sweat-based glucose monitoring device with multistage transdermal drug delivery module. Sci Adv [Internet]. 2017 Mar 8;3(3):e1601314. Available from: http://advances.sciencemag.org/lookup/doi/10.1126/sciadv.1601314

Liang M, Yan X. Nanozymes: From New Concepts, Mechanisms, and Standards to Applications. Acc Chem Res [Internet]. 2019 Aug 20;52(8):2190–200. Available from: https://pubs.acs.org/doi/10.1021/acs.accounts.9b00140

Lee P-C, Li N-S, Hsu Y-P, Peng C, Yang H-W. Direct glucose detection in whole blood by colorimetric assay based on glucose oxidase-conjugated graphene oxide/MnO 2 nanozymes. Analyst [Internet]. 2019;144(9):3038–44. Available from:

http://xlink.rsc.org/?DOI=C8AN02440E

Ray C, Dutta S, Sarkar S, Sahoo R, Roy A, Pal T. Intrinsic peroxidase-like activity of mesoporous nickel oxide for selective cysteine sensing. J Mater Chem B [Internet]. 2014 Jul 18;2(36):6097. Available from: http://xlink.rsc.org/?DOI=C4TB00968A

Zhong M, Chi M, Ma F, Zhu Y, Wang C, Lu X. Dual Responsive Enzyme Mimicking of Ternary Polyaniline–MnO 2 –Pd Nanowires and Its Application in Colorimetric Biosensing. ACS Sustain Chem Eng [Internet]. 2018 Dec 3;6(12):16482–92. Available from: https://pubs.acs.org/doi/10.1021/acssuschemeng.8b03567

Satterfield CN. Chemical reaction engineering, Octave Levenspiel, Wiley, New York(1972). AIChE J [Internet]. third. 1973 Jan;19(1):21–2. Available from: http://scholar.google.com/scholar?hl=en&btnG=Search&q=intitle:chemical+reaction+engineering#0

Liu Y, Zhu G, Yang J, Yuan A, Shen X. Peroxidase-like catalytic activity of Ag3PO4 nanocrystals prepared by a colloidal route. PLoS One. 2014;9(10):3–9.

Torng W, Altman RB. High precision protein functional site detection using 3D convolutional neural networks. Valencia A, editor. Bioinformatics. 2019 May 1;35(9):1503–12. Available from: https://academic.oup.com/bioinformatics/article/35/9/1503/5104336

Daniel RM, Dines M, Petach HH. The denaturation and degradation of stable enzymes at high temperatures. Biochem J. 1996 Jul 1;317(1):1–11. Available from: https://portlandpress.com/biochemj/article/317/1/1/31738/The-denaturation-and-degradation-of-stable-enzymes

Wu, J.; Wang X.; Wang Q.; Lou Z.; Li S.; Zhu Y.; Qin L.; Wei H. Nanomaterials with enzyme-like characteristics (nanozymes): next-generation artificial enzymes (II). Chem Soc Rev. 2019;48(4):1004–76.

Jiang B, Duan D, Gao L, Zhou M, Fan K, Tang Y, et al. Standardized assays for determining the catalytic activity and kinetics of peroxidase-like nanozymes. Nat Protoc. 2018 Jul 2;13(7):1506–20. Available from: http://www.nature.com/articles/s41596-018-0001-1

Wang X, Tang CL, Liu JJ, Zhang HZ, Wang J. Ultra-small CuS Nanoparticles as Peroxidase Mimetics for Sensitive and Colorimetric Detection of Uric Acid in Human Serum. Chinese J Anal Chem. 2018 May;46(5):e1825–31. Available from: https://linkinghub.elsevier.com/retrieve/pii/S1872204017610831

Golchin J, Golchin K, Alidadian N, Ghaderi S, Eslamkhah S, Eslamkhah M, et al. Nanozyme applications in biology and medicine: an overview. Artif Cells, Nanomedicine, Biotechnol. 2017 Aug 18;45(6):1069–76. Available from: https://www.tandfonline.com/doi/full/10.1080/21691401.2017.1313268

Khan AA, Rahmani AH, Aldebasi YH, Aly SM. Biochemical and Pathological Studies on

Peroxidases –An Updated Review. Glob J Health Sci. 2014 May 13;6(5). Available from: http://ccsenet.org/journal/index.php/gjhs/article/view/35689

Everse J, Coates PW. Role of peroxidases in Parkinson disease: a hypothesis. Free Radic Biol Med. 2005 May;38(10):1296–310. Available from: https://linkinghub.elsevier.com/retrieve/pii/S0891584905000365

Gao L, Zhuang J, Nie L, Zhang J, Zhang Y, Gu N, et al. Intrinsic peroxidase-like activity of ferromagnetic nanoparticles. Nat Nanotechnol. 2007 Sep 26;2(9):577–83. Available from: http://www.nature.com/articles/nnano.2007.260

Song Y, Qu K, Zhao C, Ren J, Qu X. Graphene Oxide: Intrinsic Peroxidase Catalytic Activity and Its Application to Glucose Detection. Adv Mater. 2010 Mar 5;22(19):2206–10. Available from: http://doi.wiley.com/10.1002/adma.200903783

Huang JY, Lin HT, Chen TH, Chen CA, Chang HT, Chen CF. Signal Amplified Gold Nanoparticles for Cancer Diagnosis on Paper-Based Analytical Devices. ACS Sensors. 2018 Jan 26;3(1):174–82. Available from: https://pubs.acs.org/doi/10.1021/acssensors.7b00823

Liu F, He J, Zeng M, Hao J, Guo Q, Song Y, et al. Cu–hemin metal-organic frameworks with peroxidase-like activity as peroxidase mimics for colorimetric sensing of glucose. J Nanoparticle Res. 2016 May 15;18(5):106. Available from: http://link.springer.com/10.1007/s11051-016-3416-z

Tripathi A, Harris KD, Elias AL. Peroxidase-Like Behavior of Ni Thin Films Deposited by Glancing Angle Deposition for Enzyme-Free Uric Acid Sensing. ACS Omega. 2020 Apr 28;5(16):9123–30. Available from: https://pubs.acs.org/doi/10.1021/acsomega.9b04071

Feng L, Zhang L, Zhang S, Chen X, Li P, Gao Y, et al. Plasma-Assisted Controllable Doping of Nitrogen into MoS_2 Nanosheets as Efficient Nanozymes with Enhanced Peroxidase-Like Catalysis Activity. ACS Appl Mater Interfaces. 2020 Apr 15;12(15):17547–56. Available from: https://pubs.acs.org/doi/10.1021/acsami.0c01789

Tang Y, Allen BL, Kauffman DR, Star A. Electrocatalytic Activity of Nitrogen-Doped Carbon Nanotube Cups. J Am Chem Soc. 2009 Sep 23;131(37):13200–1. Available from: https://pubs.acs.org/doi/10.1021/ja904595t

Zhou W, Hou D, Sang Y, Yao S, Zhou J, Li G, et al. MoO_2 nanobelts@nitrogen self-doped MoS_2 nanosheets as effective electrocatalysts for hydrogen evolution reaction. J Mater Chem A. 2014;2(29):11358–64. Available from: http://xlink.rsc.org/?DOI=c4ta01898b

Huang L, Chen J, Gan L, Wang J, Dong S. Single-atom nanozymes. Sci Adv. 2019;5(5).

Bae G, Kim H, Choi H, Jeong P, Kim DH, Kwon HC, et al. Quantification of Active Site Density and Turnover Frequency: From Single-Atom Metal to Nanoparticle Electrocatalysts. JACS Au. 2021 May 24;1(5):586–97. Available from: https://pubs.acs.org/doi/10.1021/jacsau.1c00074

Grüner C, Reeck P, Jacobs P-P, Liedtke S, Lotnyk A, Rauschenbach B. Gold coated metal nanostructures grown by glancing angle deposition and pulsed electroplating. Phys Lett A. 2018 May;382(19):1287–90. Available from: https://linkinghub.elsevier.com/retrieve/pii/S0375960118302536

Hawkeye MM, Brett MJ. Glancing angle deposition: Fabrication, properties, and applications of micro- and nanostructured thin films. J Vac Sci Technol A Vacuum, Surfaces, Film. 2007;25(5):1317. Available from: http://scitation.aip.org/content/avs/journal/jvsta/25/5/10.1116/1.2764082

Singer N, Pillai RG, Johnson AID, Harris KD, Jemere AB. Nanostructured nickel oxide electrodes for non-enzymatic electrochemical glucose sensing. Microchim Acta. 2020 Apr 3;187(4):196. Available from: http://link.springer.com/10.1007/s00604-020-4171-5

Barranco A, Borras A, Gonzalez-Elipe AR, Palmero A. Perspectives on oblique angle deposition of thin films: From fundamentals to devices. Prog Mater Sci. 2016 Mar;76:59–153. Available from: https://linkinghub.elsevier.com/retrieve/pii/S0079642515000705

Lin D, Harris KD, Chan NWC, Jemere AB. Nanostructured indium tin oxide electrodes immobilized with toll-like receptor proteins for label-free electrochemical detection of pathogen markers. Sensors Actuators B Chem. 2018 Mar;257:324–30. Available from: https://linkinghub.elsevier.com/retrieve/pii/S0925400517320543

Dulac M, Melet A, Harris KD, Limoges B, Galardon E, Balland V. An optical H_2S biosensor based on the chemoselective Hb-I protein tethered to a transparent, high surface area nanocolumnar electrode. Sensors Actuators B Chem. 2019 Jul;290:326–35. Available from: https://linkinghub.elsevier.com/retrieve/pii/S0925400519304903

Vohrer U. Interfacial engineering of functional textiles for biomedical applications. In: R. Shishoo, editor. Plasma Technologies for Textiles. 1st ed. Woodhead Publishing; 2007. p. 202–27. Available from: https://linkinghub.elsevier.com/retrieve/pii/B9781845690731500081

Li G, Wu X, Guo H, Guo Y, Chen H, Wu Y, et al. Plasma Transforming $Ni(OH)_2$ Nanosheets into Porous Nickel Nitride Sheets for Alkaline Hydrogen Evolution. ACS Appl Mater Interfaces [Internet]. 2020 Feb 5;12(5):5951–7. Available from: https://pubs.acs.org/doi/10.1021/acsami.9b20887

Meftah A, Gharibshahi E, Soltani N, Yunus W, Saion E. Structural, Optical and Electrical Properties of PVA/PANI/Nickel Nanocomposites Synthesized by Gamma Radiolytic Method. Polymers (Basel). 2014 Sep 24;6(9):2435–50. Available from: http://www.mdpi.com/2073-4360/6/9/2435

Chandrabhan Shende R, Muruganathan M, Mizuta H, Akabori M, Sundara R. Chemical Simultaneous Synthesis Strategy of Two Nitrogen-Rich Carbon Nanomaterials for All-Solid-State Symmetric Supercapacitor. ACS Omega. 2018 Dec 31;3(12):17276–86. Available from: https://pubs.acs.org/doi/10.1021/acsomega.8b02835

Han M, Liu Q, He J, Song Y, Xu ZCS and MP of C and HPNN, Zhu JM. Controllable Synthesis and Magnetic Properties of Cubic and Hexagonal Phase Nickel Nanocrystals. Adv Mater. 2007 Apr 20;19(8):1096–100. Available from: https://onlinelibrary.wiley.com/doi/10.1002/adma.200601460

Barrientos L, Rodriguez - Llamazares S, Merchani J, Jara P, Yutronic N, Lavayen V. Unveiling the structure of Ni/Ni oxide nanoparticles system. J Chil Chem Soc. 2009 Dec;54(4). Available from: http://www.scielo.cl/scielo.php?script=sci_arttext&pid=S0717-97072009000400014&lng=en&nrm=iso&tlng=en

Nazir S, Bano S, Munir S, Fahad Al-Ajmi M, Afzal M, Mazhar K. "Smart" nickel oxide based core-shell nanoparticles for combined chemo and photodynamic cancer therapy. Int J Nanomedicine. 2016 Jul;Volume 11:3159–66. Available from: https://www.dovepress.com/quotsmartquot-nickel-oxide-based-corendashshell-nanoparticles-for-comb-peer-reviewed-article-IJN

Hengne AM, Samal AK, Enakonda LR, Harb M, Gevers LE, Anjum DH, et al. Ni–Sn-Supported ZrO_2 Catalysts Modified by Indium for Selective CO_2 Hydrogenation to Methanol. ACS Omega. 2018 Apr 30;3(4):3688–701. Available from: https://pubs.acs.org/doi/10.1021/acsomega.8b00211

Karki V, Debnath AK, Kumar S, Bhattacharya D. Synthesis of co-sputter deposited Ni–Ti thin alloy films and their compositional characterization using depth sensitive techniques. Thin Solid Films. 2020 Mar;697:137800. Available from: https://linkinghub.elsevier.com/retrieve/pii/S004060902030016X

Tanaka S, Masud MK, Kaneti YV, Shiddiky MJA, Fatehmulla A, Aldhafiri AM, et al. Enhanced Peroxidase Mimetic Activity of Porous Iron Oxide Nanoflakes. ChemNanoMat. 2019 Apr 4;5(4):506–13. Available from: https://onlinelibrary.wiley.com/doi/abs/10.1002/cnma.201800487

Smirnov A, Hausner D, Laffers R, Strongin DR, Schoonen MA. Abiotic ammonium formation in the presence of Ni-Fe metals and alloys and its implications for the Hadean nitrogen cycle. Geochem Trans. 2008 Dec 19;9(1):5. Available from: https://geochemicaltransactions.biomedcentral.com/articles/10.1186/1467-4866-9-5

Josephy PD, Eling T, Mason RP. The horseradish peroxidase-catalyzed oxidation of 3,5,3',5'-tetramethylbenzidine. Free radical and charge-transfer complex intermediates. J Biol Chem. 1982;257(7):3669–75.

Carrell C, Kava A, Nguyen M, Menger R, Munshi Z, Call Z, et al. Beyond the lateral flow assay: A review of paper-based microfluidics. Microelectron Eng. 2019 Feb;206:45–54. Available from: https://linkinghub.elsevier.com/retrieve/pii/S0167931718305069

Song HJ, Shin HJ, Chung Y, Lee JC, Lee MK. X-ray absorption and photoelectron spectroscopic study of plasma-nitrided SiO_2 film. J Appl Phys. 2005 Jun;97(11):113711. Available from: http://aip.scitation.org/doi/10.1063/1.1927283

Sun J, Li C, Qi Y, Guo S, Liang X. Optimizing Colorimetric Assay Based on V_2O_5 Nanozymes for Sensitive Detection of H_2O_2 and Glucose. Sensors. 2016 Apr 22;16(4):584. Available from: http://www.mdpi.com/1424-8220/16/4/584

Trawczyńska I. New Method of Determining Kinetic Parameters for Decomposition of Hydrogen Peroxide by Catalase. Catalysts. 2020 Mar 12;10(3):323. Available from: https://www.mdpi.com/2073-4344/10/3/323

Lian J, Liu P, Jin C, Shi Z, Luo X, Liu Q. Perylene diimide-functionalized CeO_2 nanocomposite as a peroxidase mimic for colorimetric determination of hydrogen peroxide and glutathione. Microchim Acta. 2019 Jun 6;186(6):332. Available from: http://link.springer.com/10.1007/s00604-019-3439-0

Gao L, Fan K, Yan X. Iron Oxide Nanozyme: A Multifunctional Enzyme Mimetic for Biomedical Applications. Theranostics. 2017;7(13):3207–27. Available from: http://www.thno.org/v07p3207.htm

Chen J, Xu F, Zhang Q, Li S. N-doped MoS_2-nanoflowers as peroxidase-like nanozymes for total antioxidant capacity assay. Anal Chim Acta. 2021 Oct;1180:338740. Available from: https://linkinghub.elsevier.com/retrieve/pii/S0003267021005663

Lou Z, Zhao S, Wang Q, Wei H. N-Doped Carbon As Peroxidase-Like Nanozymes for Total Antioxidant Capacity Assay. Anal Chem. 2019 Dec 3;91(23):15267–74. Available from: https://pubs.acs.org/doi/10.1021/acs.analchem.9b04333

Bao Y-W, Hua X-W, Ran H-H, Zeng J, Wu F-G. Metal-doped carbon nanoparticles with intrinsic peroxidase-like activity for colorimetric detection of H_2O_2 and glucose. J Mater Chem B. 2019;7(2):296–304. Available from: http://xlink.rsc.org/?DOI=C8TB02404A

Cui M, Zhou J, Zhao Y, Song Q. Facile synthesis of iridium nanoparticles with superior peroxidase-like activity for colorimetric determination of H_2O_2 and xanthine. Sens. Actuators. B. 2016 Nov 27;243(2017):203-210. Available from: https://linkinghub.elsevier.com/retrieve/pii/S0925400516319438

Ju P, Xiang Y, Xiang Z, Wang M, Zhao Y, Zhang D, et al. BiOI hierarchical nanoflowers as novel robust peroxidase mimetics for colorimetric detection of H_2O_2. RSC Adv. 2016;6(21):17483–93. Available from: http://xlink.rsc.org/?DOI=C6RA00368K

Ai L, Li L, Zhang C, Fu J, Jiang J. MIL-53(Fe): A Metal-Organic Framework with Intrinsic Peroxidase-Like Catalytic Activity for Colorimetric Biosensing. Chem - A Eur J. 2013 Nov 4;19(45):15105–8. Available from: http://doi.wiley.com/10.1002/chem.201303051

Lin T, Zhong L, Guo L, Fu F, Chen G. Seeing diabetes: visual detection of glucose based on the intrinsic peroxidase-like activity of MoS_2 nanosheets. Nanoscale. 2014;6(20):11856–62. Available from: http://xlink.rsc.org/?DOI=C4NR03393K

Cai S, Han Q, Qi C, Lian Z, Jia X, Yang R, et al. $Pt_{74}Ag_{26}$ nanoparticle-decorated ultrathin MoS_2 nanosheets as novel peroxidase mimics for highly selective colorimetric detection of

H_2O_2 and glucose. Nanoscale. 2016;8(6):3685–93. Available from: http://xlink.rsc.org/?DOI=C5NR08038J

Dong Y, Zhang H, Rahman ZU, Su L, Chen X, Hu J, et al. Graphene oxide–Fe_3O_4 magnetic nanocomposites with peroxidase-like activity for colorimetric detection of glucose. Nanoscale [Internet]. 2012;4(13):3969. Available from: http://xlink.rsc.org/?DOI=c2nr12109c

Guo Y, Deng L, Li J, Guo S, Wang E, Dong S. Hemin−Graphene Hybrid Nanosheets with Intrinsic Peroxidase-like Activity for Label-free Colorimetric Detection of Single-Nucleotide Polymorphism. ACS Nano. 2011 Feb 22;5(2):1282–90. Available from: https://pubs.acs.org/doi/10.1021/nn1029586

Liu M, Zhao H, Chen S, Yu H, Quan X. Stimuli-responsive peroxidase mimicking at a smart graphene interface. Chem Commun. 2012;48(56):7055. Available from: http://xlink.rsc.org/?DOI=c2cc32406g

Lin L, Song X, Chen Y, Rong M, Zhao T, Wang Y, et al. Intrinsic peroxidase-like catalytic activity of nitrogen-doped graphene quantum dots and their application in the colorimetric detection of H_2O_2 and glucose. Anal Chim Acta. 2015 Apr;869:89–95. Available from: https://linkinghub.elsevier.com/retrieve/pii/S0003267015002020

Omidfar K, Khorsand B, Larijani B. Development of a new sensitive immunostrip assay based on mesoporous silica and colloidal Au nanoparticles. Mol Biol Rep. 2012 Feb 21;39(2):1253–9. Available from: http://link.springer.com/10.1007/s11033-011-0856-5

Liu Y, Zhan L, Qin Z, Sackrison J, Bischof JC. Ultrasensitive and Highly Specific Lateral Flow Assays for Point-of-Care Diagnosis. ACS Nano. 2021 Mar 23;15(3):3593–611. Available from: https://pubs.acs.org/doi/10.1021/acsnano.0c10035

Reis C, Sousa E, Serpa J, Oliveira R, Oliveira R, Santos J. Design of immobilized enzyme biocatalysts: Drawbacks and opportunities. Quim Nova. 2019 July; 42(7):1-16 Available from: https://www.scielo.br/j/qn/a/cBRd9MXMLCQSry9bXwrNtNc/?lang=en

Christodouleas DC, Kaur B, Chorti P. From Point-of-Care Testing to eHealth Diagnostic Devices (eDiagnostics). ACS Cent Sci. 2018 Dec 26;4(12):1600–16. Available from: https://pubs.acs.org/doi/10.1021/acscentsci.8b00625

Mohamad NR, Marzuki NHC, Buang NA, Huyop F, Wahab RA. An overview of technologies for immobilization of enzymes and surface analysis techniques for immobilized enzymes. Biotechnol Biotechnol Equip. 2015 Mar 4;29(2):205–20. Available from: http://www.tandfonline.com/doi/abs/10.1080/13102818.2015.1008192

Hasegawa K, Minakata K, Suzuki M, Suzuki O. The standard addition method and its validation in forensic toxicology. Forensic Toxicology [Internet]. 2021 June;39:311-333. Avaialble from: https://doi.org/10.1007/s11419-021-00585-8

Gillissen B, Burkle L, Andre B, Kuhn C, Rentsch, Brandl B, Frommer WB, A new family of high-affinity transporters for adenine, cytosine, and purine derivativatives in

Arabidopsis. Plant Cell [Internet]. 2000 Feb, 12(2): 291-300. Available from: 10.1105/tpc.12.2.291